

Taking the Pulse of Polymerization Kinetics: A Systematic PLP-SEC Study of Industrially Relevant (Meth)acrylates

Zur Erlangung des akademischen Grades eines
DOKTORS DER NATURWISSENSCHAFTEN
(Dr. rer. nat.)

von der KIT-Fakultät für Chemie und Biowissenschaften
des Karlsruher Instituts für Technologie (KIT)

genehmigte
DISSERTATION
von

Dipl. Chem. Katrin Blandine Kockler

aus
Birkenfeld, Deutschland

Dekan: Prof. Dr. Willem Klopper
Referent: Prof. Dr. Christopher Barner-Kowollik
Korreferent: Prof. Dr. Manfred Wilhelm
Tag der mündlichen Prüfung: 25.04.2017

Die vorliegende Arbeit wurde im Zeitraum von März 2014 bis März 2017 unter Anleitung von Prof. Christopher Barner-Kowollik am Karlsruhe Institut für Technologie (KIT) - Universitätsbereich angefertigt.

*No amount of experiments can ever proof me right, but a single experiment
can proof me wrong.*

Albert Einstein

I'm gonna have to science the shit out of this!

Mark Watney (The Martian)

Abstract

Knowledge of the fundamental kinetic data of elemental reaction steps is critical for the synthesis of polymers with well-defined properties. Access to kinetic rate coefficients for free radical polymerization (FRP) processes allows for the prediction of space-time yields, heat generation, or properties of the polymeric products in large scale production as well as the modelling and selection of suitable controlling agents for reversible deactivation radical polymerization (RDRP) techniques as for example the industrially frequently used reversible addition-fragmentation chain transfer (RAFT) polymerization or nitroxide-mediated polymerization (NMP).

In the present thesis the database of precise monomer specific propagation rate coefficients, k_p , and Arrhenius parameters is extended and the comparison of different monomers allows for the determination of trends and family type behaviors among designated monomer groups. The first-time kinetic investigation of five branched acrylates in solution – namely *tert*-butyl acrylate, isobornyl acrylate, benzyl acrylate, 2-ethylhexyl acrylate, and 2-propylheptyl acrylate – and six nitrogen-containing (branched) methacrylates in bulk – i.e. 2-(*N*-ethylanilino)ethyl methacrylate, 2-morpholinoethyl methacrylate, 2-(1-piperidyl)ethyl methacrylate, 2-(*N,N*-diethylamino)ethyl methacrylate, 2-(*N,N*-dimethylamino)ethyl methacrylate, and 3-(*N,N*-dimethylamino)propyl methacrylate – compared with literature known data enables the identification of structure - propagation rate - relations. A family type behavior for nitrogen-containing methacrylates – where the heteroatom is separated from the ester moiety by an ethyl linker – was observed and may be attributed to comparable steric demands and polarity as key factors. For acrylates with branched ester side chains in solution, no trends could be detected and no clear analogous behavior between branched acrylates in solution and in bulk was identified, leading to the necessity of a direct determination of monomer specific Arrhenius parameters of the propagation rate coefficient for each branched acrylate of interest. Reasons for the lack of detectable trends throughout the series of branched acrylates may be a combination of entropic and enthalpic effects originating in the missing α -methyl substituent compared to the branched methacrylates which are exhibiting a family type behavior. For the precise investigation of secondary propagation rate coefficients for acrylate monomers at elevated temperatures (above 30°C), pulse repetition rates of up to 500 Hz are mandatory to prevent potential side reactions interfering with linear chain growth such as backbiting, therefore, a high frequency Excimer laser was employed for the studied monomers. The findings of the current study are based on the careful determination of monomer specific temperature

dependent propagation rate coefficients and Arrhenius parameters for eleven acrylic and methacrylic monomers via the pulsed laser polymerization – size exclusion chromatography (PLP-SEC) method, a method recommended by the IUPAC working party on *Modeling of Kinetics and Processes of Polymerization* for the critical evaluation of propagation rate coefficients. For an accurate SEC calibration, polymer specific Mark-Houwink-Kuhn-Sakurada (MHKS) parameters need to be employed and are determined during the course of the present thesis for the six nitrogen-containing methacrylates via a triple detection SEC setup and measurement of narrowly distributed polymer samples generated via reversible addition-fragmentation chain transfer polymerization and polymerization with a thiol as transfer agent, since no MHKS parameters for the investigated polymers are known in the literature. The herein investigated methacrylates constitute the first extended group of nitrogen-containing methacrylates investigated via PLP-SEC, adding to the hitherto first and only investigated N-containing methacrylate ureidoethyl methacrylate (UMA). All data obtained during the current study are critically compared to literature known data to extend the understanding of trends and family type behaviors.

Furthermore, studies of the influence of Lewis acids on the propagation rate coefficient and degree of transfer to polymer and defect structures of methyl acrylate were performed via PLP-SEC. A general rate accelerating effect of the Lewis acid on the propagation reaction of MA was observed and the propagation rate coefficient, k_p , increased depending on the employed temperature. At -12 °C an increase in k_p of approximately 18% is reported, while at 10 °C an increase of close to 30% is observed.

Zusammenfassung

Für die Darstellung wohldefinierter Polymere ist die genaue Kenntnis über fundamentale kinetische Daten elementarer Reaktionsschritte notwendig. Informationen über kinetische Geschwindigkeitskoeffizienten für Prozesse der freien radikalischen Polymerisation (FRP) ermöglichen die Vorhersage von Raum-Zeit Ausbeuten, Hitzeentwicklung oder der Eigenschaften polymerer Produkte in der Massenproduktion sowie die Auswahl von passenden Kontrollreagenzien für eine Vielzahl industriell relevanter Polymerisationstechniken im Bereich der Reversiblen Deaktivierungs Radikalischen Polymerisation (RDRP), wie z.B. die Reversible Additions Fragmentierungs Kettenübertragungs (RAFT) Polymerisation oder Nitroxid-vermittelte Polymerisation (NMP). In der vorliegenden Arbeit wird die Datenbank der monomerspezifischen Wachstumsgeschwindigkeitskoeffizienten, k_p , und Arrhenius Parameter erweitert und anhand von Vergleichen der einzelnen Monomere untereinander werden übergeordnete Trends und Familienverhalten untersucht. Die erstmaligen kinetischen Untersuchungen von fünf verzweigten Acrylaten in Lösung – *tert*-Butylacrylat, Isobornylacrylat, Benzylacrylat, 2-Ethylhexylacrylat und 2-Propylheptylacrylat – sowie sechs stickstoffhaltiger Methacrylate in Substanz – 2-(*N*-Ethylanilino)ethylmethacrylat, 2-Morpholinoethylmethacrylat, 2-(1-Piperidyl)ethylmethacrylat, 2-(*N,N*-Diethylamino)ethylmethacrylat, 2-(*N,N*-Dimethylamino)ethylmethacrylat und 3-(*N,N*-Dimethylamino)propylmethacrylat – erlauben im Zusammenhang mit literaturbekannten Datensätzen die Etablierung von Struktur – Geschwindigkeitskoeffizienten – Beziehungen. Für die stickstoffhaltigen Methacrylate, deren Heteroatom durch einen Ethyl-Linker von der Estergruppe separiert ist, konnte ein Familienverhalten entdeckt werden, das hauptsächlich auf einen vergleichbaren sterischen Anspruch und ähnliche Polaritäten der Monomere zurückzuführen ist. Für die Gruppe der Acrylate mit verzweigten Seitenketten in Lösung konnten keine Trends festgestellt werden und auch ein analoges Verhalten zu den verzweigten Acrylaten in Substanz ist nicht vollständig gegeben, was zu der Notwendigkeit führt, für jedes Monomer von Interesse separat die monomerspezifischen Wachstumsgeschwindigkeitskoeffizienten und Arrhenius Parameter zu bestimmen. Erklärungen für das Fehlen eines erkennbaren Trends innerhalb der Reihe der verzweigten Acrylate können möglicherweise auf eine Kombination aus entropischen und enthalpischen Effekten zurückgeführt werden, die aus dem Fehlen der α -Methylgruppe entsteht, verglichen zu der Reihe der verzweigten Methacrylate, die ein Familienverhalten aufweisen. Für die genaue Untersuchung der sekundär propagierenden Geschwindigkeitskoeffizienten der Acrylatmonomere bei erhöhten Temperaturen (über 30°C) sind hohe

Laserpulsfrequenzen von bis zu 500 Hz notwendig, um mögliche Nebenreaktionen wie das sogenannte “backbiting“ (Radikalübertragung vom Ende der Polymerkette auf das Polymerrückgrad), die das lineare Wachstum der Polymerketten beeinträchtigen, zu unterdrücken. Deshalb wurde in der vorliegenden Arbeit ein hochfrequenter Excimer Laser zur Durchführung der Versuche genutzt. Die Erkenntnisse, die im Laufe dieser Arbeit gewonnen wurden, basieren auf einer sorgfältigen Bestimmung der monomerspezifischen, temperaturabhängigen Wachstumsgeschwindigkeitskoeffizienten und Arrhenius Parameter für elf acrylische und methacrylische Monomere mittels der Puls laser Polymerisations – Größenausschlusschromatographie (PLP-SEC), der von der IUPAC Arbeitsgruppe für *Modeling of Kinetics and Processes of Polymerization* empfohlenen Methode für die Bestimmung von Wachstumsgeschwindigkeitskoeffizienten. Für eine akkurate SEC-Kalibrierung werden polymerspezifische Mark-Houwink-Kuhn-Sakurada (MHKS) Parameter eingesetzt, welche im Laufe der vorliegenden Arbeit für die sechs stickstoffhaltigen Polymethacrylate bestimmt wurden mittels dreifach detektierter Größenausschlusschromatographie-Messungen eng verteilter Polymerproben, die per RAFT Polymerisation und Polymerisation mit Thiol als Transferreagenz hergestellt wurden, da zu diesen Polymeren bisher keine MHKS Parameter in der Literatur bekannt sind. Die in dieser Arbeit untersuchten Methacrylate stellen die erste größere Gruppe von stickstoffhaltigen Methacrylaten dar, die mittels PLP-SEC untersucht wurde und reißen sich ein mit dem zu diesem Zeitpunkt ersten und einzigen untersuchten stickstoffhaltigen Methacrylat Ureidoethylmethacrylat (UMA). Alle Daten, die im Laufe der vorliegenden Arbeit aufgenommen wurden, werden kritisch mit den bekannten Literaturdaten verglichen, um das Verständnis der vorliegenden Trends und Familienverhalten zu erweitern.

Desweiteren wurde der Einfluss von Lewis Säuren auf den Wachstumsgeschwindigkeitskoeffizienten und den Anteil an Transfer zum Polymerrückgrad sowie Defektstrukturen anhand von Methylacrylat mittels PLP-SEC untersucht. Ein genereller Anstieg der Geschwindigkeit der Propagationsreaktion von MA wurde beobachtet, dessen Ausmaß abhängig von der Polymerisationstemperatur ist. Bei $-12\text{ }^{\circ}\text{C}$ wurde ein Anstieg von k_p um circa 18% festgestellt, während bei $10\text{ }^{\circ}\text{C}$ eine Beschleunigung der Propagationsgeschwindigkeit um bereits etwa 30% zu beobachten war.

Publications Arising from the Thesis

- 1. No Apparent Correlation of k_p with Steric Hindrance for Branched Acrylates**
K. B. Kockler, A. P. Haehnel, F. Fleischhaker, M. Schneider-Baumann, A. M. Misske, C. Barner-Kowollik, *Macromol. Chem. Phys.* **2015**, *216*, 1573–1582.
- 2. Determining Free-Radical Propagation Rate Coefficients with High Frequency Lasers: Current Status and Future Perspectives – invited feature article**
K. B. Kockler, A. P. Haehnel, T. Junkers, C. Barner-Kowollik, *Macromol. Rapid Commun.* **2016**, *37*, 123–134.
- 3. Investigating the Propagation Kinetics of a Novel Class of Nitrogen Containing Methacrylates via PLP-SEC**
K. B. Kockler, F. Fleischhaker, C. Barner-Kowollik, *Polym. Chem.* **2016**, *7*, 4342–4351.
- 4. Free Radical Propagation Rate Coefficients of N-Containing Methacrylates: Are we Family?**
K. B. Kockler, F. Fleischhaker, C. Barner-Kowollik, *Macromolecules* **2016**, *49*, 8572–8580.

Additional Publications

- 1. Solvent Effects on Acrylate k_p in Organic Media? – A Systematic PLP-SEC Study**
A. P. Haehnel, B. Wenn, K. Kockler, T. Bantle, A. M. Misske, F. Fleischhaker, T. Junkers, C. Barner-Kowollik, *Macromol. Rapid Commun.* **2014**, *5*, 2029–2037.
- 2. Solvent Effects on Acrylate k_p in Organic Media? – A Systematic PLP-SEC Study – Statement to the Response**
A. P. Haehnel, B. Wenn, K. Kockler, T. Bantle, A. M. Misske, F. Fleischhaker, T. Junkers, C. Barner-Kowollik, *Macromol. Rapid Commun.* **2015**, *36*, 1984–1986.
- 3. A Complete Kinetic Study of a Versatile Functional Monomer: Acetoacetoxyethyl Methacrylate (AAEMA)**
A. Zoller, K. B. Kockler, M. Rollet, C. Lefay, D. Gigmes, C. Barner-Kowollik, Y. Guillaneuf, *Polym. Chem.* **2016**, *7*, 5518–5525.
- 4. An alternative method to estimate the bulk backbiting rate coefficient in acrylate radical polymerization**
Y. W. Marien, P. H. M. Van Steenberge, K. B. Kockler, C. Barner-Kowollik, M.-F. Reyniers, D. R. D’hooge, G. B. Marin, *Polym. Chem.* **2016**, *7*, 6521–6528.
- 5. Estimating Photodissociation Quantum Yields from PLP-SEC Peak Heights**
Y. W. Marien, P. H. M. Van Steenberge, K. B. Kockler, C. Barner-Kowollik, M.-F. Reyniers, G. B. Marin, D. R. D’hooge, **2017**, *in press*.

Contents

Abstract	i
Zusammenfassung	iii
1. Introduction	1
1.1. Motivation and Aim of the Research Program	2
1.2. Free Radical Polymerization (FRP)	3
1.3. Polymerization Techniques - Controlling dispersities	6
1.3.1. Reversible Addition-Fragmentation Chain Transfer Polymerization (RAFT)	7
1.3.2. Radical Polymerization with Chain Transfer Agent	10
1.4. Pulsed-Laser Polymerization - Size Exclusion Chromatography (PLP-SEC)	12
1.4.1. SEC-Analysis and Determination of Absolute Molecular Weights	22
1.4.2. Arrhenius Relations and Determination of Arrhenius Parameters	25
2. Branched Acrylates in Solution	29
2.1. MHKS Parameters	33
2.2. Arrhenius Parameters	35
2.3. Trends and Family Type Behavior	39
2.3.1. Comparison to Linear Acrylates and Branched Methacrylates .	45
3. Nitrogen-Containing Methacrylates	53
3.1. MHKS Parameters	57
3.2. Arrhenius Parameters	61
3.3. Trends and Family Type Behaviour	64
3.3.1. Expanding the Family	68
3.3.2. Comparison to UMA	76
3.3.3. Comparison to Cyclic Methacrylates	79
3.3.4. Comparison to Branched Methacrylates	82
4. Lewis Acid-mediated PLP	87
4.1. Polymerization of Methyl Acrylate with LiNTf ₃	90
5. Conclusion	99

6. Experimental Section	103
6.1. Materials	103
6.2. Pulsed Laser Polymerization Experiments	103
6.3. Characterization Methods	105
6.3.1. Size-Exclusion Chromatography	105
6.3.2. Triple-Detection SEC	106
6.3.3. Density Measurements	106
6.3.4. UV measurements	107
6.4. Polymerization Techniques	107
6.4.1. Reversible Addition-Fragmentation Chain Transfer Polymer- ization	107
6.4.2. Polymerization With Chain Transfer Agent	108
7. Abbreviations	109
A. Appendix	125
A.1. Chapter 2: Branched Acrylates in Solution	125
A.2. Chapter 3: Nitrogen Containing Methacrylates	137
A.3. Chapter 4: PLP with Lewis Acids	166
Curriculum Vitae	173
Publications and Conference Contributions	175
Acknowledgements	177

List of Figures

1.1.	General kinetics of a free radical polymerization reaction.	3
1.2.	Backbiting mechanism of an acrylic macroradical with a six-membered transition state.	5
1.3.	A mid chain radical (MCR) alongside its possible reaction pathways propagation and β -scission.	5
1.4.	General principle of RDRP.	7
1.5.	Mechanism of RAFT polymerization.	8
1.6.	Overview of appropriate Z- and R-groups for the selection of suitable RAFT agents.	9
1.7.	General mechanism of chain transfer to CTA.	11
1.8.	Structures of typical photoinitiators alongside all initiators employed in the current study.	14
1.9.	Example of chain growth during PLP.	15
1.10.	Typical PLP generated molecular weight distribution with its first derivative.	16
1.11.	S-shaped curve showing the frequency dependency of acrylate systems at low pulse repetition rates.	18
1.12.	Schematic setup of a MALLS detector.	23
1.13.	Typical Arrhenius plot with linear fit.	26
2.1.	Monomer Landscape of Branched Acrylates.	31
2.2.	Arrhenius plots of branched Acrylates in solution.	37
2.3.	Dependance of the Arrhenius parameters on the ester side chain for branched acrylates.	40
2.4.	Dependence of the propagation rate coefficients on the ester side chain for branched acrylates.	42
2.5.	Combined Arrhenius plot for branched acrylates in solution.	44
2.6.	Dependence of the propagation rate on the ester side chain for the homologous series of branched acrylates.	47
3.1.	Monomer Landscape of Nitrogen-Containing Methacrylates.	56
3.2.	MHKS plots for nitrogen-containing methacrylates.	58
3.3.	Arrhenius plots of nitrogen-containing methacrylates in bulk.	62
3.4.	Propagation rate coefficients for NEAEMA, MOMA, and PipEMA.	65

3.5.	Combined Arrhenius plot for NEAEMA, MOMA, and PipEMA.	66
3.6.	Combined Arrhenius plots and propagation rate coefficients for DEAEMA, DMAEMA, and DMAPMAE.	68
3.7.	Combined Arrhenius plots and propagation rate coefficients for DEAEMA, NEAEMA, MOMA, and PipEMA.	70
3.8.	Combined Arrhenius plots and propagation rate coefficients for DMAEMA, NEAEMA, MOMA, and PipEMA.	71
3.9.	Combined Arrhenius plots and propagation rate coefficients for DMAPMAE, NEAEMA, MOMA, and PipEMA.	72
3.10.	Arrhenius parameters of DMAPMAE, PipEMA, DEAEMA, and DMAEMA.	73
3.11.	Combined Arrhenius fits for nitrogen-containing methacrylates.	75
3.12.	Combined propagation rate coefficients of N-ethyl methacrylates and UMA.	77
3.13.	Linear Arrhenius fits for N-ethyl methacrylates and UMA.	78
3.14.	Combined propagation rate coefficients of N-ethyl methacrylates and cyclic methacrylates.	80
3.15.	Linear Arrhenius fits for N-ethyl methacrylates and cyclic methacrylates.	81
3.16.	Combined propagation rate coefficients of N-ethyl methacrylates and branched methacrylates.	83
3.17.	Linear Arrhenius fits for N-ethyl methacrylates and branched methacrylates.	84
4.1.	Possible coordinations of Lewis acid during radical polymerization.	88
4.2.	UV spectra of photoinitiators with and without Lewis acid.	92
4.3.	Frequency series for MA in presence and absence of the Lewis acid at -12 °C.	94
4.4.	Frequency series for MA in presence and absence of the Lewis acid at 10 °C.	94
4.5.	Propagation rate coefficients at different frequencies at -15 °C.	95
4.6.	Molecular weight distributions and their first derivatives for MA in the presence and absence of LiNTf ₃	96
4.7.	Arrhenius plot for MA in the presence and absence of LiNTf ₃	97
A.1.	Representative molecular weight distributions and their first derivatives of benzyl acrylate (BnA) in 1M solution in butyl acetate.	126
A.2.	Representative molecular weight distributions and their first derivatives of 2-ethylhexyl acrylate (EHA) in 1M solution in butyl acetate.	127

A.3. Representative molecular weight distributions and their first derivatives of <i>iso</i> -bornyl acrylate (<i>i</i> BoA) in 1M solution in butyl acetate.	128
A.4. Representative molecular weight distributions and their first derivatives of 2-propylheptyl acrylate (PHA) in 1M solution in butyl acetate.	129
A.5. Representative molecular weight distributions and their first derivatives of <i>tert</i> -butyl acrylate (<i>t</i> BA) in 1M solution in butyl acetate.	130
A.6. Temperature dependent densities for the herein studied monomers BnA, EHA, <i>i</i> BoA, PHA, and <i>t</i> BA in 1 molar solution in BuAc.	136
A.7. Representative molecular weight distributions and their first derivatives of 2-(<i>N</i> -ethylamino)ethyl methacrylate (NEAEMA) in bulk.	138
A.8. Representative molecular weight distributions and their first derivatives of 2-morpholinoethyl methacrylate (MOMA) in bulk.	139
A.9. Representative molecular weight distributions and their first derivatives of 2-(1-piperidyl)ethyl methacrylate (PipEMA) in bulk.	140
A.10. Representative molecular weight distributions and their first derivatives of 2-(<i>N,N</i> -diethylamino)ethyl methacrylate (DEAEMA) in bulk.	141
A.11. Representative molecular weight distributions and their first derivatives of 2-(<i>N,N</i> -dimethylamino)ethyl methacrylate (DMAEMA) in bulk.	142
A.12. Representative molecular weight distributions and their first derivatives of 3-(<i>N,N</i> -dimethylamino)propyl methacrylate (DMAPMAE) in bulk.	143
A.13. Temperature dependent densities for the herein studied monomers NEAEMA, MOMA, PipEMA, DEAEMA, DMAEMA, and DMAPMAE in bulk.	150
A.14. Representative triple detection SEC traces for NEAEMA.	151
A.15. Representative triple detection SEC traces for MOMA.	152
A.16. Representative triple detection SEC traces for PipEMA.	153
A.17. Representative triple detection SEC traces for DEAEMA.	154
A.18. Representative triple detection SEC traces for DMAEMA.	155
A.19. Representative triple detection SEC traces for DMAPMAE.	156
A.20. Temperature dependent densities for MA in bulk with 5-10 mol% Lewis acid.	166
A.21. Representative molecular weight distributions and their first derivatives of methyl acrylate in bulk.	166
A.22. Representative molecular weight distributions and their first derivatives of methyl acrylate with LiNTf ₃	167

List of Tables

1.1. Summary of trends and family type behaviors.	21
2.1. Collation of monomer and polymer specific physical data for branched acrylates.	34
2.2. Arrhenius parameters for branched acrylates in solution.	36
3.1. Collation of monomer and polymer specific physical data for nitrogen-containing methacrylates.	60
3.2. Arrhenius parameters for nitrogen-containing methacrylates in bulk.	63
A.1. Detailed PLP sample conditions, absolute molecular weights, and resulting propagation rates for BnA 1M in BuAc	131
A.2. Detailed PLP sample conditions, absolute molecular weights, and resulting propagation rates for EHA 1M in BuAc	132
A.3. Detailed PLP sample conditions, absolute molecular weights, and resulting propagation rates for <i>i</i> BoA 1M in BuAc	133
A.4. Detailed PLP sample conditions, absolute molecular weights, and resulting propagation rates for PHA 1M in BuAc	134
A.5. Detailed PLP sample conditions, absolute molecular weights, and resulting propagation rates for ^t BA 1M in BuAc	135
A.6. Detailed PLP sample conditions, absolute molecular weights, and resulting propagation rates for NEAEMA in bulk.	144
A.7. Detailed PLP sample conditions, absolute molecular weights, and resulting propagation rates for MOMA in bulk.	145
A.8. Detailed PLP sample conditions, absolute molecular weights, and resulting propagation rates for PipEMA in bulk.	146
A.9. Detailed PLP sample conditions, absolute molecular weights, and resulting propagation rates for DEAEMA in bulk.	147
A.10. Detailed PLP sample conditions, absolute molecular weights, and resulting propagation rates for DMAEMA in bulk.	148
A.11. Detailed PLP sample conditions, absolute molecular weights, and resulting propagation rates for DMAPMAE in bulk.	149
A.12. Weight average molecular weights and intrinsic viscosities employed to determine the MHKS parameters for NEAEMA, MOMA, and PipEMA.	157

A.13. Weight average molecular weights and intrinsic viscosities employed to determine the MHKS parameters for DEAEMA, DMAEMA, and DMAPMAE.	158
A.14. Detailed sample conditions and resulting isolated yield for the RAFT polymerization of NEAEMA in bulk.	159
A.15. Detailed sample conditions and resulting isolated yield for the polymerization with thiol as transfer agent for NEAEMA in bulk.	160
A.16. Detailed sample conditions and resulting isolated yield for the RAFT polymerization of MOMA in bulk.	160
A.17. Detailed sample conditions and resulting isolated yield for the polymerization with thiol as transfer agent for MOMA in bulk.	160
A.18. Detailed sample conditions and resulting isolated yield for the polymerization with thiol as transfer agent for PipEMA in 50% solution in THF.	161
A.19. Detailed sample conditions and resulting isolated yield for the polymerization with thiol as transfer agent for DEAEMA in bulk.	162
A.20. Detailed sample conditions and resulting isolated yield for the polymerization with thiol as transfer agent for DMAEMA in bulk.	163
A.21. Detailed sample conditions and resulting isolated yield for the polymerization with thiol as transfer agent for DMAPMAE in bulk.	165
A.22. Detailed PLP sample conditions for MA in bulk at 10 °C.	168
A.23. Detailed PLP sample conditions for MA in bulk with the addition of LA at 10 °C.	169
A.24. Detailed PLP sample conditions for MA in bulk at -12 °C.	169
A.25. Detailed PLP sample conditions for MA in bulk with the addition of LA at -12 °C.	170
A.26. Detailed sample conditions for MA in the presence and absence of Lewis acid at 10 to 50 Hz.	170
A.27. Detailed sample conditions of MA incorporated into the Arrhenius plot.	171

*If we knew what it was we were doing,
it would not be called research, would it?*

Albert Einstein

1

Introduction

In academia as well as industry detailed knowledge of the mechanisms and kinetics of polymerization processes is crucial for the synthesis of tailor-made polymers for specialized applications. The control over, for example, chain branching, stereoregularity, or composition of (block)co-polymers is a highly desired goal in free radical polymerization. Understanding the fundamental chemical processes and kinetic background of elemental reaction steps enables the facilitation of large-scale industrial production of polymeric materials by allowing for the prediction of reaction heat and space–time yield and therefore the appropriate reactor designs and procedures. For small-scale applications and academia as well, knowledge of monomer specific rate data is mandatory e.g. for the design of suitable reaction agents for reversible addition-fragmentation chain transfer (RAFT) polymerization^[1-4] or nitroxide mediated polymerization (NMP)^[5-7] and to allow for kinetic modeling and prediction of microstructures.^[8-10] Experimentally inaccessible kinetic data are made available via rate coefficients for propagation or termination reactions^[11] and the modelling of e.g. entire polymerization mechanisms and processes such as atom transfer radical polymerization (ATRP) or single electron transfer – living radical polymerization (SET-LRP) is made possible.^[12-15]

Monomer families that are of great interest for industrial applications are acrylates and methacrylates. (Meth)acrylates can readily be polymerized because of their reactive double bond and are noted for their transparency, elasticity, and resistance towards breakage. A wide variety of industrially relevant products is based on (meth)acrylates, such as coatings, adhesives, electronics, lubricants, and cosmetics.^[16] Poly(methacrylates) can be used for aircraft parts, security glass, safety goggles, or construction panels.

Poly(methyl methacrylate) (PMMA) – being the most common poly(methacrylate) – finds various medicinal applications as well, including dental prothesis or bone substitutes. Methacrylates containing heteroatoms are utilized in home- and personal care products, paper chemicals, or flocculation agents^[16] and are interesting candidates for friction modifiers, printing inks, adhesion promoters, dispersion agents, and biomedical and electrooptical applications.^[17–26]

Understanding fundamental principles and detailed kinetic investigations of the FRP process are necessary to effectively manipulate the polymerization pathways to gain control and e.g. suppress non-desired side reactions to create precise and well-defined products. Therefore assessing precise rate coefficients is highly important for industrial and academic purposes alike.

1.1. Motivation and Aim of the Research Program

The current work is an investigation into one of the most important reaction steps in free radical polymerization (FRP) processes, the chain propagation, to provide insight into the underlying kinetic data, and to strive for a better understanding of the polymerization behavior of certain monomer classes. Due to numerous applications in many industrial and academic fields, acrylates and methacrylates constitute important monomer families. Their versatility and ease of accessibility makes them highly attractive reactants for a wide variety of commonly used products. In the current work, the emphasis lies on:

- the kinetic investigation of several (meth)acrylic monomers via the deduction of
 - propagation rate coefficients
 - Mark-Houwink-Kuhn-Sakurada parameters
 - Arrhenius parameters
- the identification of overarching trends or family type behaviors among certain monomer classes with regard to their ester side chains to give direction to predictions of yet unstudied monomers
- the provision of possible explanations for detected trends and family type behaviors or their absence
- an insight into the influence of Lewis acids on the formation of defect structures and mid chain radicals during FRP

1.2. Free Radical Polymerization (FRP)

Radical polymerization bears advantages compared to ionic polymerization including mild reaction conditions, low environmental impact, or versatility, for example regarding potential reaction media (bulk, solution, suspension, emulsion) or feasible monomers.^[27,28] Hence, free radical polymerization (FRP) is one of the most important industrial methods for the synthesis of polymers and employed for approximately 50% of industrially produced polymers.^[29] The underlying mechanism of FRP is described in the current thesis since it is the basis of the herein employed pulsed laser polymerization (PLP) method and the reversible addition-fragmentation chain transfer (RAFT) polymerization technique as well as the polymerization with chain transfer agent. FRP is based on a chain reaction^[30] consisting of five elementary reaction steps as depicted in Figure 1.1:

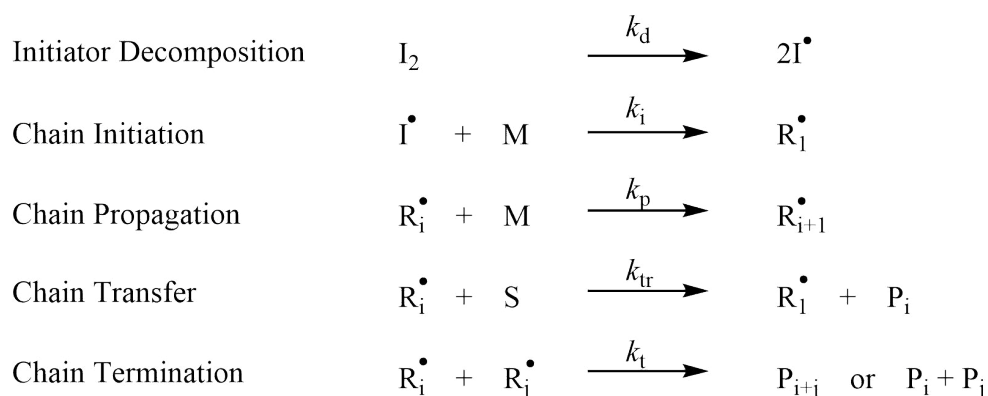


Figure 1.1.: General kinetics of a free radical polymerization reaction. For further information refer to the main text. Adapted from Ref [31] with permission of John Wiley and Sons.

1) **Initiator Decomposition:** Radicals are formed via homolytic cleavage of thermally or photochemically reactive initiator molecules with an initiator efficiency f and a unimolecular rate coefficient k_d .

2) **Chain Initiation:** The previously generated (primary) radicals add to the C=C double bond of monomer molecules with typical rate coefficients of $k_d \approx 10^{-5} \text{ L}\cdot\text{mol}^{-1}\cdot\text{s}^{-1}$ and $k_i > 10^4 \text{ L}\cdot\text{mol}^{-1}\cdot\text{s}^{-1}$ forming a single bond and more stable secondary radical.

3) **Chain Propagation:** A repetitive addition of radicals to monomer units bearing a double bond takes place with a propagation rate of $k_p = 10^2 - 10^4 \text{ L}\cdot\text{mol}^{-1}\cdot\text{s}^{-1}$ leading to the formation of macromolecular chains. On-going research focuses on different factors influencing the propagation rate coefficient. A dependency of k_p on the

chain length of the propagating macroradicals is suggested in several publications. [32,33]

4) Chain Termination: Growing chains can terminate either via recombination or disproportionation. Recombination describes the reaction of two radical sites that leads to a “dead” macromolecular chain (not able to propagate further). On the other hand, disproportionation includes the abstraction of a hydrogen atom, leading to a saturated (“dead”) chain and a new double bond bearing macromolecule able to undergo further propagation. Termination rate coefficients are diffusion controlled and since diffusion is strongly influenced by the size of the polymer chains as well as the viscosity of the reaction medium leading to the so called Trommsdorff effect at higher conversions, k_t is chain length and conversion dependent [34–38] with values of approx. $10^{8\pm 1} \text{ L}\cdot\text{mol}^{-1}\cdot\text{s}^{-1}$.

5) Chain Transfer: Competitive reactions to linear propagation are transfer reactions that, contrary to chain termination reactions, result in the creation of a new radical site (the radical is not destroyed, but transferred). Radicals can be transferred with a rate coefficient k_{tr} to low molecular weight species such as solvent, transfer agents, or monomers as well as to other polymeric chains. The radical species formed by transfer to monomer is often resonance stabilized and thus does not encourage further propagation. [39] Due to an increase of polymeric species in the reaction medium, transfer to polymer becomes increasingly important at higher conversions. The radicals formed via transfer to polymer are usually tertiary (so-called mid chain radicals (MCRs)) and therefore are more stable due to a positive inductive effect of the substituents. The increased stability of the radical site results in a decreased propagation rate coefficient as well as increased radical lifetime – similar to the lifetime of intermediate RAFT radicals [8,40,41] – amplifying the possibility of further side reactions. The formation of MCRs is especially important in the polymerization of acrylic monomers, where the intramolecular abstraction of a hydrogen atom via a six-membered cyclic transition state (the so-called “backbiting” reaction) transfers the radical site to the polymer backbone thereby leading to the formation of short chain branches [42–44] as shown in Figure 1.2.

Via the addition of further monomer units the MCRs are converted to secondary propagating radicals (SPRs) and – depending on intramolecular or intermolecular transfer – lead to short or long chain branching of the polymer molecule. Another possible formation of SPRs from MCRs is β -scission, forming a SPR and an unsaturated macromolecule. [45,46] MCRs can furthermore be terminated via disproportionation or recombination, the latter resulting in a 3- or 4-arm star polymer. The main possible follow-up reactions of MCRs are depicted in Figure 1.3. [8,40,47]

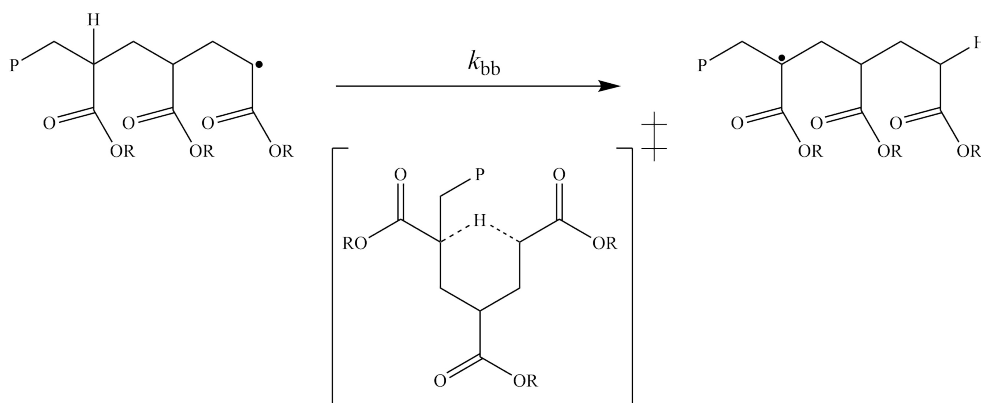


Figure 1.2.: Backbiting mechanism of an acrylic macroradical with a six-membered transition state. Figure adapted from Ref [28] with permission of John Wiley and Sons.

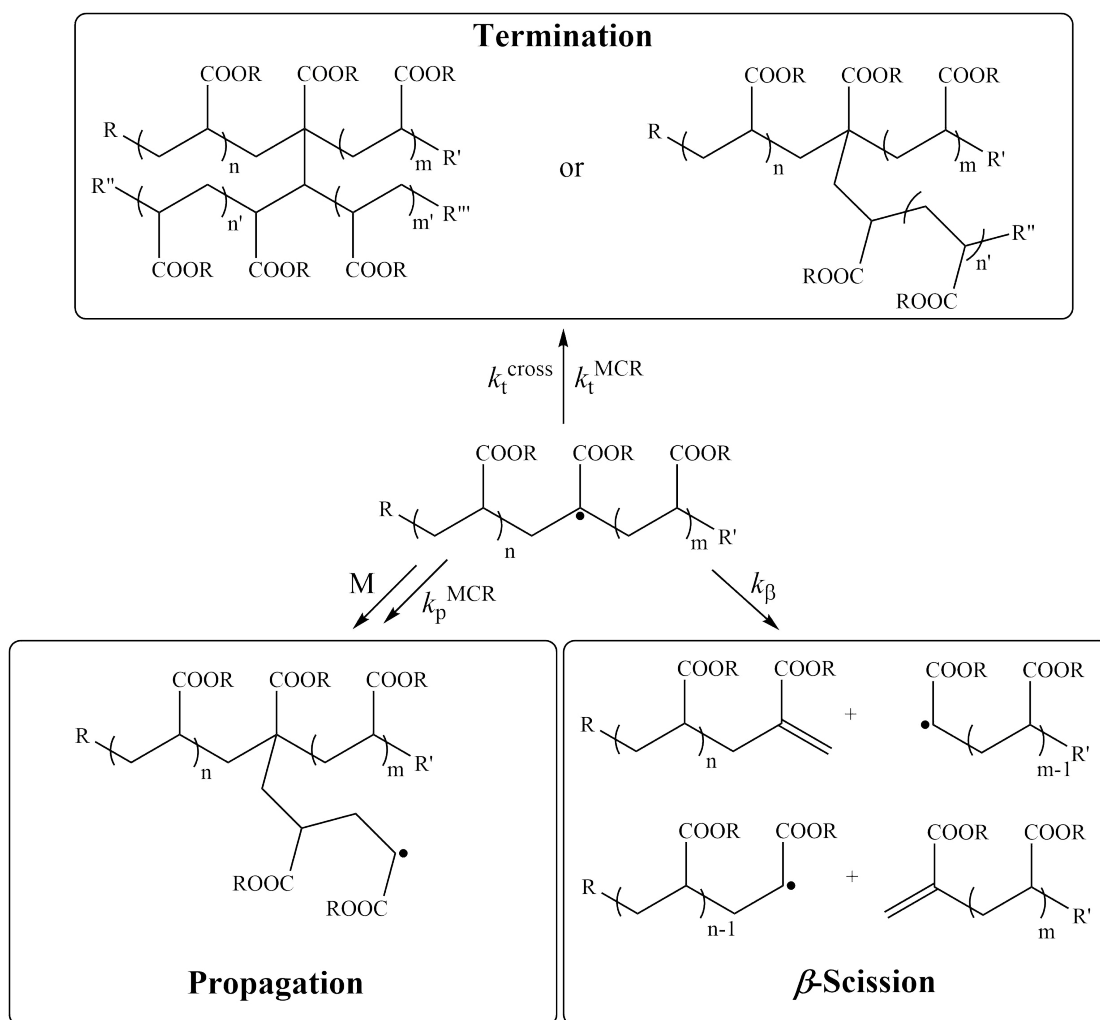


Figure 1.3.: A mid chain radical (MCR) alongside its possible reaction pathways propagation and β -scission. Reprinted from Ref [40] with permission of John Wiley and Sons.

FRP is a robust polymerization process tolerating a wide range of monomers as well as reaction conditions such as the presence of water or other protic impurities, providing theoretical dispersities \bar{D} between 1.5 and 2.0 depending on the type of termination, although in reality mostly higher dispersities are produced due to an increase of transfer and termination reactions with increasing conversion and the consumption of the monomer, leading to lower produced molecular weights. However, only limited control over polymeric architecture or functionality can be achieved. Several polymerization techniques have been developed to significantly reduce termination reactions and gain efficient control over architecture and end-group functionality via reversible termination or degenerative chain transfer.^[48]

1.3. Polymerization Techniques - Controlling dispersities

Radical polymerization is the most important technique for the production of polymeric materials in academia as well as industry. One of the disadvantages of free radical polymerization is the uncontrolled termination reactions leading to broad molecular weight distributions. According to Equation 1.1, an increase in the concentration of free radicals leads to a squared increase in the termination rate.

$$r_t = k_t[P^\cdot]^2 \quad (1.1)$$

Therefore decreasing the amount of free radicals in the reaction mixture enables a minimization of termination reactions and therefore better control. In controlled radical polymerization (CRP) the concentration of free radicals (propagating species) is reduced to approximately 10^{-9} to 10^{-7} mol·L⁻¹.^[49] CRP combines the advantages of radical polymerization and ionic polymerization – like inexpensive production of blockpolymers or the ability to introduce polar monomers in blockcopolymers – without their drawbacks, therefore being a highly industrially and academically relevant polymerization technique. During the last decade, effort has been made to develop several reversible deactivation radical polymerization (RDRP) techniques like RAFT, NMP, SET-LRP, and ATRP to gain better control over conventional FRP and introducing characteristics of living polymerization.^[50] However, the International Union of Pure and Applied Chemistry (IUPAC) urges to refrain from the term “living“ when addressing RDRP techniques, since they do not display all properties necessary to be termed a living process.^[51] Using RDRP, termination reactions are not entirely suppressed, but a majority of the macromolecules are kept in a stable, dormant state due to a deactivation

of the propagating site (see Figure 1.4.^[52] RDRP techniques allow for distinguished control over the molecular weight due to linear increase of the degree of polymerization vs. conversion and facilitate the fine-tuning of microstructure leading to high end group fidelity and low dispersities.

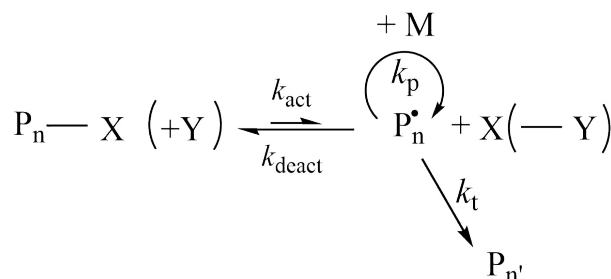


Figure 1.4.: General Principle of RDRP techniques. Deactivation is favored over activation. Although termination is reduced, it is not complete suppressed.

Though not considered CRP, another useful way to reduce dispersities during radical polymerization is the use of chain transfer agents (CTA) like mercaptanes or halocarbons. The two polymerization techniques employed in the current study to produce polymeric samples with dispersities around 2.0 for the determination of Mark-Houwink-Kuhn-Sakurada parameters as described in chapter 1.4.1 are RAFT polymerization and radical polymerization with a CTA and will be described in detail in the following subsections.

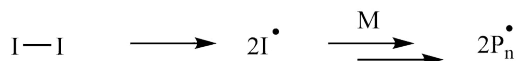
1.3.1. Reversible Addition-Fragmentation Chain Transfer Polymerization (RAFT)

Reversible addition fragmentation chain transfer (RAFT) polymerization is one of the most versatile RDRP methods for imparting living characteristics to FRP.^[3,53,54] The main advantages of RAFT polymerization are the suitability for most monomers including (meth)acrylates, tolerance of unprotected functionalities, the possibility of polymerization in aqueous or protic media and the cost effectiveness compared to other competitive techniques. Almost 20 years ago – in 1998 – a group of Australian researchers from the Commonwealth Scientific and Industrial Research Organisation (CSIRO) reported the successful control of radical polymerization by employing dithioesters as chain transfer agents.^[4] While the Australian group termed their findings reversible addition fragmentation chain transfer (RAFT) polymerization, a group of French researchers independently reported the MADIX (macromolecular design by interchange of xanthanes) technique based on the same mechanism.^[55,56] The underlying mechanism is

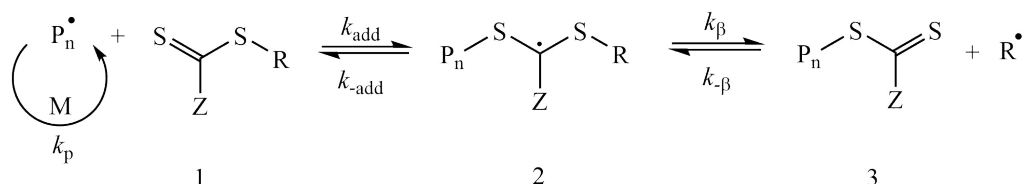
1. Introduction

based on degenerative chain transfer events and the accepted mechanism is composed of a sequence of addition-fragmentation equilibria as shown in Figure 1.5

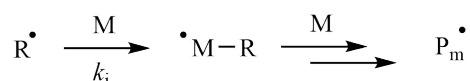
Initiation



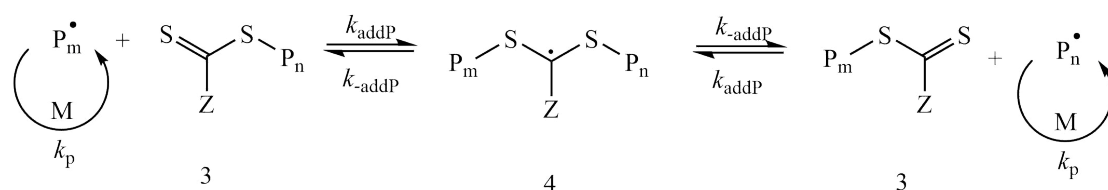
Reversible Chain Transfer (Pre-equilibrium)



Reinitiation



Chain Equilibrium



Termination



Figure 1.5.: Mechanism of RAFT polymerization. Adapted from Ref [3] with permission of CSIRO Publishing.

The initiation, propagation, and termination steps follow the same basic mechanism as in conventional FRP reactions. However, during the early stages of the polymerization the propagating radicals add to the dithioester compound and fragmentation of the intermediate radical (2) into a macroRAFT agent (3) and a new radical occurs. The newly formed radical is able to start polymeric chain growth via re-initiation. After several propagation steps, the growing polymer chain P_m^{\bullet} forms another intermediate radical species (4) with the macroRAFT agent (3) and a rapid exchange of the polymeric radical via the chain equilibrium releases another polymeric chain (P_n^{\bullet}) which starts further propagation. In contrast to conventional FRP, the rapid equilibrium between dormant species and propagating chains results in an equal probability to grow for all chains leading to low dispersities.

An advantage of the RAFT mechanism compared to other RDRP methods like NMP or ATRP is that the overall radical concentration is not reduced during the polymerization process, theoretically suppressing the retardation. Nevertheless, in practise retardation and hybrid effects (initial increase to high molecular weights and elevated dispersities) are often observed ^[1] due to cross-termination or slow fragmentation of the intermediate radicals (2 and 4) ^[41,57,58], or the occurrence of the less favoured addition of the propagating radicals to the initial dithioester species (1), respectively. To efficiently control the polymerization reaction, the choice of suitable RAFT agents for a specific monomer is crucial. ^[54] A detailed guide for the choice of appropriate RAFT agents was provided by Moad, Rizzardo, and Thang in 2005. ^[3] To function as an efficient RAFT agent, the dithioester must contain a R-group that can be effectively expelled from the initial RAFT agent (1) – therefore it must be sufficiently stable – while also being able to re-initiate the polymerization of the monomer ($k_i > k_p$). The initial RAFT agent (1), as well as the polymeric RAFT agent (3), should display a high k_{add} . The Z-group influences the exchange of the propagating chains by stabilizing the intermediate radicals (2 and 4) that should be able to rapidly fragment (high k_{β}) without leading to side reactions. The intermediate radical (2) should partition in favor of the products ($k_{\beta} > k_{-app}$). Figure 1.6 depicts a summary of appropriate RAFT agents for different types of monomers.

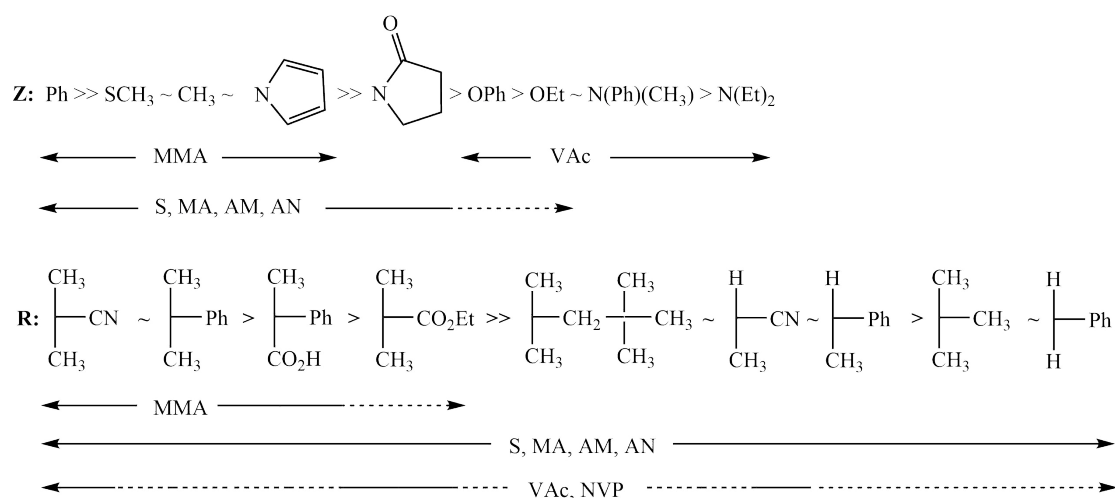


Figure 1.6.: Overview of appropriate Z- and R-groups for the selection of suitable RAFT agents. Z-groups: Decrease of addition rates/Increase of fragmentation rates from left to right. R-groups: Decrease of fragmentation rates from left to right. Dashed lines indicate partial control (i.e. control of molecular weight but poor polydispersity or substantial retardation in the case of VAc). Adapted from Ref [3] with permission of CSIRO Publishing.

For the polymerization of more activated monomers such as methacrylates, aromatic dithioesters are among the most efficient RAFT agents. However, the aromatic substituents render them more sensitive towards hydrolysis and may lead to retarda-

tion when used in high concentrations.^[59,60] For the polymerization of methacrylates the choice of the R-group is crucial and some of the most effective RAFT agents display a tertiary cyanoalkyl group. The first successfully employed RAFT agents for the polymerization of methacrylates include cumyl dithiobenzoate and tertiary cyanoalkyldithiobenzoates.^[61] Dithiocarbonates as well as dithiocarbamates and trithiocarbonates can undergo aminolysis in the same way as carbonates or carbamates when employed for the polymerization of amine containing monomers leading to the destruction of the RAFT agent. Tolerated monomer functionalities, however, include tertiary amino methacrylates such as 2-(*N,N*-dimethylamino)ethyl methacrylate (DMAEMA)^[62–65] and comparable nitrogen containing methacrylates as employed in the current study.

1.3.2. Radical Polymerization with Chain Transfer Agent

Chain transfer reactions can be unavoidable side reactions with several types of reaction components during radical polymerization or can be deliberately introduced by the use of a CTA. A chain transfer is considered a polymerization reaction which transfers the radical of a growing chain to another molecule. Transfer reactions can be:^[30,66]

- **Transfer to monomer:** Growing polymer chains are able to abstract an atom from unreacted monomer, transferring the active site from the chain to the monomer. Transfer to monomer determines the theoretical maximum molecular weight achievable by a given monomer. In radical polymerization, transfer to monomer is less important, however, is included here for the sake of completeness.
- **Transfer to polymer:** A growing polymer chain transfers the active site to an already existing polymer chain. Transfer to polymer often occurs towards the end of radical polymerizations at high conversions when the majority of the monomer is consumed and a high concentration of polymer chains is present, leading to chain branching as the new radical site is located along the polymer backbone.
- **Transfer to solvent:** When polymerization reactions are performed in solution, a non-inert solvent can react as a CTA resulting in low molecular weight polymers.
- **Transfer to chain transfer agent:** CTAs display at least one weak chemical bond which enables the transfer reaction. Thiols, disulfides, or halomethanes, as well as other molecules with easily abstractable H-atoms are commonly used CTAs and are sometimes called *modifiers* or *regulators*.^[67] Chain transfer processes

mediated by a CTA occur according to the mechanism shown in Figure 1.7. A propagating polymer chain carrying a radical site (P_n^\bullet) reacts with the CTA (represented by R-X). The previously propagating chain is terminated and forms a polymer P_n -X while the radical site is transferred to the CTA, forming a new radical R^\bullet which is able to react with monomer molecules to form new propagating chains.

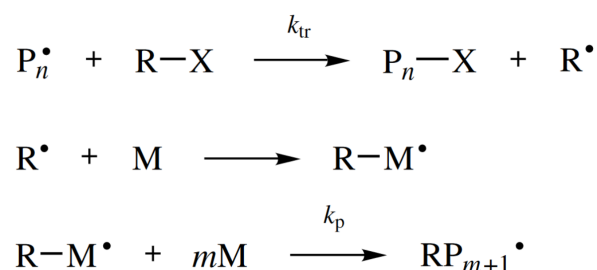


Figure 1.7.: General mechanism of a chain transfer mediated by a chain transfer agent. In the case of the current study, X refers to a hydrogen atom and R to the thiyl rest. Adapted from Ref [68] with permission from John Wiley and Sons.

The first time chain transfer was proposed in 1930 by Taylor and Jones, investigating the thermal decomposition of methyl alkyls in hydrogen-ethylene mixtures.^[69] Certain observed side reactions and product mixtures suggested the involvement of ethyl radicals and could best be described by postulating a transfer of the radical site to other reactants. The US Rubber Reserve Company was the first institution to make industrial use of CTAs during World War II. The addition of a mercaptan modifier to their rubber recipe significantly changed the properties of the product and replaced the need for additional production steps to soften the initially hard rubber. This effect was found to be due to a decrease in molecular weight of the polymer chains and concomitantly an increase of the polymerization rate was reported.^[70] In 1937, Flory already incorporated the concept of transfer to CTAs in his mathematical considerations to explain the observation of reduced average chain lengths compared to chain length predicted by rate considerations alone.^[71] The general understanding of CTAs was progressed during the 1940's and 50's and Mayo *et al.* delivered the basis for rate determination of chain transfer reactions.^[72-74] Employing the Mayo-Equation 1.2,^[73] it is possible to calculate the average degree of polymerization when using defined amounts of monomer and transfer agent.

$$\frac{1}{DP_n} = C \cdot \frac{[Trans]}{[M]} + \frac{1}{DP_0} \quad (1.2)$$

With DP_n being the degree of polymerization with addition of a CTA, DP_0 the degree of polymerization without the addition of a CTA, $[Trans]$ the concentration of transfer agent, $[M]$ the monomer concentration, and C the chain transfer constant defined as k_{tr}/k_p .

Chain transfer can be employed to regulate the molecular weight and to some extent to introduce chain end functionalities as well. End functionalized polymers with low molecular weight found applications in automotive coatings for low-volatile-organic content (VOC) formulations.^[75] In FRP, thiols are the most commonly used CTAs and a number of functional thiols as for example mercaptoethanol or methyl thioglycoate were employed for the preparation of end-functionalized copolymers^[76-78] for application as emulsifiers, thermoplastic elastomers, or adhesives.^[79] The chain transfer constant of thiols is dependent on the reaction conditions and type of monomer. Due to the electrophilic nature of the thiyl radical produced during the transfer step, thiols react with an increased rate with nucleophilic radicals than electrophilic ones, leading to a higher C_{tr} with styrene or vinyl esters than with (meth)acrylates for example.^[68] The molecular weight is inversely proportional to the concentration of the CTA, therefore targeting certain molecular weights is possible and the same reaction procedures (temperature, reaction time) can be used to produce polymeric samples covering a wide range of molecular weights by varying the concentration of the added CTA.

In the current study, polymerization with a thiol as transfer agent was employed to prepare polymeric samples for the determination of MHKS parameters since in contrast to RAFT polymerizations it bears the advantage of yielding high molecular weights in short reaction times of just up to one hour while still giving dispersities suitable for the intended purposes.

1.4. Pulsed-Laser Polymerization - Size Exclusion Chromatography (PLP-SEC)

Though for many years the determination of precise monomer specific propagation rate coefficients is targeted in polymer chemistry with several experimental methods,^[28,80] most attempts to gain knowledge of those highly important kinetic data had several disadvantages and up until the 1990's many varying – and often not reproducible – data were reported from different laboratories.^[80] The deduced k_p values were commonly beset with inconsistent error rates varying up to and above 50% depending on the applied method and often showed wide disparities, were contradictory to each other, or not reproducible at all. Many inconsistencies between the different literature known data –

apart from the fact that many studies were conducted under widely different reaction conditions – could be attributed to the experimental difficulties with a commonly used method to determine the propagation rate coefficients, namely the rotating sector method. For the original rotating sector experiment employed by Nagy *et al.* in 1983,^[81] a nonlaser light source was utilized. To achieve a pulsed illumination, a rotating disk was placed between the sample and the light source, featuring cut out portions to mimic the light and dark periods. The periods of illumination could be varied by rotating the disk at different frequencies and varying the dark-to-light ratio r of cut out and non-cut out sectors. The main objective of the rotating sector method is the determination of the parameter τ_s , defining the “average lifetime of a growing radical“ under steady-state polymerization according to Equation 1.3 with $[M]$ being the monomer concentration and $(R_p)_s$ the rate of polymerization under steady-state conditions.^[28]

$$\tau_s = \frac{k_p[M]}{2k_t(R_p)_s} \quad (1.3)$$

Apart from the broad pulses generated via the rotating disc compared to the sharp pulses produced with a pulsed laser, the main drawback of the rotating sector method was the determination of k_p only in conjunction with the termination rate as $k_p/k_t^{1/2}$. Although the original rotating sector method has been further enhanced, one of the advantages of the PLP-SEC method is the ability to determine individual propagation rate coefficients without being coupled to k_t . The PLP-SEC method is a combination of an experimental (PLP) and analytical (SEC) technique vital to the effective characterization of FRP and was reported in 1977 by Aleksandrov *et al.*^[82] and further developed by Olaj and coworkers in the following years.^[83–85] The technique was declared the method of choice by the IUPAC for the determination of propagation rate coefficients. In 1995 the IUPAC working party on *Modeling of Kinetics and Processes in Polymerization* was called into presence and started benchmarking propagation rate coefficients for several monomers.^[9,86–92] To date a broad database of propagation rate coefficients determined via the PLP-SEC method is available and the technique is well established and understood.^[82,93,94] An overview of important monomer systems investigated via PLP-SEC in the last three decades is given by Beuermann and Buback^[93] as well as the author of the present thesis.^[95] A more detailed description of particular monomer classes will, however, be given in the subsequent chapters when they are compared to monomers investigated in the course of this thesis.

The PLP method is based on the generation of photoinitiator radicals in defined time intervals (controlled via the frequency of the laser pulses). Typical photoinitiators^[92]

1. Introduction

are depicted in Figure 1.8 alongside all initiators employed in the current study with 2,2-dimethoxy-2-phenylacetophenone (DMPA) being the most important one.

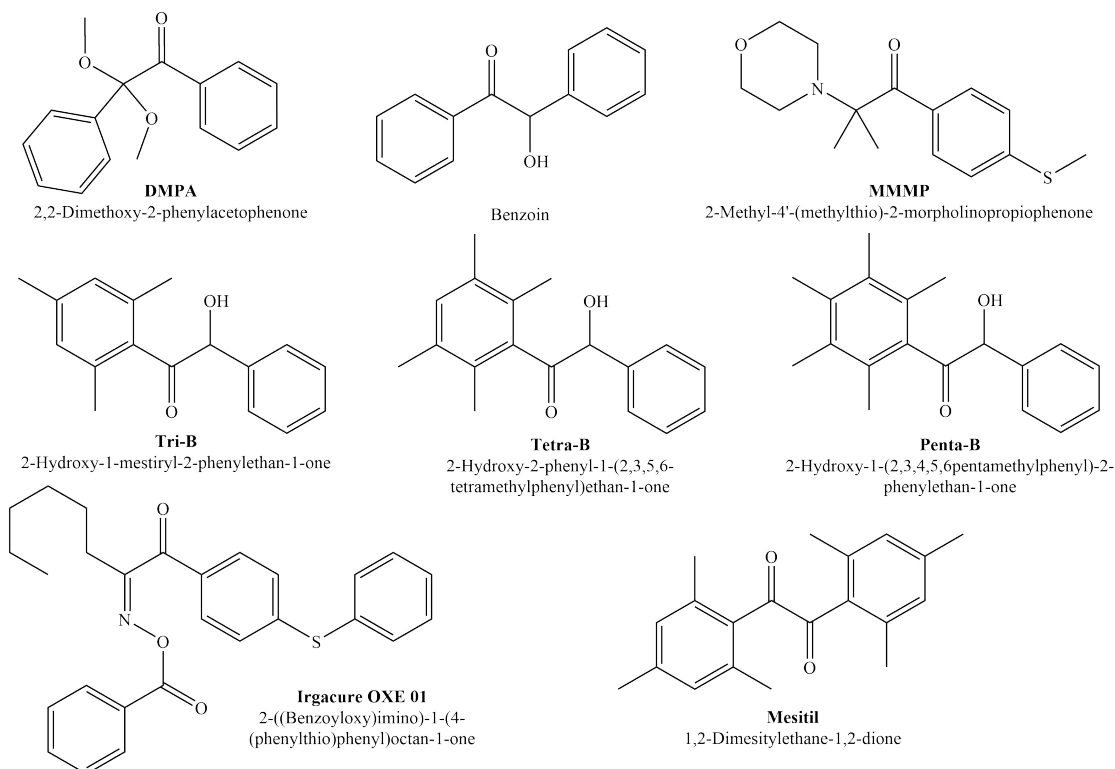


Figure 1.8.: Structures of typical photoinitiators such as DMPA, benzoin, and MMMP, alongside all additional photoinitiators employed in the current study: Tri-B, Tetra-B, Penta-B, Mesityl, and Irgacure OXE 01

The first laser pulse generates initiator radicals and the propagation reaction takes place. The second (as well as each consecutive) laser pulse generates new initiator radicals which start new propagating chains and lead to the termination of the majority of already growing polymer chains. However, not all polymer chains will be terminated after the second pulse. A minority of chains will continue propagation for more than one dark time (the time between two consecutive laser pulses, see Figure 1.9). The molecular weight of the terminated chains, M_i , is dependant on the propagation rate coefficient, k_p , and is proportional to the number of dark times the propagating chain survived. Chains propagating for two or three dark times will exhibit molecular weights twice or three times as high as for the chains terminated after one dark time, respectively. The accumulation of polymer chains surviving one, two, three,... dark times leads to a multimodal SEC distribution with one, two, three,... local maxima in their first derivative (see Figure 1.10). In the current study, polymer chains surviving up to seven

dark times could be observed and exemplary PLP distributions of the herein investigated monomers are depicted in the Appendix A.

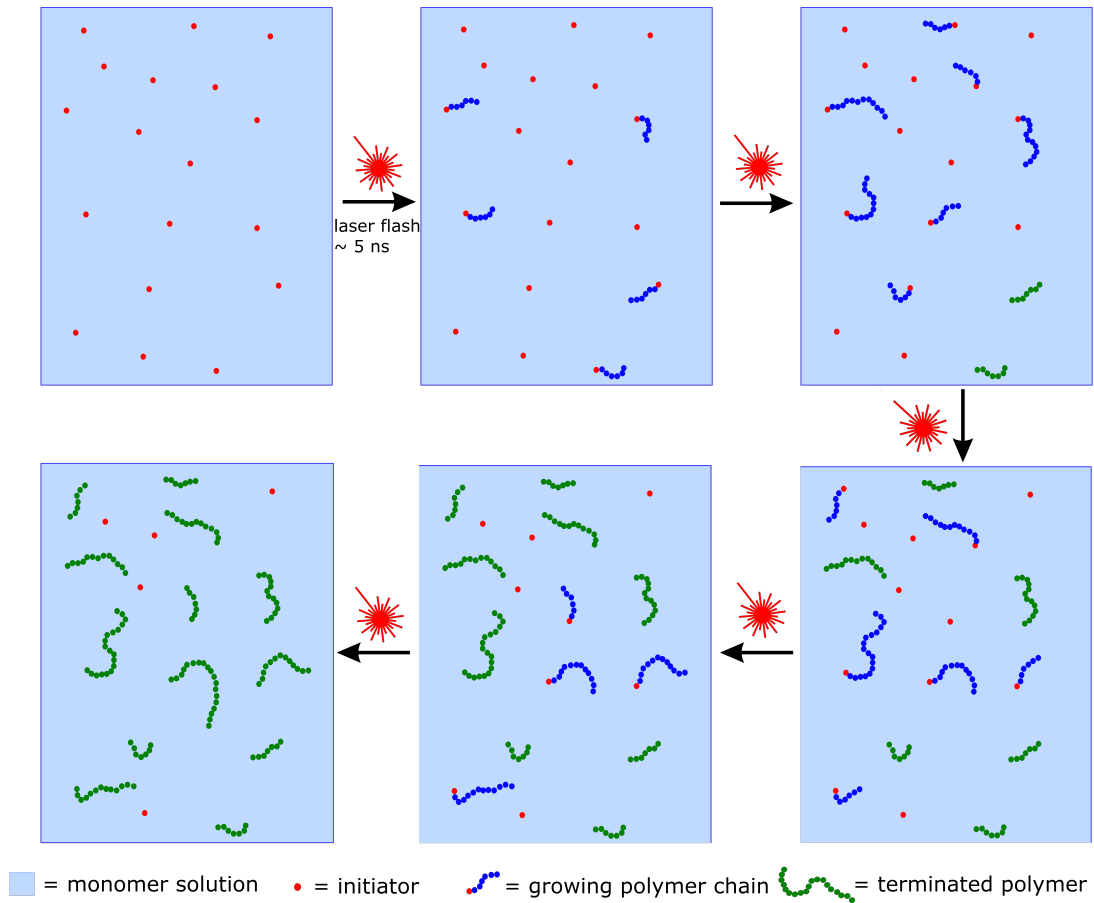


Figure 1.9.: Example of chain growth during PLP. Consecutive laser pulses will start the propagation of new chains as well as end the propagation of previously growing chains.

The molecular weights of the maxima in the first derivatives of the PLP distribution can be employed to determine the propagation rate coefficients according to Equation 1.4.

$$L_i = \frac{M_i}{M_M} = i \cdot k_p \cdot c_M \cdot t_0 \quad (1.4)$$

where L_i is the degree of polymerization, M_i the molecular weight of the respective inflection point, M_M the molecular weight of the monomer, i the number of the inflection point, c_M the monomer concentration, and t_0 , the dark time. According to the stationary state, the monomer concentration is assumed to be constant during the experiment and equals the initial monomer concentration of the sample, which is calculated via the temperature dependent density function (Equation 1.5)

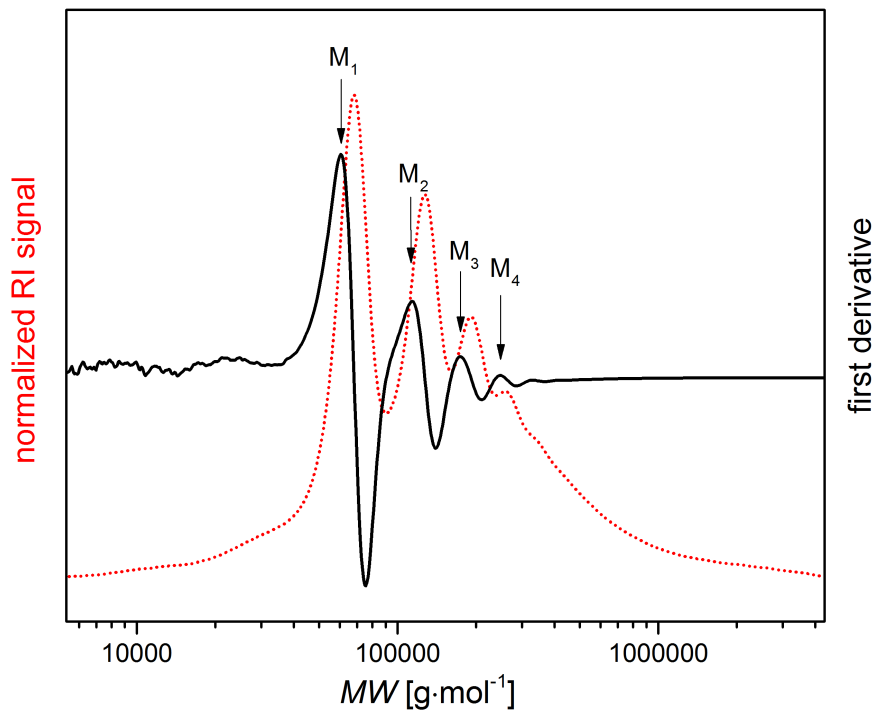


Figure 1.10.: Typical PLP generated molecular weight distribution with its first derivative. M_i describes the molecular weight of a polymer chain surviving for i dark times.

$$\rho = \rho_0 - b \cdot T \quad (1.5)$$

where ρ_0 is the density at 0 °C and b is the slope density function determined over an extended range of temperatures T . Temperature dependent density functions for all monomers investigated in the current study are given in the Appendix A. A theoretical study concerning factors influencing the accuracy of the determined propagation rate coefficients noted that the most robust access to precise molecular weights for the calculation of k_p is given by employing the logarithmic molecular weight distribution.^[96] Based on the modeling of PLP-SEC experiments, the study showed, when plotting the molecular weight on a logarithmic scale, the position of the inflection points and, thus, the propagation rate coefficients, are less influenced by experimental SEC broadening.^[96] In a theoretical study from 1995, Sarnecki *et al.* reported the so-called low and high termination rate limits, that described if the propagation rate coefficient is best determined via the inflection point or the maximum of the MWD depending

on the “radical concentration of chain length zero generated per laser pulse“, c_R^0 .^[97] At low concentrations of laser induced radicals and thus at low termination rates, the radical concentration half-value life is of the order of the pulse period. In this case, the inflection point of the MWD gives the most reliable results for k_p . At high termination rates, due to high start concentrations of radicals, the radical concentration half-value life is much shorter than the pulse period, leading to the best results for k_p when employing the maximum of the MWD. Although it is not easy to assess if the high termination limit is operative, it is rather difficult to achieve such high initial radical concentrations experimentally,^[98] thus employing the inflection points of the MWD for the determination of the propagation rate coefficients is generally preferred for PLP-SEC experiments.

The observation of different chain lengths with $M_1 = \frac{1}{2} M_2 = \frac{1}{3} M_3$ etc. is one of the consistency criteria of the PLP-SEC method. Other consistency criteria and requirements for successful PLP experiments are:

- at least two visible inflection points
- k_p invariant to variation of the frequency (reaction governed by PLP, solely secondary propagating radicals)
- $k_{p,1}/k_{p,2}$ near unity
- k_p invariant to variation of pulse number, photoinitiator concentration, or laser pulse energy (and therefore invariant to the amount of produced radicals per pulse)

An assumption made in Equation 1.4 is that c_M equals the initial monomer concentration. For this assumptions to be valid and to obtain reliable propagation rate coefficients, it is mandatory to stop the polymerization reaction at low conversions to stay in the range of ideal kinetics. Detailed descriptions of the criteria and requirements for PLP-SEC experiments are given in the benchmarking publications of the working party *Modeling of Kinetics and Processes in Polymerization*.^[89,90,92] It is furthermore assumed that all macroradicals are equally reactive towards propagation. This consideration is especially important regarding the propagation reaction of acrylate systems where the formation of MCRs plays an important role as noted previously. The frequency of transfer reactions is sufficient to lead to a considerable amount of MCRs, occurring via the backbiting reaction.^[99] The formation of tertiary radicals due to backbiting results in an apparent propagation rate coefficients, k_p^{app} , consisting of secondary and tertiary propagating radicals, $k_{p,sec}$ and $k_{p,tert}$, leading to errors in the determined k_p

and a blurring of the PLP distribution. As depicted in Figure 1.11, for acrylate systems a frequency dependency of the propagation rate coefficient can be detected, leading to an S-shaped curve when plotting k_p^{app} vs. frequency. To obtain reliable propagation rate coefficients, the plateau of the S-shaped curve has to be reached, where k_p is no longer dependent on the applied laser frequency. Thus, to eliminate errors in k_p arising from the concurrent detection of tertiary and secondary propagating radicals and to avoid a blurring of the PLP traces, it is necessary to ensure that the time between consecutive laser pulses is shorter than the average time needed to undergo transfer to polymer reactions, therefore, the highest available laser frequencies have to be employed.

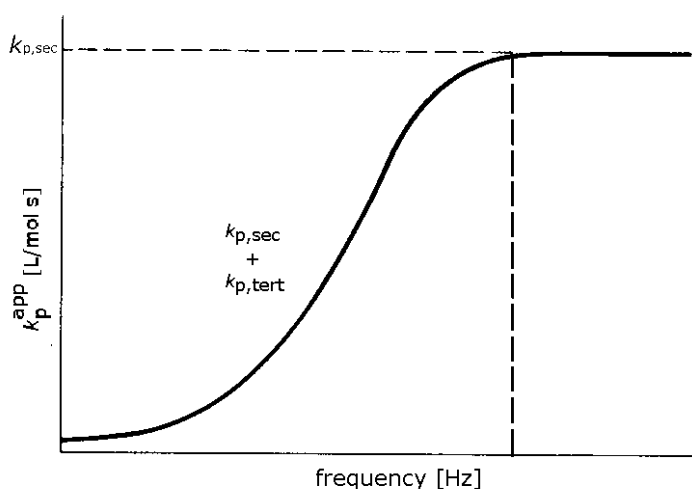


Figure 1.11.: S-shaped curve showing the frequency dependency of acrylate systems at low pulse repetition rates. To obtain reliable secondary propagation rate coefficients, the frequencies have to be sufficiently high to reach the plateau of the curve.

Determination of the propagation rate coefficient via the PLP-SEC method is possible for homo- as well as copolymerizations. However, when studying the propagation rate coefficients for copolymers, SEC calibration for each copolymer composition is required.^[93] For some exceptions, as for example found for the copolymerization of styrene and MMA, SEC calibration can be achieved employing Mark-Houwink-Kuhn-Sakurada parameters determined by linear interpolation between the parameters of the corresponding homopolymers.^[100] Theoretical studies aimed at the description of $k_{p,\text{copo}}$ employing different models. The terminal model (TM), where the propagation reactivity is assumed to be determined by the terminal unit at the propagating radical site was shown to work for copolymerization reactions,^[101] however, Fukuda *et al.* found the penultimate model to be more accurate, where the terminal as well as penultimate unit at the propagating radical site influence the reactivity.^[102] A more detailed description of the different models for the determination of propagation rate coefficient

during copolymerization processes is available in the literature.^[103–105] Starting in the 1980's, a variety of copolymer systems was investigated employing the PLP-SEC method such as methyl methacrylate with perdeuterated methyl methacrylate,^[106] substituted styrenes,^[107–109] styrene with different methacrylates,^[110–114] and various other monomer combinations.^[115,116] Extensive PLP-SEC studies of the copolymerization of acrylates with methacrylates has been published^[105,117,118] and a summary of the systems investigated via PLP-SEC until the early 2000's is given by Beuermann *et al.*^[93] Apart from binary copolymerization, ternary systems have been studied by PLP-SEC as well, for example a styrene–methyl methacrylate–methyl acrylate system^[119] and *p*-methoxystyrene–styrene–methyl methacrylate.^[120]

Besides PLP coupled with SEC, the determination of k_p is possible employing the matrix assisted laser desorption and ionisation time of flight (MALDI-ToF) mass spectrometry. Band broadening of the SEC traces and the need for calibration are often mentioned drawbacks of the PLP-SEC method, while MALDI-ToF is an absolute method for the determination of molecular weights and can furthermore be employed to analyze branched polymers.^[121] However, broad polymers can lead to mass discrimination effects that can result in errors of the determined rate coefficients.^[122–125] PLP coupled with MALDI has, for example, been employed to investigate the influence of primary radical concentrations on the propagation rate coefficient and to determine the k_p for a series of linear alkyl acrylates,^[121] fast acrylates containing heteroatoms (tetrahydrofurfuryl acrylate, THFA, and (R)- α -acryloyloxy- β,β -dimethyl- γ -butyrolactone, ADBL),^[126] and a copolymerization of styrene and MMA.^[122] Furthermore, PLP-based models are employed to determine other important intrinsic rate coefficients in addition to k_p , such as the backbiting rate, k_{bb} , for acrylate systems.^[11,127–129]

To date, the PLP method was not only employed to determine the propagation rates of a wide variety of monomer systems, but also overarching trends and family type behaviors among defined monomer groups are reported. For a series of linear (meth)acrylates, a steady increase of the propagation rate coefficient with increased ester side chain length was reported.^[121,130] For methacrylates with branched^[131] and cyclic^[88] ester side chains a family type behavior was described, leading to joint Arrhenius parameters for the investigated monomers, collated in Table 1.1.^a

In the current study, a series of branched acrylates in solution as well as methacrylates with nitrogen-containing ester side chains are investigated with regards to trends

^a In a previous publication, ΔE_A is given with 2 kJ·mol⁻¹ for the linear methacrylates and 3 kJ·mol⁻¹ for branched methacrylates^[130] However, inspection of the activation energies shows that ΔE_A for the linear methacrylates is ~3 kJ·mol⁻¹ (20.52 - 23.38 kJ·mol⁻¹) and less than 2 kJ·mol⁻¹ for the branched methacrylates (20.72 - 22.11 kJ·mol⁻¹).

and family type behavior among their propagation rate coefficients and Arrhenius parameters to broaden the understanding of the underlying kinetics of free radical polymerizations of (meth)acrylates. A detailed description of the to date detected trends will be given in Chapter 2 and 3.

Table 1.1.: Summary of the monomer families with trends and family type behaviors, Arrhenius parameters of joint Arrhenius fits, increase of propagation rate coefficients at 50 °C, and variations of activation energy within the monomer group. Adapted with permission from ref [132].

monomers	trend or family type behavior	joint Arrhenius plot A [L·mol ⁻¹ ·s ⁻¹]	EA [kJ·mol ⁻¹]	increase of k_p ^{50°C} per add. CH ₂ group compared to MA / MMA	ΔEA within family
Linear methacrylates [89,131]	bulk linear increase in k_p with increasing ester side chain	n/a	n/a	~30 L·mol ⁻¹ ·s ⁻¹ (3 - 4 %)	~3 kJ·mol ⁻¹
Branched methacrylates [130,131]	bulk almost identical $k_{p,s}$ irrespective of chemical nature of ester side chain	2.23·10 ⁶	20.96	n/a	~2 kJ·mol ⁻¹
Methacrylates with cyclic ester side chain [88]	bulk almost identical $k_{p,s}$ irrespective of chemical nature of ester side chain	5.0·10 ⁶	22.3	n/a	~3 kJ·mol ⁻¹
Linear acrylates [130,131,133]	bulk linear increase in k_p with increasing ester side chain	n/a	n/a	~550 L·mol ⁻¹ ·s ⁻¹ (2 %)	~4 kJ·mol ⁻¹
Branched acrylates [131,132]	solution tendency of increasing k_p with increasing ester side chain	n/a	n/a	n/a	n/a
	bulk no trend / family type behavior observable	n/a	n/a	n/a	~4 kJ·mol ⁻¹
	solution no trend / family type behavior observable	n/a	n/a	n/a	~3 kJ·mol ⁻¹
N-ethyl methacrylates [134,135]	bulk almost identical $k_{p,s}$ irrespective of chemical nature of ester side chain	1.55·10 ⁶	19.69	n/a	~1 kJ·mol ⁻¹

1.4.1. SEC-Analysis and Determination of Absolute Molecular Weights

For the determination of the propagation rate coefficients, polymeric samples generated by pulsed-laser polymerization are analyzed via SEC measurements to obtain the typical PLP patterned elugrams. The molecular weight at the inflection points is employed to calculate the propagation rate coefficients k_p for each specific monomer, therefore, the use of accurate molecular weights is mandatory to determine reliable monomer specific data. During the SEC measurement, the polymeric molecules are separated via their hydrodynamic volume, thus, molecules displaying the same hydrodynamic volume elute at the same time. Already many years ago, it was established that the main limitation to the determination of precise propagation rate coefficients via PLP is an accurate calibration of the SEC.^[136] To convert the retention time into accurate molecular weight, calibration is needed and is often achieved by measurement of several standards with low dispersities and known molecular weights. However, for unknown or not yet fully investigated polymers such standards are generally not available. For the determination of the molecular weights via SEC analysis, two methods can be employed: direct measurement or universal calibration.^[137] For direct measurement a triple-detection setup with a concentration sensitive detector (RI or UV), light scattering (e.g. MALLS or LALLS), and viscometry detector is the most common setup.^[138–140] In the case of the current study, for the measurement of the PLP generated samples applying the universal calibration is favored over the direct measurement via a triple-detection SEC setup since multi-detector setups are often limited to high molecular weights. To achieve reliable statements on the absolute molecular weight with MALLS detection, MW above approximately $50\,000\text{ g}\cdot\text{mol}^{-1}$ are necessary for reliable signals especially for macromolecular species with poor light scattering properties and in the low molecular weight range, high sample concentrations need to be employed in order to produce detectable signals.^[141] Ideally, during PLP experiments the laser settings are tuned to give first inflection points between $10\,000$ and $20\,000\text{ g}\cdot\text{mol}^{-1}$ leading to high uncertainties or a loss of detector signal when directly analyzed via MALLS detection. Changing the experimental settings in a way to obtain polymeric chains with first inflection points above $50\,000\text{ g}\cdot\text{mol}^{-1}$ increases the risk of a loss of the PLP structure in the MWD and especially in the case of acrylic monomers gives rise to side reactions such as backbiting. Another reason for an increased uncertainty of the molecular weights derived from the MALLS detector signal is the accurate sample concentration that needs to be employed for measurements with a triple-detection setup. Furthermore, inappropriate signal alignment of the different detectors can lead to significant deviations in the calculated molecular weight distribution.^[142–146] To measure MWDs of

unknown polymers without employing mass sensitive detectors, universal calibration can be employed. Universal calibration was initially introduced in 1967 by Grubisic *et al.* [147] and is mostly based on the application of Mark-Houwink-Kuhn-Sakurada (MHKS) parameters. Employing universal calibration with polymer specific MHKS parameters, the accuracy of the molecular weight and, therefore, the propagation rate coefficients is strongly dependent on the employed sets of parameters. [148] In the case of the current study, for the determination of MHKS parameters, narrowly distributed polymer samples are analyzed via a triple detection SEC setup comprised of a refractive index (RI), light scattering (MALLS), and viscometry (visco) detector to gain the absolute weight averaged molecular weight M_w and the intrinsic viscosity $[\eta]$. [149] Light scattering ranks among the few absolute methods to determine the molecular weight as well as shape and conformation of polymeric samples. [141] During analysis with a MALLS detector, the collimated, polarized light beam of a laser is directed at the sample cell containing a solution of the macromolecules of interest and the scattered light is detected by multiple detectors situated at specific angular locations (see Figure 1.12). The intensity of the light scattered from the macromolecules depends on the dipoles induced by the oscillating electric field of the light and, thus, on the polarizability of the macromolecules and the concentration in solution and is directly proportional to the molar mass of the molecules. The angular dependence within the horizontal plane, however, gives information about the size of the measured macromolecule. To determine the molecular weight of a broadly distributed polymer sample, separation via SEC and subsequent analysis via MALLS leads to light scattering data at each elution volume which can be employed to determine the molar mass of the sample.

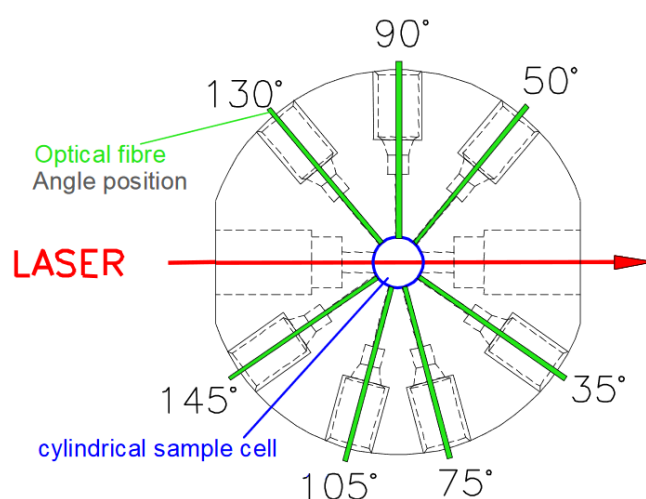


Figure 1.12.: Schematic setup of a multi angle laser light scattering (MALLS) detector on the example of the SLD 7000 detector from PPS Mainz as employed in the current thesis. [150].

The MHKS parameters K and α can be determined according to the well established Mark-Houwink-Kuhn-Sakurada Equation 1.6. [151]

$$[\eta] = K \cdot M^\alpha \quad (1.6)$$

To obtain reliable results, the determination of $[\eta]$ and M_w for several polymer samples spanning a wide molecular weight range is conducted in the current thesis. When plotted on a log scale, the slope of the $[\eta]$ vs. M_w plot corresponds to the exponent α while the y-intercept corresponds to the prefactor K (cf. Figures in Chapter 3.1). A wide variety of MHKS parameters for polymers synthesized under various reaction conditions and analyzed in different solvents can already be found in the literature. [80] Since the microstructure of the polymeric samples can have a significant impact on the MHKS parameters, for acrylic monomers prone to chain branching reactions under FRP conditions the use of MHKS parameters obtained from samples generated via PLP is advisable for the determination of reliable propagation rate coefficients. For the investigated acrylates, MHKS parameters prepared under suitable conditions can be found in the literature.^b [10, 130, 131, 152] For the methacrylic systems employed in the current thesis no MHKS parameters were available and were thus determined in the course of the study. Polymer samples with dispersities below 2.0 were generated via RAFT polymerization or polymerization with a transfer agent and subsequently analyzed via a triple detection SEC setup with MALLS, RI, and visco detector. To obtain reliable MHKS parameters, a wide molecular weight range was covered. At a given retention time the hydrodynamic volume of two polymers are assumed to be identical, thus giving the possibility to re-calculate the molecular weight of the PLP generated samples measured via universal calibration against narrowly distributed poly(styrene) and poly(methyl methacrylate) standards employing the polymer specific MHKS parameters according to Equation 1.7. [153, 154] For the acrylic monomers employed in the current study the SEC elugrams were recorded using the polymer specific MHKS parameters. For the methacrylates, p(MMA) MHKS are used for the SEC analysis and the obtained molecular weights are afterwards re-calculated employing the polymer specific parameters.

^b For poly(benzyl acrylate) no MHKS parameters were available in the literature. However, all attempts to produce narrowly distributed samples with a suitable microstructure – e.g. fractionation of broadly distributed PLP samples – were not successful. For the determination of propagation rate coefficients for benzyl acrylate, MHKS parameters of p(^tBA) have been employed therefore the obtained k_p and Arrhenius parameters have to be treated with caution.

$$K_1 \cdot M_1^{1+\alpha_1} = K_2 \cdot M_2^{1+\alpha_2} \quad (1.7)$$

The MHKS equation is known to properly describe the $[\eta]$ vs. M_w relation in a molecular weight range above 10 000 g·mol⁻¹. However, since the intrinsic viscosity no longer follows a simple power – law relation at lower molecular weights, significant deviations can be detected.^[155]

The MHKS parameters employed for the determination of the absolute molecular weights of the herein investigated monomers are collated in the respective chapters.

1.4.2. Arrhenius Relations and Determination of Arrhenius Parameters

In the current study the SEC elugrams of all PLP generated samples are computationally smoothed and the molecular weight at the inflection points, M_i , is determined via the local maxima of the first derivative. According to Equation 1.4, the molecular weights at the inflection points can be employed to calculate the propagation rate coefficient k_p . Propagation rates calculated in this manner follow the Arrhenius Equation 1.8.

$$k_p = A \cdot e^{\frac{-E_A}{RT}} \quad (1.8)$$

The Arrhenius equation is a relation to describe the relationship between temperature and rate coefficient and was named after Svante Arrhenius, who first proposed the equation in 1889.^[156] The equation is of high importance for the calculation of activation energies and can best be seen as an empirical relationship^[157] related to the Eyring equation used in transitional state theory.^[158] When the propagation rate coefficients are recorded over an expanded temperature range, they can be presented in the form of an Arrhenius plot, showcasing $\ln(k_p)$ vs. T^{-1} , giving a linear fit as depicted in Figure 1.13.

According to Equation 1.9 the linear fit can be employed to calculate the Arrhenius parameters with the slope representing the activation energy, E_A , and the y-intercept corresponding to the frequency factor (or pre-factor) A.

$$\ln(k) = \ln(A) - \frac{E_A}{RT} \quad (1.9)$$

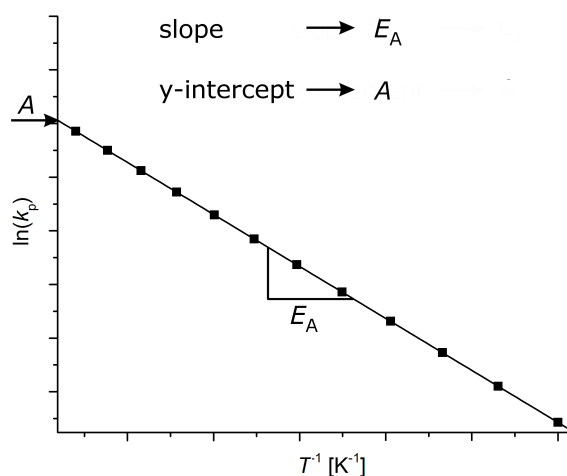


Figure 1.13.: Typical $\ln(k_p)$ vs. T^{-1} plot with linear fit. The activation energy, E_A can be calculated employing the slope of the fit while the frequency factor, A , corresponds to the y-intercept.

Although equation 1.9 has some inherent errors due to an actual temperature dependence of the prefactor ^[66] – leading to a slight increase of A with increasing temperature – the weak temperature dependence is negligible compared to the temperature dependence of the exponential factor. It is also reasonable to assume an independency of the activation energy on the temperature considering the relatively small temperature range kinetic studies are generally undertaken in.

As described in chapter 1.4 on page 17, several consistency criteria need to be fulfilled for the determination of reliable propagation rate coefficients and Arrhenius parameters. Therefore in the current thesis, all samples incorporated in the calculation of k_p and thus the determination of Arrhenius parameters have been checked for consistency:

- To ascertain a PLP governed polymerization with solely secondary propagating radicals, different frequencies have been applied at the same temperature and pulse number. Only samples where the molecular weight of the inflection points was inversely proportional to the frequency (thus, no change in k_p was observed with varying frequency) were incorporated into the final Arrhenius plots. In the current thesis, for the methacrylates frequencies between 4 and 120 Hz have been applied. For the acrylates, 50 to 500 Hz were employed since especially for elevated temperatures the acrylate typical transfer reactions become increasingly important. The formation of mid chain radicals substantially influences the propagation rate, since those more stable tertiary radicals propagate significantly slower

than the secondary radicals.^[8] To avoid the formation of MCRs and therefore a deceleration of the propagation reaction, the highest possible pulse repetition rates have to be employed to guarantee the determination of solely secondary propagating radicals. At higher temperatures, however, a pulse repetition rate of 500 Hz is not sufficient anymore to assure the suppression of tertiary radicals, leading to k_p values consisting of a mixture of secondary and tertiary propagation rates with generally high deviations of $k_{p,1}/k_{p,2}$ from unity. It should be avoided to incorporate such mixed propagation rates into the Arrhenius plots, therefore in the current study only values with a $k_{p,1}/k_{p,2}$ ratio close to 1 have been employed for the determination of Arrhenius parameters.

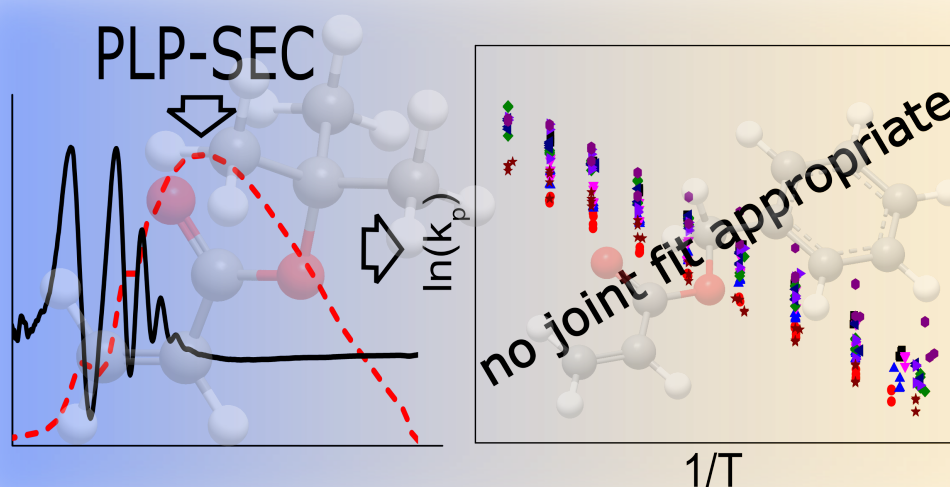
- At a given temperature and pulse repetition rate at least two different pulse numbers have been applied to exclude an influence of the degree of conversion on k_p . Only samples showing no significant change in propagation rate with changing pulse numbers have been included in the final plots. No significant change was assessed if the difference in k_p did not exceed the assumed SEC error of 10-15% occurring at multiple injections of the same sample. To obey the assumption of an infinitesimally low conversion and therefore assumed constant monomer concentration, c_M , it was strived to use a pulse number as low as possible while still obtaining a sufficiently high amount of polymer and a sufficiently good signal-to-noise ratio in the SEC analysis. For the investigated acrylates, pulse numbers between 800 and 1200 have been applied while for the methacrylates 300 to 1600 pulses gave best results and stayed within the boundaries of accepted deviations.
- To assure the independence of the propagation rate coefficient of pulse energy as well as photoinitiator concentration, the pulse energy was varied between 2 to 5 mJ (acrylates) and 1.5 to 2 mJ (methacrylates), respectively and the photoinitiator concentration ranged from 5 to 20 mmol·L⁻¹. Only samples that showed no significant deviation of k_p with varying pulse energy or photoinitiator concentration were included in the final Arrhenius plots.

Due to the half logarithmic scale of the Arrhenius plot experimental errors in k_p lead to increased errors at elevated temperatures (corresponding to higher k_p values) therefore significantly increasing the error in the frequency factor. To reliably calculate Arrhenius parameters, van Herk and co-workers proposed a mathematical procedure to determine A and E_A via a non-linear fit of the Arrhenius expression.^[94] Thus, the program CONTOUR V2.0.2^[159] was employed to specify the Arrhenius parameters, which

utilizes constant errors for each incorporated data point as estimated absolute error ranges. According to and in agreement with an extended set of PLP-SEC experiments the error ranges for acrylates were assumed to be approx. 15% while for methacrylates an error range of 10% was estimated. The resulting data are provided in the corresponding chapters in Tables 2.2 and 3.2 and are within the boundaries of the 95% joint confidence intervals represented by the error ranges stated in the respective tables. The reported Arrhenius parameters lie in the center of the symmetric 75, 90, and 95% joint confidence contours as depicted in the following chapters.

2

Branched Acrylates in Solution^a



In the current chapter, possible trends and family type behavior of the propagation rate coefficient as a function of the steric demand and ester side chain conformation of a series of branched acrylates in 1M solution in butyl acetate (BuAc) is investigated. Butyl acetate is a commonly employed solvent for acrylate polymerizations since it mimics the properties of butyl acrylate without interfering with the polymerization process as it does not feature the ability to polymerize. In addition, it features similar viscosity and polarity as a wide range of other alkyl acrylates. As described in Chapter 1.4.2, the investigation of acrylate monomers calls for high laser frequencies especially at elevated temperatures. Until the 2000's, the state-of-the-art of frequency accessible via high-energy pulsed lasers was limited to 100 Hz and therefore investigations of k_p were

^a Parts of this chapter are reproduced with permission from Kockler, K. B., Haehnel, A. P., Fleischhaker, F., Schneider-Baumann, M., Misske, A. M., Barner-Kowollik, C. "No Apparent Correlation of k_p with Steric Hindrance for Branched Acrylates", *Macromol. Chem. Phys.*, **2015**, 216, 1573–1582. Copyright (2015) Wiley-VCH

restricted to relatively slowly propagating monomers such as styrene or MMA.^[90,92] Determination of propagation rate coefficients of faster propagating monomers such as acrylates was hardly possible and not feasible at temperatures above 30 °C.^[9] The low pulse repetition rates did not prove sufficient to suppress the typical acrylate transfer reactions such as backbiting, leading to the formation of less reactive radicals and therefore a blurring of the PLP pattern and composition of $k_{p,sec}$ and $k_{p,tert}$. The above noted transfer processes occurred predominantly at temperatures exceeding ambient conditions^[99] but were already noted at sub-zero temperatures as well.^[160] With high frequency pulsed lasers becoming available in the last decade, it is possible to determine precise propagation rates above ambient temperature for rapidly propagating monomers whose radicals are able to undergo inter- and intramolecular chain transfer processes. The first PLP experiments employing pulse repetition rates of 500 Hz were carried out in 2008 on *n*-butyl acrylate and confirmed the propagation rates determined earlier with 100 Hz lasers.^[161] In the case of vinyl acetate, however, an increase of k_p of close to 25% was detected when pulsing with a frequency of 500 Hz compared to 100 Hz,^[162] showing the necessity to employ the highest available pulse rates to obtain reliable data as already discussed in Chapter 1.4.

The detection of trends and family type behavior for defined groups of monomers aids to understand the underlying effects and influences of the chemical structure on the propagation rate coefficient. Describing trends and family behaviors provides the opportunity to estimate propagation rate coefficients for not yet investigated monomers fitting into the proposed families without the need of individual measurements. Interesting observations have been made regarding the determination of k_p of a series of linear (meth)acrylates and branched acrylates. For linear acrylates as well as linear methacrylates, a linear increase of k_p with increasing ester side chain length was observed when going from methyl acrylate (MA) to behenyl acrylate (BeA) and methyl methacrylate (MMA) to behenyl methacrylate (BeMA), respectively.^[89,93,131,143,163] The linear acrylates displayed an increase in k_p of 550 L·mol⁻¹·s⁻¹ (2-3%) per additional CH₂ group and the propagation rate of linear methacrylates increased by approximately 30 L·mol⁻¹·s⁻¹ (3-4%) per additional CH₂ group at 50 °C. For branched methacrylates, a family type behavior was identified^[130,131] giving the possibility to describe investigated monomers *i*DeMA, EHMA, PHMA, TDA-MA, TND-MA, and C17MA with a joint set of Arrhenius parameters reading $A=2.82\cdot 10^6$ L·mol⁻¹·s⁻¹ and $E_A=21.51$ kJ·mol⁻¹. Interestingly, a group of branched acrylates investigated in bulk by Haehnel *et al.* did not show any trends in their propagation rate coefficients, nor was a family type behavior observed.^[131]

The focus of the current chapter lies on the study of branched acrylates in 1M solution

in BuAc to investigate with regards to differences between solution and bulk data, as well as differences between branched and linear acrylates and branched acrylates and methacrylates, respectively and the search for possible trends within the investigated monomer class. The monomers investigated in the current chapter are presented in Figure 2.1 alongside the structures of the previously studied linear acrylates and branched methacrylates that will be discussed in this chapter.

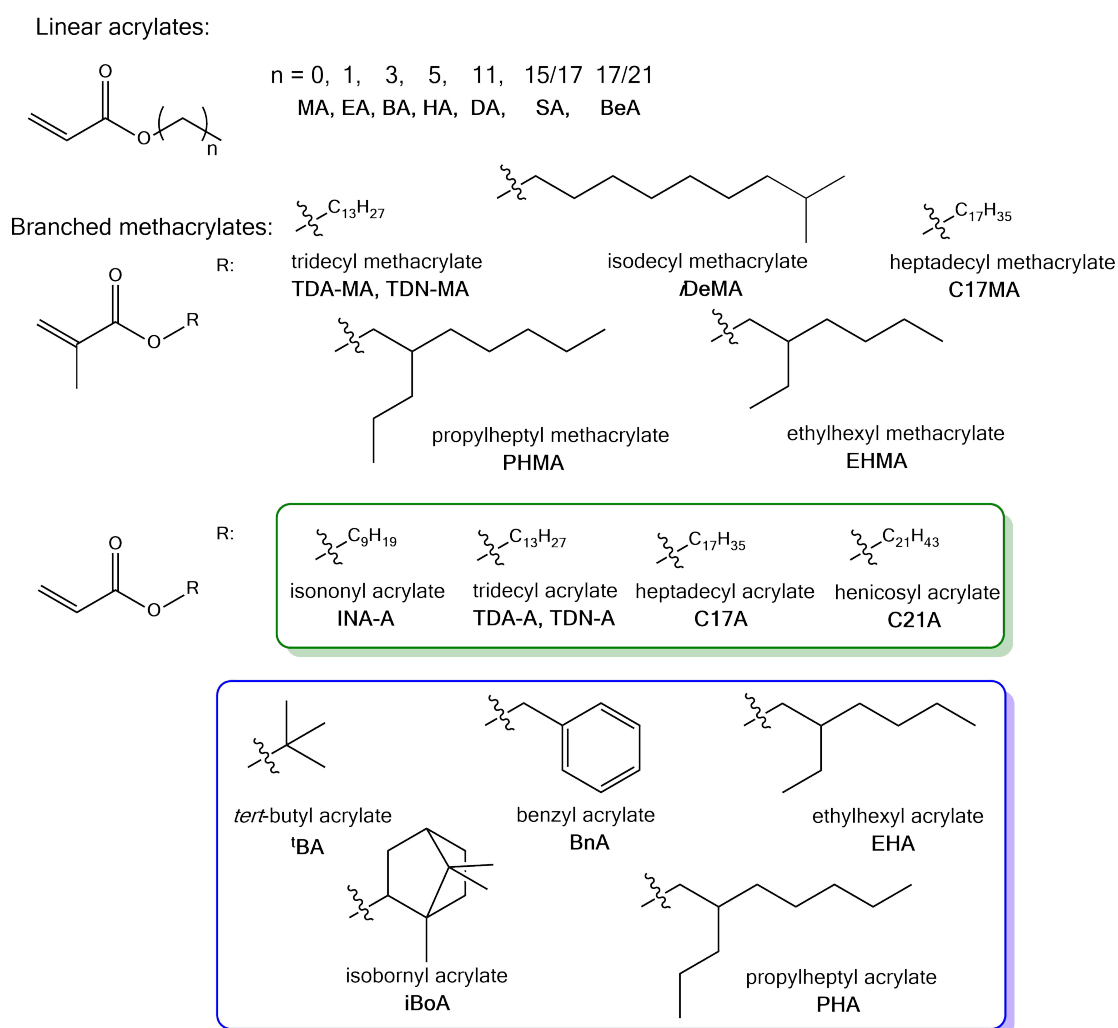


Figure 2.1.: Monomer Landscape. The branched acrylates investigated in solution in the current study are highlighted in the blue box and were previously studied^[131] in bulk. Branched acrylates additionally investigated in bulk^[131] are highlighted in the green box. Linear acrylates showing a trend in their propagation rate coefficient (methyl acrylate, MA; ethyl acrylate, EA; butyl acrylate, BA; hexyl acrylate, HA; dodecyl acrylate, DA; stearyl acrylate, SA; and behenyl acrylate, BeA) as well as branched methacrylates displaying a family type behavior (TDA-MA/TDN-MA, *i*DeMA, C17MA, PHMA, and EHMA) are critically compared to the data determined in the course of this work.

The investigated monomers are highlighted in the blue box of Figure 2.1. Branched acrylates investigated in solution by Haehnel *et al.* [131] and incorporated into the current study are shown in the green box. In previous studies, the Arrhenius parameters and propagation rate coefficients were reported for a series of linear acrylates, namely: methyl acrylate (MA), [164] ethyl acrylate (EA), [121] butyl acrylate (BA), [99] hexyl acrylate (HA), [121] dodecyl acrylate (DA), [165] stearyl acrylate (SA), [131] and behenyl acrylate (BeA), [131] as well as a family of branched methacrylates: *iso*-decyl methacrylate (*i*DeMA), [163] 2-ethylhexyl methacrylate (EHMA), [163] 3-propylheptyl methacrylate (PHMA), [130] tridecyl methacrylates (TDN-MA and TDA-MA), [131] and heptadecyl methacrylate (C17MA). [130] Furthermore, ten branched acrylates were investigated in bulk: *tert*-butyl acrylate (*t*BA), [152] benzyl acrylate (BnA), [121] *iso*-bornyl acrylate (*i*BoA), [152] 2-ethylhexyl acrylate (EHA), [10] 2-propylheptyl acrylate (PHA), [131] *iso*-nonyl acrylate (INA-A), [131] tridecyl acrylates (TNA-A and TDN-A), [131] heptadecyl acrylate (C17A), [131] and hencicosyl acrylate (C21A); [131] the latter five being investigated in 1M solution in BuAc as well. To complete the series of branched acrylates in solution and provide a solid base for the comparison of solution and bulk data, *t*BA, BnA, *i*BoA, EHA, and PHA are investigated in 1M solution in BuAc. In addition to the broadening of the database of available monomer specific propagation rate coefficients, this chapter aims at the investigation of the series of branched acrylates in solution for the detection of possible trends within the monomer series, the comparison to branched acrylates in bulk to check for possible solvent effects, and to gain insight into the underlying effects that cause the kinetic differences between branched acrylates and linear acrylates or branched methacrylates, respectively.

2.1. MHKS Parameters

The need for polymer specific MHKS parameters to obtain reliable molecular weights of the inflection points and therefore precise k_p values was already addressed in chapter 1.4.1. With the exception of benzyl acrylate, for the investigated branched acrylates, MHKS parameters were available in the literature. However, the microstructure of the polymer samples with regards to the occurrence and amount of chain branching can have an influence on their conformation in solution, therefore influencing their hydrodynamic volume and ultimately the derived MHKS parameters. Especially long chain branches occurring due to random transfer to polymer reactions may have a significant effect on the MWD. [166,167] The MHKS parameters for EHA, t BA, and i BoA were not determined using PLP generated samples, hence the microstructures may vary and the application of these MHKS parameters can lead to additional errors in the determined propagation rate coefficients. However, to ensure the comparability to the previously published bulk data, the same MHKS parameters are employed in the current study for the determination of k_p in solution.

For benzyl acrylate, no monomer specific MHKS parameters could be found in the literature, (bulk k_p data published by Willemse *et al.* were determined via MALDI-ToF-MS coupled with PLP, thus no MHKS parameters were needed) therefore, attempts have been made to determine these parameters in the course of the current study. Broadly distributed polymer samples of BnA were generated via PLP, combined, and subsequently freed from remaining monomer and other impurities by precipitation in cold methanol. The purified polymer was dissolved in tetrahydrofuran (THF) and fractionated via a preparative SEC column. The resulting sample fractions need to be analyzed via the triple detection SEC setup. However, several problems were encountered during the fractionation process. The main drawback was the insolubility in THF of most of the sample fractions after separation and drying, making an analysis via triple detection SEC impossible. An additional problem occurring after fractionation was that the selected fractions were still quite broad when reanalyzed via SEC. A possible reason for the insolubility of the samples and the apparently high dispersities even after fractionation might be due to a crosslinking of the polymer. For the fractionation process, unstabilized THF was employed and the solvent was subsequently evaporated over night. Since the fractionated polymer was either still broadly distributed or insoluble after drying, a crosslinking of the polymer chains due to the formation of radicals from the unstabilized THF could be the cause. After several unsuccessful attempts to obtain reliable polymer specific MHKS parameters for BnA, the PLP samples of BnA were analyzed employing $p(t$ BA) MHKS parameters. Parameters of poly(benzyl

methacrylate), pBnMA, were provided by Hutchinson *et al.* in 1998^[168] and are, to date, the only reported data for a monomer containing an aromatic system in direct proximity of the ester functionality, thus, employing the MHKS of the methacrylate for the corresponding acrylate appears to be a logical choice. However, the effect of the α -methyl group on the polymer conformation and the differences in persistence length and rigidity of the polymer backbone compared to the corresponding acrylate significantly influence the resulting K and α . Considering these significant conformational differences, the application of MHKS parameters of an acrylate type monomer with comparable steric hindrance seems to be the more appropriate choice. Nevertheless, employing non-specific MHKS parameters for the determination of molecular weights is beset with an additional error and the resulting k_p data and Arrhenius parameters should be treated with caution. The MHKS parameters employed for the determination of propagation rate coefficients are displayed in Table 2.1 alongside the molecular weights of the monomers and the temperature-dependent densities.

Table 2.1.: Collation of monomer and polymer specific physical data of the acrylates investigated in the current study alongside additional monomers to complete the series of branched acrylates. The molecular weight of the monomer (MW) as well as the temperature-dependent densities in 1M solution in BuAc (ρ_0 , b) and the MHKS parameters in THF at 35 °C (K , α) are stated. For BnA, p(^tBA) MHKS parameters were applied since no parameters for p(BnA) were available. MHKS parameters were taken from the stated references.

monomer	MW [g·mol ⁻¹]	ρ_0 [g·mL ⁻¹]	b [g·mL ⁻¹ ·°C]	K [cm ³ ·g ⁻¹]	α
tBA ^[152]	128.17	0.90353	10.4000 x 10 ⁻⁴	19.7 x 10 ⁻³	0.66
BnA ^[152]	162.19	0.92844	10.2000 x 10 ⁻⁴	19.7 x 10 ⁻³	0.66
iBoA ^[152]	208.3	0.92514	9.9290 x 10 ⁻⁴	5.00 x 10 ⁻³	0.75
EHA ^[10]	184.28	0.90237	9.9883 x 10 ⁻⁴	9.85 x 10 ⁻³	0.719
PHA ^[130]	212.3	0.89972	9.8140 x 10 ⁻⁴	5.55 x 10 ⁻³	0.743
INA-A ^[131]	198.3	0.90159	9.8790 x 10 ⁻⁴	8.36 x 10 ⁻³	0.707
TDA-A ^[131]	254.41	0.997	9.5521 x 10 ⁻⁴	7.88 x 10 ⁻³	0.692
TDN-A ^[131]	254.41	0.89957	9.5381 x 10 ⁻⁴	3.65 x 10 ⁻³	0.76
C17A ^[130]	310.51	0.89799	9.2113 x 10 ⁻⁴	2.60 x 10 ⁻³	0.762
C21A ^[131]	366.62	0.89792	8.9060 x 10 ⁻⁴	4.81 x 10 ⁻³	0.715

2.2. Arrhenius Parameters

Critical to understanding the kinetic behavior, appropriate Arrhenius parameters need to be determined. The following is a thorough evaluation of various branched acrylates in order to carefully characterize the selected monomers. Employing the polymer specific MHKS parameters for the SEC analysis taken from the stated references, the obtained SEC elugrams of the PLP generated polymers give the accurate molecular weights of the inflection points and valid propagation rate coefficients can be determined. Plotting k_p against the temperature on a $\ln(k_p)$ vs. T^{-1} scale, the Arrhenius parameters can be deduced using the y-intercept and the slope of the linear fit. Figure 2.2 depicts the Arrhenius plots for the investigated branched acrylates in 1M solution in BuAc: *tert*-butyl acrylate, 2-propylheptyl acrylate, isobornyl acrylate, 2-ethylhexyl acrylate, and benzyl acrylate. The obtained Arrhenius parameters, A and E_A , alongside their corresponding error margins as well as the propagation rate coefficients at 50 °C, $k_p^{50^\circ\text{C}}$, and the investigated temperature interval are collated in Table 2.2. The detailed sample conditions of all PLP generated samples corresponding to the data points incorporated into the Arrhenius plots are stated in Tables A.1 to A.5 in the Appendix A alongside representative SEC elugrams for each investigated monomer (see Figures A.1 to A.5). The Arrhenius parameters and corresponding error margins stated in Table 2.2 were calculated using the program CONTOUR V2.0.2 by van Herk^[159,169] with constant absolute error margins of 15% as standard deviations and the average errors of each data point lie well within the initially assumed error range (ranging from 2.1% for *t*BA to 5.8% for PHA). The error ranges stated in Table 2.2 are the boundaries of the 95% joint confidence interval and all data points can be fitted within the 95% probability. The frequency factors show the typical magnitude of 10^6 to 10^7 L·mol⁻¹·s⁻¹ (for acrylates generally higher than for methacrylates) and the scattering of the data points incorporated into the Arrhenius plots lie within an error range correlated to the error margins of approximately 2 kJ·mol⁻¹ in the activation energy characteristic for acrylates. Due to the extrapolated nature of the linear fit and the comparably narrow temperature range, small errors in the slope of the fit can result in high uncertainties in the y-intercept, leading to significantly higher error ranges for the prefactor A than the activation energy E_A .

Table 2.2.: Arrhenius parameters with error margins, propagation rate coefficients at 50 °C, and investigated temperature intervals for branched acrylates in 1M solution. Data for BnA have been calculated employing the MHKS parameters for p(^tBA). Reprinted with permission from [132]. Copyright 2015 Wiley-VCH.

monomer	A [L·mol ⁻¹ ·s ⁻¹]	±	E _A [kJ·mol ⁻¹]	±	k _p ^{50°C} [L·mol ⁻¹ ·s ⁻¹]	T-interval [°C]
^t BA	11.2 x 10 ⁶	-2.19 x 10 ⁶ 3.69 x 10 ⁶	16.45	-0.64 0.67	24600	-7 to 60
BnA	12.8 x 10 ⁶	-4.84 x 10 ⁶ 1.98 x 10 ⁷	16.12	-1.76 1.85	30700	-5 to 60
iBoA	4.81 x 10 ⁶	-1.31 x 10 ⁶ 3.01 x 10 ⁶	15.35	-1 1.06	15900	-6 to 60
EHA	6.16 x 10 ⁶	-2.21 x 10 ⁶ 5.67 x 10 ⁶	15.59	-1.47 1.37	18600	-6 to 60
PHA	5.83 x 10 ⁶	-2.24 x 10 ⁶ 1.12 x 10 ⁷	15.24	-1.86 2.08	20000	-8 to 60
Following data taken from Ref [131]						
INA-A	16.6 x 10 ⁶	-6.41 x 10 ⁵ 3.99 x 10 ⁶	17.63	-1.93 2.31	23500	-10 to 70
TDA-A	9.63 x 10 ⁶	-2.71 x 10 ⁵ 9.28 x 10 ⁶	16.18	-1.02 1.33	23500	-10 to 70
TDN-A	15.9 x 10 ⁶	-6.69 x 10 ⁵ 6.18 x 10 ⁷	17.52	-2.19 2.9	23500	-10 to 70
C17A	6.24 x 10 ⁶	-2.55 x 10 ⁵ 1.42 x 10 ⁶	14.73	-2.12 2.29	26000	-12 to 70
C21A	8.16 x 10 ⁶	-3.18 x 10 ⁵ 1.74 x 10 ⁶	16.50	-1.98 2.25	23400	-9 to 70

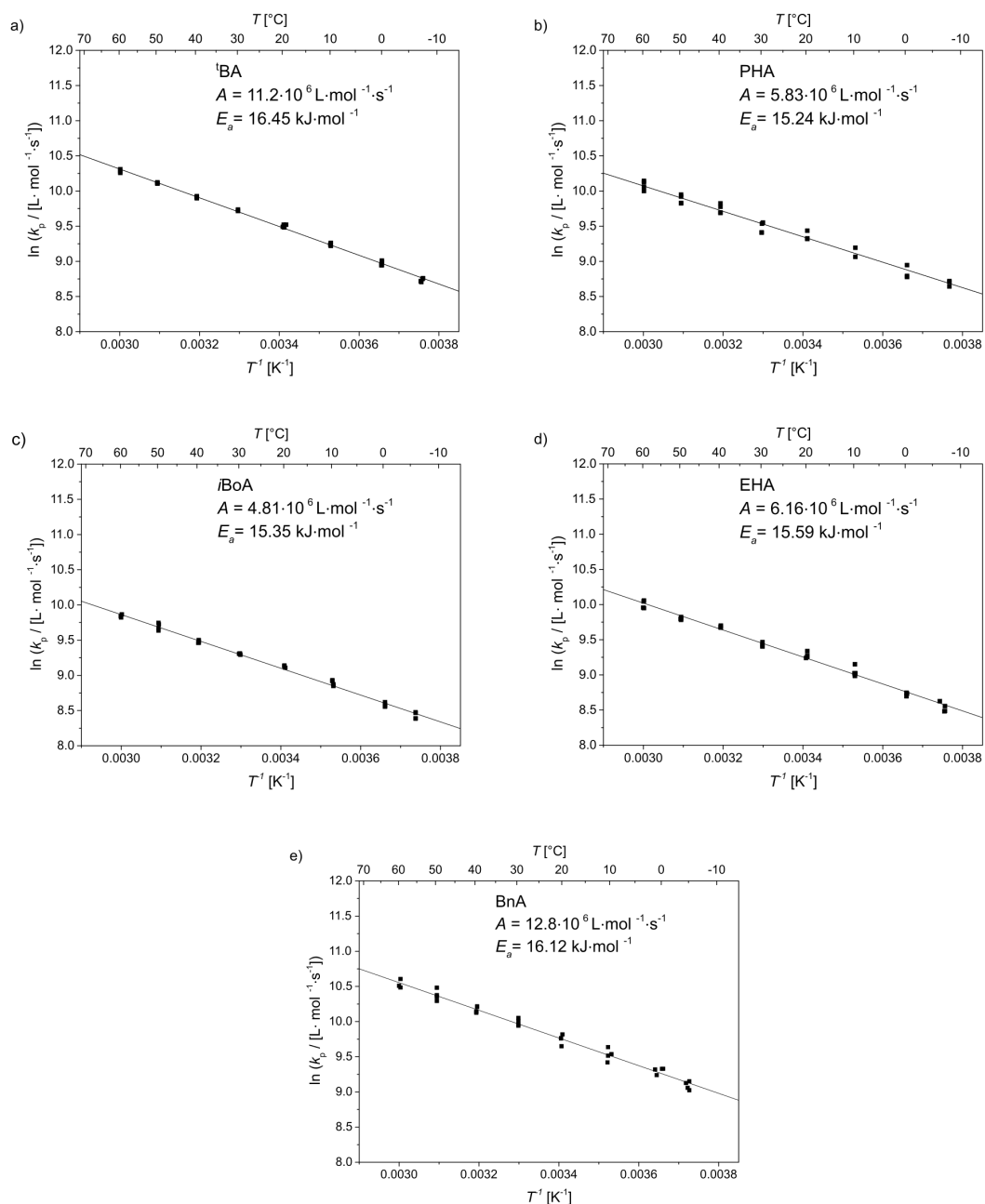


Figure 2.2.: $\ln(k_p)$ versus T^{-1} plots for the determination of Arrhenius parameters for branched acrylates in 1M solution in BuAc for a) *tert*-butyl acrylate (^tBA), b) 2-propylheptyl acrylate (PHA), c) isobornyl acrylate (*i*BoA), d) 2-ethylhexyl acrylate (EHA), e) benzyl acrylate (BnA). For p(BnA) MHKS parameters of p(^tBA) were applied. The corresponding monomer structures are depicted in Figure 2.1. The Arrhenius parameters are collated in Table 2.2 jointly with the associated error margins. Adapted with permission from ref [132]. Copyright 2015 Wiley-VCH.

All depicted Arrhenius plots display a strict linear behavior of the propagation rate coefficients over the entire studied temperature interval and for none of the data significantly deviations from linearity are observed in any of the depicted graphs. For the acrylates investigated in the current study, temperatures from -8 °C to 60 °C were investigated, mainly limited due to a loss of the typical PLP distribution in the SEC chromatogram at elevated temperatures, leading to the inability to clearly detect a second inflection point or deviations of $k_{p,1}/k_{p,2}$ from unity, respectively. For acrylate monomers, the deviation of the propagation rate coefficient to lower values at elevated temperatures is based on the increasing importance of transfer to polymer reactions such as backbiting and the formation of MCRs. [11,99] The simultaneous growth of secondary and tertiary propagating radicals leads to a mixture of $k_{p,sec}$ and $k_{p,tert}$ and an overall decreased k_p^{app} . [8,170,171] For a more detailed discussion of the side reaction interfering with the determination of a solely secondary propagating k_p refer to chapter 1.2 on FRP. To prevent a loss of the PLP structure and the mixture of concurrently growing secondary and tertiary radicals at elevated temperatures, even higher pulse repetition rates need to be employed. High-energy pulsed lasers with frequencies of up to 1000 Hz just recently became available, [172,173] however, their potential to broaden the assessible temperature range for acrylates might be limited. More interesting aspects of applying kHz lasers lie in the investigation of backbiting rates or quasi continuous irradiation. Another reason for deviations of the data from linearity lies in the chain length dependence (CLD) of the propagation rate coefficient [32] for small macroradicals, especially in the low temperature range where propagation is slow and deviations to higher k_p values can occur. These deviations, however, were not observed in the current study since the pulse repetition rate has been adjusted accordingly in the low temperature ranges to consistently obtain polymeric samples displaying their first inflection points at a molecular weight close to 10 000 - 20 000 g·mol⁻¹. As stated previously, only samples with a $k_{p,1}/k_{p,2}$ ratio close to 1 should be included into the data set for the Arrhenius plots to avoid the incorporation of samples influenced by non-PLP governed reactions such as backbiting, leading to a mix of secondary and tertiary propagating radicals (see Figure 1.11 in Chapter 1.4). $k_{p,1}/k_{p,2}$ values of each sample included in the final Arrhenius plots lie between 0.95 and 1.17 and are collated in Tables A.1 to A.5 in the Appendix A.

2.3. Trends and Family Type Behavior

The results reported in the previous section are reviewed with respect to trends and family type behavior within the investigated monomer series. Subsequently, the results will be compared to literature known data of linear acrylates and branched methacrylates and a hypothesis for the differences between the monomer families is tendered. A comparison of the Arrhenius parameters within the investigated series of branched acrylates shows a parallel behavior between the frequency factor and the activation energy, however, no systematic trends can be detected within the monomer series, arranged in the most likely order of increasing steric demand (see Figure 2.3). Interestingly, no analogous behavior can be detected between the solution and bulk data. While in solution the activation energy as well as the frequency factor seem to scatter around a horizontal line at approximately $16 \text{ kJ}\cdot\text{mol}^{-1}$ and $1 \times 10^7 \text{ L}\cdot\text{mol}^{-1}\cdot\text{s}^{-1}$, the bulk data show a tendential decrease of both, A and E_A , when going to monomers with longer ester side chains and higher steric demands. The activation energy seems to vary independently of the actual size or steric demand of the ester side chain in the range of approximately $3 \text{ kJ}\cdot\text{mol}^{-1}$ in solution and $5 \text{ kJ}\cdot\text{mol}^{-1}$ in bulk. The parallel behavior of A and E_A is attributed to the acquisition of A via extrapolation of the determined slope of the Arrhenius plot. Since the slope is proportional to the activation energy, the frequency factor exhibits basically the same behavior: higher/lower activation energies lead to higher/lower frequency factors. On a physicochemical level, this parallel behavior of A and E_A can be explained by the interaction with the transition state (TS). Stronger interactions of the ester side chain with the TS lead to a decrease of the activation energy. Concomitantly, a more pronounced interaction of the TS increases the hindrance of the torsion and internal rotation, ultimately lowering the frequency factor.^[33] Using *ab initio* calculations, Heuts *et al.* reported a penultimate unit effect, leading to an increase in hindrance of the torsion when changing to a bulkier ester side chain, decreasing the frequency factor.^[174] These findings fit well for the observations made in bulk for the series of branched acrylates, however, the solution data do not follow these predictions. A possible influence of the solvent on the transition state – although not observed for other monomer classes – should therefore not be fully ruled out.

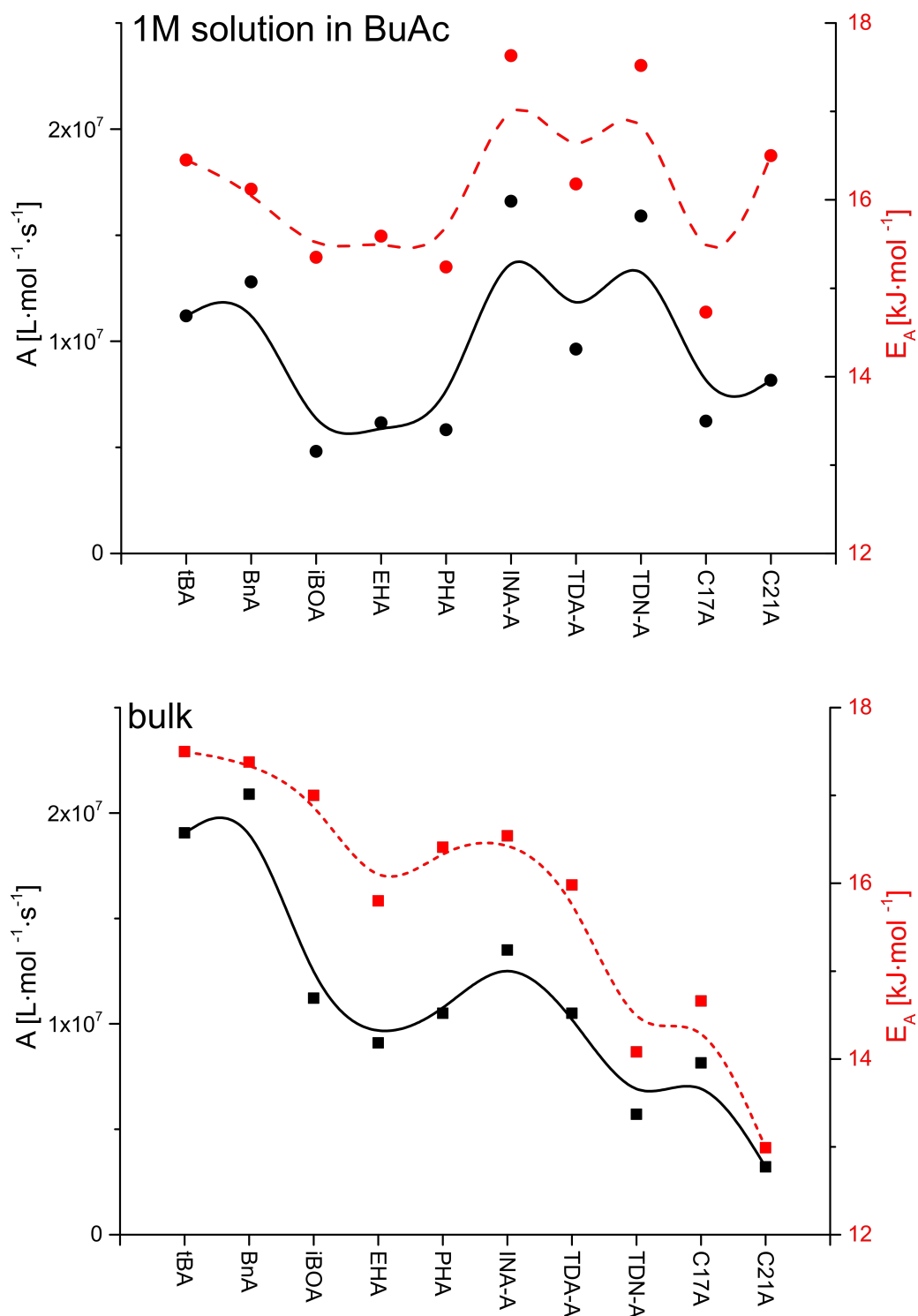


Figure 2.3.: Dependence of the Arrhenius parameters on the ester side chain for branched acrylates in 1M solution (upper part) as well as bulk (lower part). Monomers are depicted in the most likely order of increasing steric demand from left to right. Neither for E_A (red line) nor the pre-factor (black line) a trends is detectable and no analogous behavior is detected between bulk and solution data. The lines are no fits and solely for guiding the eye.

During their investigation of linear methacrylates, Beuermann *et al.* already noted the non-analogous behavior of Arrhenius parameters and propagation rate coefficients within the studied monomer family.^[89] Although they were not able to detect a systematic variation of the activation energies and frequency factors of the investigated methacrylates, a distinctive trend of k_p depending on the ester side chain could be described. It is clearly necessary to closely inspect the propagation rate coefficients of each monomer to arrive at a valid statement on possible global trends or family type behaviors within investigated monomer families. An overview of the k_p data for the branched acrylates investigated in the current study as well as the five additional acrylates described by Haehnel *et al.* is given in Figure 2.4 and the corresponding k_p values at 50 °C are collated in Table 2.2. Propagation rates are derived from the monomer specific Arrhenius parameters via Equation 1.8 and depicted for three temperatures (-50, 0, and 50 °C). The values calculated for 0 and 50 °C are in perfect agreement with the experimentally determined data. Direct measurements of k_p below 10 °C was not possible with the experimental setup employed in the current study. Extrapolations of the propagation rates based on the Arrhenius parameters to higher temperatures, however, are beset with larger errors due to the logarithmic nature of the Arrhenius plot, therefore the depicted data are limited to the experimental upper temperature limit. By plotting the data in such a manner, trends within the monomer series can be readily detected and an arrangement of the monomers in the most likely order of increasing steric demand is possible. For better comparison of the depicted data, k_p values are plotted on the same scale for solution (upper part) and bulk (lower part).

2. Branched Acrylates in Solution

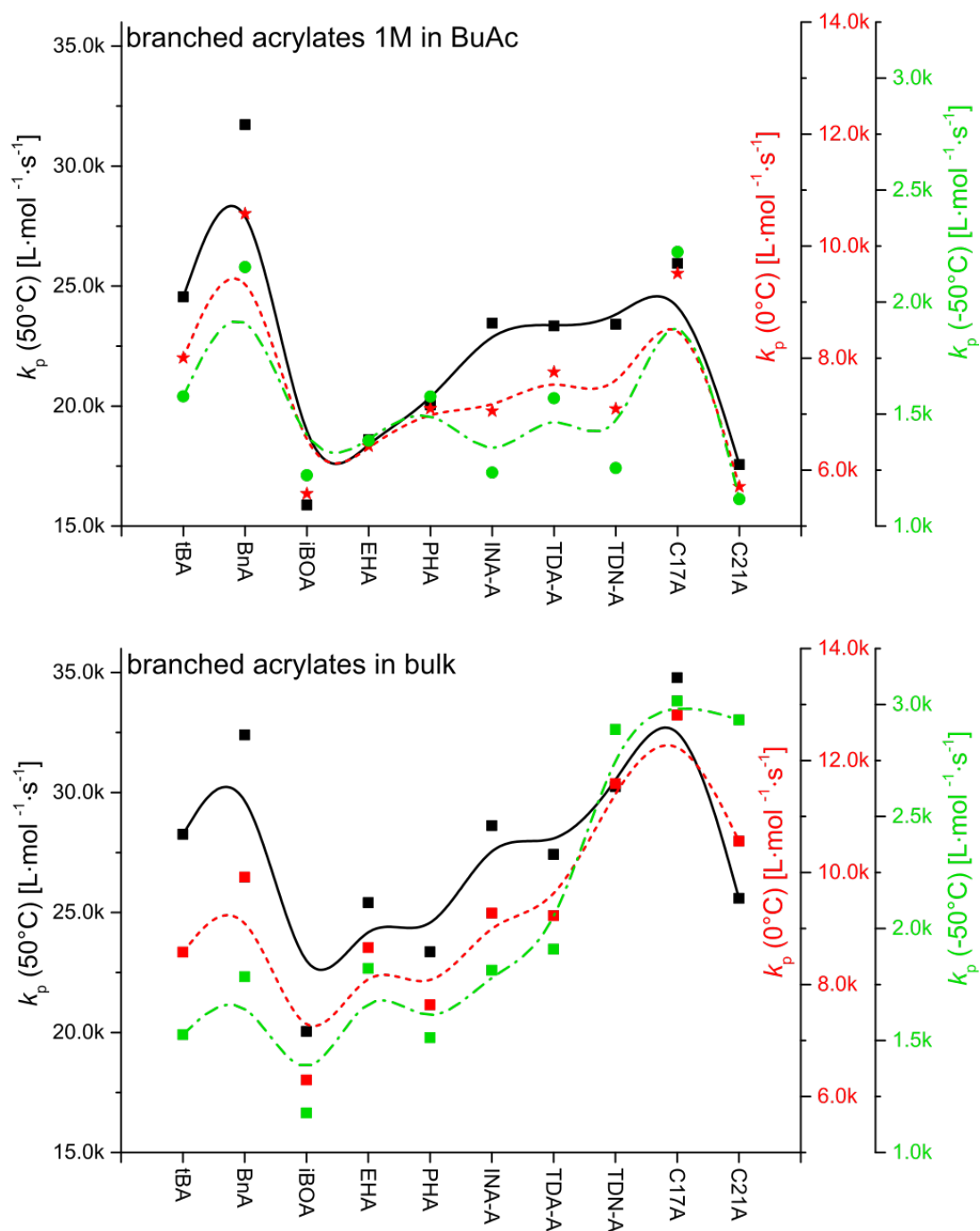


Figure 2.4.: Dependence of the propagation rate coefficients on the ester side chain for branched acrylates in 1M solution (upper part) as well as bulk (lower part) at different temperatures: left scale, black solid line: $k_p^{50^\circ\text{C}}$; right inner scale, red dashed line: $k_p^{0^\circ\text{C}}$; right outer scale, green dot-dashed line: $k_p^{-50^\circ\text{C}}$. For better comparison of the data, scales are the same for solution and bulk. Monomers are depicted in the most likely order of increasing steric demand. The lines are no fits and solely for guiding the eye. Adapted from ref [132] with permission from Wiley-VCH.

Having a closer look at Figure 2.4, it is evident that in contrast to the branched methacrylates, branched acrylates do not show a family type behavior, neither can a distinctive trend within the monomer series be identified. A tendency of increasing propagation rate coefficients with increasing length and steric demand of the ester side chain can be observed from *i*BoA to C17A in bulk. However, this trend is clearly not followed by the most bulky monomer, C21A. Especially in 1M solution, C21A displays significantly decreased propagation rates, being the second slowest propagating monomer within the investigated series. In bulk, the deviations of C21A to lower propagation rates becomes more distinct at higher temperatures due to the notably lower activation energy, leading to a less pronounced increase in k_p with increasing temperature. In solution, however, the activation energy of C21A is considerably higher and in good agreement with the other monomers of the series, leading to a less pronounced difference between the depicted temperatures. INA-A through C21A comprises a homologous series of monomers featuring ester side chains derived from an oligomerization of *n*-butene, yet no trend can be described within that series. The slight increase of k_p from INA-A to C17A in bulk is not present in solution, where INA-A, TDA-A, and TDN-A feature the exact same propagation rates at 50 °C. The significantly higher k_p for benzyl acrylate (considering the comparably low steric demand and low number of carbon atoms of the ester side chain) can possibly be explained by “enthalpic effects [...] related to the electronic interaction of the phenyl ring and its interaction with the unpaired electron“ of the radical site, according to Willemse and Herk.^[121] This elevated propagation rate of BnA seems to be even more pronounced in solution, however, it needs to be kept in mind that for the solution data of BnA, non-specific MHKS parameters have been applied and, therefore, the data need to be handled with caution.

Although similarities can be observed between the bulk and solution data – elevated k_p for ^tBA and BnA, significantly lower k_p for C21A, and slight increase of k_p when going from *i*BoA to C17A – no constant analogous behavior is observed. The differences in propagation rate between bulk and solution range from 13% to 32% at 50 °C (i.e. k_p (^tBA) bulk: 28 300 L·mol⁻¹·s⁻¹, solution: 24 600 L·mol⁻¹·s⁻¹; k_p (C21A) bulk: 25 600 L·mol⁻¹·s⁻¹, solution: 17 600 L·mol⁻¹·s⁻¹). While in solution, PHA features a slightly higher propagation rate than EHA over the entire temperature range, in bulk k_p (PHA) is below k_p (EHA) for all depicted temperatures. Additionally, C21A features the second lowest propagation rate in solution for all depicted temperatures, while in bulk k_p (C21A) lies above *i*BoA, EHA, and PHA at 50 °C and even possesses the third and second highest k_p at 0 °C and -50 °C, respectively. These observations are surprising since they are in contrast to previous findings for other monomer families. For linear alkyl acrylates for example, it was demonstrated that differing monomer concentration

from bulk to solution did indeed result in a variation of $k_p^{50^\circ\text{C}}$ of approximately 5 to 20%. Yet the global trend of increasing propagation rate with increasing number of carbon atoms in the ester side chain was clearly observed for bulk as well as solution and no significant difference could be detected even when going to very dilute conditions.^[133] However, for several monomers and solvent conditions, variations of the propagation rate coefficients between bulk and solution have been reported.^[93, 175–178] As described previously, a similar non-analogous behavior is observed for A and E_A between solution and bulk data, as for the example ^tBA displays a decrease in activation energy by approximately $2 \text{ kJ}\cdot\text{mol}^{-1}$ when going from bulk to solution, while the E_A of C21A increases by $3.5 \text{ kJ}\cdot\text{mol}^{-1}$, making it not advisable to predict Arrhenius parameters in solution based on bulk data and vice versa. The non-family type behavior of the branched acrylates in solution is also evident when inspecting the joint Arrhenius plot in Figure 2.5.

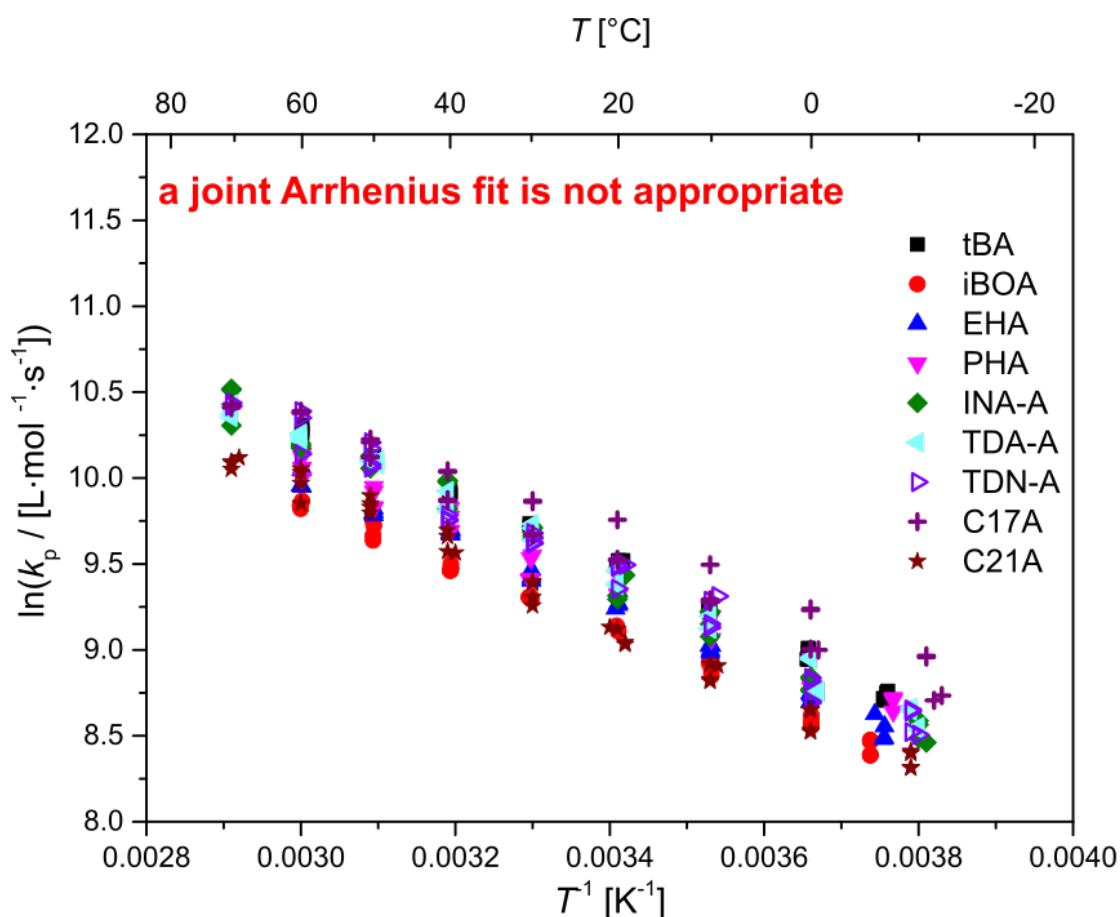


Figure 2.5.: Combined Arrhenius plot for branched acrylates in 1M solution in BuAc. A joint linear fit is clearly not appropriate. Adapted from ref [132] with permission from Wiley-VCH.

Over the entire investigated temperature range, the data scattering between different monomers in the series is significantly larger than the scattering within different samples of one monomer. Although a SEC error of approximately 15% is inevitable, the scattering of the propagation rates between different monomers unquestionably exceeds the boundaries of the error margins, therefore, a joint Arrhenius fit is not appropriate and neither trends nor a family type behavior could be described within the investigated series of branched acrylates.

The presented data demonstrate the need for direct measurements and individual determination of the monomer specific propagation rate coefficients and Arrhenius parameters for each branched acrylate of interest, in solution and bulk alike.

2.3.1. Comparison to Linear Acrylates and Branched Methacrylates

The following chapter's objective is to provide a hypothesis for the possible reasons for the non-observable trends within the investigated series of branched acrylates and a comparison to the trends detected for linear acrylates as well as branched methacrylates. As stated previously, a linear increase of the propagation rate coefficient with increasing ester side chain length was reported for the series of methyl acrylate (MA), ethyl acrylate (EA), butyl acrylate (BA), hexyl acrylate (HA), dodecyl acrylate (DA), stearyl acrylate (SA), and behenyl acrylate (BeA).^[89,131] To describe these findings, two possible explanations are given:^[179] destabilizations of the radical site leading to alterations in the transition state or pre-structuring of the monomers, respectively. The attacking propagating radical is delocalized in the TS and stabilized by the polar ester moiety, however, increasing the ester side chain leads to an increased (non-polar) alkyl content causing a decrease of the ester moiety concentration and reduction of the radical stabilization. Therefore the reaction of the radicals with the double bond of other monomer units is accelerated since "a repulsive potential energy surface facilitates leaving the TS in the direction of the product radical".^[179] Beuermann *et al.* also stated that long alkyl chains can effectively shield the polar interactions of the ester moiety, thus reducing the rotational barriers of the TS, leading to changes in the propagation rate.^[176] Alternatively, a pre-structuring of the reaction solution is considered as a possible explanation of the observed increase in propagation rate. Due to the long non-polar linear alkyl chains, the monomers are able to align in a fashion that puts the acrylic ester groups in close proximity to each other. This alignment results in a propagation of closely situated monomer units leading to an alteration in the local concentration of the monomer and, therefore, an apparently elevated propagation rate. Longer ester side chains induce a more pronounced pre-structuring, causing a visible

trend of k_p in the series of linear acrylates.

However, both explanatory approaches do not seem to be relevant for the branched acrylates. Although a tendency of increased k_p might be inferred from *i*BoA to C17A, no global trend is observable. While the described trend for linear acrylates is detected in bulk as well as solution (since the solvent does not seem to have a significant impact on the TS or a possible pre-structuring of the reaction solution), the distinct differences for branched acrylates are contradictory to the given hypotheses. For the homologous series from INA-A to C21A (enlarged and displayed in Figure 2.6 for better comparison), the trend observed for the linear acrylates might be slightly detectable in bulk, yet fully negligible in solution, where especially INA-A, TDA-A, and TDN-A display the same propagation rates. In both cases, solution as well as bulk, C21A does not follow any trend or family type behavior and clearly contradicts any possible trend. A pre-structuring of the reaction mixture of branched acrylates is relatively unlikely considering the highly branched, sterically demanding ester side chains.

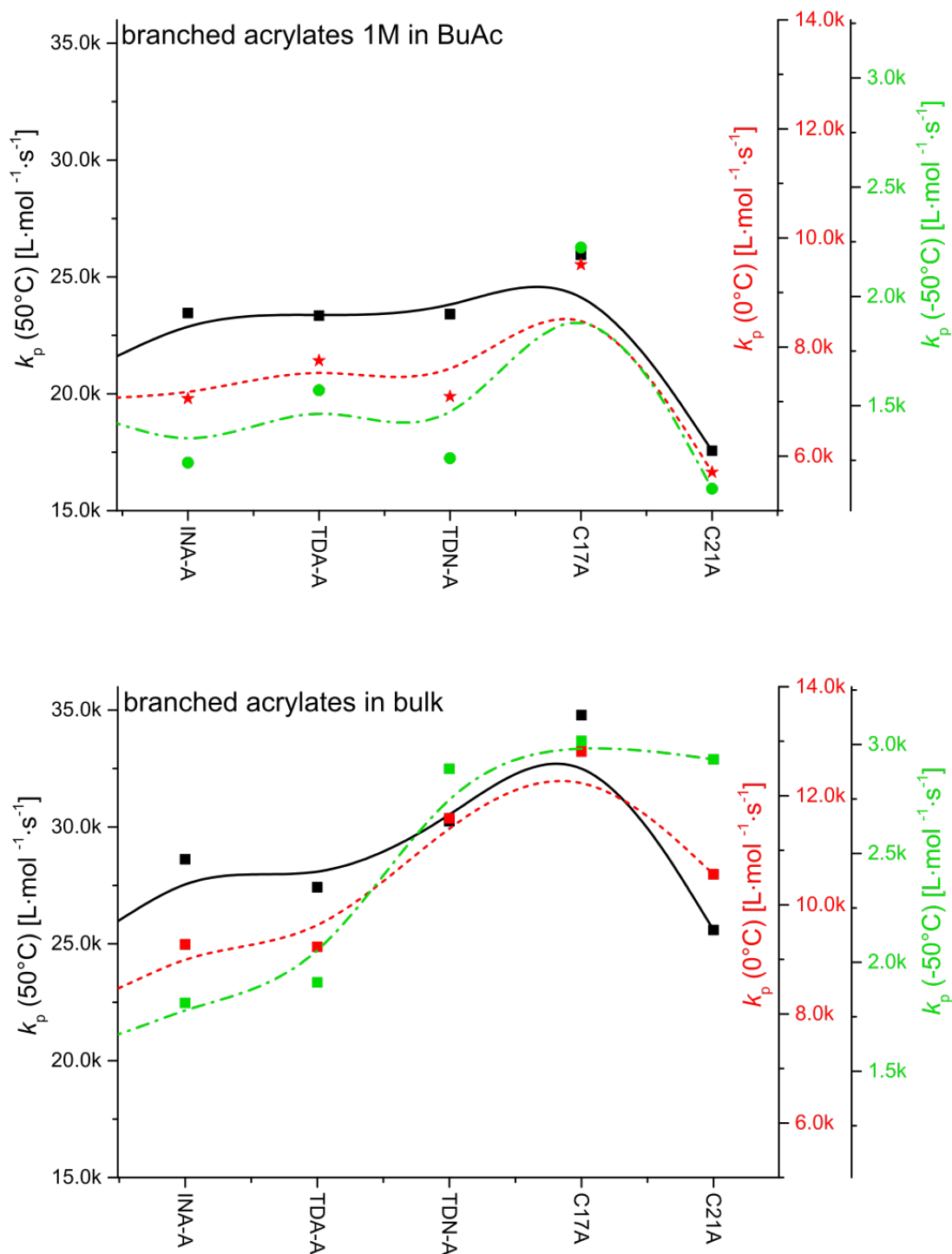


Figure 2.6.: Dependence of the propagation rate coefficients on the ester side chain for the homologous series of INA-A, TDA-A, TDN-A, C17A, and C21A in 1M solution in BuAc (upper part) and bulk (lower part). For better comparison of the data, scales are the same for solution and bulk.

In contrast to the linear acrylates and methacrylates, no increase in k_p was detected for branched methacrylates, instead a family type behavior could be described. Isodecyl methacrylate (*i*DeMA), 2-ethylhexyl methacrylate (EHMA), 2-propylheptyl methacrylate (PHMA), tridecyl methacrylates (TDN-MA and TDA-MA), and heptadecanyl methacrylate (C17MA) in bulk featured remarkably similar propagation rates over the investigated temperature range with experimental k_p values located within the SEC error margins of approximately 15% and can be described by a joint Arrhenius fit.^[130] A previously investigated group of methacrylates with cyclic ester side chains showing a family type behavior, containing isobornyl methacrylate (*i*BoA), cyclohexyl methacrylate (cHMA), benzyl methacrylate (BnMA), and glycidyl methacrylate (GMA), displayed propagation rates approximately 30% higher than for the branched methacrylates.^[87,88] The two studied butyl methacrylates (*i*BMA^[163] and ^tBMA^[180]) display significantly lowered propagation rates compared to cyclic as well as branched methacrylates. In both cases – bulk as well as solution – butyl acrylate displays lower propagation rate coefficients than benzyl acrylate (as is the case for the corresponding methacrylates). However, isobornyl acrylate also exhibits significantly lower k_p values than benzyl acrylate, being the slowest propagating monomer in the investigated series of branched methacrylates compared to BnA as the fastest (solution) or second fastest (bulk) propagating monomer, respectively. This finding is in strong contrast to the description of the corresponding methacrylates BnMA and *i*BoMA with joint parameters. Although for ^tBA and BnA analogies to ^tBMA and BnMA can be observed, the remaining monomers of the investigated series do not follow the same behavior as detected for the methacrylates. The similar propagation rate coefficients observed for INA-A through C17A in solution are not followed by EHA, PHA, and C21A and no evidence of a possible family type behavior can be found in bulk.

For the family of branched methacrylates, the exact shape and branching points of the ester side chain seem not to significantly influence the propagation rate as long as a certain degree of steric demand is present. An exchange of the ester side chain with a comparably bulky chain results in just slight changes of the propagation rate coefficient, implying that the exact chemical nature of the ester side chain is not the main influencing factor. As described above, a pre-structuring of the monomer units appears to be unlikely for sterically demanding and highly branched monomers, they rather seem to behave in a first approximation as spherical objects with similar kinetic properties if similar steric demands are assumed. The branched acrylates discussed in the current study exhibit the exact same ester side chains as the previously investigated branched methacrylates, yet do not follow the same trends in the propagation rate coefficients. These differences are most probably based on the α -methyl substituent –

the only structural difference between the branched acrylates and the corresponding methacrylates – and its influence on the transition state of the propagating reaction. The differences in steric demand, the positive inductive (+I) effect of the α -methyl group, and the changes it induces in the electronic energy levels, rotational degrees of freedom, or the stiffness of the polymer backbone significantly influence the diffusion behavior of the monomers as well as macromolecules. Due to the α -methyl substituent, the methacrylates exhibit a shielding of the dipole character of the ester functionality as well as an increased tendency of the lateral polymer chain to a helical arrangement while for acrylates, no such tendency is reported.^[181] Taking into account the high impact of the α -methyl substituent on the TS and general reactivity of the branched methacrylates, it comes as no surprise that the lack of this α -methyl group has a significant impact on the propagation rate and leads to a more pronounced influence of the specific ester side chain on the propagation reaction. The differences in the kinetic behavior of the branched acrylates compared to the corresponding methacrylates seems to be based on a combination of enthalpic and entropic effects, originating in the methacrylates' α -methyl substituent.

The differences in steric demand of the ester side chain result in different rotational barriers of the transition state. For methacrylates, the main influence on the rotational barriers is given by the α -methyl substituent and its steric interactions with the side chains, thus the actual differences of the side chains on the transition state are less pronounced than for the corresponding acrylates. The differences in steric demand and rotational hindrance, resulting in a lower entropy of the polymer chain, are also reflected in significant differences of the glass transition temperatures (T_g): Acrylates display an approximately 80-100 °C lower T_g than methacrylates, since the acrylic polymer backbone is more flexible and features a lower degree of order.^[182] To describe the influence of enthalpy, entropy, and temperature on the free Gibbs energy of the transition state of a radical propagation, the Gibbs-Helmholtz-Equation 2.1 can be employed.^[183] The Gibbs equation can not only be used to describe the overall reaction process, but to provide a description of the energy barrier of the transition state that needs to be overcome for a successful reaction.

$$\Delta G^\ddagger = \Delta H^\ddagger - T \cdot \Delta S^\ddagger \quad (2.1)$$

Furthermore, the Eyring Equation 2.2 shows the correlation of the Gibbs energy of the transition state (ΔG^\ddagger) and the propagation rate (k) with k_B being the Boltzmann constant, h the Planck's constant, and R the gas constant.

$$k = \frac{k_B T}{h} \cdot \exp\left(\frac{-\Delta G^\ddagger}{RT}\right) \quad (2.2)$$

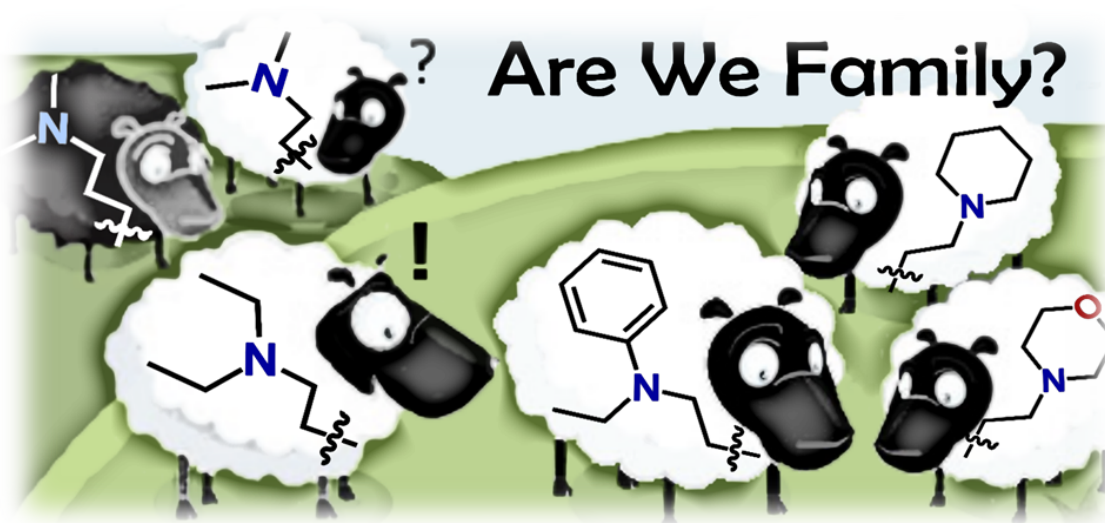
Acrylates display a higher reactivity compared to methacrylates, reflected in their higher propagation rate coefficients. Therefore, ΔG is comparably lower for acrylates (note that a more negative Gibbs energy implies a more favorable forward reaction) and to overcome the higher degree of order present in methacrylic systems and to set the polymer chains in motions, more thermal energy is necessary. Exchanging the ester side chain with a bulkier unit, the stiffness of the polymer backbone will be increased and the entropy of the polymer chain is lowered. The higher the stiffness of the polymer backbone and, therefore, the degree of order of the polymer chain, the more entropy is lost during the polymerization process. A more positive contribution of the entropy to the overall free reaction energy promotes a slower propagating reaction and therefore lower k_p . The differences in ΔS^\ddagger lead to fluctuations in the Gibbs energy depending on the steric demand of the ester side chain. For acrylates, the stiffness of the polymer backbone is mainly governed by the differences in steric demand of the ester side chains, resulting in an influence of the chemical nature of the side chain on the propagation rate. The stiffness in poly(methacrylates), however, is especially defined by the α -methyl substituent. An alteration of the ester side chain therefore insignificantly alters the stiffness of the backbone and the resulting variation in entropy during the polymerization reaction. The influence of the ester side chain on the propagation reaction are visible for the tridecyl acrylates TDA-A and TDN-A, that only differ in the degree of branching of the ester side chain (characterized by the isoindex of TDA = 3.1 and TDN = 2.1). Both monomers display the same ratio of alkyl chain to ester moiety, therefore, the effect of destabilization of the attacking radical should not vary for both acrylates. The different k_p values become even more pronounced at lower temperatures, and the lowered k_p observed for TDA-A seems to be attributed to the higher degree of branching (and hence higher steric influence on the transition state), leading to higher rotational barriers and a stronger decrease in entropy. Interestingly these differences could not be observed in solution, where TDA-A and TDN-A display very similar propagation over the entire temperature range, again suggesting that a solvent influence on the transition state can not be fully ruled out.

In addition to the varying relative contribution of the ester side chain to the differences in entropy for acrylates (solely influenced by the ester side chain) and methacrylates (influenced by ester side chain, but mainly governed by the α -methyl substituent), the electronic differences are reflected in the different contributions to the enthalpy of the

reaction. Exchanging the ester side chain also leads to fluctuations of ΔH^\ddagger , mainly governed by the electronic configuration of the reactants. As mentioned previously, the high propagation rate of the only aromatic monomer, BnA, regarding its comparably low number of carbon atoms, could be attributed to electronic interactions of the phenyl ring with the radical site^[121] and its effects on the reaction enthalpy. Exchanging alkyl side chains with one another should not have a significant effect on the electronic environment of the reactants due to the distance of the side chain to the radical center and the lack of a conjugation therewith. However, Zammit *et al.*^[143] described the possibility of through-space interactions of the ester side chain on the terminal unit of the radical with the unpaired electron if the chain is long enough to be coiled and, therefore, lie quite close to the radical center. This interaction would lead to a form of steric hindrance that lowers the propagation rate coefficient. This explanation might be of interest for the significantly lowered k_p observed for C21A, however, does not seem to apply even for the longest alkyl chains of the linear (meth)acrylates that still follow the trend of increasing propagation rate with increasing ester side chain length. Although the electronic environment of the acrylates might just slightly be altered when exchanging the ester side chains, it is indisputably altered by the addition of the α -methyl group present for the methacrylic monomers. For methacrylates, the contribution of the electronic situation of the tertiary radical site on the enthalpy of the transition state is critically more important than the comparably low fluctuations caused by the ester side chains. Taking these entropic and enthalpic effects into account, the variations of ΔH^\ddagger and ΔS^\ddagger caused by the exchange of the ester side chains between the different monomers is distinctively more significant for the change in the free Gibbs energy of the transition state for acrylates than for methacrylates, where both aspects are mainly defined by the electronic and steric effects of the α -methyl substituent and its shielding character. In Equation 2.2, the Gibbs free energy is correlated with the propagation rate via an exponential term, thus for the acrylates small variations of the Gibbs energy caused by the exchange of the ester side chains are likely to be embodied in considerably higher fluctuations of the propagation rate coefficients. While for the methacrylate the k_p values of the various monomers are located within the error ranges of the SEC measurement, the influences of the side chains on k_p for acrylates is sufficiently strong to exceed the error margins, leading to a loss of detectable family type behavior.

3

Nitrogen-Containing Methacrylates^a



The current chapter investigates possible trends and family type behaviors of the propagation rate coefficient for a novel class of nitrogen-containing methacrylates in bulk. As described previously, poly(methacrylates) constitute important materials for industrial applications and are widely found in home and personal care products, paper chemicals, electronics, adhesives, etc.^[16] Methacrylates containing nitrogen atoms in their ester side chains are interesting candidates for friction modifiers, printing inks, adhesion promoters, dispersion agents, or biomedical and electrooptic applications.^[17–26] In previous publications, efforts were made to identify trends among a group of methacrylates with branched ester side chains (isobutyl methacrylate (*i*BMA), *tert*-butyl methacry-

^a Parts of this chapter are reproduced with permission from Kockler, K. B., Fleischhaker, F., Barner-Kowollik, C. "Investigating the Propagation Kinetics of a Novel Class of Nitrogen-Containing Methacrylates via PLP-SEC", *Polym. Chem.*, **2016**,*7*, 4342–4351. Copyright (2016) Royal Society of Chemistry as well as Kockler, K. B., Fleischhaker, F., Barner-Kowollik, C. "Free Radical Propagation Rate Coefficients of N-Containing Methacrylates: Are We Family?", *Macromolecules*, **2016**,*49*, 8572–8580. Copyright (2016) American Chemical Society

late (^tBMA), isodecyl methacrylate (*i*DeMA), 2-ethylhexyl methacrylate (EHMA), 2-propylheptyl methacrylate (PHMA), tridecyl methacrylates (TDN-MA and TDA-MA), and heptadecyl methacrylate (C17MA))^[130,131,163,180,184], as well as methacrylates with cyclic ester side chains (cyclohexyl methacrylate (cHMA), benzyl methacrylate (BnMA), glycidyl methacrylate (GMA), and isobornyl methacrylate (*i*BoMA)^[88]. For the branched methacrylates *i*DeMA, EHMA, PHMA, and C17MA^[130] as well as the cyclic methacrylates^[88] family type behaviors were reported with joint Arrhenius parameters of $A = 2.39 \cdot 10^6 \text{ L} \cdot \text{mol}^{-1} \cdot \text{s}^{-1}$, $E_A = 21.16 \text{ kJ} \cdot \text{mol}^{-1}$ and $A = 4.24 \cdot 10^6 \text{ L} \cdot \text{mol}^{-1} \cdot \text{s}^{-1}$, $E_A = 21.90 \text{ kJ} \cdot \text{mol}^{-1}$, respectively. Besides the noted alkyl (meth)acrylates, the investigation of monomers with more complex ester side chains became attractive and kinetic data for (meth)acrylates with urethane or hydroxyl functionalized side chains were determined via PLP-SEC. The database was extended by the monomers ethoxyethyl acrylate (EEA),^[152] 2-(phenylcarbamoyloxy)ethyl acrylate (PhCEA), 2-(phenylcarbamoyloxy)isopropyl acrylate (PhCPA), 2-(hexylcarbamoyloxy)ethyl acrylate (HCEA), 2-(hexylcarbamoyloxy)isopropyl acrylate (HCPA)^[185], and hydroxypropylcarbamate acrylate (HPCA)^[186] as well as 2-hydroxyethyl acrylate (HEA)^[187], 2-hydroxyethyl methacrylate (HEMA)^[165], and 2-hydroxypropyl methacrylate (HPMA).^[168], being mainly acrylate monomers. It is interesting to note that excluding HEA, all investigated heteroatom-containing acrylates featured activation energies comparably lower to the typical values of E_A observed for acrylate monomers (approximately $14 \text{ kJ} \cdot \text{mol}^{-1}$ compared to $17\text{-}19 \text{ kJ} \cdot \text{mol}^{-1}$).

Almost 30 years after the establishment of PLP-SEC as a method of choice for the investigation of propagation rate coefficients, the method was utilized to expand the understanding of fundamental kinetics for a wide variety of monomer systems. However, despite the high interest of nitrogen-containing methacrylates for industrial applications, they have surprisingly rarely been investigated with regard to their underlying reaction kinetics. Only in 2014, the first nitrogen-containing methacrylate was studied via PLP-SEC, reporting the propagation rate coefficients for ureidoethyl methacrylate (UMA).^[186] Due to the high melting point above $40 \text{ }^\circ\text{C}$, an investigation of UMA in bulk was experimentally challenging because of the quite narrow accessible temperature range. Thus, the monomer was solely studied in solution in *N,N*-dimethylacetamide (DMAc), leaving possible effects of the solvent on the propagation rate coefficient unknown. A deeper investigation into the fundamental kinetics of nitrogen-containing methacrylates thus seems to be of high interest.

As noted in the previous chapter, describing family type behavior for a group of monomers featuring certain distinct characteristics (as e.g. a similar chemical nature of the ester side chain) allows for the understanding of underlying influences of said char-

acteristics and provides the possibility to estimate further propagation rate coefficients of unknown monomers. Therefore, the focus of the current chapter lies on the study of six nitrogen-containing methacrylates in bulk to pay attention to this, as of yet, barely studied monomer group. The novel set of monomers will be investigated for overarching trends and family type behavior and will be critically compared to the previously studied UMA as well as the families of cyclic and branched methacrylates. During the current study, the MHKS parameters, propagation rate coefficients, and Arrhenius parameters of the monomers 2-(*N*-ethyl-anilino)ethyl methacrylate (NEAEMA), 2-morpholinoethyl methacrylate (MOMA), 2-(1-piperidyl)ethyl methacrylate (PipEMA), 2-(*N,N*-diethylamino)ethyl methacrylate (DEAEMA), 2-(*N,N*-dimethylamino)ethyl methacrylate (DMAEMA), and 3-(*N,N*-dimethylamino)propyl methacrylate (DMAPMAE) are carefully determined and the obtained data will be put into relation to the literature known methacrylate families. The polymers analyzed via triple SEC measurement for the determination of the MHKS parameters are generated via RAFT polymerization and polymerization with a thiol as CTA, respectively. Although monomers containing amine functions are known to undergo side reactions with, for example, the thiocarbonyl functionality of RAFT agents^[188,189], the nitrogen-containing methacrylates investigated in the current study and polymerized via RAFT polymerization gave reasonable results. The monomers investigated in this work are depicted in the blue box in Figure 3.1 alongside the previously studied UMA. The methacrylates with cyclic and branched ester side chains displaying family type behavior and discussed in the current chapter, are depicted in the green boxes in Figure 3.1.

3. Nitrogen-Containing Methacrylates

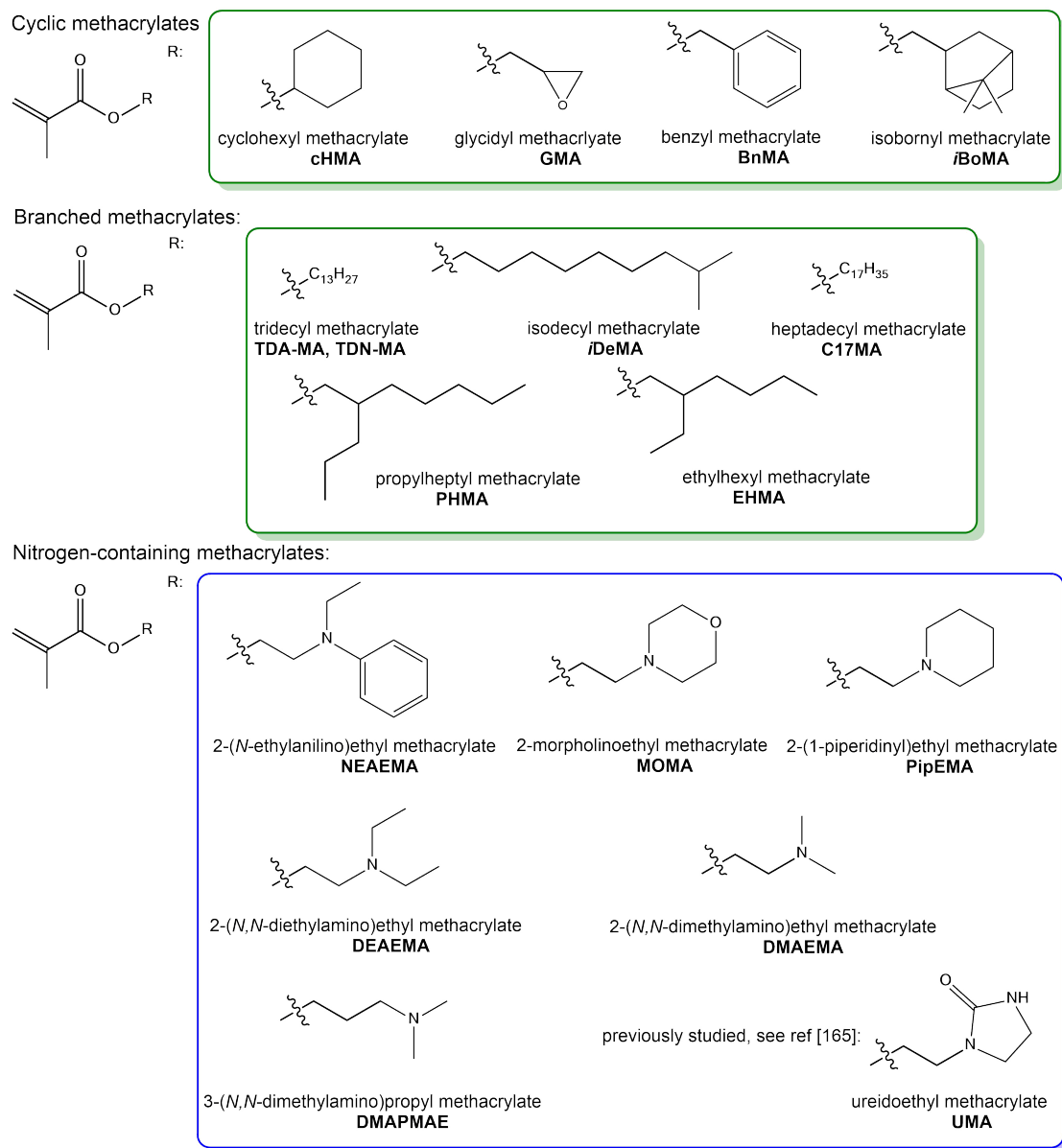


Figure 3.1.: Monomer Landscape. The nitrogen-containing methacrylates investigated in the current study are depicted in the blue box alongside the first investigated N-containing methacrylate ureidoethyl methacrylate (UMA): 2-(*N*-ethylanilino)ethyl methacrylate (NEAEMA), 2-morpholinoethyl methacrylate (MOMA), 2-(1-piperidyl)ethyl methacrylate (PipEMA), 2-(*N,N*-diethylamino)ethyl methacrylate (DEAEMA), 2-(*N,N*-dimethylamino)ethyl methacrylate (DMAEMA), and 3-(*N,N*-dimethylamino)propyl methacrylate (DMAPMAE). Methacrylates that showed a family type behavior are depicted in the green boxes: cHMA, GMA, BnMA, and iBoA as the family of cyclic methacrylates as well as TDA-MA, TDN-MA, iDeMA, C17MA, PHMA, and EHMA as a family of branched methacrylates.

3.1. MHKS Parameters

In Chapter 1.4.1, the need for polymer specific MHKS parameters for the correct determination of monomer specific propagation rate coefficients was already emphasized. For a most precise determination of the propagation rate coefficients and Arrhenius parameters, the microstructure of the polymer samples employed for the determination of the MHKS parameters should be the same as for the samples employed in the Arrhenius plots. For methacrylates, the microstructure of the polymers, regarding possible chain branching, does not vary as much as for the acrylates between samples generated via different polymerization types. The formation of MCRs and transfer to polymer reactions during conventional free radical polymerization of methacrylates is negligible, thus the microstructure and, therefore, the hydrodynamic volume of the polymer samples is not significantly influenced by the polymerization method. Other important conditions for the application of suitable MHKS parameters are the solvent and temperature employed for the determination of the parameters, since both can influence the elution behavior of the polymer during SEC measurement. In the case of methacrylates – due to the less pronounced influence of the polymerization method – it is generally possible to employ literature known MHKS parameter determined under the same solvent and temperature conditions as the polymer samples of interest. However, no MHKS parameters were known in literature for neither of the investigated nitrogen-containing methacrylates, making the generation of polymeric samples for the determination of MHKS parameters inevitable. To determine the MHKS parameters of NEAEMA, MOMA, PipEMA, DEAEMA, DMAEMA, and DMAPMAE in the course of the current study, polymer samples of each monomer were generated via RAFT polymerization or polymerization with dodecanethiol as a chain transfer agent to obtain polymers with dispersities of up to 2.0. The obtained polymer samples were subsequently repeatedly analyzed via a triple detection SEC setup with THF as eluent at 35 °C, employing the exact sample concentration as well as the refractive index increment, dn/dc , describing the change of the refractive index with a change of sample concentration. To calculate the exact monomer concentrations at the temperature of the measurement, the temperature-dependent density functions are employed.

3. Nitrogen-Containing Methacrylates

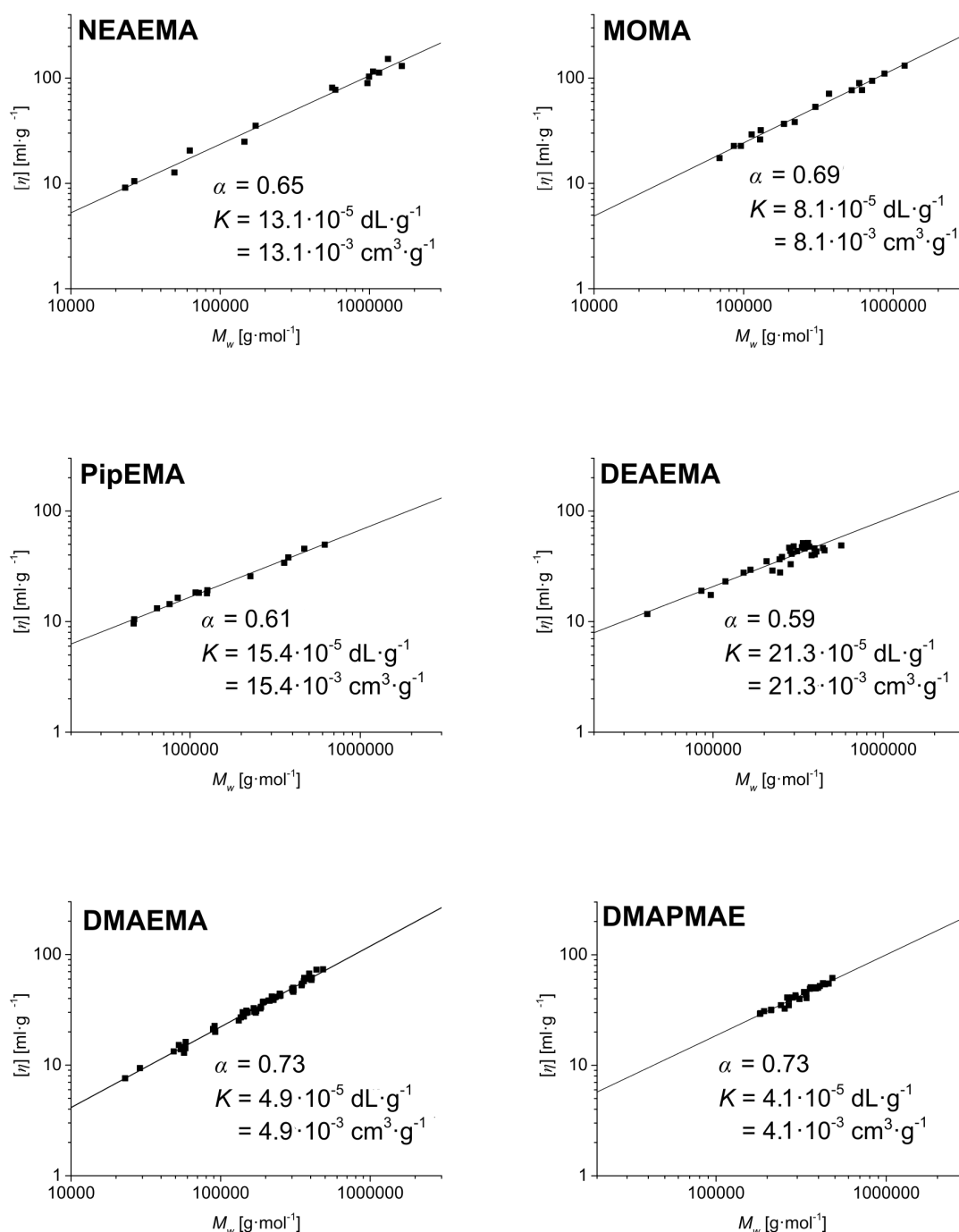


Figure 3.2.: $[\eta]$ vs. M_w plots with linear fits for the determination of MHKS parameters in THF at 35 °C for nitrogen-containing methacrylates: poly(2-(*N*-ethylanylino)ethyl methacrylate) (pNEAEMA), poly(2-morpholinoethyl methacrylate) (pMOMA), poly(2-(1-piperidyl)ethyl methacrylate) (pPipEMA), poly(2-(*N,N*-diethylamino)ethyl methacrylate) (pDEAEMA), poly(2-(*N,N*-dimethylamino)ethyl methacrylate) (pDMAEMA), and poly(3-(*N*-dimethylamino)propyl methacrylate) (pDMAPMAE). The corresponding monomer structures are depicted in Figure 3.1. The resulting MHKS parameters are collated in Table 3.1. Adapted with permission from refs. [134] and [135]. Copyright 2016 Royal Society of Chemistry and American Chemical Society.

Plotting the intrinsic viscosities, $[\eta]$, versus the molecular weight, M_w , the MHKS parameters can be deduced from the slope and y-intercept of the linear fit. The slope of the linear fit corresponds to the α exponent and the y-intercept refers to the prefactor K , as previously noted (see Chapter 1.4.1). All nitrogen-containing methacrylates investigated in the current study show a strict linear behavior in the MHKS plots depicted in Figure 3.2 over a wide molecular weight range (in case of NEAEMA over two orders of magnitude). For the most reliable results, MHKS parameters should only be applied for polymeric samples within the molecular weight range at which those parameters were determined^[143]. However, as described in Chapter 1.4.1, the molecular weight range can be experimentally restricted especially in the low molecular weight range due to the decreased quality of MALLS signals for low molecular weight species. Broadening the investigated molecular weight range significantly enhances the accuracy of the determined MHKS parameters and allows for more reliable extrapolations.

In the case of DEAMEA, a higher deviation of the data points compared to the other investigated monomers is observed. However, the reliability of the stated MHKS parameters was confirmed by several remeasurements of the polymer samples and no deviations exceeding the SEC error ranges were observed. While for NEAEMA, MOMA, PipEMA, DEAEMA, and DMAEMA the obtained molecular weights spanned over at least one order of magnitude, for DMAPMAE only a limited molecular weight range could be covered. Attempts to obtain acceptable SEC traces below approximately 150 000 $\text{g}\cdot\text{mol}^{-1}$ and above 500 000 $\text{g}\cdot\text{mol}^{-1}$ were not successful. Yet, the obtained data points feature a strict linear behavior with very low deviations of the data from linearity, allowing for the determination of suitable MHKS parameters. In the case of NEAEMA and MOMA, molecular weights well over $1\cdot 10^6$ $\text{g}\cdot\text{mol}^{-1}$ could be obtained. For the four remaining monomers, no molecular weights above approximately $6\cdot 10^5$ $\text{g}\cdot\text{mol}^{-1}$ were achieved, even when significantly reducing the concentration of the CTA. For most monomers, it was not possible to obtain analyzable SEC traces for low molecular weight samples (<30 000 $\text{g}\cdot\text{mol}^{-1}$) due to a poor signal to noise ratio, leading to the impossibility to determine a clear maximum of the signal. For NEAEMA and DMAEMA, polymer samples with molecular weights as low as 23 000 $\text{g}\cdot\text{mol}^{-1}$ could be incorporated into the MHKS plots since they gave analyzable SEC traces and clearly supported the linear trend of the higher molecular weight samples.

Representative triple detection SEC traces of the polymer samples employed for the determination of the MHKS parameters are depicted in Figures A.14 to A.19 in Appendix A. The obtained weight average molecular weights (M_w), intrinsic viscosities ($[\eta]$), as well as dispersities, D , are collated in Tables A.12 and A.13 in Appendix A. The MHKS parameters determined for the nitrogen-containing methacrylates and employed for

the calculation of the propagation rate coefficients are displayed in Table 3.1 alongside the molecular weights of the monomers, the refractive index increments, the glass transition temperatures, and the temperature dependent densities.

Table 3.1.: Collation of monomer and polymer specific physical data of the methacrylates investigated in the current study. The molecular weight of the monomer (MW) as well as the temperature-dependent densities in bulk (ρ_0 , b), the refractive index increment, the glass transition temperatures, and the MHKS parameters in THF at 35 °C (K , α) are stated.

monomer	MW [g·mol ⁻¹]	ρ_0 [g·mL ⁻¹]	b [g·m ⁻¹ ·°C]	dn/dc [mL·g ⁻¹]	T_g [°C]	K [cm ³ ·g ⁻¹]	α
NEAEMA	233.3	1.05665	8.4416×10^{-4}	0.144	38	13.1×10^{-3}	0.650
MOMA	199.2	1.06603	9.0284×10^{-4}	0.103	44	8.1×10^{-3}	0.695
PipEMA	197.2	0.99507	8.8055×10^{-4}	0.103	26	15.4×10^{-3}	0.607
DEAEMA	185.3	0.94290	8.8723×10^{-4}	0.089	-15	21.35×10^{-3}	0.597
DMAEMA	157.2	0.95453	9.5491×10^{-4}	0.086	0	4.98×10^{-3}	0.729
DMAPMAE	171.2	0.94294	9.0342×10^{-4}	0.079	-6	4.09×10^{-3}	0.731

In general, the determination of MHKS parameters is also possible employing just a single broadly distributed polymer sample.^[152] During a triple detection SEC measurement, $[\eta]$ can be deduced for each elution increment of the sample, leading to a $[\eta]$ vs. M_w plot containing several $[\eta]$ - M_w relations of a single polymer sample. However, the main disadvantages of this method compared to the evaluation of several polymer samples, is the higher possibility of experimental errors as well as the limitation to a more narrow molecular weight range. Deviations of the calculated sample concentration or refractive index increment from the actual values or uncertainties in the SEC measurement (i.e. misalignment of the detector signals) lead to errors in each determined $[\eta]$ - M_w set, since the method relies on the measurement of a single sample and is, therefore, more susceptible to a single evaluation error. Employing a wide set of different polymer samples for the determination of MHKS parameters, however, covers a wider range of molecular weights and provides the possibility to easily detect samples that do not fit a linear $[\eta]$ - M_w relation.

Although MHKS parameters correlate with the hydrodynamic volume and, therefore, the flexibility of the eluting macromolecules, a MHKS parameter – structure relation does not seem to be present. For the nitrogen-containing polymers investigated in the current chapter, the prefactor varies from 4.09 to $21.35 \cdot 10^{-3}$ cm³·g⁻¹ and α from 0.597 to 0.731 without obvious correlations to the actual monomer structure. To date, a broad database of different MHKS parameters is reported, spanning over a wide variety of monomers, different polymerization techniques, and solvent or temperature conditions,^[80] yet no overarching trends have been proposed.

3.2. Arrhenius Parameters

In analogy to Chapter 2.2, the MHKS parameters determined for the nitrogen-containing methacrylates are employed to obtain accurate molecular weights of the inflection points of the SEC elugrams and determine reliable propagation rate coefficients and Arrhenius parameters. After analyzing the PLP generated polymer samples via SEC measurement employing universal calibration against narrowly distributed p(MMA) standards, the molecular weight at the inflection points can be recalculated according to Equation 1.7 employing the polymer specific MHKS parameters. The Figure 3.3 depicts the Arrhenius plots for the investigated nitrogen-containing methacrylates in bulk: 2-(*N*-ethylanilino)ethyl methacrylate, 2-morpholinoethyl methacrylate, 2-(1-piperidyl)ethyl methacrylate, 2-(*N,N*-diethylamino)ethyl methacrylate, 2-(*N,N*-dimethylamino)ethyl methacrylate, and 3-(*N,N*-dimethylamino)propyl methacrylate. Table 3.2 collates the obtained Arrhenius parameters A and E_A as well as the corresponding error margins. The propagation rate coefficients at 50 °C are provided for better comparison. Detailed sample conditions of all polymeric samples generated via PLP and incorporated into the final Arrhenius plots are collated in Tables A.6 to A.11 in the Appendix A alongside representative SEC elugrams for each investigated monomer (see Figures A.7 to A.12). Arrhenius parameters and error margins stated in Table 3.2 are calculated using the program CONTOUR V2.0.2 by van Herk^[159,169] with constant absolute error margins of 10% as standard deviations. The average errors of each data point lie well within the initially assumed error range, ranging from 2.9% for DMAEMA to 8.0% for DMAPMAE. The error ranges stated in Table 3.2 are the boundaries of the 95% joint confidence interval and all data points can be fitted within the 95% probability. The frequency factors lie in the typical magnitude for methacrylates around $2 \cdot 10^6 \text{ L} \cdot \text{mol}^{-1} \cdot \text{s}^{-1}$, being significantly lower than for acrylate type monomers. As previously described for the branched acrylates, the error ranges calculated for the prefactor A are significantly higher than errors for the activation energy, due to the extrapolated nature of the linear fit leading to higher uncertainties in the y-intercept when errors in the slope are assumed.

3. Nitrogen-Containing Methacrylates

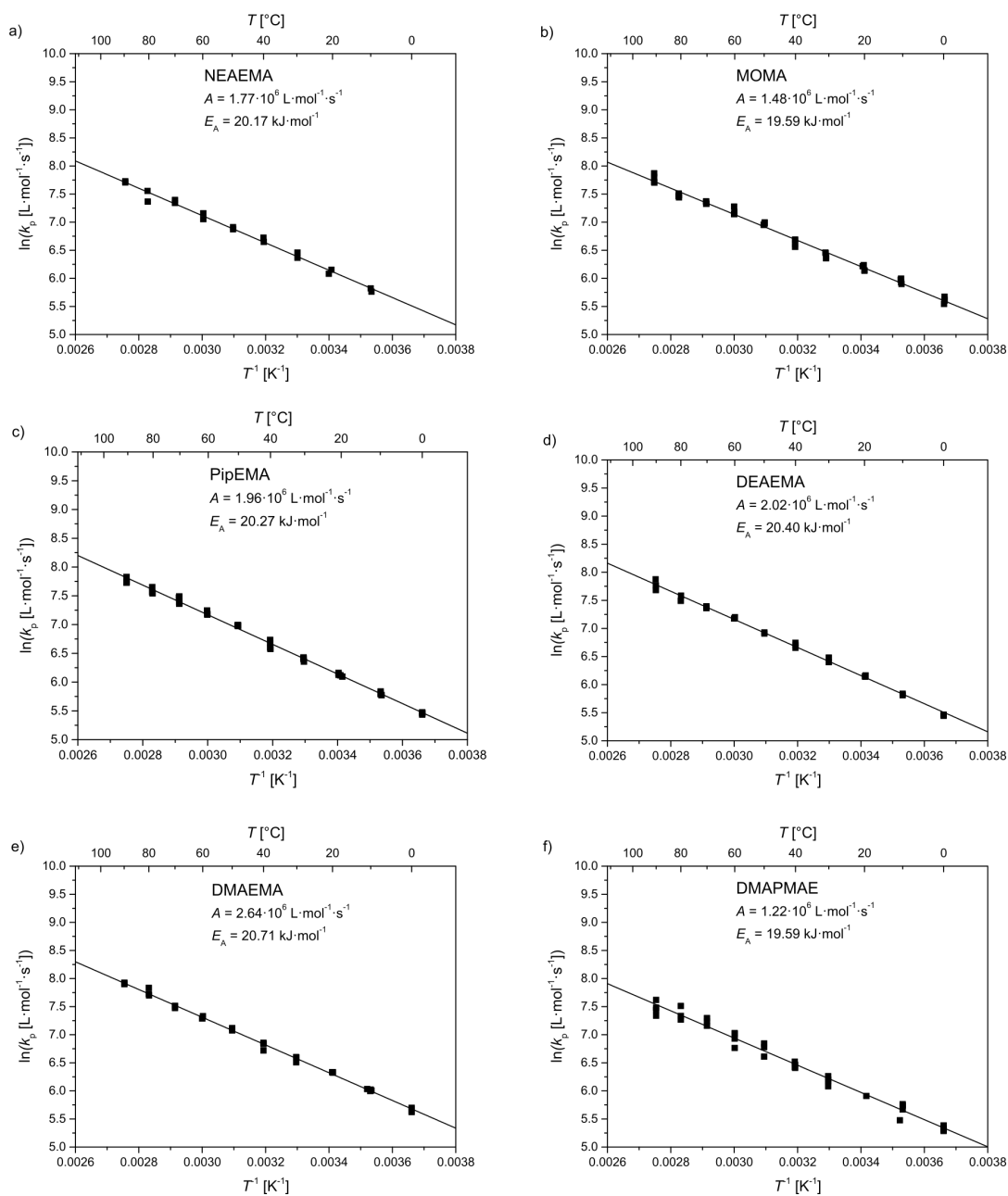


Figure 3.3.: $\ln(k_p)$ versus T^{-1} plots for the determination of Arrhenius parameters for nitrogen-containing methacrylates for a) 2-(*N*-ethylanylino)ethyl methacrylate (NEAEMA), b) 2-morpholinoethyl methacrylate (MOMA), c) 2-(1-piperidyl)ethyl methacrylate (PipEMA), d) 2-(*N,N*-diethylamino)ethyl methacrylate (DEAEMA), e) 2-(*N,N*-dimethylamino)ethyl methacrylate (DMAEMA), and e) 3-(*N,N*-dimethylamino)propyl methacrylate (DMAPMAE). The corresponding monomer structures are depicted in Figure 3.1. The Arrhenius parameters are collated in Table 3.2 jointly with the associated error margins. Adapted with permission from refs. [134] and [135].

Table 3.2.: Arrhenius parameters with error margins, propagation rate coefficients at 50 °C, and investigated temperature intervals for nitrogen-containing methacrylates in bulk. ^aJoint Arrhenius parameters can be described for NEAEMA, MOMA, PipEMA, and DEAEMA. Adapted with permission from refs. [134] and [135].

monomer	A [L·mol ⁻¹ ·s ⁻¹]	\pm	E_A [kJ·mol ⁻¹]	\pm	$k_p^{50^\circ\text{C}}$ [L·mol ⁻¹ ·s ⁻¹]	T -interval [°C]
NEAEMA	1.77×10^6	-7.51×10^5 5.74×10^6	20.17	-2.57 2.87	972	0 to 90
MOMA	1.48×10^6	-5.80×10^5 4.22×10^6	19.59	-2.12 2.72	1008	0 to 91
PipEMA	1.96×10^6	-6.46×10^5 2.92×10^6	20.27	-1.47 1.97	1036	0 to 90
DEAEMA	2.07×10^6	-7.89×10^5 3.89×10^6	20.45	-2.02 2.28	1024	0 to 90
DMAEMA	2.64×10^6	-7.90×10^5 1.98×10^6	20.71	-1.31 1.32	1185	0 to 90
DMAPMAE	1.22×10^6	-5.35×10^5 8.02×10^6	19.59	-2.74 3.83	831	0 to 90
Joint Fit ^a	1.55×10^6	-5.66×10^5 3.88×10^6	19.69	-1.76 2.6	1021	

The Arrhenius plots of all nitrogen-containing methacrylates investigated in the current study showed a clear linear behavior over the depicted temperature range and no significant deviations from linearity are observed for any of the data points. For methacrylates, the acrylate typical side reactions such as backbiting, leading to composites of $k_{p,\text{sec}}$ and $k_{p,\text{tert}}$ and blurring of the PLP typical SEC distribution are mainly negligible. Therefore, lower pulse frequencies are sufficient to obtain suitable PLP patterns and higher temperatures can be applied. For the methacrylates investigated in the current study, temperature ranges of 0 to 90 °C were employed and for all monomers at least three – in some cases even up to seven – inflection points could be detected. The data points obtained for DMAPMAE display higher deviations from the linear fit than observed for the other investigated monomers and feature the highest error (8.0%), yet none of the data points exceed the previously stated error limit of 10%. Solely samples fulfilling the consistency criteria – displaying at least two inflection points, independency of k_p on the initiator concentration, pulse energy, or pulse frequency, and a $k_{p,1}/k_{p,2}$ ratio of close to unity – are incorporated into the final Arrhenius plots.

$k_{p,1}/k_{p,2}$ values of each sample included in Figure 3.3 lie between 0.92 and 1.1 and are collated in Tables A.6 to A.11 in the Appendix A. For NEAEMA, MOMA, PipEMA, and DEAEMA, a set of joint Arrhenius parameters can be described and will be discussed in detail in the subsequent section.

3.3. Trends and Family Type Behaviour

In the current chapter, the reported propagation rate coefficients and Arrhenius parameters are discussed with respect to trends and family type behavior within the investigated monomer group of nitrogen-containing methacrylates. The first group of nitrogen-containing methacrylates investigated in the course of the current study comprise NEAEMA, MOMA, and PipEMA. The family type behavior observed within this group will be critically compared to the first investigated nitrogen-containing methacrylate UMA as well as the families of cyclic and branched methacrylates and a hypothesis for the differences between the monomer families will be tendered. Subsequently, the ester side chain will be systematically altered with respect to spacer length and branching length to identify the boundaries of the proposed family.

Examining the Arrhenius parameters for NEAEMA, MOMA, and PipEMA, it is apparent that the prefactors as well as activation energies of the monomers lie in close proximity to each other. To enable a valid statement on a possible family type behavior, an inspection of the propagation rate coefficients at different temperatures is necessary. An overview of the k_p data of NEAEMA, MOMA, and PipEMA is provided in Figure 3.4 and the propagation rate coefficients at 50 °C are additionally stated in Table 3.2. The depicted propagation rate coefficients are derived from the monomer specific Arrhenius parameters according to Equation 1.8 for -50, 0, 50, and 100 °C. The calculated values are in good agreement with the experimentally obtained data. By plotting k_p against the monomers, it is evident that the data are almost identical for all depicted temperatures and a family type behavior can readily be observed. For the lower temperatures, the propagation rate coefficients for MOMA deviate to higher k_p values, while PipEMA displays slight deviations to larger k_p values at elevated temperatures. However, these deviations do not exceed approximately 14% for MOMA at the lowest depicted temperature ($k_p^{50^\circ\text{C}} = 38.4 \text{ L}\cdot\text{mol}^{-1}\cdot\text{s}^{-1}$ for MOMA vs. $33.6 \text{ L}\cdot\text{mol}^{-1}\cdot\text{s}^{-1}$ for NEAEMA) and 7% for PipEMA at the highest depicted temperature ($k_p^{100^\circ\text{C}} = 2849.0 \text{ L}\cdot\text{mol}^{-1}\cdot\text{s}^{-1}$ for PipEMA vs. $2657.1 \text{ L}\cdot\text{mol}^{-1}\cdot\text{s}^{-1}$ for NEAEMA), being acceptable error ranges within the temperatures relevant for applications and lying within the generally assumed SEC error margins.

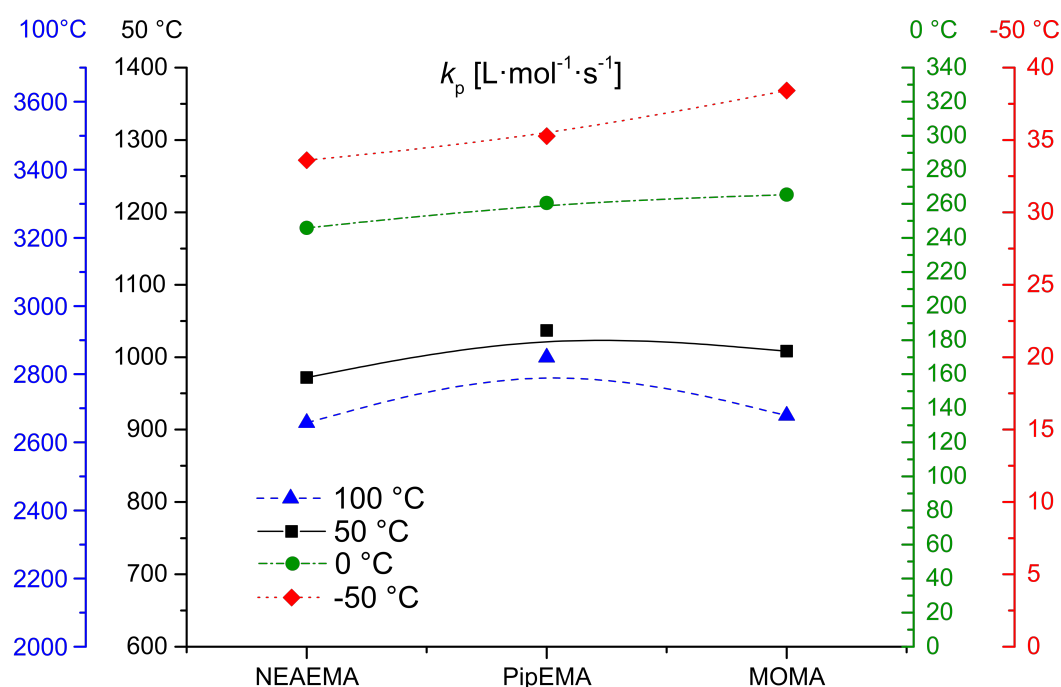


Figure 3.4.: Propagation rate coefficients for 2-(*N*-ethylanilino)ethyl methacrylate (NEAEMA), 2-morpholinoethyl methacrylate (MOMA), and 2-(1-piperidyl)ethyl methacrylate (PipEMA) at different temperatures: Left outer scale, blue dashed line = $k_p(100^\circ\text{C})$; left inner scale, black solid line = $k_p(50^\circ\text{C})$; right inner scale, green dot-dashed line = $k_p(0^\circ\text{C})$; right outer scale, red dotted line = $k_p(-50^\circ\text{C})$. The lines are no fits and solely for guiding the eye. Reprinted with permission from ref. [134]. Copyright 2016 Royal Society of Chemistry.

For all depicted temperatures, NEAEMA features the lowest propagation rates, yet still in an acceptable range to describe a family type behavior for NEAEMA, MOMA, and PipEMA. The different behavior of k_p at lowered/elevated temperatures is caused by the variations in the activation energy, descending from the different slopes of the Arrhenius plot. Comparing the monomer structures of MOMA and PipEMA depicted in Figure 3.1, it stands to reason that these deviations of k_p at lowered/elevated temperatures are found in the only structural difference between the two monomers, namely the oxygen atom within the morpholino group. Although this oxygen atom seems to be rather chemically unreactive, it might be able to induce dipoles, leading to a positively polarized carbon atom in its direct proximity and a negatively polarized oxygen atom. Such a polarization of the morpholino ring can possibly lead to a pre-structuring of the monomer solution with an opposed alignment of the ester side chains, enhancing the propagation rate coefficient. For the majority of the investigated temperature range, this effect seems to be quite negligible, yet lowers the activation energy in a way that, due to the reduced slope of the Arrhenius plot, a decrease of k_p in the sub-zero temperature range is observed. However, it needs to be kept in mind that the temperatures for the

experimentally assessed k_p data did not range below 0 °C and the data depicted at -50 °C are solely values extrapolated from the determined Arrhenius parameters. Since no melting points for NEAEMA, MOMA, and PipEMA are known so far, it is not certain to which degree it is possible to conduct bulk experiments at decreased temperatures and, therefore, no final statement can be made on how reliable these values are compared to experimentally obtained data.

An inspection of the deduced Arrhenius parameters shows a close correlation of the data for NEAEMA, MOMA, and PipEMA and the observation of a family type behavior becomes even more evident when combining the Arrhenius plots to a joint fit as depicted in Figure 3.5. The Arrhenius parameters for the joint fit read $A=1.83 \cdot 10^6 \text{ L}\cdot\text{mol}^{-1}\cdot\text{s}^{-1}$ and $E_A=20.14 \text{ kJ}\cdot\text{mol}^{-1}$ and features an average error of the data points of 5.4%, lying well within the errors obtained for the single monomers (between 4.6 and 6.0%).

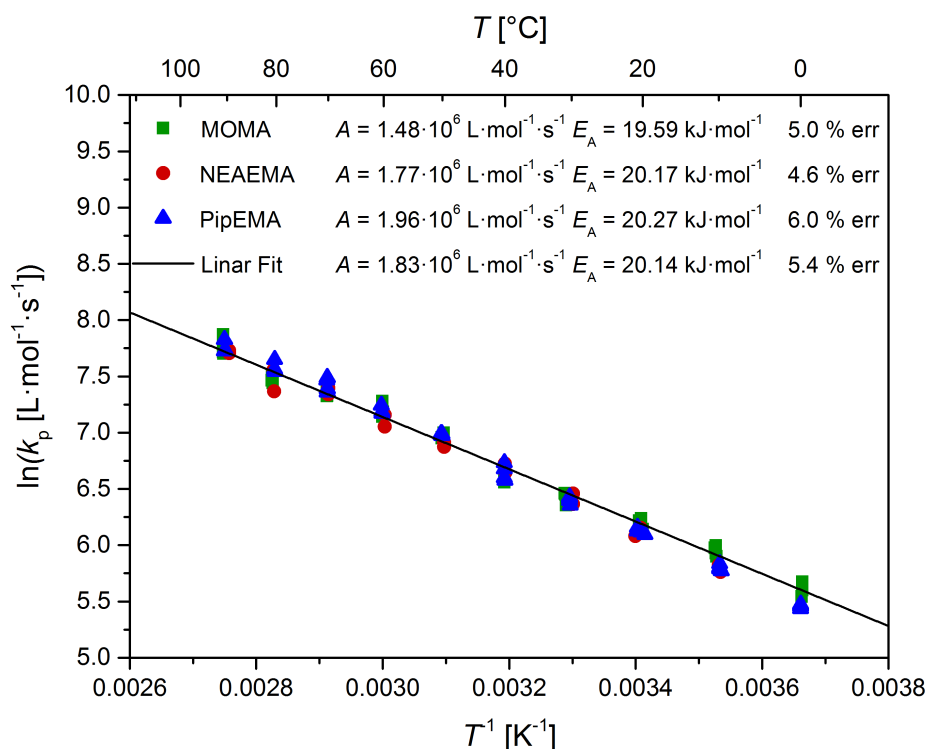


Figure 3.5.: Combined Arrhenius plot for 2-(*N*-ethylanilino)ethyl methacrylate (NEAEMA), 2-morpholinoethyl methacrylate (MOMA), and 2-(1-piperidyl)ethyl methacrylate (PipEMA) in bulk. A joint linear fit can be applied. Reprinted with permission from ref [134]. Copyright 2016 Royal Society of Chemistry.

Comparable to the single Arrhenius plots, for each data point an error of 10% in the propagation rate coefficients was assumed for the calculation of the joint fit, lying well above the calculated error of 5.4%.

As previously noted, in the case of the methacrylates with branched ester side chains, the exact structure, shape, and position of the branching point of the side chain was not found to have a major impact on the propagation rate coefficient as long as a similar steric demand was present.^[130] This description seems to be valid for the observations made for NEAEMA, MOMA, and PipEMA and is supported by *ab initio* and semi-empirical quantum calculations by Heuts *et al.*^[174] In the case of methacrylates, Heuts proposed that the main influence of the hindrance to internal rotations is governed by the methyl and carbonyl groups at the radical terminus, not the ester side chain. The increase in propagation rate coefficients with increasing ester side chain length was attributed to the increase in molar mass, influencing the vibrational and rotational partition functions. However, these *ab initio* calculations were only performed for non-polar, small monomer systems such as ethylene or methacrylates with small alkyl ester side chains, and just theoretically transferred to more complex monomer systems, since for direct calculations of more challenging monomers a high level of computational resources is required. In the case of the nitrogen-containing methacrylates, additional focus needs to be placed on the polarity of the ester side chain. As already mentioned in the case of possibly induced polarities in the morpholino ring of MOMA, the polarity of the ester side chain should also have an influence on the Arrhenius parameters due to a stronger interaction with the transition state. A more pronounced polarity of the ester side chain leads to a stronger influence with the transition state, resulting in a lowering of the activation energy, as observed in the case of MOMA compared to PipEMA. In addition, this more pronounced interaction with the transition state is expected to result in an increased hindrance of the internal rotations, ultimately lowering the frequency factor. Taking these considerations into account (transition state mainly influenced by α -methyl group, higher k_p with increased monomer mass, and influence of polar side chains on the transition state), a family type behavior can be expected among methacrylic monomers with comparable molar masses and ester side chains that exhibit comparable polarities and similar steric demands.

3.3.1. Expanding the Family

After the description of a family type behavior for NEAEMA, MOMA, and PipEMA it is of high interest to further investigate how the structure of the ester side chain may influence the propagation rate for nitrogen-containing methacrylates and where the boundaries of the proposed family lie. To achieve a deeper insight into the possible influence of the ester side chain, two strategies are pursued: A stepwise reduction of the number of CH_2 groups situated at the nitrogen atom starting from PipEMA over DEAEMA to DMAEMA and the subsequent extension of the alkyl linker between the ester moiety and the nitrogen atom from DMAEMA to DMAPMAE. Therefore, DEAEMA, DMAEMA, and DMAPMAE (see Figure 3.1) are investigated with respect to their propagation rate coefficients and critically compared to the previously proposed family.

The left hand side of Figure 3.6 displays the combined Arrhenius plots for DEAEMA, DMAEMA, and DMAPMAE and it is evident that the monomers do not qualify for a joint Arrhenius fit. Although single data points of DEAEMA and DMAEMA overlap, it is clearly visible that the data scattering within each monomer is significantly lower than the scattering between the different monomers, and no single fit would be appropriate. On the right hand side of Figure 3.6, the propagation rate coefficients over an extended temperature range are displayed with the monomers arranged in order as investigated and as they will be discussed in the current chapter.

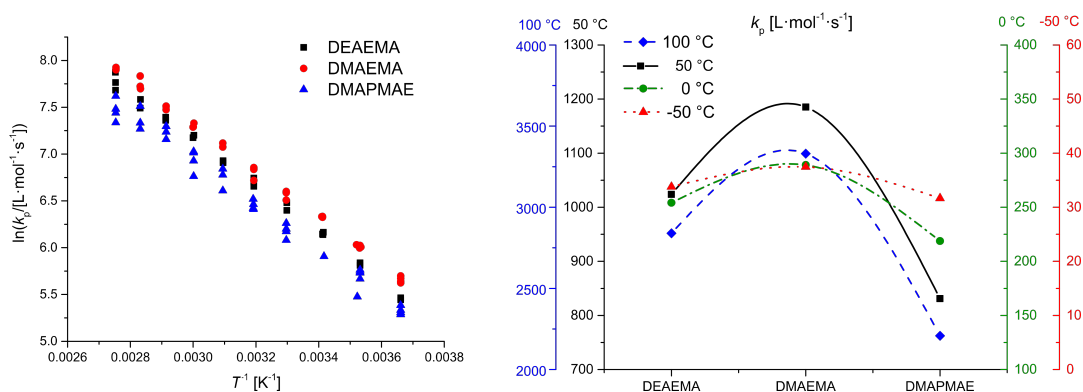


Figure 3.6.: Left: Combined Arrhenius plots for 2-(*N,N*-diethylamino)ethyl methacrylate (DEAEMA), 2-(*N,N*-dimethylamino)ethyl methacrylate (DMAEMA), and 3-(*N,N*-dimethylamino)propyl methacrylate (DMAPMAE) in bulk. A joint linear fit is not appropriate. Right: Propagation rate coefficients for DEAEMA, DMAEMA, and DMAPMAE at different temperatures: blue dashed line = 100 °C, black solid line = 50 °C, green dot-dashed line = 0 °C, and red dotted line = -50 °C. The monomers are displayed in order as investigated and discussed in the text. The lines are no fits and solely for guiding the eye. Reprinted with permission from ref [135]. Copyright 2016 American Chemical Society.

The depicted k_p values are calculated employing the Arrhenius parameters and are in good agreement with the experimentally determined values. For all four depicted temperatures (-50, 0, 50, and 100 °C), DMAEMA displays elevated propagation rate coefficients while DMAPMAE exhibits significantly decreased k_p values compared to DEAEMA. Although the data seem to be in agreement for each monomer at the lowest temperature, the deviations between DMAPMAE and DMAEMA already exceed 30% at 0 °C. As mentioned earlier, no propagation rate coefficients were determined below 0 °C and since no melting points are known for the investigated monomers, it is not certain how well the data extrapolated to -50 °C reflect an actual experimental behavior. Going to elevated temperatures, the differences between the monomers becomes even more obvious, reaching up to 50% deviation between DMAPMAE and DMAEMA at 100 °C. Since the inspection of the combined Arrhenius plots and propagation rates clearly dismisses the introduction of DEAEMA, DMAEMA, and DMAPMAE in a joint family, in the following each monomer will be individually discussed and compared to the family of nitrogen-containing methacrylates.

To commence the detailed discussion of each monomer, 2-(*N,N*-diethylamino)ethyl methacrylate (DEAEMA) will be reviewed, displaying an ester side chain reduced by one CH₂ group at the piperidyl ring compared to 2-(1-piperidyl)ethyl methacrylate (PipEMA). Both Arrhenius parameters – A and E_A – determined for DEAEMA are higher than the joint parameters for NEAEMA, MOMA, and PipEMA, (see 3.5) yet lie in close proximity to the Arrhenius parameters determined for PipEMA with $A=2.07 \cdot 10^6 \text{ L} \cdot \text{mol}^{-1} \cdot \text{s}^{-1}$, $E_A=20.45 \text{ kJ} \cdot \text{mol}^{-1}$ for DEAEMA, and $A=1.96 \cdot 10^6 \text{ L} \cdot \text{mol}^{-1} \cdot \text{s}^{-1}$, $E_A=20.27 \text{ kJ} \cdot \text{mol}^{-1}$ for PipEMA. Inspection of the left hand part of Figure 3.7 shows a clear overlap of the Arrhenius plots of DEAEMA with the previously discussed nitrogen-containing methacrylates over the entire investigated temperature range and the data scattering between the different monomers does not exceed the scattering withing each depicted monomer. This close agreement of the determined propagation rate coefficients for DEAEMA with the family of nitrogen-containing methacrylates is also clearly featured in the right hand part of Figure 3.7, depicting the propagation rate coefficients for DEAEMA, NEAEMA, MOMA, and PipEMA at -50, 0, 50, and 100 °C. The depicted k_p values are calculated by employing the determined Arrhenius parameters and for all four temperature ranges, a good agreement between DEAEMA and the previously discussed monomers is observed. Differences in the propagation rate coefficient between DEAEMA and PipEMA range from 0.3% at 100 °C to 4.4% at -50 °C and between DEAEMA and the previously described family from 0.8% at 100 °C to 4.4% at -50 °C, qualifying DEAEMA for an inclusion into the family of nitrogen-containing methacrylates.

3. Nitrogen-Containing Methacrylates

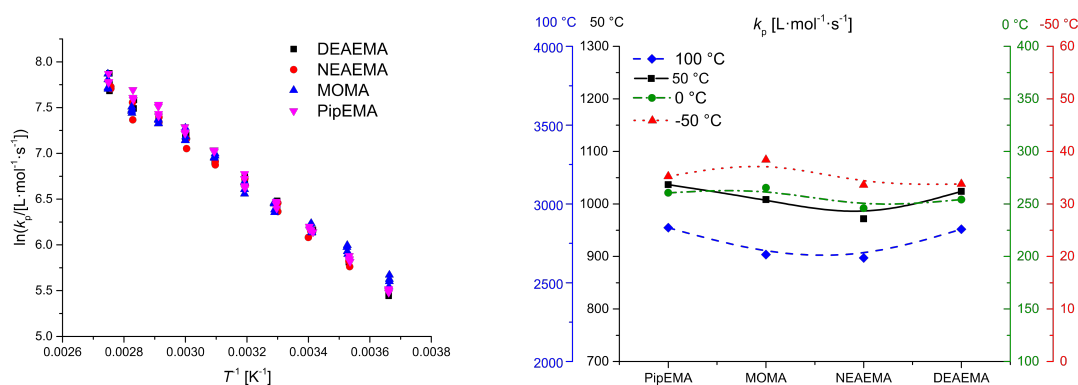


Figure 3.7.: Left: Combined Arrhenius plots for 2-(*N,N*-diethylamino)ethyl methacrylate (DEAEMA), 2-(*N*-ethylamino)ethyl methacrylate (NEAEMA), 2-morpholinoethyl methacrylate (MOMA), and 2-(1-piperidyl)ethyl methacrylate (PipEMA) in bulk. Right: Propagation rate coefficients for DEAEMA, NEAEMA, MOMA, and PipEMA at different temperatures: blue dashed line = 100 °C, black solid line = 50 °C, green dot-dashed line = 0 °C, and red dotted line = -50 °C. The lines are no fits and solely for guiding the eye. Reprinted with permission from ref [135]. Copyright 2016 American Chemical Society.

In the subsequent step, the side chains at the nitrogen atom will be reduced by two additional CH₂ groups, leading to 2-(*N,N*-dimethylamino)ethyl methacrylate (DMAEMA). Again, reducing the CH₂ groups resulted in an increase in the Arrhenius parameters, giving $A=2.64 \cdot 10^6$ L·mol⁻¹·s⁻¹ and $E_A=20.71$ kJ·mol⁻¹. However, the increase in Arrhenius parameters also results in elevated propagation rate coefficients as can be seen in Figure 3.8. In the combined Arrhenius plots on the left hand side of the figure, several data points for DMAEMA seem to partly overlap with PipEMA at higher temperatures and with MOMA in the lower temperature regions, however, no overlap with NEAEMA is observed and the scattering between the different monomers exceeds the scattering within the data for DMAEMA. Over the entire investigated temperature range, DMAEMA lies at the top end of the depicted Arrhenius plots. A closer look at the right hand part of Figure 3.8 shows a good agreement of the k_p values for DMAEMA with the previously investigated monomers at the lowest temperature -50 °C, yet clearly starts to deviate to higher propagation rate coefficients at 0 °C. The elevated activation energy of DMAEMA leads to a steeper slope and consequently to a faster increase of the propagation rate coefficient with increasing temperature, resulting in higher deviations from the proposed family at elevated temperatures. The differences in k_p between DMAEMA and PipEMA range from already 6.2% at -50 °C up to 17% at 100 °C and between DMAEMA and the joint fit for NEAEMA, MOMA, and PipEMA between 6.2% at -50 °C and 20% at 100 °C, just exceeding the SEC error margins of approximately 15%. Thus, DMAEMA appears to lie just at the edge of the proposed family, however,

due to the more pronounced deviations of k_p with increasing temperature, an inclusion into the family of nitrogen-containing methacrylates seems to be not advisable.

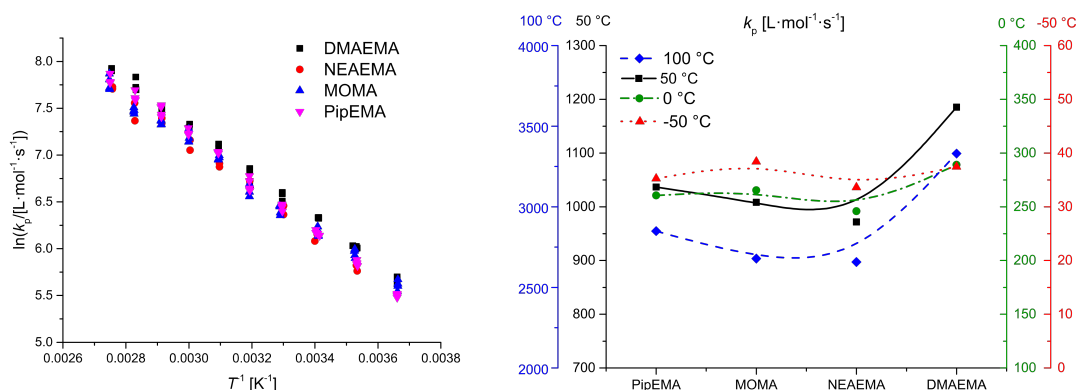


Figure 3.8.: Left: Combined Arrhenius plots for 2-(*N,N*-dimethylamino)ethyl methacrylate (DMAEMA), 2-(*N*-ethylamino)ethyl methacrylate (NEAEMA), 2-morpholinoethyl methacrylate (MOMA), and 2-(1-piperidyl)ethyl methacrylate (PipEMA) in bulk. Right: Propagation rate coefficients for DMAEMA, NEAEMA, MOMA, and PipEMA at different temperatures: blue dashed line = 100 °C, black solid line = 50 °C, green dot-dashed line = 0 °C, and red dotted line = -50 °C. The lines are no fits and solely for guiding the eye. Reprinted with permission from ref [135]. Copyright 2016 American Chemical Society.

To conclude the investigation of additional nitrogen-containing methacrylates and the influence of an alteration of the ester side chain length on the propagation rate coefficient, 3-(*N,N*-dimethylamino)propyl methacrylate (DMAPMAE) is examined, featuring an additional CH_2 group in the alkyl linker between the ester moiety and the nitrogen atom compared to DMAEMA. When expanding the ester side chain, the Arrhenius parameters are significantly lowered to $A=1.22\cdot 10^6 \text{ L}\cdot\text{mol}^{-1}\cdot\text{s}^{-1}$ and $E_A=19.59 \text{ kJ}\cdot\text{mol}^{-1}$. According to the explanation by Heuts *et al.*,^[174] changing to a more bulky unit leads to an increased hindrance of the internal rotations and lowering of the frequency factor, yet the decrease in A of DMAPMAE compared to DMAEMA seems surprisingly substantial, considering the only small change in the chemical structure. The left hand part of Figure 3.9, however, clearly shows the influence of the decreased Arrhenius parameters on the propagation rate coefficient. Over the entire investigated temperature range the Arrhenius plot for DMAPMAE lies significantly lower than the Arrhenius plots for NEAEMA, MOMA, and PipEMA. Although single data points show an overlap with the previously investigated methacrylates, the overall plot clearly lies outside of the acceptable error ranges and the description of a joint fit is not appropriate. The propagation rate coefficients depicted on the right hand side of Figure 3.9 for -50, 0, 50, and 100 °C confirm the assumptions of an exclusion of DMAPMAE from the family of nitrogen-containing methacrylates. Although the k_p value for the lowest depicted tem-

3. Nitrogen-Containing Methacrylates

perature seems to lie in acceptable range to the previously investigated methacrylates, a deviation to lower propagation rate coefficients becomes increasingly significant at elevated temperatures. The differences of the propagation rate coefficients between DMAPMAE and the joint fit for NEAEMA, MOMA, and PipEMA vary between 11.3% for -50 °C and 25.6% for 100 °C. With deviations of k_p clearly exceeding the SEC error ranges, it is evident that DMAPMAE does not qualify for an inclusion into the family of nitrogen-containing methacrylates.

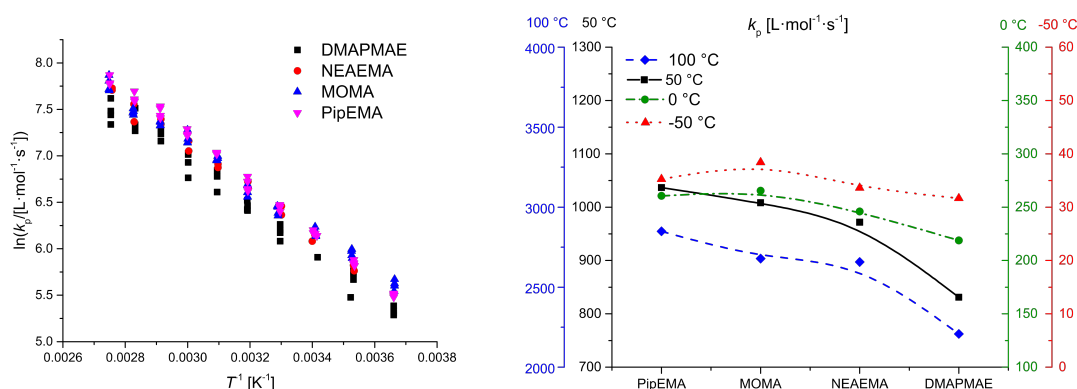


Figure 3.9.: Left: Combined Arrhenius plots for 3-(*N,N*-dimethylamino)propyl methacrylate (DMAPMAE), 2-(*N*-ethylanylino)ethyl methacrylate (NEAEMA), 2-morpholinoethyl methacrylate (MOMA), and 2-(1-piperidyl)ethyl methacrylate (PipEMA) in bulk. Right: Propagation rate coefficients for DMAPMAE, NEAEMA, MOMA, and PipEMA at different temperatures: blue dashed line = 100 °C, black solid line = 50 °C, green dot-dashed line = 0 °C, and red dotted line = -50 °C. The lines are no fits and solely for guiding the eye. Reprinted with permission from ref [135]. Copyright 2016 American Chemical Society.

The comparison of the additional nitrogen-containing methacrylates DEAEMA, DMAEMA, and DMAPMAE showed significant differences between these three monomers regarding Arrhenius parameters and propagation rate coefficients. Figure 3.10 clearly shows the increase in A and E_A with decreasing CH_2 groups when going from PipEMA to DMAEMA with A [$10^6 \text{ L}\cdot\text{mol}^{-1}\cdot\text{s}^{-1}$]=1.96 (PipEMA) to 2.07 (DEAEMA) to 2.64 (DMAEMA) and E_A [$\text{kJ}\cdot\text{mol}^{-1}$]=20.27 (PipEMA) to 20.45 (DEAEMA) to 20.71 (DMAEMA). As previously stated, due to the estimation of A via the extrapolation of the determined slope of the Arrhenius plot, A and E_A show a parallel behavior. In their studies of terminal and penultimate unit effects on the transition state, [33,174] Heuts *et al.* noted that exchanging the ester side chain with a bulkier unit leads to an increased hindrance of the torsion, lowering the frequency factor. When going from PipEMA to DMAEMA, the bulkiness of the ester side chain is reduced by the stepwise removal of CH_2 groups at

the amino function, consequently increasing the frequency factor. While removing a single CH_2 group from PipEMA to DEAEMA, just a slight increase in A is observed, due to a comparably low change in steric demand of the ester side chain. Decreasing the side chain by two more CH_2 groups, however, leads to a significantly higher increase of A attributed to a more drastic change in steric demand.

An interesting observation is certainly the significant decrease of the Arrhenius parameters and propagation rate coefficients from DMAEMA to DMAPMAE with A [$10^6 \text{ L}\cdot\text{mol}^{-1}\cdot\text{s}^{-1}$]=2.64 (DMAEMA) to 1.22 (DMAPMAE) and E_A [$\text{kJ}\cdot\text{mol}^{-1}$]=20.71 (DMAEMA) to 19.59 (DMAPMAE) leading to a difference in propagation rate coefficients of already 20% at -50°C up to 50% at 100°C . The Arrhenius plot of DMAEMA lies just slightly above the previously proposed family of nitrogen-containing methacrylates and the Arrhenius plot for DMAPMAE clearly exceeds the boundaries to significantly lower propagation rates, although both monomers merely differ by a single CH_2 group in the alkyl linker between the ester moiety and the nitrogen atom.

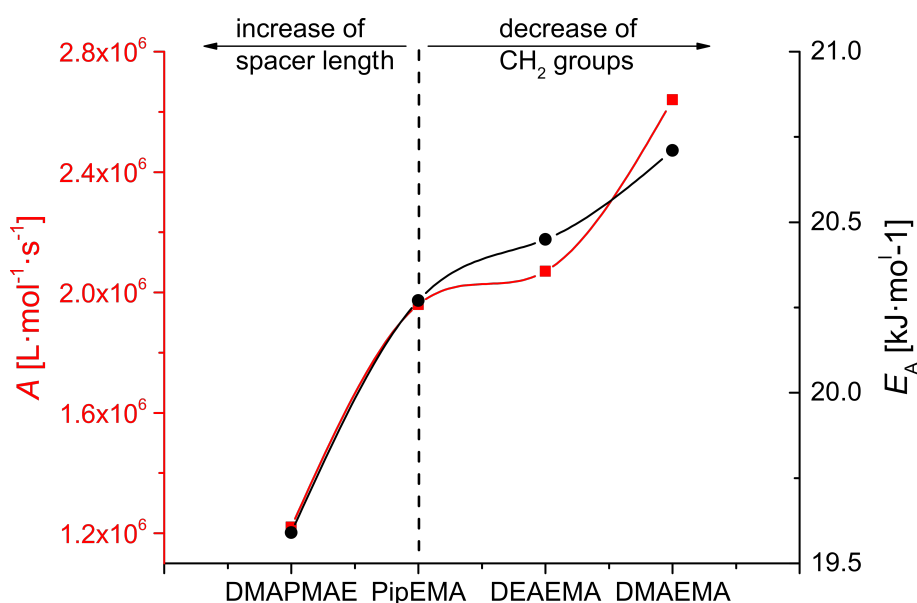


Figure 3.10. Arrhenius parameters of 3-(*N,N*-dimethylamino)propyl methacrylate (DMAPMAE), 2-(1-piperidyl)ethyl methacrylate (PipEMA), 2-(*N,N*-diethylamino)ethyl methacrylate (DEAEMA), and 2-(*N,N*-dimethylamino)ethyl methacrylate (DMAEMA). An increase in both Arrhenius parameters is observed when going from PipEMA to DMAEMA and a significant decrease in the Arrhenius parameters is observed when going to DMAPMAE. Reprinted with permission from ref [135]. Copyright 2016 American Chemical Society.

It was noted earlier that for the branched methacrylates, the exact shape and chemical structure of the ester side chain was not the major influencing factor of the propagation rate coefficient as long as the ester side chains displayed a similar steric demand.^[130] Although this hypothesis was supported by the findings for the first three monomers discussed in the current chapter (NEAEMA, MOMA, PipEMA), after expanding the investigated monomer group it is obvious that the hypothesis is not entirely transferrable for the nitrogen-containing methacrylates. The steric demand of the ester side chain is most likely not the only influencing factor, but it is also important to have a closer look at the polarities of the monomers. A more polar side chain reduces both Arrhenius parameters due to a stronger interaction with the transition state resulting in an increased hindrance of the internal rotations. In case of the branched methacrylates with their alkyl ester side chains, a difference in the polarities should not be assumed. For the nitrogen-containing methacrylates, however, the nitrogen atom holds potential for intramolecular interactions with the ester moiety. Such an intramolecular interaction can lead to induced polarities at the nitrogen atom and the carbonyl carbon, altering the electronic environment of the monomer. In the case of the investigated N-ethyl methacrylates (NEAEMA, MOMA, PipEMA, DEAEMA, DMAEMA), the nitrogen atom is situated too close to the ester moiety to favor ring formation and interacting with the propagating radical site.

For DMAPMAE, displaying a propyl linker between the ester moiety and the nitrogen atom, however, a possible convergency of the nitrogen atom and the ester moiety via the formation of a six-membered ring would lead to an interaction that significantly increases the (induced) polarity of the monomer and, therefore, the electronic environment of the propagating radical. The effect of different polarities on the propagation rate coefficient was already mentioned to describe the differences between PipEMA and MOMA, where a slight change in polarity of the morpholino ring might possibly be induced by the oxygen atom. However, in the case of MOMA, the more polar side chain is more likely to have an influence on a pre-structuring of the reaction solution and not directly on the propagating radical site due to its distance to the ester moiety. A hypothetical ring formation of the monomer as proposed for DMAPMAE, however, would have a crucial effect on the transition state due to a change in steric demand as well as a significant increase in polarity and, therefore, a change of the electronic environment of the propagating radical site, resulting in significantly reduced Arrhenius parameters.

The steric differences between PipEMA and DEAEMA due to the reduced CH₂ groups just induce a slight change in the Arrhenius parameters leading to propagation rate coefficients that do not exceed the error margins of the previously proposed family of

nitrogen-containing methacrylates. Further alteration of the ester side chain by removing two additional CH_2 groups and thus more pronounced reduction in steric demand further increases the Arrhenius parameters, resulting in elevated propagation rate coefficients and a marginal loss of the family type behavior. The possible interaction of the nitrogen atom with the ester moiety induced by the extension of the alkyl linker and the resulting significant changes in steric demand as well as electronic environment of the propagating radical site when going to DMAPMAE, leads to a considerable decrease in Arrhenius parameters and propagation rate coefficients.

The extended Arrhenius fits of DEAEMA, DMAEMA, and DMAPMAE calculated via the determined Arrhenius parameters are depicted in Figure 3.11 alongside the joint fit for NEAEMA, MOMA, and PipEMA. Inspection of Figure 3.11 shows that the Arrhenius fit for DEAEMA perfectly overlays with the joint Arrhenius fit for NEAEMA, MOMA, and PipEMA over the entire temperature range and clearly fits into the previously proposed family.

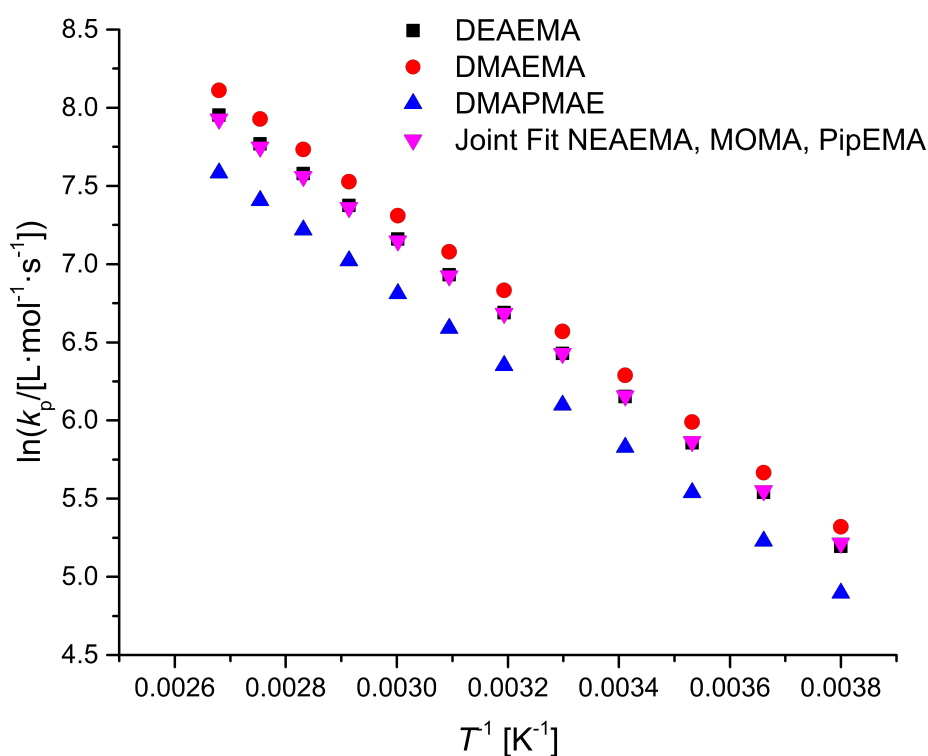


Figure 3.11.: Combined Arrhenius fits for 3-(*N,N*-dimethylamino)propyl methacrylate (DMAPMAE), 2-(*N,N*-diethylamino)ethyl methacrylate (DEAEMA), and 2-(*N,N*-dimethylamino)ethyl methacrylate (DMAEMA) as well as the joint fit for 2-(*N*-ethylamino)ethyl methacrylate (NEAEMA), 2-morpholinoethyl methacrylate (MOMA), and 2-(1-piperidyl)ethyl methacrylate (PipEMA) as calculated via the corresponding Arrhenius parameters. Reprinted with permission from ref [135]. Copyright 2016 American Chemical Society.

The propagation rate coefficients determined for DMAEMA are slightly elevated and over the entire temperature range the Arrhenius fit for DMAEMA lies just above the joint fit and although a slight converging of the fits is observable in the lower temperature ranges, no overlapping occurs until sub-zero temperatures, making it not advisable to include DMAEMA into the described family. The structural differences of DMAPMAE, resulting in significant changes in the steric demand and electronic environment of the monomer, influence the propagation rate coefficient in a way that over the entire extended temperature range the Arrhenius fit lies clearly below the joint fit for the family. No convergency or overlapping is observable, clearly disqualifying DMAPMAE for an inclusion in the family of nitrogen-containing methacrylates. It is interesting to note the differences in glass transition temperatures for the two investigated groups: While the T_g for NEAEMA, MOMA, and PipEMA lie between 26 and 44 °C, DEAEMA, DMAEMA, and DMAPMAE display lowered T_g between 0 and -15 °C (see Table 3.1). Although the glass transition temperatures are generally implying differences in physicochemical behavior, surprisingly the monomer with the lowest T_g (largest difference to the previously described family) perfectly fits into the family while DMAEMA and DMAPMAE do not display comparable propagation rate coefficients.

The addition of three nitrogen-containing methacrylates to the previously investigated NEAEMA, MOMA, and PipEMA aimed at testing the additional monomers for a possible inclusion into the family of nitrogen-containing methacrylates and to find the boundaries of the proposed family type behavior. It is found that based on different steric demands and polarities, DEAEMA qualifies for an inclusion while DMAEMA and DMAPMAE are not to be added to the family. Taking these findings into account, the updated joint fit for a family of N-ethyl methacrylates gives Arrhenius parameters of $A=1.55 \cdot 10^6 \text{ L} \cdot \text{mol}^{-1} \cdot \text{s}^{-1}$ and $E_A=19.68 \text{ kJ} \cdot \text{mol}^{-1}$.

3.3.2. Comparison to UMA

Before launching into a comparison of the proposed family of N-ethyl methacrylates to previously described methacrylic families, it is worthwhile to inspect the first investigated nitrogen-containing methacrylate, UMA (for chemical structure refer to Figure 3.1) and its relation to the newly proposed family. Although nitrogen-containing methacrylates are interesting monomers for a wide variety of industrial applications and are also of high interest for academic purposes, the first representative of this monomer group was not investigated before 2014, when Haehnel *et al.* stated the Arrhenius parameters

for UMA in DMac to be $A=2.08 \cdot 10^6 \text{ L} \cdot \text{mol}^{-1} \cdot \text{s}^{-1}$ and $E_A=19.90 \text{ kJ} \cdot \text{mol}^{-1}$. Due to the high melting point of UMA at approximately $44 \text{ }^\circ\text{C}$, the experimentally accessible temperature range was relatively narrow, making an investigation in solution more favorable. UMA still being a solid at elevated temperatures stands in contrast to most other methacrylates as well as the monomers of the family of N-ethyl methacrylates, which remain liquid even at a storage temperature of $-19 \text{ }^\circ\text{C}$. Those apparent physical differences are also reflected by differences in the glass transition temperatures of the monomers, where the T_g of UMA is remarkably high with $103 \text{ }^\circ\text{C}$.

Comparing solely the Arrhenius parameters stated for UMA with the parameters for NEAEMA, MOMA, PipEMA and DEAEMA, an inclusion of UMA into the family of N-ethyl methacrylates might seem like an appropriate choice. However, inspection of Figure 3.12 does clearly not support this assumption. UMA displays significantly higher propagation rate coefficients at all depicted temperatures with deviations from the joint parameters for the N-ethyl methacrylates of already 17% at $-50 \text{ }^\circ\text{C}$ up to 21% at $100 \text{ }^\circ\text{C}$, clearly exceeding the error margins.

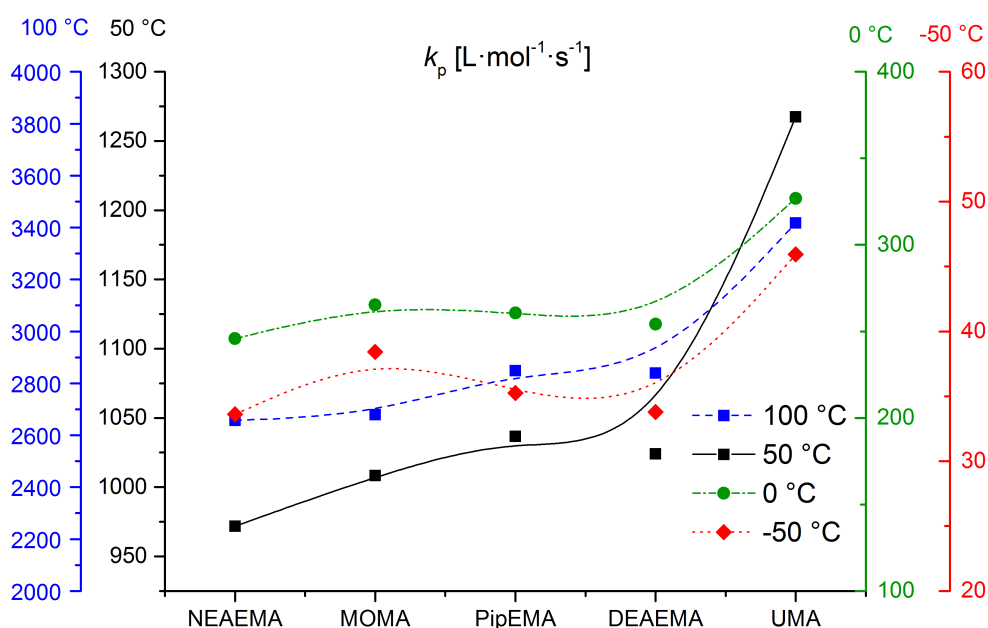


Figure 3.12.: Propagation rate coefficients for 2-(*N*-ethylanilino)ethyl methacrylate (NEAEMA), 2-morpholinoethyl methacrylate (MOMA), 2-(1-piperidyl)ethyl methacrylate (PipEMA), 2-(*N,N*-diethylamino)ethyl methacrylate (DEAEMA), and ureidoethyl methacrylate (UMA) at different temperatures. Left outer scale, blue dashed line = $k_p(100^\circ\text{C})$; left inner scale, black solid line = $k_p(50^\circ\text{C})$; right inner scale, green dot-dashed line = $k_p(0^\circ\text{C})$; right outer scale, red dotted line = $k_p(-50^\circ\text{C})$. Adapted with permission from ref [134].

Figure 3.13 displays the Arrhenius fit for UMA derived from the Arrhenius parameters stated in ref [186] as well as the joint fit for NEAEMA, MOMA, PipEMA, and DEAEMA. The elevated Arrhenius parameters compared to the parameters for the family of N-ethyl methacrylates – A [$10^6 \text{ L}\cdot\text{mol}^{-1}\cdot\text{s}^{-1}$]=2.08 (UMA) to 1.55 (family) and E_A [$\text{kJ}\cdot\text{mol}^{-1}$]=19.90 (UMA) to 19.68 (family) – lead to consequently higher $\ln(k_p)$ values for UMA over the entire temperature range and a linear behavior of the two fits without any overlapping data. UMA displays a similar molar mass as the N-ethyl methacrylates and is expected to feature a comparable steric demand.

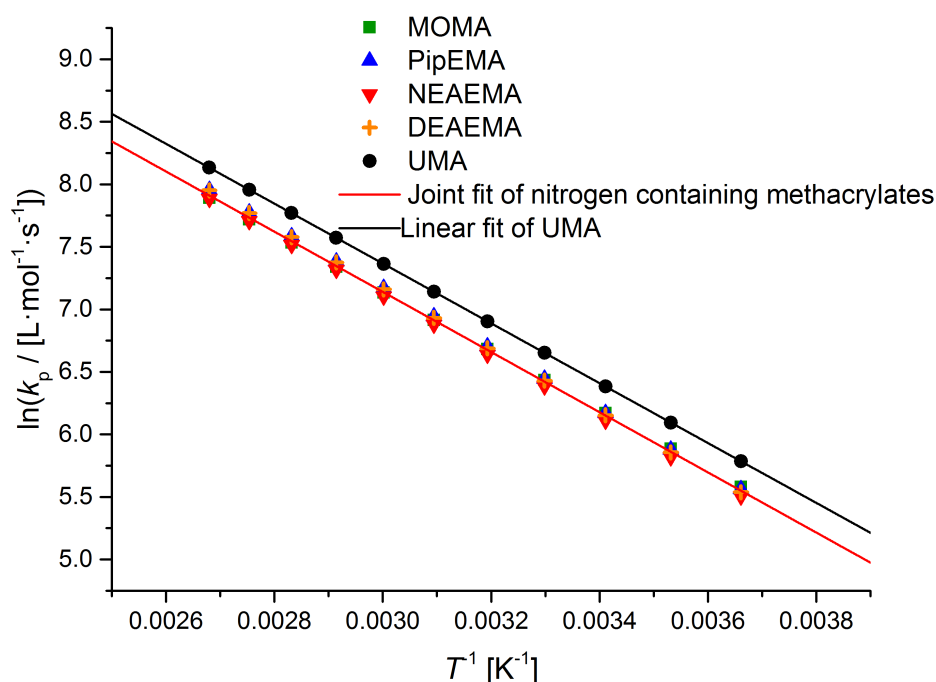


Figure 3.13.: Joint linear Arrhenius fit for the investigated N-ethyl methacrylates 2-(*N*-ethylanilino)ethyl methacrylate (NEAEMA), 2-morpholinoethyl methacrylate (MOMA), 2-(1-piperidyl)ethyl methacrylate (PipEMA), and 2-(*N,N*-diethylamino)ethyl methacrylate (DEAEMA) as well as Arrhenius fit for ureidoethyl methacrylate (UMA) derived from the Arrhenius parameters stated in ref [186]. Adapted with permission from ref [134].

Although differences in the polarity of the ester side chain might be expected due to an electron withdrawing effect of the oxygen, the main factor influencing the propagation rate coefficient might be the ability of the ureido group to form intramolecular hydrogen bonds. Hydrogen bonds between the monomer units influence the stiffness of the chain and diffusion behavior of the radicals, however, it has to be kept in mind that UMA was solely investigated in solution in DMAc. A more pronounced interaction between the transition state and the solvent due to a breakage of the intermolecular hydrogen

bonds leads to a reduced hindrance of the torsion and ultimately an increase in the propagation rate coefficient. To reliably compare the propagation rate coefficients for UMA with the family of N-ethyl methacrylates, an investigation of UMA in bulk would be preferable, since it can not yet be stated if the aforementioned effects of the intermolecular hydrogen bonds would ultimately lower the propagation rate coefficient. Although the data for UMA reported in 2014^[186] clearly do not fit into the proposed family, it is refrained from giving a final statement on a possible implementation of UMA into the family of N-ethyl methacrylates, since the solvent effects on the propagating reaction of UMA and, therefore, on the Arrhenius parameters and propagation rate coefficients are not yet fully known or understood and no bulk data are available.

3.3.3. Comparison to Cyclic Methacrylates

In 2003, Beuermann *et al.*^[88] noted the first family type behavior for a group of methacrylates featuring cyclic ester side chains, namely cyclohexyl methacrylate (cHMA), glycidyl methacrylate (GMA), benzyl methacrylate (BnMA), and isobornyl methacrylate (iBoMA) as depicted in Figure 3.1. The propagation rate coefficients for these four monomers were in close agreement to each other and could be described by joint Arrhenius parameters of $A = 4.24 \cdot 10^6 \text{ L} \cdot \text{mol}^{-1} \cdot \text{s}^{-1}$ and $E_A = 21.90 \text{ kJ} \cdot \text{mol}^{-1}$. A comparison of the family of methacrylates with cyclic ester side chains to the N-ethyl methacrylate seems interesting due to NEAEMA, MOMA, and PipEMA featuring a cyclic system in their ester side chains as well. Comparing the Arrhenius parameters for the family of cyclic methacrylates and the N-ethyl methacrylates ($A [10^6 \text{ L} \cdot \text{mol}^{-1} \cdot \text{s}^{-1}] = 4.24$ for cyclic, 1.55 for N-ethyl and $E_A [\text{kJ} \cdot \text{mol}^{-1}] = 21.90$ for cyclic, 19.68 for N-ethyl), a difference in the families seems already quite obvious. The significantly higher frequency factor implies elevated propagation rate coefficients for the cyclic methacrylates compared to the N-ethyl methacrylates, yet the elevated activation energy and, therefore, steeper slope, might suggest a convergence or even crossing of the Arrhenius plots in the lower temperature range. Inspecting Figure 3.14, it is visible that at 0 °C the propagation rate coefficient of the cyclic methacrylates is in good agreement with the N-ethyl methacrylates. While at 0 °C the k_p value is just insignificantly higher, at -50 °C it lies below the family of N-ethyl methacrylates, supporting the suggestion of a crossing of the Arrhenius plots. When going to elevated temperatures, however, the propagation rate coefficients for the cyclic methacrylates clearly divert to significantly higher values with a difference of approximately 35% at 100 °C.

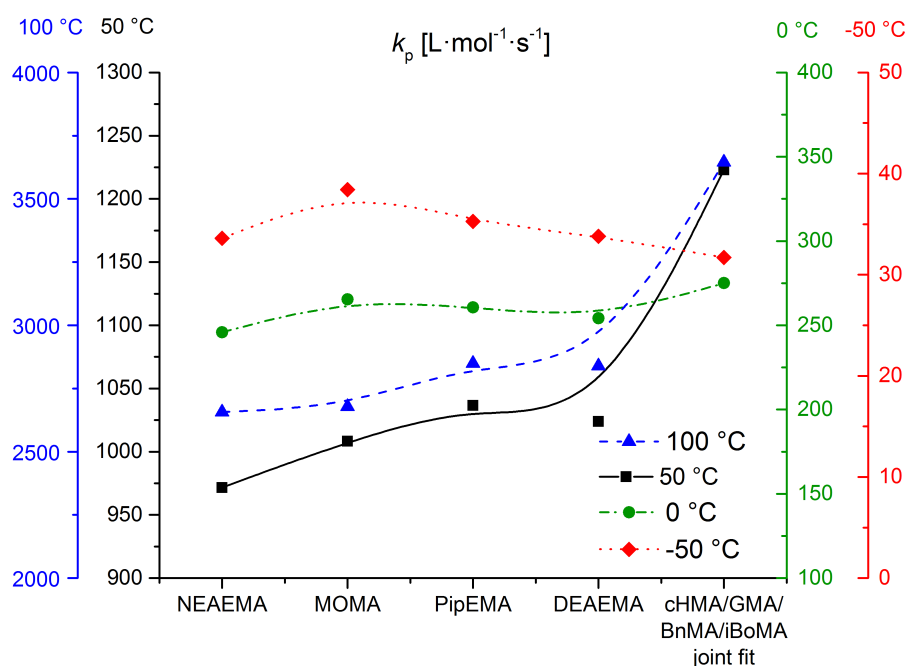


Figure 3.14.: Propagation rate coefficients for 2-(*N*-ethylamino)ethyl methacrylate (NEAEMA), 2-morpholinoethyl methacrylate (MOMA), 2-(1-piperidyl)ethyl methacrylate (PipEMA), 2-(*N,N*-diethylamino)ethyl methacrylate (DEAEMA), and a joint k_p of cyclohexyl methacrylate (cHMA), glycidyl methacrylate (GMA), benzyl methacrylate (BnMA), and isobornyl methacrylate (iBoMA) as taken from ref. [88] at different temperatures. Left outer scale, blue dashed line = $k_p(100^\circ\text{C})$; left inner scale, black solid line = $k_p(50^\circ\text{C})$; right inner scale, green dot-dashed line = $k_p(0^\circ\text{C})$; right outer scale, red dotted line = $k_p(-50^\circ\text{C})$. Adapted with permission from ref [134].

The joint Arrhenius fits for both families, as depicted in Figure 3.15, show the behavior expected after comparison of the Arrhenius parameters. At sub-zero temperatures some of the data points for the cyclic methacrylates are in agreement with the *N*-ethyl methacrylates and the fits are crossing each other due to the large differences in the activation energy and, therefore, the slope of the fit. However, the divergent nature of the fits is quite obvious when having a look at the elevated temperature range, where the propagation rate coefficients for both families increasingly move apart. As pointed out previously, the k_p values for -50°C depicted in Figure 3.14 are only theoretically calculated values and no experimental data are available for such low temperatures. Thus, no clear statement can be given on the behavior of the investigated families when going to far sub-zero temperatures.

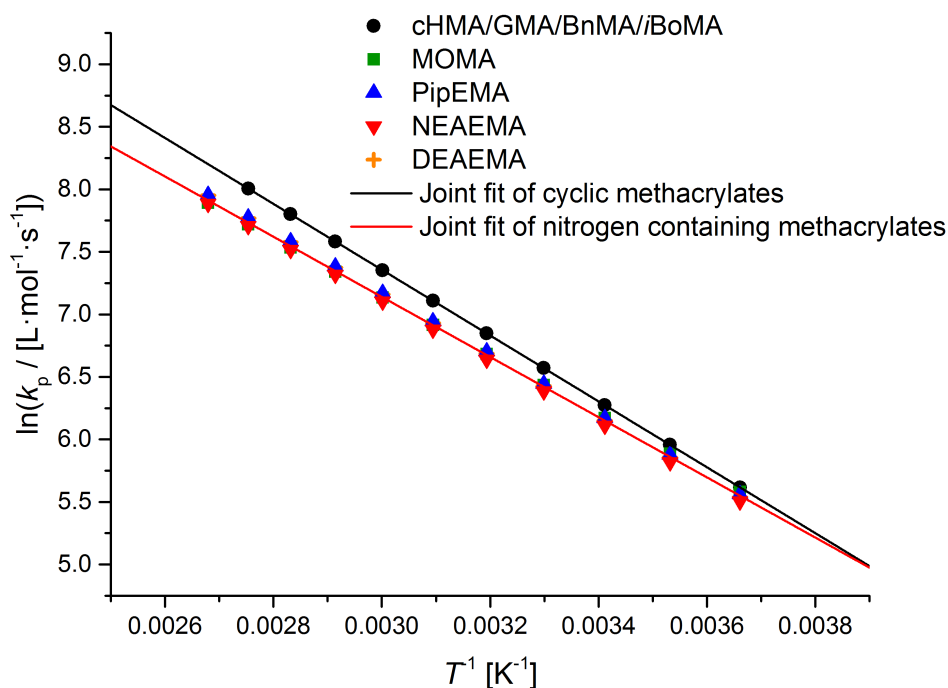


Figure 3.15.: Joint linear Arrhenius fit for the investigated N-ethyl methacrylates 2-(*N*-ethylanylino)ethyl methacrylate (NEAEMA), 2-morpholinoethyl methacrylate (MOMA), 2-(1-piperidyl)ethyl methacrylate (PipEMA), and 2-(*N,N*-diethylamino)ethyl methacrylate (DEAEMA) as well as joint Arrhenius fit for cyclohexyl methacrylate (cHMA), glycidyl methacrylate (GMA), benzyl methacrylate (BnMA), and isobornyl methacrylate (*i*BoMA) derived from the Arrhenius parameters stated in ref [88]. Adapted with permission from ref [134].

Molecular mass, steric demand, and polarity of the ester side chain were proposed to be the key influencing factors for a possible family type behavior of investigated monomers. While the N-ethyl methacrylates display slightly higher molecular masses, on first glance the steric demands seem not be considerably distinct to lead to such substantial differences in the Arrhenius parameters. However, these differences might be attributed to the varied polarities of the ester side chains between the cyclic methacrylates and N-ethyl methacrylates. Due to the more pronounced polarity of the ester side chains for the N-ethyl methacrylates, the electronic environment is altered and the double bond slightly activated. A higher polarity at the propagating radical increases the hindrance of the torsion and internal rotations, lowering the frequency factor as well as activation energy. A full explanation of the underlying effects that cause the substantial differences between the two respective families and their Arrhenius parameters and propagation rate coefficients can not yet be given, however, it is evident that the families do not qualify for an integration into a combined family with a joint Arrhenius fit.

3.3.4. Comparison to Branched Methacrylates

To place the family of N-ethyl methacrylates into the context of another previously described family of methacrylates and to complete the picture of the different family type behaviors, an evaluation of the methacrylates with branched ester side chains is mandatory. In 2013, Haehnel *et al.* ^[130] introduced a group of branched methacrylates – ethylhexyl methacrylate (EHMA), propylheptyl methacrylate (PHMA), isodecyl methacrylate (*i*DeMA), and heptadecanyl methacrylate (C17MA) – that displayed a family type behavior and can be described by a joint Arrhenius fit leading to the joint parameters of $A = 2.39 \cdot 10^6 \text{ L} \cdot \text{mol}^{-1} \cdot \text{s}^{-1}$ and $E_A = 21.16 \text{ kJ} \cdot \text{mol}^{-1}$. The comparison of the family of N-ethyl methacrylates to the branched methacrylates will be limited to the family of PHMA, *i*DeMA, EHMA, and C17MA. Since a broad variety of various branched methacrylates has been investigated, each displaying their individual Arrhenius parameters and propagation rate coefficients, a comparison to each individual methacrylate with branched ester side chain would go beyond the scope of this study. Similar to the cyclic methacrylates, in the case of the branched methacrylates, the higher frequency factor might suggest higher propagation rate coefficients than determined for the N-ethyl methacrylates with a possible convergency or even crossing of the Arrhenius plots at lower temperatures due to a higher activation energy and, therefore, steeper slope. However, the differences in the frequency factor may not be sufficiently distinctive for a reliable statement. The depiction of the propagation rate coefficients for the N-ethyl methacrylates as well as the branched methacrylates at four different temperatures (-50, 0, 50, and 100 °C) in Figure 3.16 even shows an opposite effect. Throughout the entire temperature range, the k_p values for the branched methacrylates lie below the values for the N-ethyl methacrylates. A close proximity of both families is undeniable, especially for the highest temperature where the k_p values differ by merely 5% ($k_p(100 \text{ °C}) [\text{L} \cdot \text{mol}^{-1} \cdot \text{s}^{-1}] \approx 2.600$ for branched, 2.700 for N-ethyl and $k_p(50 \text{ °C}) [\text{L} \cdot \text{mol}^{-1} \cdot \text{s}^{-1}] \approx 900$ for branched, 1000 for N-ethyl), yet by inspecting Figure 3.16 alone, it is not clear if a combination of the families is advisable.

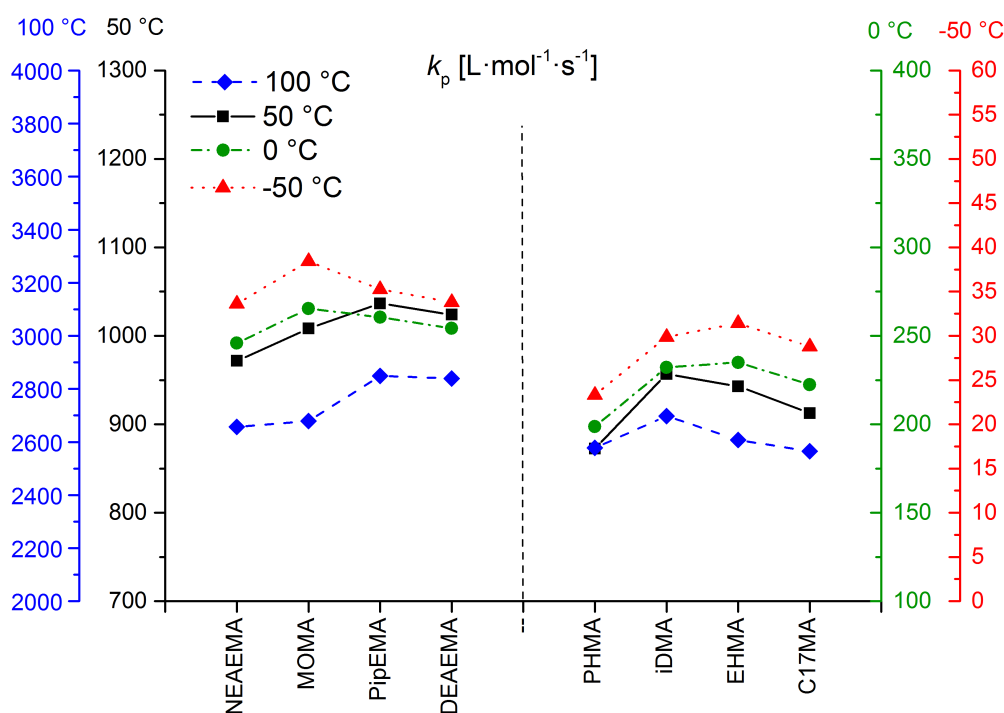


Figure 3.16.: Propagation rate coefficients for 2-(*N*-ethylanilino)ethyl methacrylate (NEAEMA), 2-morpholinoethyl methacrylate (MOMA), 2-(1-piperidyl)ethyl methacrylate (PipEMA), and 2-(*N,N*-diethylamino)ethyl methacrylate (DEAEMA) as well as 2-propylheptyl methacrylate (PHMA), isodecyl methacrylate (*i*DeMA), 2-ethylhexyl methacrylate (EHMA), and heptadecanyl methacrylate (C17MA) as taken from ref. [9] at different temperatures. Left outer scale, blue dashed line = $k_p(100^\circ\text{C})$; left inner scale, black solid line = $k_p(50^\circ\text{C})$; right inner scale, green dot-dashed line = $k_p(0^\circ\text{C})$; right outer scale, red dotted line = $k_p(-50^\circ\text{C})$. Adapted with permission from ref [134].

The question of a possible combination of the two monomer families discussed in the current section can be clarified upon the inspection of the joint Arrhenius fits for the *N*-ethyl methacrylates as well as branched methacrylates, depicted in Figure 3.17. The Arrhenius plots support the findings from Figure 3.16 of a good agreement of the propagation rate coefficients for the elevated temperature regime and as expected from the differences in the activation energy, a convergence of the Arrhenius fits at high temperatures (and a crossing of the fits, leading to the higher frequency factor for the branched methacrylates) is observed. Due to the different slopes of the fits, the differences in propagation rate coefficients are becoming more and more distinct when going to lower temperatures. The differences in k_p between the *N*-ethyl methacrylates and the branched methacrylates already reach 20% at 0 °C and even exceed 30% at the lowest depicted temperature of -50 °C.

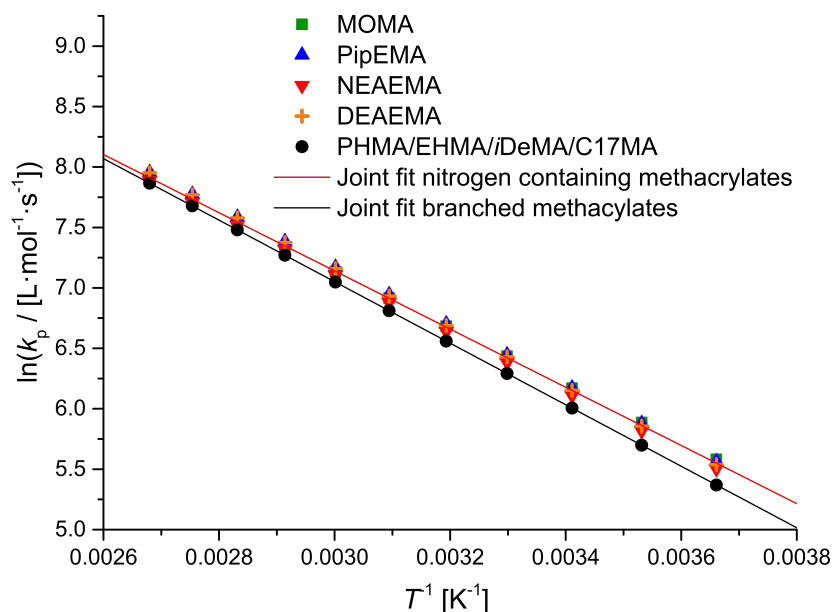


Figure 3.17.: Joint linear Arrhenius fit for the investigated N-ethyl methacrylates 2-(N-ethylanilino)ethyl methacrylate (NEAEMA), 2-morpholinoethyl methacrylate (MOMA), 2-(1-piperidyl)ethyl methacrylate (PipEMA), and 2-(N,N-diethylamino)ethyl methacrylate (DEAEMA) as well as joint Arrhenius fit for 2-propylheptyl methacrylate (PHMA), isodecyl methacrylate (iDeMA), 2-ethylhexyl methacrylate (EHMA), and heptadecanyl methacrylate (C17MA) derived from the Arrhenius parameters stated in ref [130]. Adapted with permission from ref [134].

As Figure 3.17 clearly shows that a combination of the N-ethyl methacrylates and the branched methacrylates into a joint family is not advisable when reliable values for the low temperature ranges are desired. To develop a hypothesis on the possible reasons for these observed deviations in the propagation rate coefficients and Arrhenius parameters, again, the molar mass, steric demand, and polarity of the ester side chains are considered and two different effects are observed. According to Heuts *et al.*, a higher molar mass leads to a change in the vibrational and rotational partition functions, increasing the frequency factor.^[174] The branched methacrylates, featuring the higher molar masses, also exhibit a higher steric demand, lowering the propagation rate coefficients due to an increased hindrance of the internal rotations. The N-ethyl methacrylates feature more polar ester side chains, thus, the frequency factor and activation energy – and therefore the slope of the Arrhenius fit – are comparably lower. These opposed effects of a reduced k_p due to a higher steric demand for the branched methacrylates and reduced Arrhenius parameters due to a more pronounced polarity of the ester side chains for the N-ethyl methacrylates seem to have a different impact at different temperatures. In the region of elevated temperatures, these opposing effects seem to be balanced, causing similar

propagation rate coefficients above approximately 50 °C. Going to lower temperatures, the Arrhenius fit for the N-ethyl methacrylates deviates to higher propagation rate coefficients due to the lower activation energy and, therefore, less steep descent of the fit.

As it was the case for the cyclic methacrylates as well, no final explanation for the deviations between the family of branched methacrylates and the family of N-ethyl methacrylates can be given, yet a hypothesis is developed attributing the differences in the Arrhenius parameters and propagation rate coefficients to variations in the steric demand and electronic environment of the ester side chains. However, it can be clearly observed that a combination of both families into a joint family is not advisable.

4

Lewis Acid-mediated PLP



Gaining control over the stereoselectivity of polymeric materials has been described as the “holy grail” of radical polymerization^[190] and during the last decades large effort has been placed into controlling the assembly of macromolecules towards the possibility to precisely alter the material properties and structure of radically produced polymers.^[191] Having effective control over tacticity in RDRP would provide a radical-based route to specific stereoregular polymers and significantly enhance the field of polymer synthesis. However, two key aspects of microstructural control in radical polymerization have yet to be overcome: Lack of effective stereocontrol and formation of defect structures. Almost 60 years ago, in an attempt to gain structural control, Lewis acids were first employed to examine this effect on radical polymerization.^[192] ZnCl_2 was applied for the radical polymerization of methyl methacrylate (MMA) leading to different results depending on the concentration of Lewis acid. For low concentrations, no significant stereochemical effects were reported,^[192] while later on high concentrations of ZnCl_2 were found to slightly increase the isotacticity.^[193] Since 2000 Okamoto and co-workers successfully used rare earth metal triflates ($\text{M}(\text{OTf})_3$) as controlling agents to produce

isotactic rich polymers of several methacrylates, ^[194] α -(alkoxymethyl)acrylates, ^[195] acrylamides, ^[196, 197] and methacrylamides. ^[198, 199] Although these additives increased the control of tacticity, it was not yet possible to attain stereoregularity as high as generally achieved via anionic polymerization. A lack of understanding of the interactions between growing polymer chain and Lewis acid impedes the further development of Lewis acid-mediated radical polymerization since stereoselectivity is also highly dependent on the reaction conditions such as the type of monomer, solvent, concentration, and identity of the Lewis acid. In radical polymerization, stereochemistry is determined by the relative orientation of the terminal and penultimate side-chains rather than the orientation of the incoming monomer. A rapid interconversion between *pro-meso* and *pro-racemo* conformations of the polymer terminus – both equally reactive towards propagation – leads to atactic polymers in the absence of stereocontrolling agents (refer to scenario (1) in Figure 4.1). The literature accepted mechanism of isotactic regulation first published by Matsumoto ^[200] proposes a coordination of the Lewis acid that provides an energetic preference for *meso* propagation (scenario (2)), thus yielding isotactic polymers. However, this mechanism, although frequently cited, ^[191, 201, 202] has been criticized as oversimplified. Additional types of possible coordination of the Lewis acid – coordination to the terminal side chain and monomer, scenario (3) or solely to the incoming monomer, scenario (4) – are not expected to influence the stereoselectivity in a significant way.

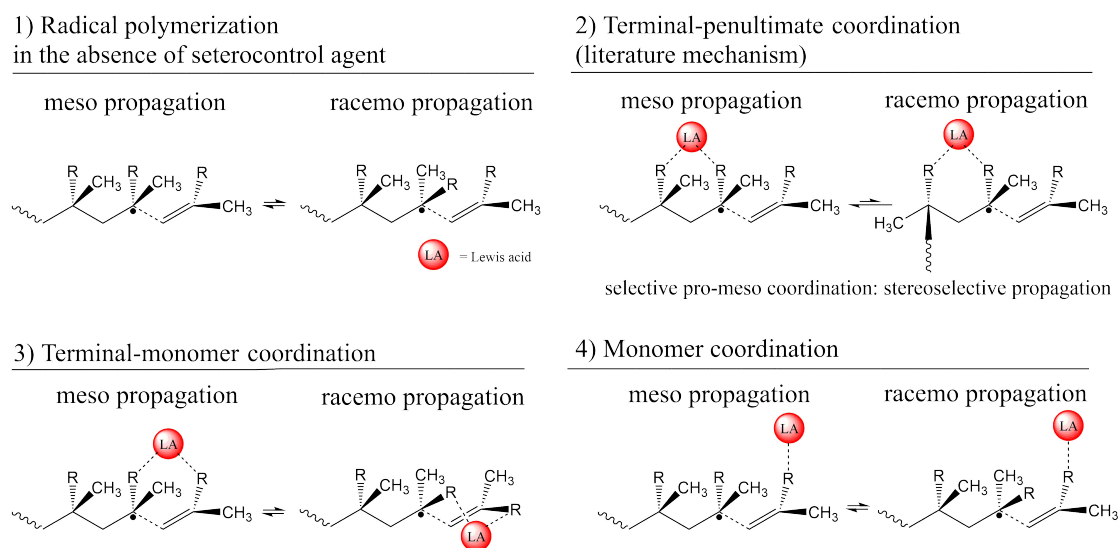


Figure 4.1.: Stereoselectivity during radical polymerization of a mono substituted alkene in the absence (1) and presence (2)-(4) of a Lewis acid. Scenarios (2)-(4) illustrate different positions of Lewis acid coordination to the polymer terminus and incoming monomer. Adapted with permission from ref [203].

The application of Lewis acids to control the tacticity of polar monomers has not proven entirely successful, however, recent work has shown that other aspects of microstructural influence can be controlled.^[204] Noble *et al.* recently investigated the influence of the Lewis acid lithium bis(trifluoromethane)sulfonamide (LiNTf₂) on the propagation of MMA via PLP-SEC experiments and computational quantum-chemical calculations.^[203] Although the Lewis acid employed in the study of Noble did not show any effect on the tacticity of the polymer, it was pointed out that catalytic activity was observed. Lewis acids were shown to catalyze homopolymerizations^[192,194,205] and due to an enhancement of propagation relative to transfer, favor end chain propagation over the formation of defect structures and therefore suppress chain branching reactions.^[94,206] A possible catalytic effect was already predicted by Clark in 1986 using *ab initio* calculations^[207] and later on experimentally confirmed by Michl *et al.*^[208] These increased propagation rates were associated with electrostatic effects without covalent interaction of the lithium cation with the monomer double bond and was said to be observable even at long distances above 4.5 Å.^[209,210]

For the rate acceleration occurring in polar systems, Clark's explanation is not satisfactory. For MMA, PLP-SEC was employed to experimentally confirm the rate accelerating properties of LiNTf₃ while the binding models were examined employing *ab initio* molecular orbital theory, showing that propagation is mainly governed by a "(pseudo)cyclization of a Li⁺ bridged terminal-monomer complex" not leading to a control over stereo regulation.^[203] Although this complex does not favor isotacticity over atactic propagation, it influences k_p due to an activation of the monomer towards propagation. Under the premise of an accelerated propagation rate and preference of linear chain propagation over branching, an investigation into acrylates is of high interest to prove the concept of suppression of side reactions and defect structures when utilizing Lewis acids in radical polymerization. As already described in chapter 1.4, for acrylates high pulse repetition rates need to be employed to prevent the formation of MCRs and therefore the occurrence of a mixture of $k_{p,sec}$ and $k_{p,tert}$ and blurring of the PLP pattern in the SEC analysis. Being able to gain better PLP traces even at low frequencies would render the need for expensive equipment redundant and gaining control over the formation of defect structures would pave the way for simpler ways to tune material properties.

4.1. Polymerization of Methyl Acrylate with LiNTf₃

To investigate the influence of Lewis acids on the propagation reaction of acrylates, methyl acrylate (MA) was studied via PLP-SEC. During free radical polymerization of MA, competing modes of propagation take place, i.e. end chain propagation vs. mid chain propagation. As previously described, mid chain radicals exhibit slower propagation rate coefficients due to the more stable nature of the radical site. When applying low pulse repetition rates, the time between two consecutive laser pulses is sufficient for intramolecular transfer reactions to take place and, thus, the formation of slowly propagating tertiary radicals leads to a blurring of the characteristic PLP traces. To overcome the formation of MCRs and the loss of PLP characteristics, higher pulse repetition rates have to be applied, however, the need for high frequencies asks for the appropriate equipment. As reported by Barner-Kowollik *et al.* in the IUPAC benchmark publication of MA, [164] even when employing a high frequency laser system at 500 Hz, a loss of PLP characteristics was observed at elevated temperatures. Therefore, another method to suppress intramolecular transfer reactions and thereof resulting defect structures is introduced with the addition of Lewis acids. Although the use of Lewis acids to influence the tacticity of the resulting polymer chain is still disputable, it has been shown that Lewis acids catalyze end chain propagation over mid chain propagation by coordination at the chain end. [94,206] In the current chapter, methyl acrylate is investigated to explore the catalytic effects of LiNTf₃ on the propagation reaction of acrylate type monomers. Therefore, two different laser setups – 500 Hz Excimer laser operating on the XeF line as well as 50 Hz Nd:YAG laser – have been employed, applying different pulse repetition rates and temperatures.

To start the investigation of the Lewis acids systems, the choice of the optimum photoinitiator is crucial. Possible interaction of the Lewis acid with the photoinitiator can lead to a shift in the absorbance of the initiator resulting in a less effective decomposition under laser irradiation. An increased triplet lifetime due to an addition of the Lewis acid to the photoinitiator can lead to problems with the initiation of the polymerization resulting in the loss of a PLP structure. Furthermore, if an interaction of the Lewis acid with the initiator takes place, the amount of Lewis acid available to interact with the propagating radical site is significantly reduced. In a study on the influence of the stronger Lewis acids ZnCl₂ and AlCl₃ on the two popular acetophenone photoinitiators methyl-4'-(methylthio)-2-morpholino-propionophenone (MMMP) and 2,2-dimethoxy-2-phenylacetophenone (DMPA), [211] a significant influence of the Lewis acid on the extinction coefficient of the photoinitiators was reported. While for DMPA an increase of the extinction coefficient was reported for the $\pi\pi^*$ transition at low wavelengths,

for MMMP a clear redshift of the absorbance maximum was detected. It is noted^[211] that the addition of Lewis acids can result in changes of the excitation dynamics of the photoinitiator and the resulting increased triplet lifetimes, slower photolysis, and lower radical concentration may negatively influence the PLP experiments. Especially at high pulse repetition rates, an increased triplet lifetime would affect the obtained MWD and lead to a loss of the PLP structure. For a deeper examination of a suitable photoinitiator for the current studies, UV spectra are recorded for each photoinitiator of interest with and without the addition of LiNTf₃. As depicted in Figure 4.2, the addition of LiNTf₃ does not lead to a shift in the spectra for Irgacure OXE01, mesitol, and tri-, tetra-, or pentamethyl benzoin. The chemical structures of the photoinitiators employed in the current study are depicted in Figure 1.8 in Chapter 1.4 and in the corresponding spectra in Figure 4.2. In the case of Irgacure OXE01, the absorbance at approximately 330 nm increases, yet no shift of the peak maximum is detected. For effective photoinitiation, photoinitiators should display a reasonable absorbance at the wavelength of the applied light source, however, a higher extinction coefficient does not necessarily correspond to a more efficient initiation.^[212,213] Test experiments with the 50 Hz Nd:YAG laser system operating at 355 nm and all available photoinitiators proved the Irgacure OXE01 to give the best defined PLP structures after SEC analysis.

4. Lewis Acid-mediated PLP

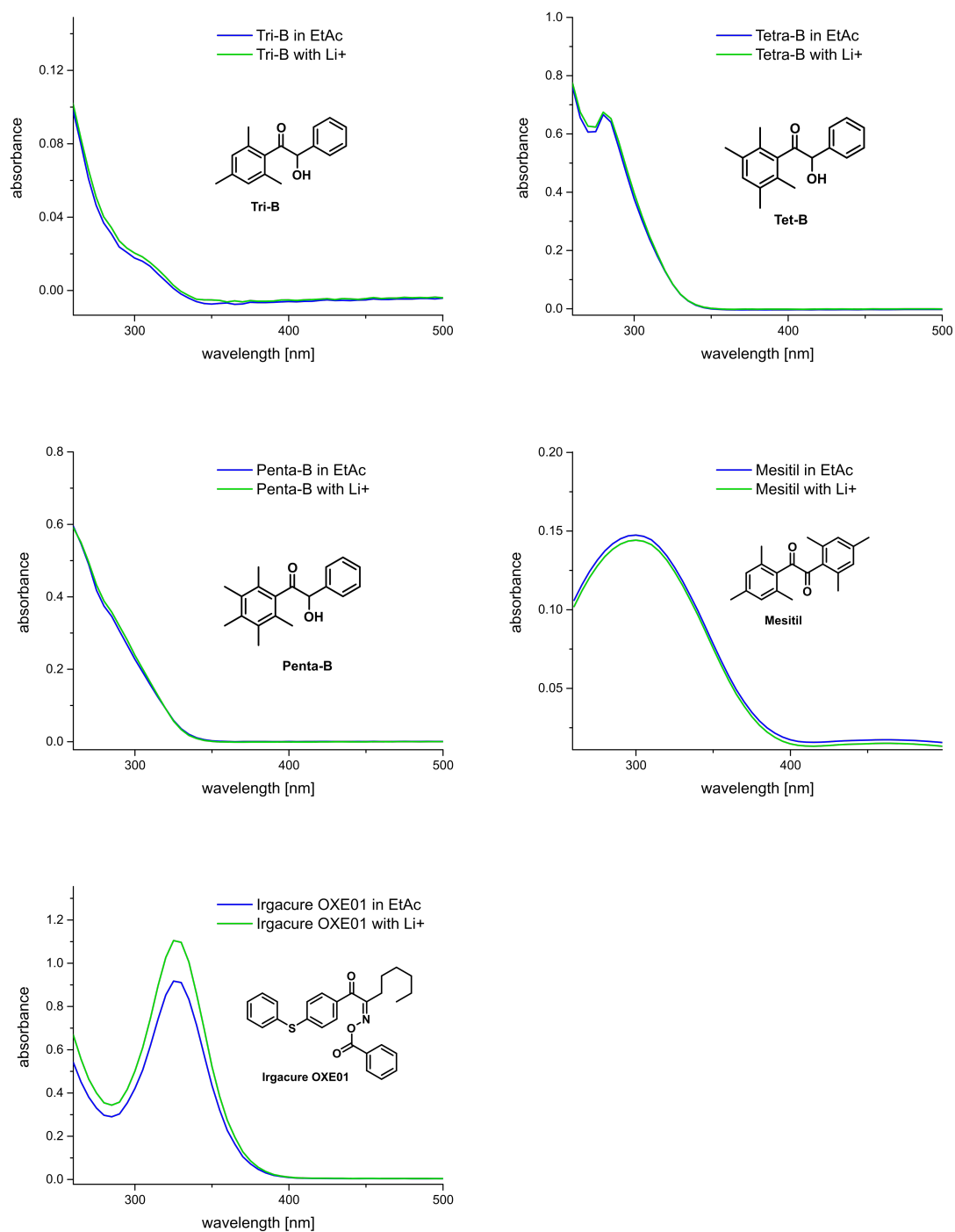


Figure 4.2.: UV spectra of the employed photoinitiators with and without the addition of 10 mol% of the Lewis acid LiNTf_3 . For none of the initiators a shift of the absorbance maximum to higher or lower wavelengths is observed.

For the direct comparison of the apparent propagation rate coefficients, k_p^{app} , and the influence of the Lewis acid on the occurrence of tertiary propagating radicals at various frequencies, the 500 Hz Excimer laser was employed to record frequency series of MA with Irgacure OXE01 as photoinitiator in the absence and presence of LiNTf₃. A first observation made during the polymerization process was the different physical properties of the produced polymer samples. Employing pure MA, the samples produced at lower frequencies featured a higher viscosity due to the higher produced molecular weights. Nevertheless, no problems occurred when dissolving the polymer in THF for the SEC analysis. The PLP samples produced with the addition of LiNTf₃, however, exhibited a significantly increased viscosity. Although an increase in viscosity is expected with higher molecular weights, a clean precipitation in methanol was not fully possible, rather an agglomeration of highly viscous, partly precipitated poly(methyl acrylate) was observed. Subsequent attempts to dissolve the agglomerated p(MA) led to a highly viscous medium and full dissolution could not be achieved even after addition of high amounts of THF. At the highest investigated temperatures of 60 °C, the pure MA started background polymerization upon heating, even before the sample was irradiated with the excimer laser, leading to a highly viscous reaction medium and no detectable PLP structures in the SEC analysis. While for the pure MA, this extensive background polymerization was merely observed at 60 °C, for some of the samples containing the Lewis acid this observation was already made at ambient temperature. Although an interaction of the Lewis acid with the photoinitiator was not observed in the UV spectra presented in Figure 4.2, photoabsorption with the Lewis acid can redshift the photoinitiation to visible light, leading to self-initiation of the polymerization and therefore a high amount of background polymerization. Apart from the experimental problems arising due to the highly viscous material – transfer of the very sticky solution to another glass vial, poor precipitation in MeOH, poor solubility for SEC analysis – extensive background polymerization can also lead to a blurring or overlap of the PLP structure and influences the determined propagation rate coefficient, since the condition of low conversion is not longer given.

Inspecting Figures 4.3 and 4.4, two effects are visible when adding LiNTf₃ to the bulk polymerization of MA: a general increase of the propagation rate coefficients and a shift of the plateau of the S-shaped curve to lower frequencies. Detailed sample conditions of all samples incorporated into the frequency series are collated in Tables A.22 to A.25 in the Appendix A.

At -12 °C, a shift of the plateau of approximately 25 Hz is observed, while at 10 °C the plateau shifts by close to 50 Hz. The rate accelerating effect of the Lewis acid is more pronounced at the elevated temperature, from approximately 18% at -12 °C to

4. Lewis Acid-mediated PLP

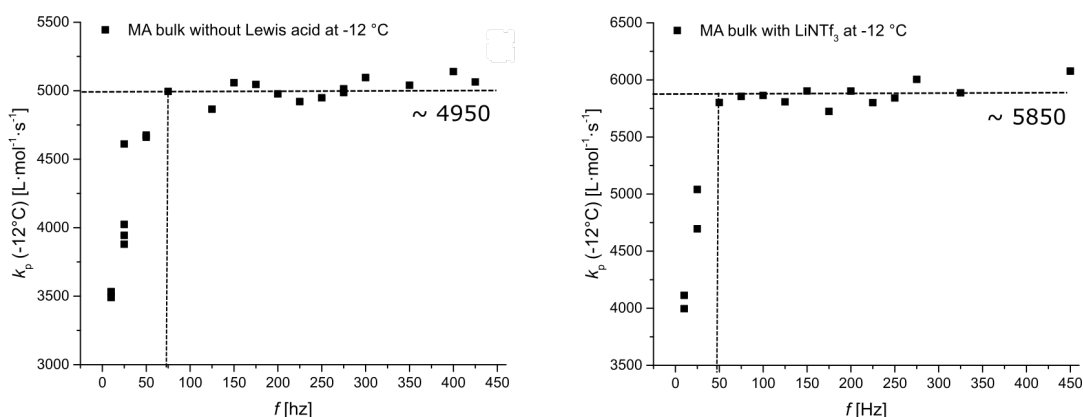


Figure 4.3.: Frequency series for MA in bulk in the absence (left) and presence (right) of LiNTf_3 at -12°C . In the presence of 5 mol% Lewis acid, a shift of the plateau of the S-shaped curve of approximately 25 Hz to lower frequencies as well as a shift to higher propagation rate coefficients is observed. Detailed sample conditions of all samples incorporated into the frequency series are collated in Tables A.24 and A.25 in the Appendix A.

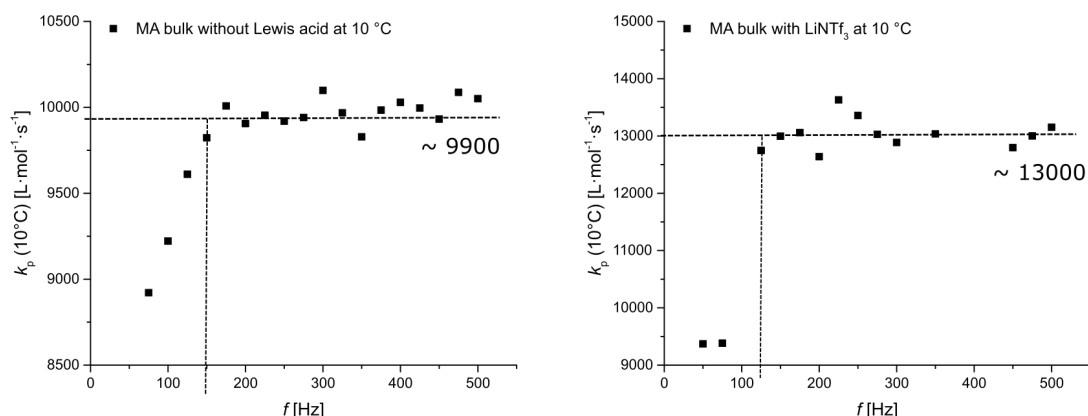


Figure 4.4.: Frequency series for MA in bulk in the absence (left) and presence (right) of LiNTf_3 at 10°C . In the presence of 10 mol% Lewis acid, a shift of the plateau of the S-shaped curve of approximately 50 Hz to lower frequencies as well as a shift to higher propagation rate coefficients is observed. Detailed sample conditions of all samples incorporated into the frequency series are collated in Tables A.22 and A.23 in the Appendix A.

30% at 10°C at the plateau of the S-shaped curve. Since the frequency series at -12°C is carried out with approximately 5 mol% LiNTf_3 and at 10°C with 10 mol% LiNTf_3 , a comparison of both data sets is not sufficient to make a statement of the temperature dependency of the rate accelerating effect of the Lewis acid. However, a comparison of the k_p data recorded at 500 Hz at -12 and 0°C with 5% LiNTf_3 shows an increase in k_p from 18% at -12°C to approximately 40% at 0°C ($k_p(-12^\circ\text{C}) = 4950$ to $5850 \text{ L}\cdot\text{mol}^{-1}\cdot\text{s}^{-1}$; $k_p(0^\circ\text{C}) = 7700$ to $11000 \text{ L}\cdot\text{mol}^{-1}\cdot\text{s}^{-1}$; refer to Table A.27 in Appendix A). As depicted on

the left hand side of Figure 4.5, recorded with the Nd:YAG Laser system, the apparent propagation rate coefficient increases faster with increasing pulse repetition rates when the Lewis acid is present, from 17% at 10 Hz to 25% difference at 25 Hz and levels out at approximately 18% when the plateau is reached for both S-shaped curves (right hand side). The final decrease in the k_p^{app} difference between the polymerizations with and without Lewis acid is due to the longer ascent of the curve for pure MA. Although the samples containing LiNTf₃ exhibit a steeper slope of the S-shaped curve – leading to an increasing difference between the two graphs – the plateau is reached earlier and the ongoing increase of k_p^{app} for MA without the Lewis acid leads to a subsequent decrease of the k_p^{app} difference until the plateau of the second S-shaped curve is reached as well. At approximately -15 °C, a frequency of 50 Hz – the highest frequency accessible with the Nd:YAG laser system – seems to be sufficient to determine the secondary propagating radicals, however, increasing the temperature shifts the plateau to higher frequencies and only composites of $k_{p,\text{sec}}$ and $k_{p,\text{tert}}$ are determined. Nevertheless, even if at higher temperatures the plateau of the S-shaped curve is not yet reached, the increase of k_p^{app} in the presence of LiNTf₃ compared to pure MA indicates a change in the propagation reaction when the Lewis acid is present.

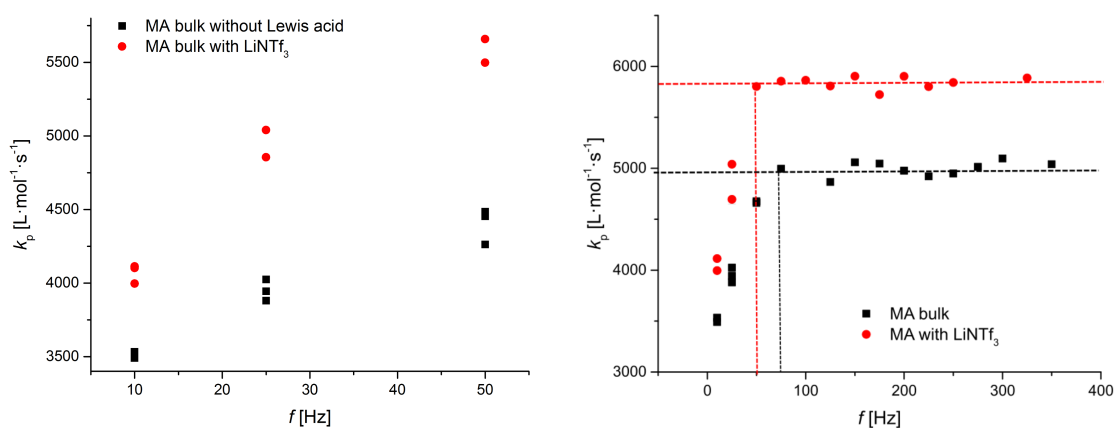


Figure 4.5.: Left hand side: Propagation rate coefficients for MA in bulk in the absence and presence of LiNTf₃ from 10 to 50 Hz at approximately -12 °C. In the presence of LiNTf₃ a steeper increase of k_p is detected with differences in k_p ranging from 17% at 10 Hz to 25% at 25 Hz. Right hand side: Frequency dependency of k_p for MA in the presence and absence of LiNTf₃ at close to -12 °C. The difference between the obtained k_p values levels out at approximately 18% at the plateau of the curve.

For the low frequencies, obtaining PLP structures with two detectable local maxima in the first derivative for the polymerizations with pure MA was challenging and the majority of the obtained PLP samples did not display the characteristic PLP distribution

or fulfill the consistency criteria. Adding the Lewis acid enhanced the detection of a second inflection point at lower pulse repetition rates, however, at high frequencies the characteristic PLP distribution was more pronounced for the polymerizations without LiNTf_3 . A possible explanation for the loss of PLP characteristics at higher flashing rates in the presence of the Lewis acid was already noted above. Although no shift of the absorbance was detected in the UV spectra when combining the photoinitiator with the Lewis acid, a possible increase of the triplet lifetime of the photoinitiator can lead to the observed blurring of the PLP distribution when going to higher pulse repetition rates. As depicted in Figure 4.6 on the example of 75 Hz at sub-zero temperatures, the addition of the Lewis acid leads to a clearer first inflection point and more pronounced second inflection point in the first derivative of the MWD at low frequencies.

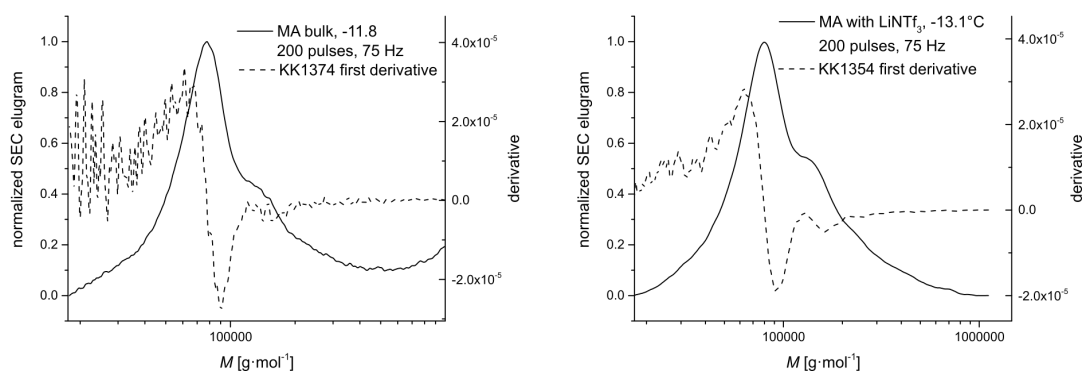


Figure 4.6.: Representative molecular weight distributions (solid lines) and their first derivatives (dotted lines) of methyl acrylate (MA) in the absence (left) and presence (right) of LiNTf_3 . The sample specific conditions are given in the diagram. A clear enhancement of the PLP structure with the addition of the Lewis acid is observed.

As discussed in the previous chapters, the determination of k_p over an extended temperature range allows for a reliable determination of Arrhenius parameters for the propagation rate coefficients. For MA, the propagation rate coefficients were investigated in the temperature range from -15 to 40 °C to allow for a comparison of the propagation behavior over an extended temperature range (see Figure 4.7).

In the case of the polymerization of MA in the absence of a Lewis acid, the determined Arrhenius parameters are determined as $A = 1.63 \cdot 10^7 \text{ L} \cdot \text{mol}^{-1} \cdot \text{s}^{-1}$ and $E_A = 17.4 \text{ kJ} \cdot \text{mol}^{-1}$ and are in good agreement with the literature known data.^[164] For the polymerization in the presence of LiNTf_3 , a small deviation to a higher frequency factor is observed due to consistently higher propagation rate coefficients. However, the determination of Arrhenius parameters should be handled with caution since the investigated temperature range as well as the available data points are relatively limited and the data do

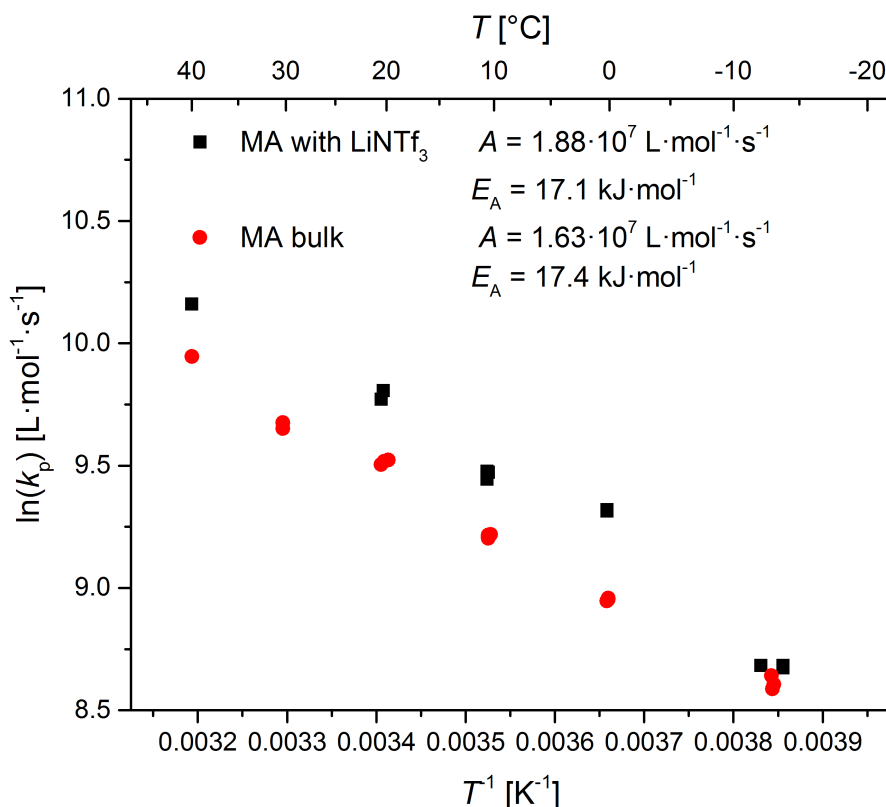


Figure 4.7.: Arrhenius plot for methyl acrylate in the absence and presence of LiNTf₃. The Arrhenius parameters of pure MA are in good agreement with the parameters reported in the literature.

not seem to follow a strict linear behavior. Starting with a deviation of below 20% at approximately -15 °C, the difference in k_p between samples polymerized in the absence and presence of the Lewis acid increases to 40% at 0 °C, but subsequently seems to decrease again to approximately 30% at 20 °C and 25% at 40 °C. Detailed sample conditions of all samples incorporated into the Arrhenius plots are collated in Table A.27 in the Appendix A. It is not yet known if a non-linear behavior of the rate accelerating effect is operational and the difference between the k_p values levels off at a certain temperature or if the deviations are caused by the limited amount of data available due to experimental difficulties to obtain valid PLP structures. The general increase in the propagation rate coefficient under the influence of a Lewis acid as well as the shift of the plateau of the S-shaped curve to lower frequencies suggest a more pronounced propagation of secondary radicals compared to tertiary radicals and a general preference of end-chain propagation over mid-chain propagation.

Although the PLP study on the influence of LiNTf₃ on the radical propagation reaction of MA revealed some interesting results, a more interdisciplinary approach seems to

be necessary to gain greater insight into the underlying mechanisms. Particularly theoretical studies and *ab initio* calculations might help to elucidate the experimentally observed effects. However, the great potential of Lewis acids to catalyze radical polymerizations and influence defect structures of acrylate type monomers could clearly be demonstrated.

*Science, my lad, is made up of mistakes,
but they are mistakes which it is useful to make,
because they lead little by little to the truth.*

Jules Verne

5

Conclusion

The extensive study of five branched acrylates in 1M solution in BuAc (^tBA, *i*BoA, BnA, EHA, and PHA) to add to the previously investigated INA-A, TDA-A, TDN-A, C17A, and C21A did not reveal global trends for the propagation rate coefficient with regard to the steric demand or chemical nature of the ester side chain and no overarching correlations between the solution and bulk data are observed. Neither can a trend among the Arrhenius parameters within the series of branched acrylates be identified and due to the differences between bulk and solution parameters (decrease of A and E_A with increased steric demand in bulk vs. scattering around a horizontal line in solution) an influence of the solvent on the propagation reaction can not be fully ruled out. With the data available at the current time, a final explanation for the observed propagation behavior of branched acrylates can not be given. The lack of global trends or family type behavior seems to be based on a combination of enthalpic and entropic effects of the ester side chains and their interaction with the transition state of the propagation reaction. The significant differences between the branched acrylates and the corresponding methacrylates are most likely based on the electronic influence of the α -methyl group on the propagating radical site. Explanations given for the trends observed in linear acrylates and branched methacrylates – destabilization of the radical site and pre-structuring of the reaction mixture, respectively – are not applicable in the case of the acrylates with branched ester side chains. Since global trends among the series of investigated and previously published acrylates with branched ester side chain can be detected, it is mandatory to individually determine the propagation rate coefficients for each monomer of interest.

For the methacrylates with nitrogen-containing ester side chains investigated in the current thesis, NEAEMA, MOMA, PipEMA, and DEAEMA display similar propagation rate coefficients over the entire investigated temperature range and can be described with joint Arrhenius parameters. However, the additionally studied monomers DMAEMA and DMAPMAE do not meet the criteria to be incorporated into the proposed family. In the case of the family of branched methacrylates reported previously, it was suggested that as soon as a certain steric demand is reached, the exact structure and chemical nature of the ester side chain is not decisive for the propagation rate coefficient anymore and k_p becomes mostly invariant to topological changes of the chain. This hypothesis is partly supported by the methacrylates investigated in the current study, however, certain limitations have to be applied. The hypothetical line of “minimum steric demand” seems to be reached between DMAEMA and DEAEMA, since the latter clearly lies within the proposed family while DMAEMA exhibits slightly elevated k_p values and just exceeds the boundaries of the family. DMAPMAE, however, displays significantly lowered propagation rate coefficients over the entire studied temperature range and an explanation based solely on the steric demand of the ester side chain seems not to be sufficient.

Furthermore, a combination of the family of N-ethyl methacrylates proposed in the current thesis and previously reported families of methacrylates with branched ester side chains and cyclic ester side chains, respectively, is found to be inappropriate. The source of these significant differences in propagation rate coefficients and Arrhenius parameters is partly based on the variation in steric demand, however, an at least equally important contribution to the observed differences is found in the polarity of the ester side chains. For the comparison of branched acrylates with branched methacrylates, the significant differences in the electronic environment of the ester moiety induced by the α -methyl group and its influence on the transition state is held liable for the absence and presence of a family type behavior, respectively. When inspecting the methacrylates with nitrogen-containing ester side chains, the differences in polarities of the ester side chain compared to alkyl chains induced by the nitrogen atom seem to additionally alter the electronic environment of the transition state. Within the series of nitrogen-containing methacrylates, similar steric demand and polarity lead to the detection of a family type behavior. In the case of DMAEMA, the steric demand seems to just exceed the boundaries to exhibit family type behavior, while for DMAPMAE the extended alkyl linker between the ester moiety and the nitrogen atom enables a hypothetical formation of a six-membered ring resulting in induced polarities at the nitrogen atom and the carbonyl carbon, significantly altering the electronic environment of the ester moiety.

A comparison of the family of N-ethyl methacrylates proposed in the current study with the first investigated nitrogen-containing methacrylate, UMA, shows a parallel behavior of the propagation rate coefficients over the investigated temperature range with UMA consistently exhibiting elevated k_p values. It has to be kept in mind that a direct comparison of UMA with the methacrylates investigated in the current thesis has to be handled with caution, since due to its high melting point, UMA has solely been investigated in solution. The influence of the solvent on the transition state is not yet investigated and it is unknown to which extend the ability of UMA to form hydrogen bonds or the breakage of said hydrogen bonds due to interactions with the solvent influences the propagation rate coefficients. However, it is clearly visible that an incorporation of UMA into the family of N-ethyl methacrylates at the current state is not appropriate.

Although there are still many unanswered questions when it comes to the addition of Lewis acids to the free radical propagation of (meth)acrylates, the investigations of the propagation reaction of methyl acrylate with the addition of LiNTf₃ clearly showcases the rate accelerating properties of the Lewis acid. In contrast to, for example, AlCl₃ and ZnCl₂, LiNTf₃ is compatible with all photoinitiators employed in the current study and no shifts in the UV spectra are observed between the pure photoinitiator and the added Lewis acid. The frequency series obtained for the PLP-SEC experiments with pure MA and MA with LiNTf₃ exhibit a shift of the plateau – where solely secondary propagating radicals are produced – to lower frequencies when the Lewis acid is added. The experiments with approximately 5 mol% of LiNTf₃ produced more pronounced PLP characteristics even at low frequencies and consistently higher propagation rate coefficients are determined. Depending on the temperature, the catalytic effect of the LiNTf₃ leads to an increase in k_p of approximately 18% at -12 °C and 30% at 10 °C at the plateau of the S-shaped curve. The enhancement of the characteristic PLP distribution at lower frequencies under the influence of LiNTf₃ as well as the shift of the plateau to lower pulse repetition rates indicates the more pronounced end-chain propagation compared to a conventional free radical polymerization of methyl acrylate. However, additional studies need to be performed to fully analyze the extend of defect structures formed in the absence and presence of the Lewis acid and to quantify the preference of end-chain over mid-chain propagation under the influence of LiNTf₃.

Although the field of PLP-SEC is already well developed and several monomer families were investigated with regards to their propagation rate coefficients and benchmark data are available, it still holds a large potential for further studies. In case of the nitrogen-containing methacrylates, the behavior of UMA in bulk would be of great interest to study the influence of hydrogen bonds as well as the investigation of ad-

ditional monomers to further push the boundaries of the proposed family. It would be worthwhile to prove if the family type behavior is truly based on the properties proposed in the current study – similar steric demand, mass, and polarity – and if additional methacrylates picked on the basis of these properties fit into the family. The Lewis acid experiments hold large potential for further investigations into, for example, the influence of various amounts of Lewis acid on k_p and number of defect structure, efficient combinations of different Lewis acids with various photoinitiators, or the influence of solvents on the rate accelerating properties of the Lewis acids. Studies of different (meth)acrylates with, for example, longer alkyl ester side chains or branched ester side chains might give additional insight into the underlying interactions and reveal if the rate accelerating and defect structure suppressing effects are dependent on the size or chemical nature of the monomer.

6

Experimental Section

In the following sections the materials employed in the current thesis are outlined as well as a description of the applied characterization and polymerization methods.

6.1. Materials

2,2-Dimethoxy-2-phenylacetophenone (DMPA, Aldrich, 99%), 4-methyl hydroquinone (MeHQ, Aldrich, 99%), hydroquinone (HQ, Fluka, >99%), azobis(isobutyronitrile) (AIBN, Aldrich, 98%), 2-cyano-2-propylbenzodithioate (CPDB, Aldrich, 97%), tetrahydrofuran (THF, HPLC grade, not stabilized), butyl acetate (BuAc, Acros, 99%), and lithium bis(trifluoromethane)sulfonamide (LiNTf₃, TCI, >98%) were used as received. *tert*-butyl acrylate (tBA, Aldrich, 98%), isobornyl acrylate (iBoA, Aldrich, technical grade), benzylacrylate (BnA, abcr, 95%), 2-ethylhexyl acrylate (EHA, Acros, >99%), 2-(diethylamino)ethyl methacrylate (DEAEMA, Aldrich, 99%, 1500 ppm MeHQ), 2-(dimethylamino)ethyl methacrylate (DMAEMA, Alfa Aesar, 97%, 0.2% MeHQ), and methyl acrylate (MA, Merck, >99%) were freed from the inhibitor by percolating over a column of basic aluminum oxide. 2-Propylheptyl acrylate (PHA, isomeric mixture with following ester groups: 2-propylheptyl / 2-propyl-4-methylhexyl / 2-propyl-5-methylhexyl / 2-isopropylheptyl = 0.93 / 0.029 / 0.039 / 0.02, <30 ppm MeHQ), 2-(*N*-ethylanilino)ethyl methacrylate (NEAEMA <30 ppm MeHQ), 2-morpholinoethyl methacrylate (MOMA <30 ppm MeHQ), 2-(1-piperidyl)ethyl methacrylate (PipEMA <30 ppm MeHQ), and 3-(*N,N*-dimethylamino)propyl methacrylate (>95%, <20 ppm MeHQ) were used as received from BASF. S,S-bis(α,α' -dimethyl- α'' -acetic acid)trithiocarbonate (TRITT) was prepared according to ref [214].

6.2. Pulsed Laser Polymerization Experiments

The experimental PLP setup employed in the current study for the determination of propagation rate coefficients of the branched acrylates as well as nitrogen-containing

methacrylates has been previously established in our group.^[10,161] For each investigated monomer, monomer stock solutions in bulk or butyl acetate and with varying initiator concentrations are prepared. The solution is transferred into sample vials (0.5 mL per sample), sealed with rubber septa and deoxygenated by purging with nitrogen for 2 to 5 minutes. The sample vials are then placed into a stainless steel sample holder and allowed to reach the desired temperature. The temperature is set with a thermostat (VWR 1196D) and monitored directly at the sample during laser irradiation. The laser beam is adjusted to hit the sample from the bottom with laser pulse energies varying from 1.5 to 2 mJ per pulse. None of the samples were exposed to a relevant temperature change exceeding 0.2 °C throughout the polymerization process. Polymerization is induced by laser pulsing at varying frequencies of up to 500 Hz employing a Coherent Xantos XS-500 laser system operated at the XeF line at 351 nm wavelength. To end the polymerization process, MeHQ dissolved in THF is added and the samples are analyzed via SEC measurement. Since most of the monomers exhibit high boiling points and therefore do not evaporate, the samples are measured without removing of the residual monomer. To ensure that the conversion does not influence the resulting propagation rate coefficients, different numbers of pulses are applied and found to be within the range of negligible monomer consumption. The experiments are tested for consistency by applying different numbers of pulses (100 to 1200), varying initiator concentrations (2.5 mmol·L⁻¹ to 20 mmol·L⁻¹), as well as varying laser pulse energies (1.5 mJ to 2 mJ). Every individual PLP distribution exhibit at least two inflection points (L_2), in case of the nitrogen-containing methacrylates up to seven inflection points could be observed. Only samples with a $k_{p,1}/k_{p,2}$ ratio between 0.95 and 1.1 are incorporated in the final Arrhenius data sets (if not stated otherwise). All $k_{p,1}/k_{p,2}$ ratios are collated in the respective Tables in the Appendix A.

An additional PLP setup has been employed for the investigation of the influence of Lewis acids on the propagation rate coefficients. For all laser conditions, a control solution containing methyl acrylate (MA) and photoinitiator as well as an experimental solution containing MA, photoinitiator, and a Lewis acid have been investigated. The solutions were transferred into a jacketed quartz windowed cell, sealed with rubber septa and degassed with nitrogen for approx. 5 minutes. Afterwards the sample was connected to a Lauda RL6 recirculating bath until equilibrated at the initially set temperature. The temperature of the sample was measured via a Testo 735-2 temperature meter fitted with a 0602 0593 probe sitting inside the sample during the course of the experiment. The temperature was logged at 1 second intervals by Testo Comfort Software X35. Temperatures of the cooling bath were set to -28 °C. Polymerization

was initiated at 355 nm with an pulse energy of 4 to 10 mJ per pulse at repetition rates of 10, 25, and 50 Hz for durations of 30 sec, 15sec, and 10 sec employing a Quantel Brilliant Nd:YAG laser. To end the polymerization process, the sample was poured into a sample vial containing methanol and hydroquinone to precipitate the polymer. The samples were left overnight to settle and afterwards three quarters of the methanol was removed via a pasteur pipette and the samples were placed into a miVac Quattro vacuum concentrator at 40°C for approx. 2 hours. The dry polymer was subsequently prepared for SEC analysis. Detailed sample conditions and $k_{p,1}/k_{p,2}$ ratios are collated in the respective Tables in the Appendix A.

6.3. Characterization Methods

For the characterization of the monomers and polymers investigated in the current thesis, different analysis and characterization methods have been employed.

6.3.1. Size-Exclusion Chromatography

SEC measurements at KIT were performed on a PL-SEC 50 Plus Integrated System, composed of an autosampler and a PLgel 5 μm bead-size guard column (50 x 7.5 mm) followed by a PLgel 5 μm Mixed E column (300 x 7.5 mm), three PLgel 5 μm Mixed C columns (300 x 7.5 mm), and a differential refractive index (RI) detector using THF as an eluent at 35 °C with a flow rate of 1 mL·min⁻¹. The SEC system is calibrated using linear poly (styrene) standards ranging from 476 to 2.5 x 10⁶ g·mol⁻¹ and linear poly(methyl methacrylate) standards ranging from 800 to 1.6 x 10⁶ g·mol⁻¹. The obtained molecular weight distributions were smoothed to remove noise from the signal and the first derivatives were used to determine the molecular weights at the inflection points. Smoothing of the signals as well as determination of the derivatives was carried out with Origin Software.^[215] In case of the branched acrylates, all SEC calculations were carried out using the polymer specific Mark-Houwink-Kuhn-Sakurada (MHKS) parameters collated in Table 2.1. For nitrogen-containing methacrylates, SEC calculations were carried out applying a universal calibration by using the poly (methyl methacrylate) MHKS parameters $K = 12.8 \cdot 10^{-3} \text{ cm}^3 \cdot \text{g}^{-1}$ and $\alpha = 0.7$. The values determined with PMMA MHKS parameters have later on been recalculated with polymer specific MHKS parameters for each polymer collated in Table 3.1. Representative PLP-SEC traces for each polymer can be found in the corresponding chapters in the Appendix A.

SEC measurements at ANU were performed on a Viscotek GPCMax SEC system

with a Viscotek TDA 305 triple detector array including a differential viscosimeter (DV), right-angle laser light scattering (RALLS), low-angle laser light scattering (LALLS), and refractive index detectors. The column set consisted of an Agilent Technologies PLgel 10 μm Guard Column (50 x 7.5 mm) and two Agilent Technologies PLgel 10 μm Mixed B columns (300 x 7.5 mm). The system was run with THF as eluent at 30°C with a flow rate of 1 mL·min⁻¹. The SEC system is calibrated using linear poly (styrene) standards and linear poly(methyl methacrylate) standards. All SEC calculations were carried out using p(MA) MHKS parameters. The obtained molecular weight distributions were smoothed to remove noise from the signal and the first derivatives were used to determine the molecular weights at the inflection points. Smoothing of the signals as well as determination of the derivatives was carried out with Origin Software. [215]

6.3.2. Triple-Detection SEC

For the analysis of the polymer samples prepared for MHKS determination, a triple detection chromatography setup consisting of a modular system (Polymer Standard Service, PSS Mainz/Agilent 1200 series) incorporating an ETA2010 viscosimeter (WGE Dr. Bures) and a multi-angle laser light scattering unit (Polymer Standard Service, PSS Mainz, SLD7000/BI-M w A, Brookhaven Instruments) is used. Two linear columns (PSS SDV-Lux-10³ Å and 10⁵ Å, 5 μm) are employed for sample separation with THF as an eluent at 35 °C and a flow rate of 1 mL·min⁻¹. The system is calibrated using poly (styrene) standards (PSS Mainz). The determination of the absolute molecular weight is achieved by employing the exact sample concentrations as well as the refractive index increments (dn/dc), collated in Table 3.1. The refractive index increments dn/dc , with n being the refractive index and c the polymer concentration, is determined for each monomer via the precisely known concentrations. For the determination of polymer specific MHKS parameters, the MALLS detector was employed to determine the weight-average molecular weight (M_w) and the intrinsic viscosity $[\eta]$ is derived from the viscosimeter signal. Both signals have been employed without any further modification (e.g. smoothing) of the residual plots. Representative triple detection SEC chromatograms (RI, MALLS, and viscosimeter signals) of polymer samples are depicted in Figures A.14 to A.19 in Appendix A.

6.3.3. Density Measurements

Measurements of the temperature-dependent densities of the monomers were performed with an Anton Paar DMA 5000 M density meter with a precision of 1 × 10 °C and 5 ×

$10^{-1} \text{ g}\cdot\text{mL}^{-1}$ and are collated in Tables 2.1 and 3.1. To prevent a polymerization process of the monomer solutions during measurements hydroquinone (HQ) was added. The temperature dependent densities of all monomers are depicted in the corresponding chapters of Appendix A.

6.3.4. UV measurements

UV spectra were recorded on a Cary-Bio 50 spectrophotometer in quartz cells with 1 cm path length. Ethyl acetate was employed as a solvent and recording of the pure EtAc showed no significant absorption in the wavelength range of interest between 250 and 500 nm. After measurements of $5 \text{ mmol}\cdot\text{L}^{-1}$ of the pure photoinitiator in EtAc, LiNTf_3 was added and the sample was measured again. Spectra containing the Lewis acids were measured immediately in sealed quartz cells to prevent potential reactions of the Lewis acids with atmospheric moisture. The resulting UV spectra are depicted in Chapter 4.1

6.4. Polymerization Techniques

For the determination of MHKS parameters for the nitrogen-containing methacrylates, polymer samples with dispersity indices of approximately 2.0 have been prepared via the following two different polymerization techniques.

6.4.1. Reversible Addition-Fragmentation Chain Transfer Polymerization

Reversible addition-fragmentation chain transfer (RAFT) polymerizations is performed in bulk solution with AIBN as initiator and cyanoisopropylidithiobenzoate (CPDB) or SS-bis(α, α' -dimethyl- α'' -acetic acid) trithiocarbonate (TRITT) as controlling agent, respectively. The initiator concentration for morpholinoethyl methacrylate (MOMA) polymerizations was approximately $9.5 \times 10^{-4} \text{ mol}\cdot\text{l}^{-1}$ and up to $6.4 \times 10^{-4} \text{ mol}\cdot\text{L}^{-1}$ for N-ethylaminoethyl methacrylate (NEAEMA) polymerizations. Detailed initiator concentrations and controlling agent concentrations for each sample are collated in Tables A.14 and A.16 of Appendix A. The polymerizations are carried out in individual class vials (approx. 1 mL per sample), sealed air tight with rubber septa and parafilm and deoxygenated by nitrogen purging for approx. 5 minutes per sample. The reactions vials are placed in a heated shaker at $66 \text{ }^\circ\text{C}$ and removed after 3.5 to 48 h. A solution of hydroquinone in THF is added to stop the polymerization process and the polymer is isolated from the monomer via dialysis against pure THF with Pectra/Por 6 Dialysis

Membrane, pre-wetted RC tubing, MWCO 1 kDa for four days. Final conversions are determined gravimetrically. The resulting polymer is analyzed using the triple detection SEC setup described previously and the obtained molecular weights ranges from $M_w = 62\,600$ to $1\,646\,000\text{ g}\cdot\text{mol}^{-1}$. Dispersities ranged from $D = 1.1$ to 2.5 .

6.4.2. Polymerization With Chain Transfer Agent

Free radical polymerization in the presence of a thiol was performed to obtain an additional set of polymers for the determination of MHKS parameters. The polymerization with chain transfer agent significantly reduces the polymerization time compared to RAFT while still ensuring a sufficiently low dispersity index. Polymerizations with chain transfer agent are performed in bulk solution for MOMA and NEAEMA with AIBN as initiator and dodecyl thiol as transfer agent. Due to the poor solubility of poly(piperidylethyl methacrylate) (p(PipEMA)) when polymerized in bulk, polymerizations of PipEMA are carried out in 50 wt% solution in butyl acetate and THF, respectively. The initiator concentration for MOMA polymerizations was 2.4×10^{-3} to $5.2 \times 10^{-3}\text{ mol}\cdot\text{L}^{-1}$, for NEAEMA polymerizations 1.1×10^{-3} to $6.0 \times 10^{-3}\text{ mol}\cdot\text{L}^{-1}$, and for PipEMA polymerizations 1.0×10^{-3} to $2.2 \times 10^{-3}\text{ mol}\cdot\text{L}^{-1}$. Thiol concentrations varied from 0.05 to 0.76 mol% for MOMA, 0.18 to 2.19 mol% for NEAEMA, and 0.07 to 0.93 mol% for PipEMA polymerizations. Detailed sample conditions are collated in Tables A.15 and A.17 to A.21 in Appendix A.

7

Abbreviations

α	Mark-Houwink-Kuhn-Sakurada parameter, exponent
AIBN	2,2'-azobis(2-methylpropionitrile)
ATRP	Atom Transfer Radical Polymerization
BA	butyl acrylate
BeA	behenyl acrylate
BeMA	behenyl methacrylate
BMA	butyl methacrylate
BnA	benzyl acrylate
BnMA	benzyl methacrylate
BuAc	butyl acetate
C17A	heptadecyl acrylate
C17MA	heptadecyl methylacrylate
C21A	hencicosyl acrylate
cHMA	<i>cyclo</i> -hexyl methacrylate
CPDB	2 cyano 2 propylbenzodithioat
\mathcal{D}	dispersity
DA	dodecyl acrylate
DEAEMA	2-(<i>N,N</i> -diethylamino)ethyl methacrylate
DMA	dodecyl methacrylate
DMAEMA	2-(<i>N,N</i> -dimethylamino)ethyl methacrylate
DMAPMAE	3-(<i>N,N</i> -dimethylamino)propyl methacrylate
DMPA	2,2-dimethoxy-2-phenylacetophenone
DMAc	<i>N,N</i> -dimethylacetamide
e.g.	for example (latin: <i>exempli gratia</i>)
EA	ethyl acrylate
EHA	2-ethylhexyl acrylate
EHMA	2-ethylhexyl methylacrylate
EMA	ethyl methacrylate
$[\eta]$	intrinsic viscosity

7. Abbreviations

FRP	Free Radical Polymerization
GMA	glycidyl methacrylate
GPC	Gel Permeation Chromatography
HA	hexyl acrylate
HCPA	(hexylcarbamoyloxy)- <i>iso</i> -propyl acrylate
HEMA	2-hydroxyethyl methacrylate
HPCA	hydroxyl- <i>iso</i> -propylcarbamate acrylate
HPMA	hydroxypropyl methacrylate
HQ	hydroquinone
i.e.	that is (id est)
<i>i</i> BMA	<i>iso</i> -butyl methacrylate
<i>i</i> BoA	<i>iso</i> -bornyl acrylate
<i>i</i> DeMA	<i>iso</i> -decyl methacrylate
INA-A	<i>iso</i> -nonyl acrylate
K	Mark-Houwink-Kuhn-Sakurada parameter, prefactor
k_p	propagation rate coefficient
LALLS	Low Angle Laser Light Scattering
LASER	Light Amplification by Stimulated Emission of Radiation
LiNTf ₃	lithium bis(trifluoromethane) sulfonamide
MA	methyl acrylate
MALLS	Multi Angle Laser Light Scattering
MCR	Mid Chain Radical
MeHQ	methyl hydroquinone
MHKS	Mark-Houwink-Kuhn-Sakurada
MMA	methyl methacrylate
M_n	number average molecular weight
MOMA	2-morpholinoethyl methacrylate
MW	molecular weight
M_w	weight average molecular weight
MWD	Molecular Weight Distribution
NEAEMA	2-(<i>N</i> -ethylanylino)ethyl methacrylate
NMP	Nitroxide Mediated Polymerization
NMR	Nuclear Magnetic Resonance
PHA	2-propylheptyl acrylate
PhCPA	(phenylcarbamoyloxy)- <i>iso</i> -propyl acrylate
PHMA	2-propylheptyl methacrylate

PipEMA	2-(1-piperidyl)ethyl methacrylate
PLP	Pulsed Laser Polymerization
PMMA	poly(methyl methacrylate)
PS	polystyrene
RAFT	Reversible Addition Fragmentation Chain Transfer
RALLS	Right Angle Laser Light Scattering
RDRP	Reversible Deactivation Radical Polymerization
RI	Refractive Index
SA	stearyl acrylate
SEC	Size Exclusion Chromatography
SMA	stearyl methacrylate
SPR	secondary propagation radical
<i>t</i> BA	<i>tert</i> -butyl acrylate
<i>t</i> BMA	<i>tert</i> -butyl methacrylate
TDA-A	tridecyl acrylate
TDA-MA	tridecyl methacrylate
TDN-A	tridecyl acrylate
TDN-MA	tridecyl methacrylate
T_g	glass transition temperature
THF	Tetrahydrofuran
TRITT	S,S-bis(α,α' -dimethyl- α'' -acetic acid)trithiocarbonate
TS	transition state

Bibliography

- [1] C. Barner-Kowollik, *Handbook of RAFT Polymerization*, Wiley-VCH Weinheim, **2008**.
- [2] K. Matyjaszewski, J.-S. Wang, *J. Am. Chem. Soc.* **1995**, *117*, 5614–5615.
- [3] G. Moad, E. Rizzardo, S. H. Thang, *Aust. J. Chem.* **2005**, *58*, 379–410.
- [4] J. Chiefari, Y. K. Chong, F. Ercole, J. Krstina, J. Jeffrey, T. P. Le, R. T. A. Mayadunne, G. F. Meijs, C. L. Moad, G. Moad, E. Rizzardo, S. H. Thang, *Macromolecules* **1998**, *31*, 5559–5562.
- [5] E. Rizzardo, G. Moad, *Macromolecules* **1995**, *28*, 8722–8728.
- [6] C. J. Hawker, A. W. Bosman, E. Harth, *Chem. Rev.* **2001**, *101*, 3661–3688.
- [7] J. Nicolas, Y. guillaneuf, C. Lefai, D. Bertin, D. Gigmes, B. Charleux, *Prog. Polym. Sci* **2013**, *38*, 63.
- [8] T. Junkers, C. Barner-Kowollik, *J. Polym. Sci. Part A: Polym. Chem.* **2008**, *46*, 7585–7605.
- [9] J. M. Asua, S. Beuermann, M. Buback, P. Castignolles, B. Charleux, R. G. Gilbert, R. A. Hutchinson, J. R. Leiza, A. N. Nikitin, J.-P. Vairon, A. M. van Herk, *Macromol. Chem. Phys.* **2004**, *205*(16), 2151–2160.
- [10] T. Junkers, M. Schneider-Baumann, S. S. P. Koo, P. Castignolles, C. Barner-Kowollik, *Macromolecules* **2010**, *43*, 10427–10434.
- [11] A. N. Nikitin, R. A. Hutchinson, M. Buback, P. Hesse, *Macromolecules* **2007**, *40*, 8631–8641.
- [12] A. P. Haehnel, S. Fleischmann, P. Hesse, K.-D. Hungenberg, C. Barner-Kowollik, *Macromol. React. Eng.* **2013**, *7*, 8–23.
- [13] M. Zhong, K. Matyjaszewski, *Macromolecules* **2011**, *44*, 2668.
- [14] M. L. Coote, C. Barner-Kowollik, *Aust. J. Chem.* **2006**, *59*, 712–718.
- [15] L. Hlalele, B. Klumperman, *Macromolecules* **2011**, *44*, 6683–6690.
- [16] R. V. Slone, *Encyclopedia of Polymer Science and Technology*, Wiley, **2010**.

- [17] O. M. Pressley, W. Zhang, A. M. Maurice US Pat.-US92122922, **2015**.
- [18] M. Scherer, R. Schweder US Pat.-US8722600, **2014**.
- [19] M. Gerst, H. Harrer, D. Wulff WO Pat.-WO2012139941, **2012**.
- [20] S. D. Pacetti US Pat.-US7244443, **2007**.
- [21] A. Kondo US Pat.-US7217743, **2007**.
- [22] T. Bolle, G. Macor WO Pat.-WO2005089957, **2005**.
- [23] S. H. Ma US Pat.-US6451950, **2002**.
- [24] S. H. Ma, W. R. Hertler US Pat.-US5648405, **1997**.
- [25] F. Foll, D. Bosc, J. Liang, A. Rousseau, B. Boutevin US Pat.-US5496899, **1996**.
- [26] R. Y. Chen US Pat.-US4143949, **1979**.
- [27] W. A. Braunecker, K. Matyjaszewski, *Prog. Polym. Sci* **2007**, *32*, 93–146.
- [28] G. Odian, *Principles of Polymerization*, Wiley-Interscience, Hoboken, New York, **2004**.
- [29] K. Matyjaszewski, *Controlled and Living Polymerizations: Radical Polymerization*, Wiley-VCH Weinheim, **2010**.
- [30] P. J. Flory, *Principles of Polymer Chemistry*, Cornell Univ. Press, Ithaca, New York, **1953**.
- [31] C. Barner-Kowollik, P. Vana, T. P. Davis, *Handbook of Radical Polymerization*, Wiley-VCH, **2003**.
- [32] J. P. Heuts, G. T. Russell, *Eur. Polym. J.* **2006**, *42*, 3–20.
- [33] J. P. Heuts, R. G. Gilbert, L. Radom, *Macromolecules* **1995**, *28*, 8771–8781.
- [34] J. Barth, M. Buback, G. T. Russell, S. Smolne, *Macromol. Chem. Phys.* **2011**, *212*, 1366–1378.
- [35] G. Johnston-Hall, A. Theis, M. J. Monteiro, T. P. Davis, M. H. Stenzel, C. Barner-Kowollik, *Macromol. Chem. Phys.* **2005**, *206*, 2047–2053.
- [36] A. Theis, A. Feldermann, N. Charton, T. P. Davis, M. H. Stenzel, C. Barner-Kowollik, *Polymer* **2005**, *46*, 6797–6809.

- [37] A. Theis, A. Feldermann, N. Charton, M. H. Stenzel, T. P. Davis, C. Barner-Kowollik, *Macromolecules* **2005**, *38*, 2595–2605.
- [38] C. Barner-Kowollik, G. T. Russell, *Prog. Polym. Sci* **2009**, *34*, 1211–1259.
- [39] J. M. G. Cowie, V. Arrighi, *Polymer: Chemistry and Physics of Modern Materials*, CRC Press, Scotland, **2008**.
- [40] C. Barner-Kowollik, T. Junkers, *J. Polym. Sci. Part A: Polym. Chem.* **2011**, *49*, 1293–1297.
- [41] A. Feldermann, M. L. Coote, M. H. Stenzel, T. P. Davis, C. Barner-Kowollik, *J. Am. Chem. Soc.* **2004**, *126*, 15915–15923.
- [42] G. E. Scott, E. Senogles, *J. Macromol. Sci: Part A* **1970**, *4*, 1105–1117.
- [43] G. E. Scott, E. Senogles, *J. Macromol. Sci: Part C* **1973**, *9*, 49–69.
- [44] G. E. Scott, E. Senogles, *J. Macromol. Sci: Part A* **1974**, *8*, 753–773.
- [45] F. Bennet, T. Roelle, T. Faecke, M.-S. Weiser, F.-K. Bruder, C. Barner-Kowollik, T. Junkers, *Macromol. Chem. Phys.* **2013**, *214*, 236–245.
- [46] J. Vandenberg, T. Junkers, *Macromolecules* **2012**, *45*, 6850–6856.
- [47] A. N. F. Peck, R. A. Hutchinson, *Macromolecules* **2004**, *37*, 5944–5951.
- [48] A. D. Jenkins, R. G. Jones, G. Moad, *Pure Appl. Chem.* **2010**, *82*, 483–491.
- [49] K. Matyjaszewski, *Controlled/Living Radical Polymerization: Progress in ATRP, NMP, and RAFT*, American Chemical Society, Washington DC, **2000**.
- [50] M. Szwarc, *Nature* **1956**, *178*, 1168–1169.
- [51] R. P. Quirk, B. Lee, *Polym. Int.* **1992**, *27*, 359–367.
- [52] K. Matyjaszewski, A. H. E. Mueller, *Controlled and Living Polymerization: From Mechanisms to Applications*, Vol. 634, Wiley-VCH Weinheim, **2009**.
- [53] G. Moad, E. Rizzardo, S. H. Thang, *Aust. J. Chem.* **2006**, *59*, 669–692.
- [54] G. Moad, E. Rizzardo, S. H. Thang, *Aust. J. Chem.* **2009**, *62*, 1402–1472.
- [55] P. Corpart, D. Charmot, T. Biadatti, S. Zard, D. Michelet, „Procédé de synthèse de polymères à blocs par polymérisation radicalaire contrôlée“, **1998**, wO Patent App. PCT/FR1998/001,316.

- [56] M. Destarac, W. Bzducha, D. Taton, I. Gauthier-Gillaizeau, S. Zard, *Macromol. Rapid Commun.* **2002**, *23*, 1049–1054.
- [57] C. Barner-Kowollik, M. Buback, B. Charleux, M. L. Coote, M. Drache, T. Fukuda, A. Goto, B. Klumperman, A. B. Lowe, J. B. McLeary, G. Moad, M. J. Monteiro, R. D. Sanderson, M. P. Tonge, P. Vana, *J. Polym. Sci. Part A: Polym. Chem.* **2006**, *44*, 5809–5831.
- [58] T. Junkers, G. Delaittre, R. Chapman, F. Guenzler, E. Chernikova, C. Barner-Kowollik, *Macromol. Rapid Commun.* **2012**, *33*, 984–990.
- [59] E. Rizzardo, M. Chen, B. Chong, G. Moad, M. Skidmore, S. H. Thang, *Macromol. Symp.* **2007**, *248*, 104–116.
- [60] Y. K. Chong, G. Moad, E. Rizzardo, M. Skidmore, S. H. Thang, *Macromolecules* **2007**, *40*, 9262–9271.
- [61] M. Eberhardt, P. Theato, *Macromol. Rapid Commun.* **2005**, *26*, 1488–1493.
- [62] S. Patel, R. G. Thakar, J. Wong, S. D. McLeod, S. Li, *Biomaterials* **2006**, *27*, 2890–2897.
- [63] H. Mori, S. Nakano, T. Endo, *Macromolecules* **2005**, *38*, 8192–8201.
- [64] P. Zhao, Q. Ling, W. Z. Wang, J. Ru, S.-B. Li, W. Huang, *Polym. Sci. Part A: Polym. Chem.* **2007**, *45*, 242–252.
- [65] N. Zhou, L. Lu, J. Zhu, X. Yang, X. Wang, X. Zhu, Z. Zhang, *Polymer* **2007**, *48*, 1255–1260.
- [66] A. D. McNaught, A. Wilkinson, *IUPAC Compendium of Chemical Terminology (The Gold Book)*, Blackwell Scientific Publications, Oxford, **1997**.
- [67] C. A. Barson, *Comprehensive Polymer Science*, Vol. 3, Pergamon, London, **1989**.
- [68] K. Matyjaszewski, T. P. Davis, *Handbook of Radical Polymerization*, John Wiley & Sons, **2002**.
- [69] H. S. Taylor, W. H. Jones, *J. Am. Chem. Soc.* **1930**, *52*, 1111–1121.
- [70] G. S. Whitby, *Synthetic Rubber*, John Wiley, NY, **1954**.
- [71] P. J. Flory, *J. Am. Chem. Soc.* **1937**, *59*, 241–253.

- [72] F. R. Mayo, *J. Am. Chem. Soc.* **1943**, *65*, 2324–2329.
- [73] R. A. Gregg, F. R. Mayo, *J. Am. Chem. Soc.* **1948**, *70*, 2373–2378.
- [74] F. R. Mayo, R. A. Gregg, M. S. Matheson, *J. Am. Chem. Soc.* **1951**, *73*, 1691–1700.
- [75] R. A. Gray, *J. Coat. Tech.* **1985**, *57*, 83–91.
- [76] B. Boutevin, A. El Idrissi, J. P. Parisi, *Makromol. Chem.* **1990**, *191*, 445–456.
- [77] B. Boutevin, J.-M. Lusinchi, Y. Pietrasanta, J.-J. Robin, *Eur. Polym. J.* **1994**, *30*, 615–619.
- [78] P. Gregor, D. Dolar, G. K. Hoesche, *J. Am. Chem. Soc.* **1955**, *77*, 3675.
- [79] G. Reiss, P. Bahadur, *Encyclopedia of Polymer Science and Engineering*, Vol. 2, Wiley, NY, **1985**.
- [80] J. Brandrup, E. H. Immergut, E. A. Grulke, A. Abe, D. R. Bloch, *Polymer Handbook*, 4. Aufl., John Wiley & Sons, New York, **1999**.
- [81] A. Nagy, D. Szalay, T. Foeldes-Berezsnich, F. Tuedoes, *Europ. Polym. J.* **1983**, *19*, 1047–1053.
- [82] A. P. Aleksandrov, N. G. Vladimir, M. S. Kitaï, I. M. Smirnova, V. V. Sokolov, *Sov. J. Quantum Electron.* **1977**, *7*(5), 547.
- [83] O. F. Olaj, I. Bitai, F. Hinkelmann, *Macromol. Chem.* **1987**, *188*(7), 1689–1702.
- [84] A. Kornherr, O. F. Olaj, I. Bitai, G. Zifferer, *Macromol. Theory Simul.* **2003**, *12*(5), 332–338.
- [85] I. Schnoell-Bitai, O. F. Olaj, *Macromol. Chem.* **1990**, *191*(10), 2491–2499.
- [86] C. Barner-Kowollik, S. Beuermann, M. Buback, P. Castignolles, B. Charleux, M. L. Coote, R. A. Hutchinson, T. Junkers, I. Lacik, G. Russell, M. Stach, A. van Herk, *Polymer Chemistry* **2014**, *5*(1), 204–212.
- [87] S. Beuermann, *Pure Appl. Chem.* **2003**, *75*(8), 1091–1096.
- [88] S. Beuermann, M. Buback, T. P. Davis, N. García, R. G. Gilbert, R. A. Hutchinson, A. Kajiwara, M. Kamachi, I. Lacik, G. T. Russell, *Macromol. Chem. Phys.* **2003**, *204*(10), 1338–1350.

- [89] S. Beuermann, M. Buback, T. P. Davis, R. G. Gilbert, R. A. Hutchinson, A. Kajiwara, B. Klumperman, G. T. Russell, *Macromol. Chem. Phys.* **2000**, *201*(12), 1355–1364.
- [90] S. Beuermann, M. Buback, T. P. Davis, R. G. Gilbert, R. A. Hutchinson, O. F. Olaj, G. T. Russell, J. Schweer, A. M. van Herk, *Macromol. Chem. Phys.* **1997**, *198*, 1545–1560.
- [91] S. Beuermann, M. Buback, P. Hesse, F. D. Kuchta, I. Lacik, A. M. van Herk, *Pure Appl. Chem.* **2007**, *79*(8), 1463–1469.
- [92] M. Buback, R. G. Gilbert, R. A. Hutchinson, B. Klumperman, F.-D. Kuchta, B. G. Manders, K. F. O’Driscoll, G. T. Russell, J. Schweer, *Macromol. Chem. Phys.* **1995**, *196*(10), 3267–3280.
- [93] S. Beuermann, M. Buback, *Prog. Polym. Sci.* **2002**, *27*(2), 191–254.
- [94] A. M. van Herk, *Macromol. Rapid Commun.* **2009**, *30*(23), 1964–1968.
- [95] K. B. Kockler, A. P. Haehnel, T. Junkers, C. Barner-Kowollik, *Macromol. Rapid Commun.* **2016**, *37*, 123.
- [96] M. Buback, M. Busch, R. A. Laemmel, *Macromol. Theory Simul.* **1996**, *5*, 845–861.
- [97] J. Sarnecki, J. Schweer, *Macromolecules* **1995**, *28*, 4080–4088.
- [98] S. Beuermann, D. A. Paquet, J. H. McMinn, R. A. Hutchinson, *Macromolecules* **1996**, *29*, 4206–4215.
- [99] C. Barner-Kowollik, T. Junkers, *J. Polym. Sci.* **2008**, *46*, 7585–7605.
- [100] M. L. Coote, M. D. Zammit, T. P. Davis, G. D. Willett, *Macromolecules* **1997**, *30*, 8182–8190.
- [101] J. Schweer, *Macromol. Chem. Theor. Simul.* **1993**, *2*, 485–502.
- [102] T. Fukuda, Y.-D. Ma, H. Inagaki, *Macromolecules* **1985**, *18*, 17–26.
- [103] M. L. Coote, T. P. Davis, *Prog. Polym. Sci.* **1999**, *24*, 1217–1251.
- [104] L. M. Morris, T. P. Davis, R. P. Chaplin, *Polymer* **2001**, *42*, 941–952.
- [105] R. A. Hutchinson, J. H. McMinn, D. A. Paquet, S. Beuermann, C. Jackson, *Ind. Eng. Chem. Res.* **1997**, *36*, 1103–1113.
- [106] O. F. Olaj, I. Schnoell-Bitai, *Makromol. Chem. Rapid. Commun.* **1990**, *11*, 459–465.

- [107] M. C. Piton, M. A. Winnik, T. P. Davis, K. F. O'Driscoll, *J. Polym. Sci. Part A: Polym. Chem.* **1990**, *28*, 2097–2106.
- [108] M. L. Coote, T. P. Davis, *Macromolecules* **1998**, *32*, 3626–3636.
- [109] D. Kukulj, T. P. Davis, *Macromolecules* **1998**, *31*, 5668–5680.
- [110] O. F. Olaj, I. Schnoell-Bitai, P. Kremminger, *Eur. Polym. J.* **1989**, *25*, 535–541.
- [111] T. P. Davis, K. F. O'Driscoll, M. C. Piton, M. A. Winnik, *J. Polym. Sci. Part C: Polym. Lett.* **1989**, *27*, 181–185.
- [112] M. L. Coote, R. Johnston, T. P. Davis, *Macromolecules* **1997**, *30*, 8191–8204.
- [113] T. P. Davis, K. F. O'Driscoll, M. C. Piton, M. A. Winnik, *Macromolecules* **1990**, *23*, 2113–2119.
- [114] W. Wang, R. A. Hutchinson, *Macromolecules* **2008**, *41*, 9011–9018.
- [115] R. A. Cockburn, R. Siegmann, K. A. Payne, S. Beuermann, T. F. L. McKenna, R. A. Hutchinson, *Biomacromolecules* **2011**, *12*, 2319–2326.
- [116] S. Beuermann, R. Siegmann, M. Drache, *J. Fluorine Chem.* **2014**, *159*.
- [117] M. Buback, A. Feldermann, C. Barner-Kowollik, I. Lacik, *Macromolecules* **2001**, *34*, 5439–5448.
- [118] E. Mueller, Dissertation, **2005**.
- [119] H. A. S. Schoonbrood, B. van den Reijen, J. B. L. de Kock, B. G. Manders, M. van Herk, A. A. L. German, *Macromol. Rapid Commun.* **1995**, *16*, 119–124.
- [120] M. L. Coote, T. P. Davis, *Polym. React. Eng.* **1999**, *7*, 363–377.
- [121] R. X. E. Willemse, M. van Herk, A. A. L. German, *Macromol. Chem. Phys.* **2010**, *211*, 539–545.
- [122] R. X. E. Willemse, M. van Herk, A. A. L. German, *J. Am. Chem. Soc.* **2006**, *128*, 4471–4480.
- [123] H. Chen, B. Guo, *Anal. Chem.* **1997**, *69*, 4399–4404.
- [124] M. W. F. Nielen, *Mass. Spectrom. Ref.* **1999**, *18*, 309–344.
- [125] C. N. McEwen, C. Jackson, B. S. Larsen, *Int. J. Mass Spectrom.* **1997**, *160*, 387–394.
- [126] C. Boukaftane, M. van Herk, A. A. L. German, *Macromol. Chem. Phys.* **2011**, *212*, 96–101.

- [127] C. Plessis, G. Arzamendi, J. M. Alberdi, M. van Herk, A. J. R. Leiza, J. M. Asua, *Macromol. Rapid Commun.* **2003**, *24*, 173–177.
- [128] J. Barth, M. Buback, P. Hesse, T. Sergeeva, *Macromolecules* **2010**, *43*, 4023–4031.
- [129] Y. W. Marien, P. H. M. van Steenberge, K. B. Kockler, C. Barner-Kowollik, M.-F. Reyniers, D. R. D’hooge, G. B. Marin, *Polym. Chem.* **2016**, *7*, 6521–6528.
- [130] A. P. Haehnel, M. Schneider-Baumann, K. U. Hildebrandt, A. M. Misske, C. Barner-Kowollik, *Macromolecules* **2013**, *46*(1), 15–28.
- [131] A. P. Haehnel, M. Schneider-Baumann, L. Arens, A. M. Misske, F. Fleischhaker, C. Barner-Kowollik, *Macromolecules* **2014**, *47*, 3483–3496.
- [132] K. B. Kockler, A. P. Haehnel, F. Fleischhaker, M. Schneider-Baumann, A. M. Misske, C. Barner-Kowollik, *Macromol. Chem. Phys.* **2015**, *216*, 1573.
- [133] A. P. Haehnel, B. Wenn, K. B. Kockler, T. Bantle, A. M. Misske, F. Fleischhaker, T. Junkers, C. Barner-Kowollik, *Macromol. Rapid Commun.* **2014**, *35*, 2029.
- [134] K. B. Kockler, F. Fleischhaker, C. Barner-Kowollik, *Polym. Chem.* **2016**, *7*, 4342–4351.
- [135] K. B. Kockler, F. Fleischhaker, C. Barner-Kowollik, *Macromolecules* **2016**, *49*, 8572–8580.
- [136] M. L. Coote, M. D. Zammit, T. P. Davis, *Trends Polym. Sci.* **1996**, *4*, 189–196.
- [137] M. L. Coote, T. P. Davis, *J. Polym. Sci. Part B: Polym. Phys.* **1999**, *37*, 2557–2570.
- [138] L. K. Kostanski, D. M. Keller, A. E. Hamielec, *J. Biochem. Biophys. Methods* **2004**, *58*, 159–186.
- [139] A. Ouano, W. Kaye, *J. Polym. Sci. Part A: Polym. Chem.* **1974**, *12*, 1151–1162.
- [140] M. A. Haney, *J. Appl. Polym. Sci.* **1985**, *30*, 3037–3040.
- [141] P. J. Wyatt, *Anal. Chim. Acta* **1993**, *272*, 1–40.
- [142] M. D. Zammit, T. P. Davis, *Polymer* **1997**, *38*, 4455–4468.
- [143] M. D. Zammit, T. P. Davis, K. G. Suddaby, *Polymer* **1998**, *39*, 5789–5798.
- [144] M. G. Pigeon, A. Rudin, *J. Appl. Polym. Sci.* **1995**, *57*, 287–301.

- [145] T. P. Davis, M. D. Zammit, *Macromol. Symp*, **1996**, *111*, 243–252.
- [146] M. D. Zammit, M. L. Coote, T. P. Davis, G. D. Willett, *Macromolecules* **1998**, *31*, 955–963.
- [147] Z. Grubisic, P. Rempp, H. Benoit, *J. Polym. Sci. Part B: Polym. Lett.* **1967**, *5*, 753–759.
- [148] C. Jackson, Y.-J. Chen, J. W. Mays, *J. Appl. Polym. Sci.* **1996**, *61*, 865–874.
- [149] T. P. Davis, M. L. Coote, *J. Polym. Sci. Part B: Polym. Ph* **1999**, *37*, 2557–2570.
- [150] „PSS Homepage, <https://www.pss-polymer.com>“, **viewed 02.2017**.
- [151] H. Mark, *Der Feste Körper*, Hirzel, Leipzig, **1938**.
- [152] B. Dervaux, T. Junkers, M. Schneider-Baumann, F. E. Du Prez, C. Barner-Kowollik, *J. Polym. Sci. Part A: Polym. Chem.* **2009**, *47*, 6641–6654.
- [153] Z. Xu, M. Song, N. Hadjichristidis, L. J. Fetters, *Macromolecules* **1981**, *14*, 1591–1594.
- [154] E. Penzel, N. Goetz, *Angew. Makromol. Chem.* **1990**, *178*, 191–200.
- [155] R. R. Chance, S. P. Baniukiewicz, D. Mintz, G. Ver Strate, *Int. J. Polym. Anal. Charact.* **1995**, *1*, 3–34.
- [156] S. A. Arrhenius, *Z. Phys. Chem.* **1889**, *4*, 96–116.
- [157] C. Kenneth, *Chemical Kinetics: The Study of Reaction RRate in Solution*, VCH Publishers, **1990**.
- [158] H. Eyring, *J. Chem. Phys.* **1935**, *3*, 107–115.
- [159] M. van Herk, A. H. van den Brand, I. Berg, „Contour V2.0.2“, **2012**.
- [160] R. X. E. Willemse, M. van Herk, A. E. Panchenko, T. Junkers, M. Buback, *Macromolecules* **2005**, *38*, 5098–5103.
- [161] C. Barner-Kowollik, F. Guenzler, T. Junkers, *Macromolecules* **2008**, *41*, 8971–8973.
- [162] T. Junkers, D. Voll, C. Barner-Kowollik, *e-Polymers* **2009**, *076*, 1618–1729.
- [163] R. A. Hutchinson, S. Beuermann, D. A. Paquet, J. H. McMinn, *Macromolecules* **1997**, *30*, 3490–3493.

- [164] C. Barner-Kowollik, S. Beuermann, M. Buback, P. Castignolles, B. Charleux, M. L. Coote, R. A. Hutchinson, T. Junkers, I. Lacik, G. Russell, M. Stach, A. van Herk, *Polym. Chem.* **2014**, *5*, 204–212.
- [165] M. Buback, C. H. Kurz, C. Schmaltz, *Macromol. Chem. Phys.* **1998**, *199*, 1721–1727.
- [166] M. Gaborieau, R. G. Gilbert, A. Gray-Weale, J. M. Hernandez, P. Castignolles, *macromol. Theory Simul.* **2007**, *16*, 13–28.
- [167] P. Castignolles, *Macromol. Rapid Commun.* **2009**, *30*, 1995–2001.
- [168] R. A. Hutchinson, S. Beuermann, D. A. Paquet, J. H. McMinn, C. Jackson, *Macromolecules* **1998**, *31*, 1542–1547.
- [169] A. M. van Herk, T. Droege, *Macromol. Theory Simul.* **1997**, *6*, 1263–1276.
- [170] E. Sato, T. Emoto, P. B. Zetterlund, B. Yamada, *Macromol. Chem. Phys.* **2004**, *205*, 1829–1839.
- [171] A. N. Nikitin, P. Castignolles, B. Charleux, J.-P. Vairon, *Macromol. Rapid Commun.* **2003**, *24*, 778–782.
- [172] „Coherent, Suppliers for LASER Systems, <https://www.coherent.com>“, **viewed 01.2017**.
- [173] „GAM LASER Inc. Homepage, Supplier for LASER Systems, <https://www.gamlaser.com>“, **viewed 01.2017**.
- [174] J. P. Heuts, Sudarko, R. G. Gilbert, *Macromol. Symp.* **1996**, *111*, 147–157.
- [175] S. Beuermann, M. Buback, V. El Rezzi, M. Jürgens, D. Nelke, *Macromol. Chem. Phys.* **2004**, *205*(7), 876–883.
- [176] S. Beuermann, M. Buback, P. Hesse, I. Lacik, *Macromolecules* **2005**, *39*, 184–193.
- [177] S. Beuermann, M. Buback, P. Hesse, S. Kuckučková, I. Lacik, *Macromol. Symp.* **2007**, *248*, 41–49.
- [178] S. C. Thickett, R. G. Gilbert, *Polymer* **2004**, *45*, 6993–6999.
- [179] A. P. Haehnel, Dissertation, Karlsruhe Institute of Technology, **2014**.
- [180] G. E. Roberts, T. P. Davis, J. P. Heuts, G. E. Ball, *Macromolecules* **2002**, *35*, 9954–9963.

- [181] I. Degirmenci, B. B. Noble, C. Y. Lin, M. L. Coote, *The Mechanism of Stereoregulation in Free-Radical Polymerization of Bulk Methacrylates. in Progress in Controlled Radical Polymerization: Mechanisms and Techniques*, Vol. 1100, American Chemical Society, Washington DC, **2012**.
- [182] F. Fleischhaker, A. P. Haehnel, A. M. Misske, M. Blanchot, S. Haremza, C. Barner-Kowollik, *Macromol. Chem. Phys.* **2014**, *215*, 1192–1200.
- [183] J. W. Gibbs, *On the Equilibrium of Heterogeneous Substances.*, Vol. 3, Transactions of the Connecticut Academy of Arts and Sciences, **1874-1778**.
- [184] P. Pascal, M. A. Winnik, D. H. Napper, R. G. Gilbert, *Makromol. Chem. Rapid Commun.* **1993**, *14*, 213–215.
- [185] C. Barner-Kowollik, F. Bennet, M. Schneider-Baumann, D. Voll, T. Roelle, T. Facke, M.-S. Weiser, F.-K. Bruder, Junker, *Polym. Chem.* **2010**, *1*, 470–479.
- [186] A. P. Haehnel, M. Stach, A. Chovancova, J. M. Rueb, G. Delaittre, A. M. Misske, I. Lacik, C. Barner-Kowollik, *Polym. Chem.* **2014**, *5*, 862–873.
- [187] K. Liang, R. A. Hutchinson, *Macromol. Rapid Commun.* **2011**, *32*, 1090–1095.
- [188] M. Deletre, G. Levesque, *Macromolecules* **1990**, *23*, 4733–4741.
- [189] X.-P. Qiu, M. A. Winnik, *Macromol. Rapid Commun.* **2006**, *27*, 1648–1653.
- [190] G. Moad, D. H. Solomon, *The Chemistry of Radical Polymerization*, Elsevier Science Ltd., Amsterdam, **2005**.
- [191] K. Satoh, M. Kamigaito, *Chem. Rev.* **2009**, *109*, 5120–5156.
- [192] F. A. Bovey, *J. Polym. Sci.* **1960**, *47*, 480–481.
- [193] T. Otsu, B. Yamada, M. J. Imoto, *Macromol. Chem.* **1966**, *1*, 61–74.
- [194] Y. Isobe, T. Nakano, Y. Okamoto, *J. Polym. Sci. Part A: Polym. Chem.* **2001**, *39*, 1463–1471.
- [195] S. Habaue, H. Baraki, Y. Okamoto, *Polym. J.* **2000**, *32*, 1017–1021.
- [196] Y. Isobe, D. Fujioka, S. Habaue, Y. Okamoto, *J. Am. Chem. Soc.* **2001**, *123*, 7180–7181.
- [197] S. Habaue, Y. Isobe, Y. Okamoto, *Tetrahedron* **2002**, *58*, 8205–8209.

- [198] Y. Suito, Y. Isobe, S. Habaue, Y. Okamoto, *J. Polym. Sci. Part A: Polym. Chem.* **2002**, *40*, 2496–2500.
- [199] Y. Isobe, Y. Suito, S. Habaue, Y. Okamoto, *J. Polym. Sci. Part A: Polym. Chem.* **2003**, *41*, 1027–1033.
- [200] S. Matsumoto, S. Nakamura, *J. Appl. Polym. Sci.* **1999**, *74*, 290–296.
- [201] J. F. Lutz, D. Neugebauer, K. Matyjaszewski, *J. Am. Chem. Soc.* **2003**, *125*, 6986–6993.
- [202] B. Ray, Y. Isobe, S. Matsumoto, S. Habaue, Y. Okamoto, M. Kamigaito, M. Saramoto, *Macromolecules* **2004**, *37*, 1702–1710.
- [203] B. B. Noble, L. M. Smith, M. L. Coote, *Polym. Chem.* **2014**, *5*, 4974–4983.
- [204] L. Hermosilla, P. Calle, P. Tiemblo, N. Garcia, L. Garrido, J. Guzman, *Macromolecules* **2013**, *46*, 5445–5454.
- [205] C. H. Bamford, A. D. Jenkins, R. Johnston, *Proc. R. Soc. London, Ser. A* **1957**, *241*, 364–375.
- [206] S. Pedron, J. Guzman, N. Garcia, *Macromol. Chem. Phys.* **2011**, *212*, 860–869.
- [207] T. Clark, *J. Chem. Soc., Chem. Commun.* **1986**, 1774–1776.
- [208] K. Vyakaranam, J. B. Barbour, J. Michl, *J. Am. Chem. Soc.* **2006**, *128*, 5610–5611.
- [209] T. Clark, *J. Am. Chem. Soc.* **2006**, *128*, 11278–11285.
- [210] A. H. Horn, T. Clark, *J. Am. Chem. Soc.* **2003**, *125*, 2809–2816.
- [211] B. B. Noble, A. C. Mater, L. M. Smith, M. L. Coote, *Polym. Chem.* **2016**, *7*, 6400–6412.
- [212] E. Frick, C. Schweigert, B. B. Noble, H. A. Ernst, A. Lauer, Y. Liang, D. Voll, M. L. Coote, A.-N. Unterreiner, C. Barner-Kowollik, *Macromolecules* **2016**, *49*, 80–89.
- [213] D. E. Fast, A. Lauer, J. P. Menzel, A.-M. Kelterer, G. Gescheidt, C. Barner-Kowollik, *Macromolecules* **2017**.
- [214] J. T. Lai, D. Filla, R. Shea, *Macromolecules* **2002**, *35*, 6754–6756.
- [215] „OriginLab Corporation, Northampton, MA01060, USA. Origin Pro 9.0G“.



Appendix

A.1. Chapter 2: Branched Acrylates in Solution

For each monomer investigated in the current study, exemplary molecular weight distributions (MWD) obtained via SEC analysis are provided alongside tables with the specific PLP conditions of all samples incorporated into the final Arrhenius plots as well as the temperature dependent density curves. Parts of this chapter, including figures were reproduced with permission from Kockler, K. B.; Haehnel, A. P.; Fleischhaker, F.; Schneider-Baumann, M.; Misske, A. M.; Barner-Kowollik, C. *Macromol. Chem. Phys.* **2015**, *216*, 1573–1582. Copyright (2016) WILEY-VCH Verlag GmbH & Co. KGaA, Weinheim

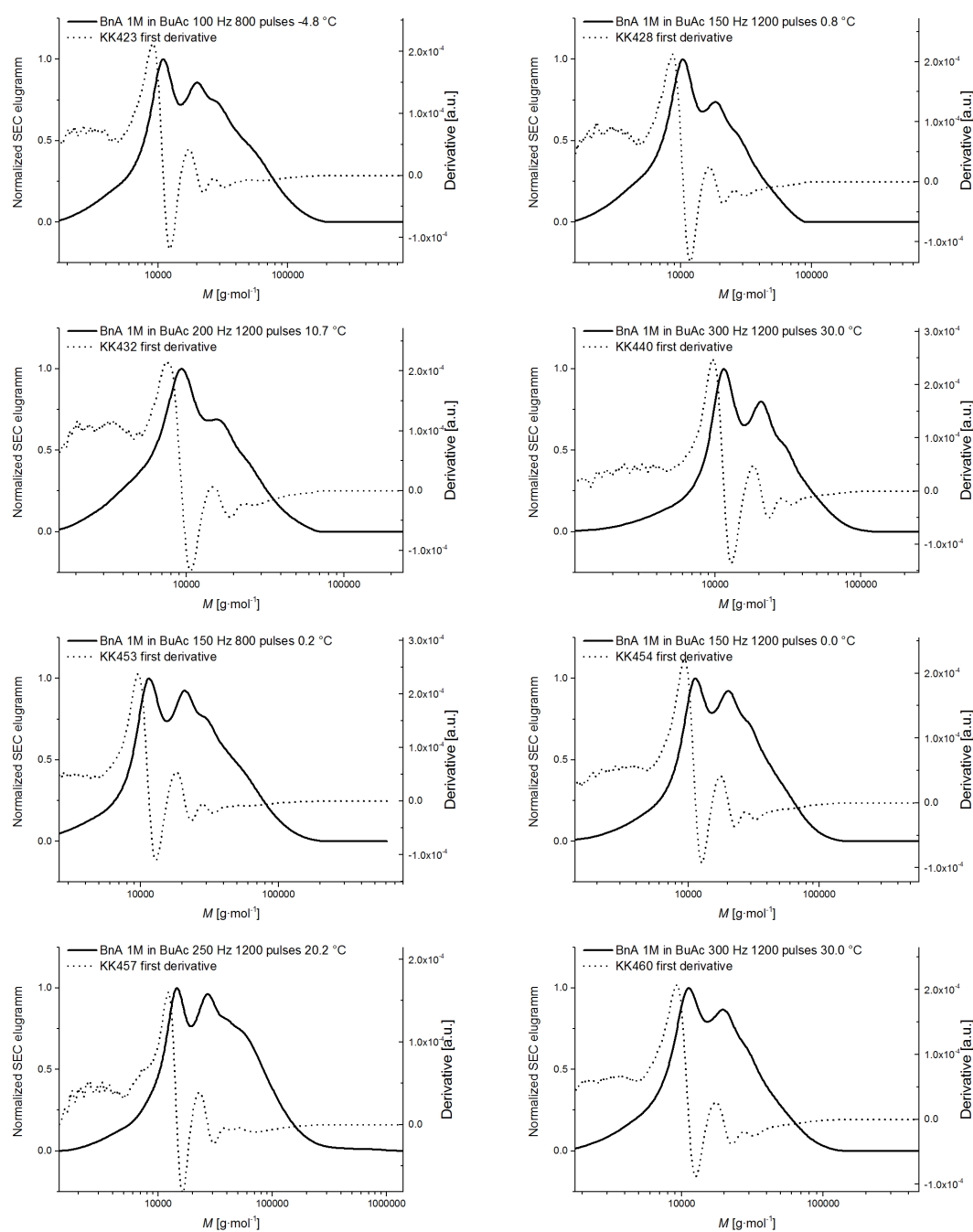


Figure A.1.: Representative molecular weight distributions (solid lines) and their first derivatives (dotted lines) of benzyl acrylate (BnA) in 1M solution in butyl acetate. The sample specific conditions are given in the corresponding diagram and collated in Table A.1. For all samples incorporated into the final Arrhenius plot, the typical PLP structure with at least two inflection points is observed.

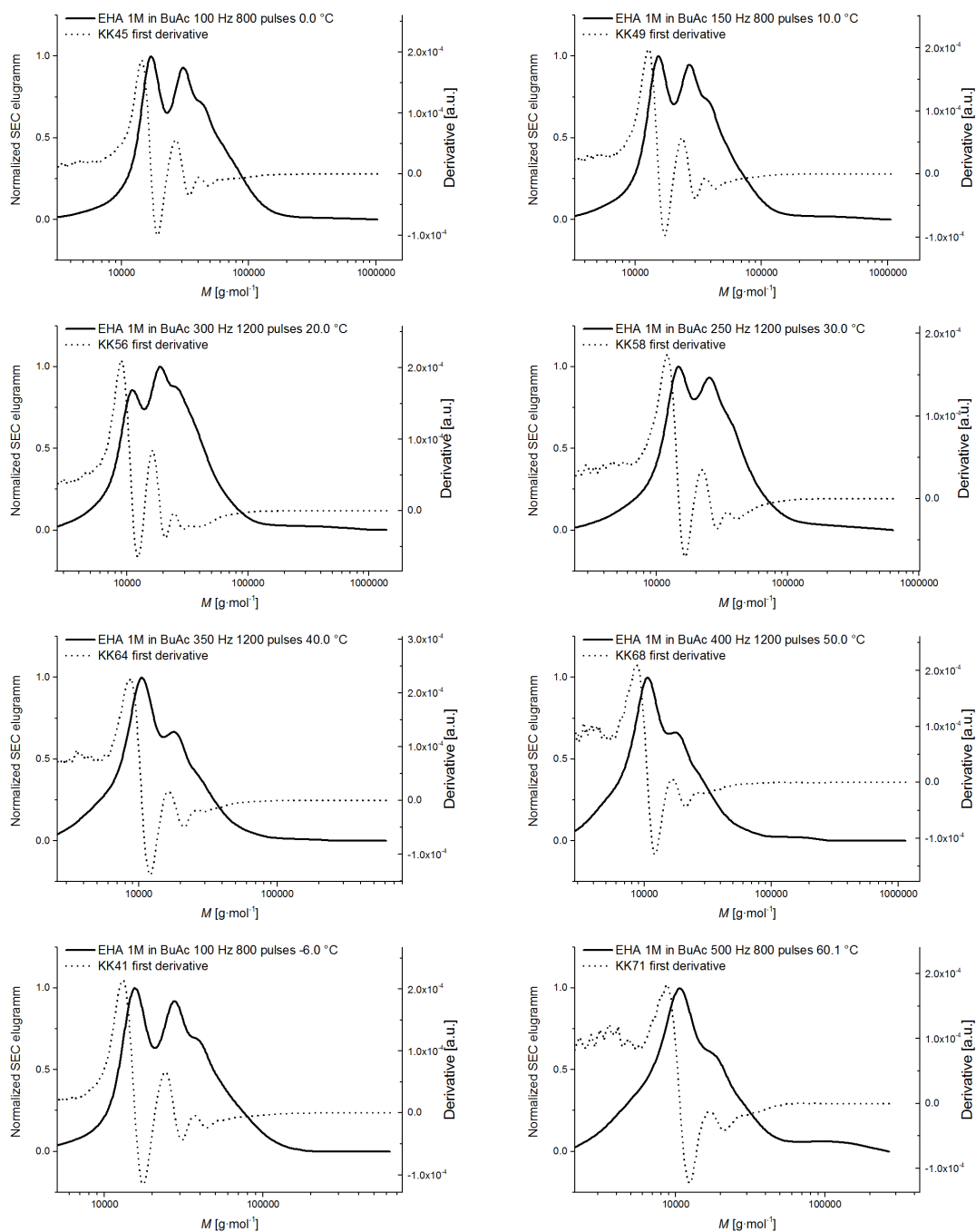


Figure A.2.: Representative molecular weight distributions (solid lines) and their first derivatives (dotted lines) of 2-ethylhexyl acrylate (EHA) in 1M solution in butyl acetate. The sample specific conditions are given in the corresponding diagram and collated in Table A.2. For all samples incorporated into the final Arrhenius plot, the typical PLP structure with at least two inflection points is observed.

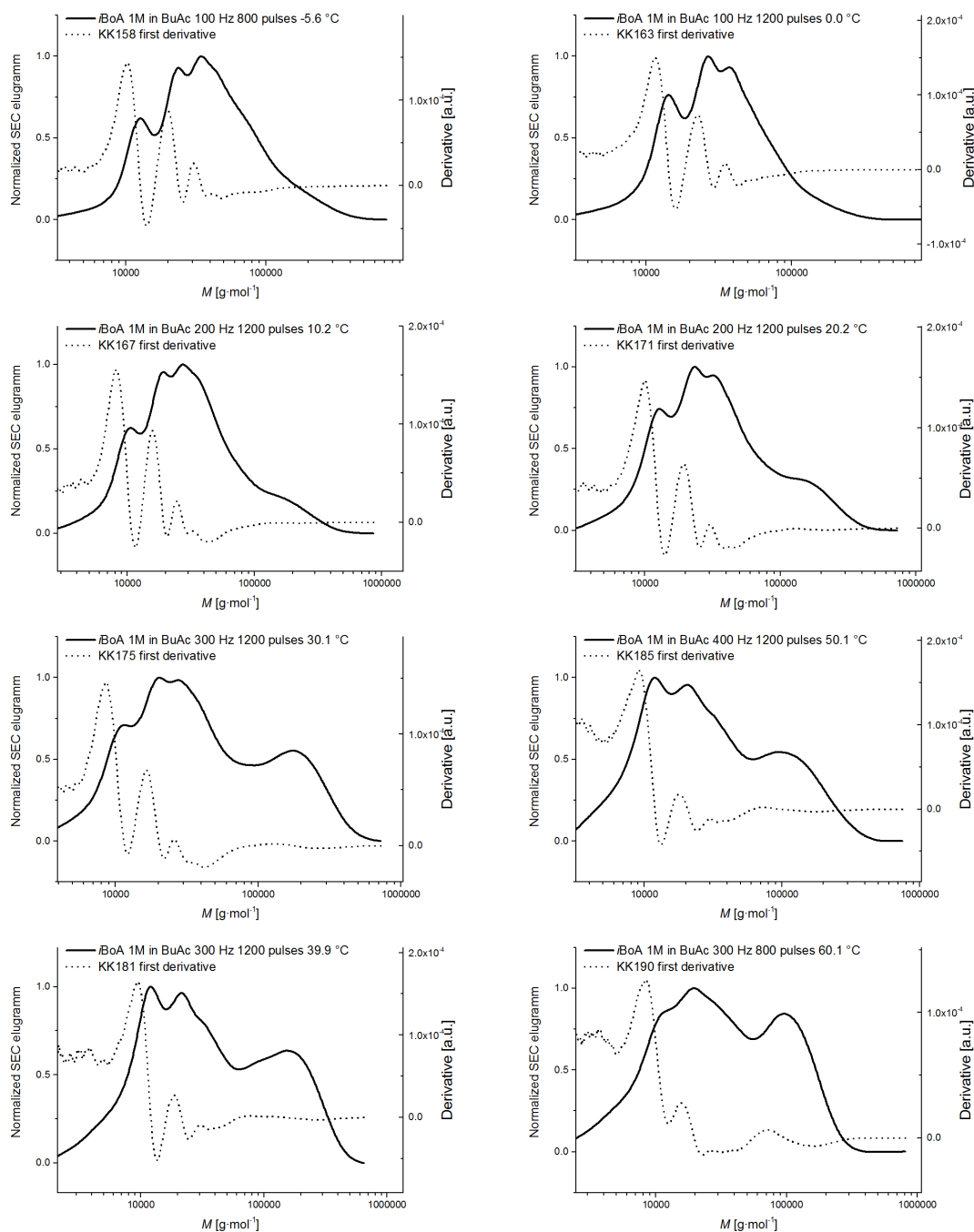


Figure A.3.: Representative molecular weight distributions (solid lines) and their first derivatives (dotted lines) of *iso*-bornyl acrylate (*i*BoA) in 1M solution in butyl acetate. The sample specific conditions are given in the corresponding diagram and collated in Table A.3. For all samples incorporated into the final Arrhenius plot, the typical PLP structure with at least two inflection points is observed.

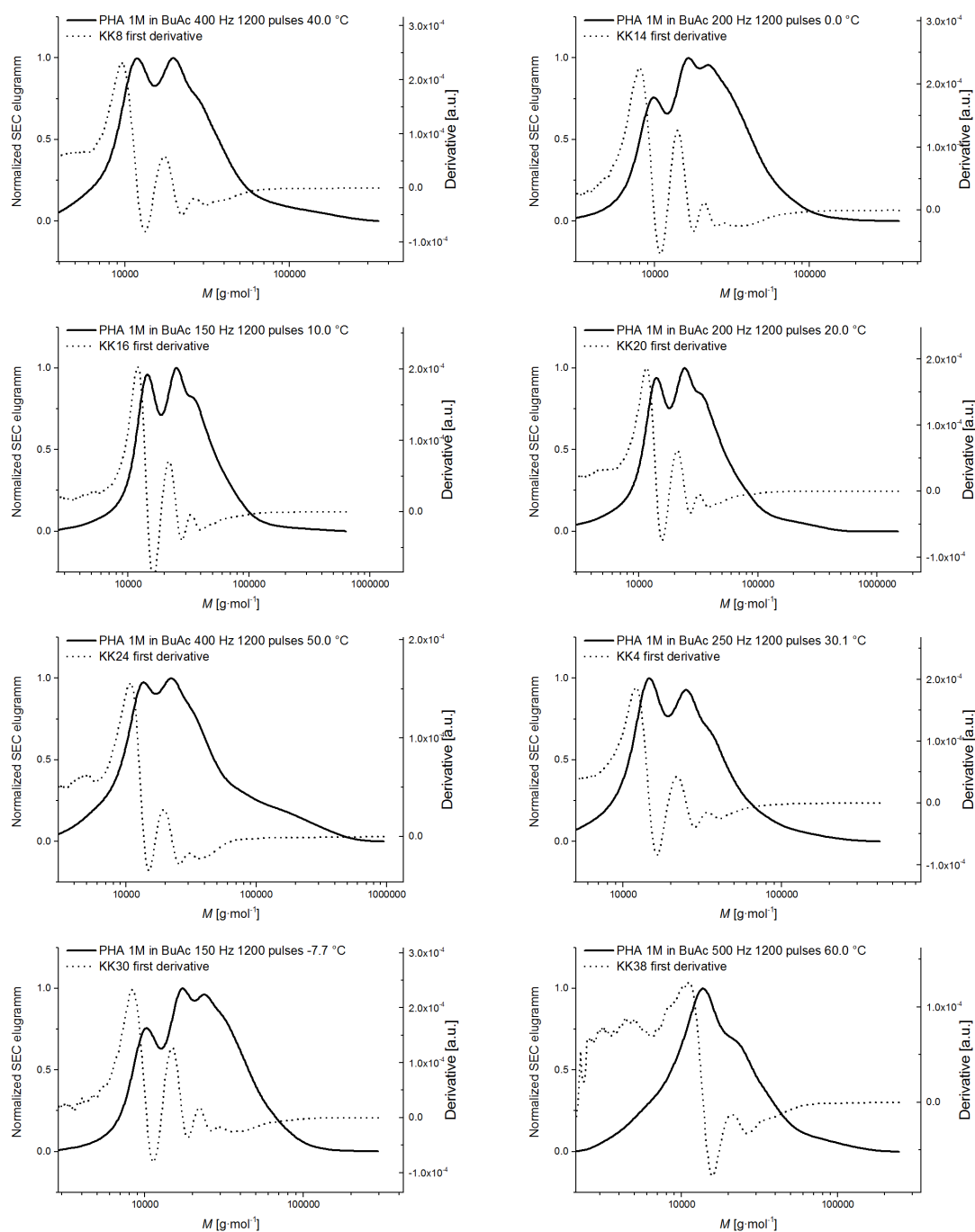


Figure A.4.: Representative molecular weight distributions (solid lines) and their first derivatives (dotted lines) of 2-propylheptyl acrylate (PHA) in 1M solution in butyl acetate. The sample specific conditions are given in the corresponding diagram and collated in Table A.4. For all samples incorporated into the final Arrhenius plot, the typical PLP structure with at least two inflection points is observed.

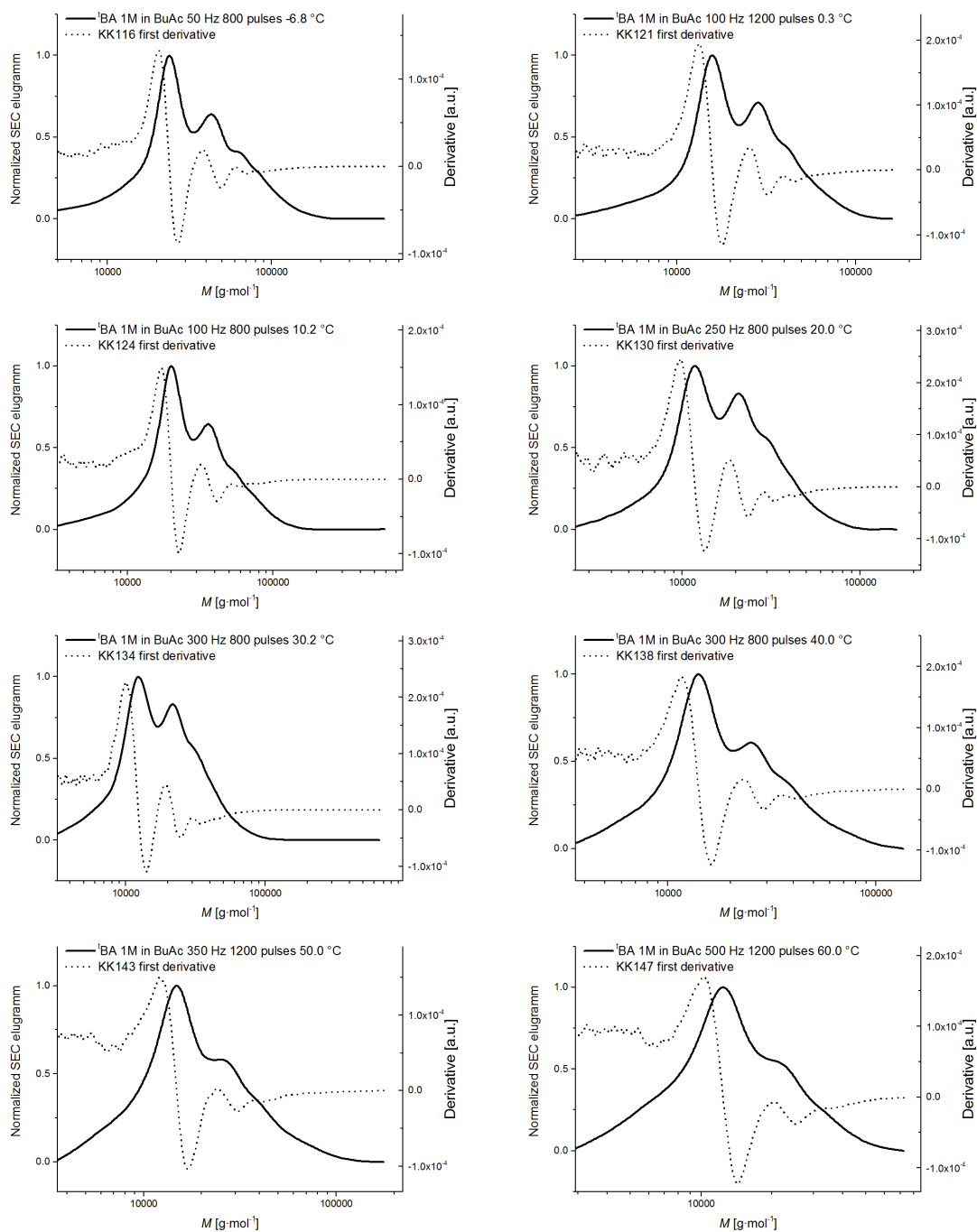


Figure A.5.: Representative molecular weight distributions (solid lines) and their first derivatives (dotted lines) of *tert*-butyl acrylate (*t*BA) in 1M solution in butyl acetate. The sample specific conditions are given in the corresponding diagram and collated in Table A.5. For all samples incorporated into the final Arrhenius plot, the typical PLP structure with at least two inflection points is observed.

Table A.1.: Detailed PLP sample conditions of all samples incorporated in the final Arrhenius plot, absolute molecular weights of the first and second inflection point, as well as the resulting propagation rate coefficients for benzyl acrylate (BnA) 1M in BuAc. Since no MHKS parameters were available for this monomer, ^tBA MHKS parameters were used.

sample	f Hz	n -	θ °C	T^{-1} 10^{-3} K^{-1}	$\ln(k_p)$ -	k_{p1}/k_{p2} -	M1 $\text{g}\cdot\text{mol}^{-1}$	M2 $\text{g}\cdot\text{mol}^{-1}$	c_M $\text{mol}\cdot\text{L}^{-1}$	k_{p1} $\text{mol}\cdot\text{L}^{-1}\cdot\text{s}^{-1}$	k_{p2} $\text{mol}\cdot\text{L}^{-1}\cdot\text{s}^{-1}$
KK421	50	800	-4.8	3.726	9.024	0.998	22034	44160	1.04	8300	8317
KK423	100	800	-4.8	3.722	9.0576	0.965	22779	47192	1.04	8583	8891
KK422	50	1200	-4.5	3.726	9.1513	1.049	12512	23845	1.04	9426	8982
KK424	100	1200	-4.2	3.718	9.1264	1.042	12197	23418	1.04	9194	8827
KK454	150	1200	0.0	3.641	9.3185	0.997	19589	39298	1.032	11142	11176
KK453	150	800	0.2	3.645	9.2394	1.035	18104	34988	1.032	10294	9947
KK426	75	1200	1.2	3.532	9.5364	0.995	18104	36388	1.04	13854	13923
KK425	75	800	1.5	3.522	9.4195	1.01	16094	31871	1.04	12326	12205
KK429	100	800	10	3.523	9.6365	1.032	9998	19377	1.04	15313	14839
KK431	200	800	10.7	3.523	9.5145	1.038	8850	17046	1.04	13555	13054
KK432	200	1200	10.7	3.405	9.7649	0.966	17998	37249	1.04	17411	18017
KK430	100	1200	10.8	3.407	9.6493	1.016	8018	15777	1.04	15510	15261
KK457	250	1200	20.2	3.299	10.0522	0.994	9893	19907	1.032	23206	23348
KK435	250	800	20.4	3.195	10.2065	1.039	9789	18846	1.04	27077	26065
KK434	125	1200	20.5	3.195	10.2171	1.038	9893	19058	1.04	27366	26359
KK455	125	800	20.5	3.095	10.4813	1.042	11148	21395	1.032	35643	34202
KK439	300	800	30	3.095	10.3513	1.051	9789	18634	1.04	31296	29788
KK458	150	800	30	3.003	10.6065	1.004	9998	19907	1.032	40395	40217
KK459	150	1200	30	3.003	10.4846	1.032	8850	17151	1.032	35758	34649
KK460	300	1200	30	3.658	9.3272	1.038	9893	19058	1.032	11239	10825
KK443	350	800	39.8	3.661	9.3287	1.044	9893	18952	1.032	11256	10782
KK444	350	1200	39.8	3.405	9.7608	1.023	17892	34988	1.032	17340	16953
KK465	250	800	40	3.409	9.8179	1.041	9476	18210	1.041	18360	17642
KK466	250	1200	40	3.299	9.9415	0.989	17681	35742	1.041	20774	20997
KK447	400	800	50	3.299	9.9593	0.969	17998	37142	1.032	21147	21820
KK448	400	1200	50	3.299	10.0109	1.053	9476	17998	1.032	22267	21147
KK472	300	800	50	3.193	10.1258	1.031	12617	24485	1.041	24979	24237
KK473	300	1200	50	3.193	10.1423	1.03	12827	24912	1.041	25395	24660
KK451	500	800	59.8	3.095	10.3759	1.011	13353	26407	1.032	32076	31717
KK452	500	1200	59.8	3.095	10.2939	1.018	12302	24165	1.032	29551	29024
KK478	350	1600	60.2	2.999	10.5094	1.016	12932	25446	1.041	36659	36065
KK480	350	1200	60.2	2.999	10.5094	1.043	12932	24805	1.041	36659	35157

Table A.2.: Detailed PLP sample conditions of all samples incorporated in the final Arrhenius plot, absolute molecular weights of the first and second inflection point, as well as the resulting propagation rate coefficients for 2-ethylhexyl acrylate (EHA) 1M in BuAc.

sample	f Hz	n -	θ °C	T^{-1} 10^{-3} K^{-1}	$\ln(k_p)$ -	k_{p1}/k_{p2} -	M1 $\text{g}\cdot\text{mol}^{-1}$	M2 $\text{g}\cdot\text{mol}^{-1}$	c_M $\text{mol}\cdot\text{L}^{-1}$	k_{p1} $\text{mol}\cdot\text{L}^{-1}\cdot\text{s}^{-1}$	k_{p2} $\text{mol}\cdot\text{L}^{-1}\cdot\text{s}^{-1}$
KK81	50	800	-6.9	3.743	9.7748	1.056	19800	37500	1.035	5192	4917
KK82	50	1200	-6.9	3.743	9.8299	1.06	18500	34900	1.035	4851	4576
KK105	50	1200	-6.8	3.661	8.4816	1.073	18400	34300	1.035	4825	4497
KK41	100	800	-6	3.532	8.6417	1.065	10600	19900	1.031	5578	5236
KK42	100	1200	-6	3.529	8.6417	1.076	10600	19700	1.031	5578	5183
KK45	100	800	0.0	3.411	8.7191	1.068	11800	22100	1.031	6209	5814
KK73	100	800	0.1	3.411	9.408	1.062	12000	22600	1.036	6285	5918
KK74	100	1200	0.1	3.411	9.6887	1.062	12000	22600	1.036	6285	5918
KK76	100	1200	0.1	3.411	9.6943	1.053	12000	22800	1.036	6285	5971
KK85	100	800	0.1	3.299	9.9207	1.032	11400	22100	1.035	5979	5795
KK49	150	800	10	3.194	8.7073	1.082	10500	19400	1.031	8288	7656
KK79	250	800	10.1	3.194	9.825	1.091	7200	13200	1.036	9427	8642
KK87	100	800	10.1	3.194	9.9487	1.034	15400	29800	1.035	8077	7815
KK88	100	1200	10.1	3.193	9.825	1.031	15200	29500	1.035	7972	7736
KK50	150	1200	10.2	3.095	8.791	1.066	10500	19700	1.031	8288	7774
KK53	200	800	20	3.095	8.7763	1.075	10000	18600	1.031	10524	9787
KK54	200	1200	20	3.002	8.9462	1.074	10100	18800	1.031	10629	9892
KK55	300	800	20	3.001	8.9462	1.075	7200	13400	1.031	11366	10576
KK56	300	1200	20	3.002	9.064	1.083	7200	13300	1.031	11366	10498
KK90	150	1200	20.3	3.66	10.1439	1.036	13100	25300	1.035	10306	9952
KK58	250	1200	30	3.66	9.064	1.065	9800	18400	1.031	12892	12102
KK92	150	1200	30	3.66	10.1239	1.066	15400	28900	1.034	12123	11375
KK93	200	800	30	3.53	9.9993	1.031	11800	22900	1.034	12385	12018
KK94	200	1200	30	3.756	10.0587	1.013	11600	22900	1.034	12175	12018
KK61	300	800	39.9	3.756	9.194	1.056	10400	19700	1.036	16341	15476
KK62	300	1200	39.9	3.66	9.194	1.041	10100	19400	1.036	15869	15241
KK63	350	800	39.9	3.53	9.3263	1.048	8800	16800	1.036	16131	15398
KK64	350	1200	40	3.53	9.3177	1.061	8700	16400	1.036	15948	15031
KK65	300	800	50	3.408	9.4355	1.027	11500	22400	1.036	18069	17598
KK68	400	1200	50	3.299	9.4355	1.073	8800	16400	1.036	18436	17179
KK101	200	800	50	3.299	9.7829	1.034	16900	32700	1.035	17727	17150
KK102	200	1200	50.1	3.299	9.7946	1.065	17100	32100	1.035	17937	16836
KK69	400	800	60	3.095	9.5503	0.99	10000	20200	1.036	20950	21159
KK72	500	1200	60	3.094	9.4126	0.989	8900	18000	1.036	23306	23568
KK71	500	800	60.1	3.001	9.5341	1.035	8800	17000	1.036	23045	22259
KK103	300	800	60.2	3.754	9.9563	1.027	13400	26100	1.035	21084	20533

Table A.3.: Detailed PLP sample conditions of all samples incorporated in the final Arrhenius plot, absolute molecular weights of the first and second inflection point, as well as the resulting propagation rate coefficients for *iso*-bornyl acrylate (*i*BoA) 1M in BuAc.

sample	f Hz	n -	θ °C	T^{-1} 10^{-3} K^{-1}	$\ln(k_p)$ -	k_{p1}/k_{p2} -	M1 $\text{g}\cdot\text{mol}^{-1}$	M2 $\text{g}\cdot\text{mol}^{-1}$	c_M $\text{mol}\cdot\text{L}^{-1}$	k_{p1} $\text{mol}\cdot\text{L}^{-1}\cdot\text{s}^{-1}$	k_{p2} $\text{mol}\cdot\text{L}^{-1}\cdot\text{s}^{-1}$
KK156	50	800	-5.6	3.738	8.3905	1.067	19100	35800	1.041	4405	4128
KK157	50	1200	-5.6	3.738	8.3853	1.07	19000	35500	1.041	4382	4094
KK158	100	800	-5.6	3.738	8.4662	1.03	10300	20000	1.041	4751	4613
KK159	100	1200	-5.6	3.738	8.4758	1.025	10400	20300	1.041	4797	4682
KK162	100	800	0.0	3.661	8.6189	1.03	12000	23300	1.041	5535	5374
KK163	100	1200	0.0	3.661	8.585	1.022	11600	22700	1.041	5351	5236
KK193	75	1200	0.0	3.532	8.5541	1.028	14900	29000	1.034	5188	5049
KK195	50	1200	0.0	3.529	8.5608	1.061	22500	42400	1.034	5223	4921
KK164	100	800	10	3.529	8.8487	1.049	15100	28800	1.041	6965	6642
KK196	100	800	10	3.409	8.8744	1.048	15200	29000	1.021	7147	6817
KK166	200	800	10.2	3.409	8.9313	1.045	8200	15700	1.041	7565	7242
KK167	200	1200	10.2	3.299	8.919	1.032	8100	15700	1.041	7473	7242
KK198	150	800	20	3.298	9.108	1.024	12800	25000	1.021	9027	8816
KK199	150	1200	20	3.194	9.108	1.036	12800	24700	1.021	9027	8710
KK170	200	800	20.2	3.194	9.1397	1.025	10100	19700	1.041	9318	9087
KK171	200	1200	20.2	3.194	9.1297	1.031	10000	19400	1.041	9226	8949
KK172	150	800	30	3.094	9.2931	1.068	15700	29400	1.041	10863	10171
KK174	300	800	30.1	3.094	9.3121	0.994	8000	16100	1.041	11071	11140
KK201	150	1200	30.2	3.095	9.3058	1.083	15600	28800	1.021	11002	10156
KK203	200	1200	30.3	3.094	9.3058	1.017	11700	23000	1.021	11002	10814
KK179	150	1200	39.9	3.661	9.4636	1.098	18500	33700	1.034	12883	11734
KK180	300	800	39.9	3.661	9.5008	1.016	9600	18900	1.034	13370	13161
KK181	300	1200	39.9	3.532	9.4797	1.011	9400	18600	1.034	13091	12952
KK206	150	800	40	3.411	9.46	1.117	18200	32600	1.021	12836	11496
KK184	400	800	50	3.411	9.7239	0.994	9000	18100	1.034	16712	16805
KK182	200	800	50.1	3.297	9.6668	1.083	17000	31400	1.034	15784	14577
KK183	200	1200	50.1	3.295	9.6369	1.071	16500	30800	1.034	15320	14298
KK185	400	1200	50.1	3.193	9.7459	1.028	9200	17900	1.034	17084	16620
KK214	500	800	60	2.999	9.8667	1.025	8200	16000	1.021	19277	18807
KK212	400	800	60.2	2.999	9.8218	0.985	9800	19900	1.021	18431	18713
KK213	400	1200	60.2	2.999	9.8218	1.043	9800	18800	1.021	18431	17678
KK210	300	800	60.3	3.002	9.8395	1.081	13300	24600	1.021	18760	17349

Table A.4.: Detailed PLP sample conditions of all samples incorporated in the final Arrhenius plot, absolute molecular weights of the first and second inflection point, as well as the resulting propagation rate coefficients for 2-propylhexyl acrylate (PHA) 1M in BuAc.

sample	f Hz	n -	θ °C	T^{-1} 10^{-3} K^{-1}	$\ln(k_p)$ -	k_{p1}/k_{p2} -	M1 $\text{g}\cdot\text{mol}^{-1}$	M2 $\text{g}\cdot\text{mol}^{-1}$	c_M $\text{mol}\cdot\text{L}^{-1}$	k_{p1} $\text{mol}\cdot\text{L}^{-1}\cdot\text{s}^{-1}$	k_{p2} $\text{mol}\cdot\text{L}^{-1}\cdot\text{s}^{-1}$
KK27	100	800	-7.7	3.3	8.6417	1.083	11800	21800	0.982	5663	5231
KK28	100	1200	-7.7	3.298	8.6417	1.098	11800	21500	0.982	5663	5159
KK29	150	800	-7.7	3.193	8.7191	1.149	8500	14800	0.982	6119	5327
KK30	150	1200	-7.7	3.193	8.7073	1.128	8400	14900	0.982	6047	5363
KK11	100	800	0.0	3.193	8.791	1.105	13700	24800	0.982	6575	5951
KK12	100	1200	0.0	3.193	8.7763	1.098	13500	24600	0.982	6479	5903
KK13	200	800	0.0	3.095	8.9462	1.151	8000	13900	0.982	7679	6671
KK14	200	1200	0.0	3.095	8.9462	1.143	8000	14000	0.982	7679	6719
KK15	150	800	10	3.661	9.064	1.101	12000	21800	0.982	8638	7847
KK16	150	1200	10	3.661	9.064	1.101	12000	21800	0.982	8638	7847
KK17	250	800	10	3.661	9.194	1.131	8200	14500	0.982	9838	8698
KK18	250	1200	10	3.661	9.194	1.131	8200	14500	0.982	9838	8698
KK19	200	800	20	3.532	9.3263	1.099	11700	21300	0.982	11230	10222
KK20	200	1200	20	3.532	9.3177	1.105	11600	21000	0.982	11134	10078
KK21	300	800	20	3.532	9.4355	1.137	8700	15300	0.982	12526	11014
KK22	300	1200	20	3.532	9.4355	1.176	8700	14800	0.982	12526	10654
KK3	250	800	29.9	3.411	9.5503	1.122	12400	22100	1.039	14049	12520
KK4	250	1200	30.1	3.411	9.5341	1.109	12200	22000	1.039	13823	12463
KK33	125	800	30.2	3.411	9.4126	1.107	21800	39400	1.049	12241	11062
KK34	125	1200	30.2	3.411	9.408	1.11	21700	39100	1.049	12185	10978
KK5	200	800	40	3.095	9.6887	1.106	17800	32200	1.039	16134	14593
KK6	200	1200	40	3.095	9.6943	1.129	17900	31700	1.039	16225	14367
KK7	400	800	40	3.002	9.825	1.103	10200	18500	1.039	18491	16769
KK8	400	1200	40	3.767	9.7748	1.109	9700	17500	1.039	17584	15862
KK10	200	1200	50	3.767	9.8299	1.165	20500	35200	1.039	18581	15953
KK23	400	800	50	3.767	9.9207	1.116	10600	19000	0.982	20348	18237
KK24	400	1200	50	3.767	9.9487	1.118	10900	19500	0.982	20924	18716
KK9	200	800	50	3.297	9.825	1.143	20400	35700	1.039	18491	16179
KK26	500	1200	60	3.297	10.1439	1.087	10600	19500	0.982	25435	23396
KK38	500	1200	60	3.002	10.1239	1.042	11100	21300	1.049	24931	23921
KK39	500	800	60	3.002	9.9993	1.077	9800	18200	1.049	22012	20439
KK40	500	1200	60	3.002	10.0587	1.01	10400	20600	1.049	23359	23135

Table A.5.: Detailed PLP sample conditions of all samples incorporated in the final Arrhenius plot, absolute molecular weights of the first and second inflection point, as well as the resulting propagation rate coefficients for *tert*-butyl acrylate (^tBA) 1M in BuAc.

sample	f Hz	n -	θ °C	T^{-1} 10^{-3} K^{-1}	$\ln(k_p)$ -	k_{p1}/k_{p2} -	M1 $\text{g}\cdot\text{mol}^{-1}$	M2 $\text{g}\cdot\text{mol}^{-1}$	c_M $\text{mol}\cdot\text{L}^{-1}$	k_{p1} $\text{mol}\cdot\text{L}^{-1}\cdot\text{s}^{-1}$	k_{p2} $\text{mol}\cdot\text{L}^{-1}\cdot\text{s}^{-1}$
KK119	100	1200	-7.2	3.754	8.7597	0.991	8426	17004	1.032	6372	6429
KK118	100	800	-7.1	3.756	8.75	0.992	8345	16832	1.032	6310	6364
KK117	50	1200	-6.9	3.759	8.706	1.029	15973	31060	1.032	6039	5872
KK116	50	800	-6.8	3.76	8.7167	1.01	16144	31964	1.032	6104	6043
KK121	100	1200	0.3	3.656	8.946	0.987	10152	20564	1.032	7677	7775
KK122	150	800	0.3	3.657	9.0092	1.017	7210	14180	1.032	8178	8042
KK123	150	1200	0.3	3.657	8.9866	0.994	7049	14180	1.032	7996	8042
KK120	100	800	0.4	3.657	8.946	0.979	10152	20739	1.032	7677	7841
KK124	100	800	10.2	3.529	9.2185	1.007	13333	26483	1.032	10082	10013
KK126	200	800	10.2	3.528	9.2628	1.001	6968	13926	1.032	10539	10531
KK127	200	1200	10.2	3.529	9.2513	0.995	6888	13841	1.032	10418	10466
KK125	100	1200	10.3	3.529	9.2374	1.012	13587	26840	1.032	10274	10148
KK131	250	1200	19.5	3.409	9.5201	1.005	7210	14350	1.032	13630	13565
KK129	150	1200	19.9	3.412	9.4819	0.993	11567	23288	1.032	13120	13208
KK130	250	800	20	3.411	9.5201	0.999	7210	14435	1.032	13630	13645
KK128	150	800	20.2	3.417	9.4891	0.993	11651	23465	1.032	13215	13308
KK132	150	800	30.2	3.297	9.7152	1.008	14606	28989	1.032	16567	16441
KK133	150	1200	30.2	3.297	9.7152	1.033	14606	28271	1.032	16567	16034
KK134	300	800	30.2	3.297	9.7354	0.98	7452	15203	1.032	16906	17244
KK135	300	1200	30.2	3.297	9.7354	0.992	7452	15032	1.032	16906	17051
KK136	200	800	40	3.193	9.9261	1.003	13502	26929	1.03	20457	20400
KK137	200	1200	40	3.193	9.9135	1.004	13333	26572	1.03	20201	20130
KK138	300	800	40	3.193	9.9074	0.979	8835	18041	1.03	20079	20500
KK139	300	1200	40	3.193	9.8981	0.975	8753	17954	1.03	19893	20402
KK140	250	800	50	3.095	10.1239	0.994	13164	26483	1.03	24931	25078
KK141	250	1200	50	3.095	10.1174	0.994	13079	26304	1.03	24771	24909
KK143	350	1200	50	3.095	10.107	0.965	9245	19168	1.03	24513	25412
KK148	200	800	50	3.002	10.1048	1.002	16144	32236	1.03	24460	24420
KK144	400	800	60	3.002	10.3094	0.967	9904	20476	1.03	30013	31024
KK145	400	1200	60	3.002	10.2581	0.964	9410	19517	1.03	28514	29570
KK147	500	1200	60	3.095	10.2801	0.969	7695	15887	1.03	29146	30088
KK155	300	1200	60	3.002	10.2997	0.952	13079	27465	1.03	29725	31210

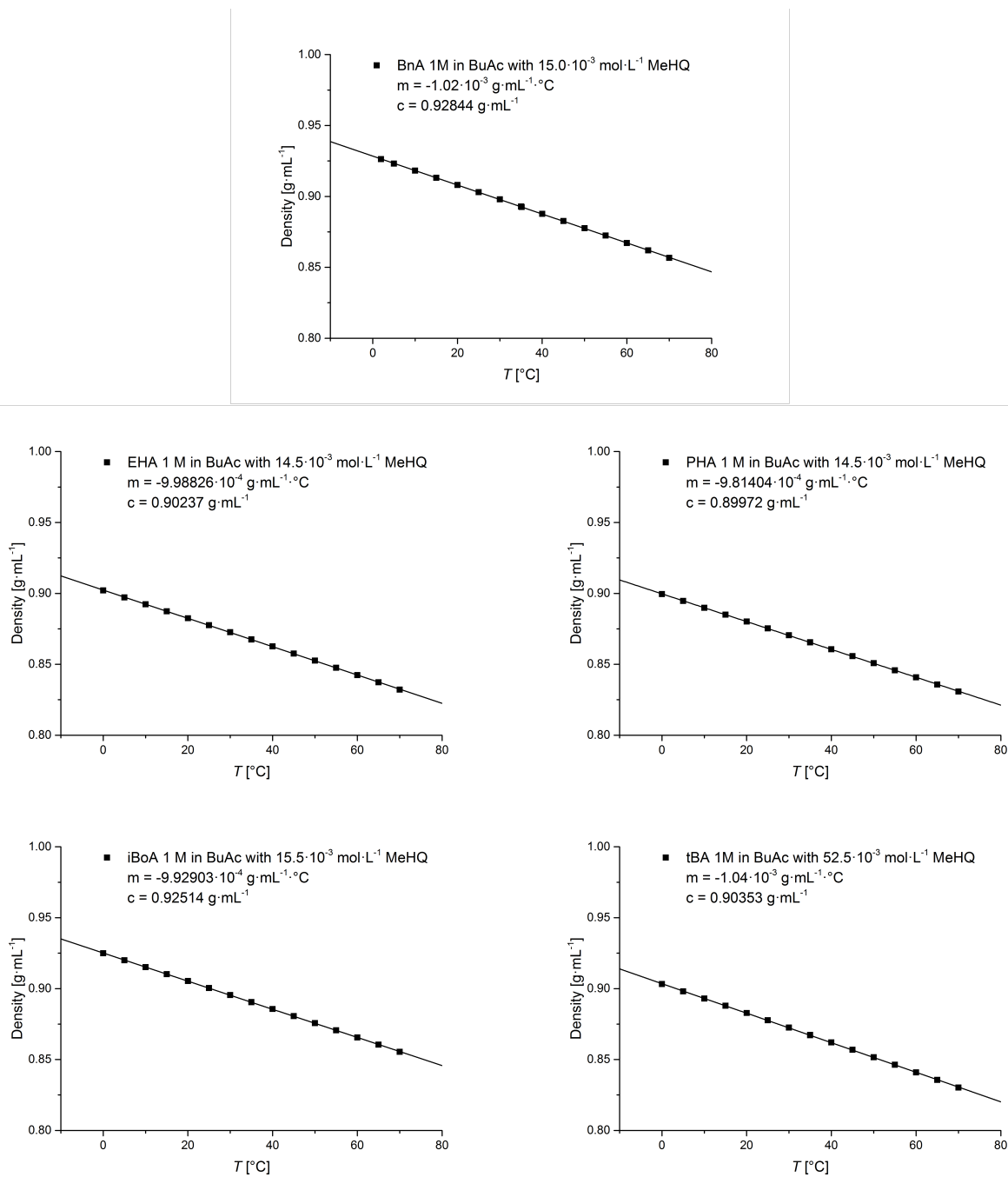


Figure A.6.: Temperature dependent densities for the herein studied monomers BnA, EHA, iBoA, PHA, and tBA in 1 molar solution in BuAc. To prevent the solutions from polymerizing inside the measurement device, methyl hydroquinone (MeHQ) was added. The temperature dependent densities are furthermore collated in Table 2.1 in Chapter 2.

A.2. Chapter 3: Nitrogen Containing Methacrylates

For each monomer investigated in the current study, exemplary molecular weight distributions (MWD) obtained via SEC analysis are provided alongside tables with the specific PLP conditions of all samples incorporated into the final Arrhenius plots as well as the temperature dependent density curves. Tables collating the molecular weights and intrinsic viscosities to determine the MHKS parameters alongside exemplary triple detection SEC traces of all samples incorporated into the final MHKS plot are depicted. Furthermore detailed sample conditions for the preparation of polymer samples for the determination of MHKS parameters are collated. Parts of this chapter, including figures were reproduced with permission from Kockler, K. B.; Fleischhaker, F.; Barner-Kowollik, C. *Polym. Chem.* **2016**, *7*, 4342–4351. Copyright (2016) Royal Society of Chemistry and Kockler, K. B.; Fleischhaker, F.; Barner-Kowollik, C. *Macromolecules* **2016**, *49*, 8572–8580. Copyright (2016) American Chemical Society.

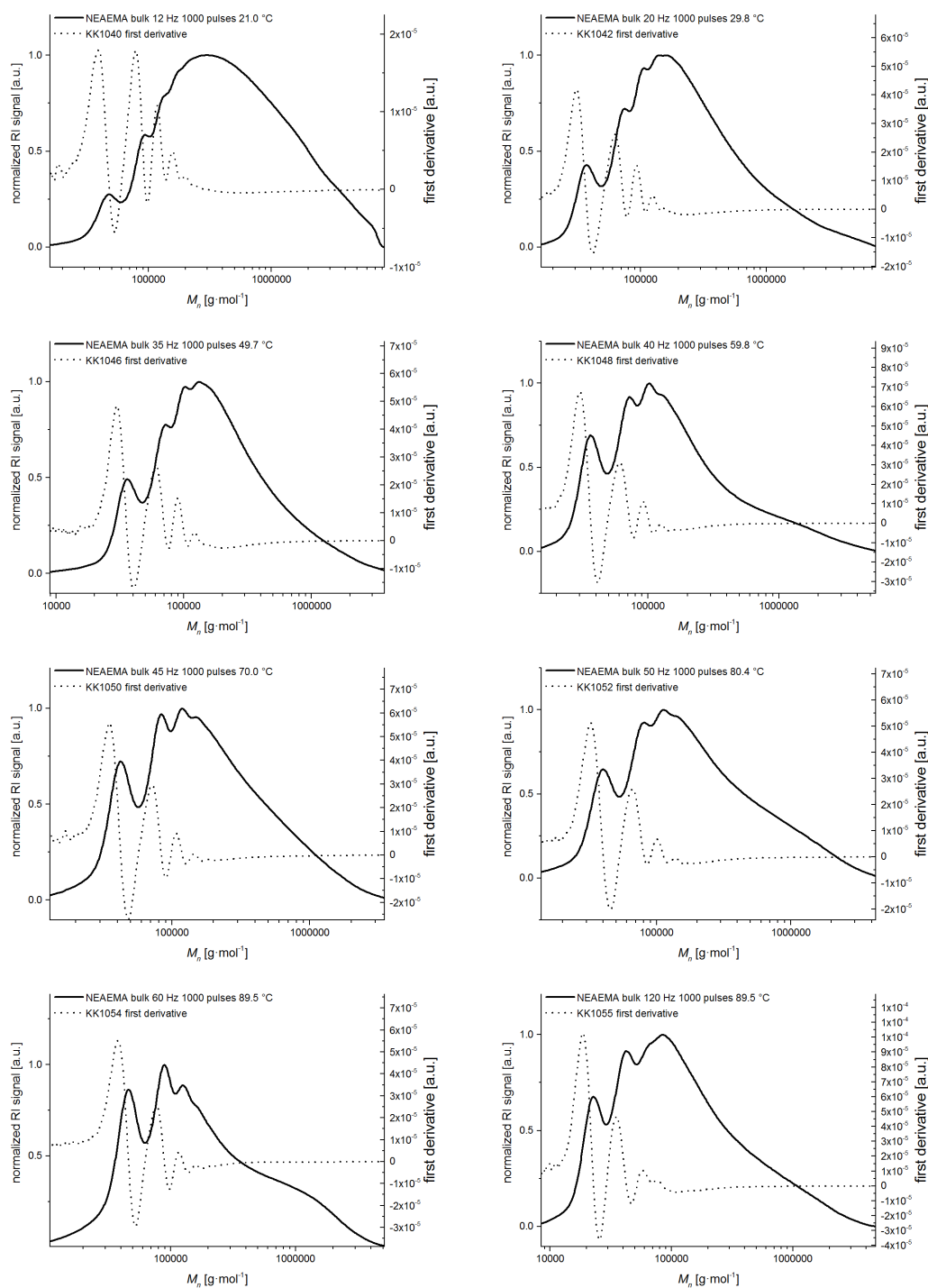


Figure A.7.: Representative molecular weight distributions (solid lines) and their first derivatives (dotted lines) of 2-(*N*-ethylanilino)ethyl methacrylate (NEAEMA) in bulk. The sample specific conditions are given in the corresponding diagram and collated in Table A.6. For all samples incorporated into the final Arrhenius plot, the typical PLP structure with at least two inflection points is observed.

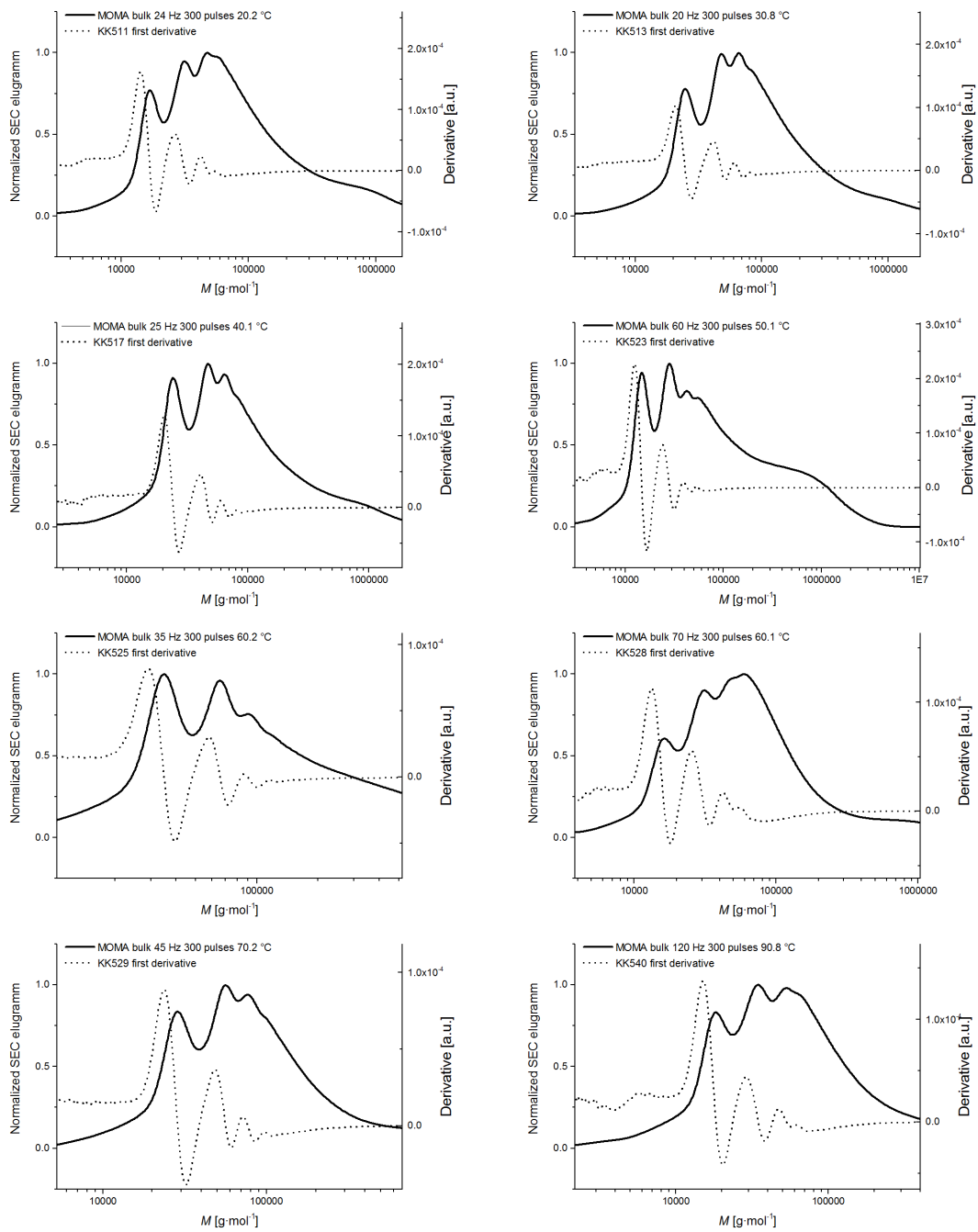


Figure A.8.: Representative molecular weight distributions (solid lines) and their first derivatives (dotted lines) of 2-morpholinoethyl methacrylate (MOMA) in bulk. The sample specific conditions are given in the corresponding diagram and collated in Table A.7. For all samples incorporated into the final Arrhenius plot, the typical PLP structure with at least two inflection points is observed.

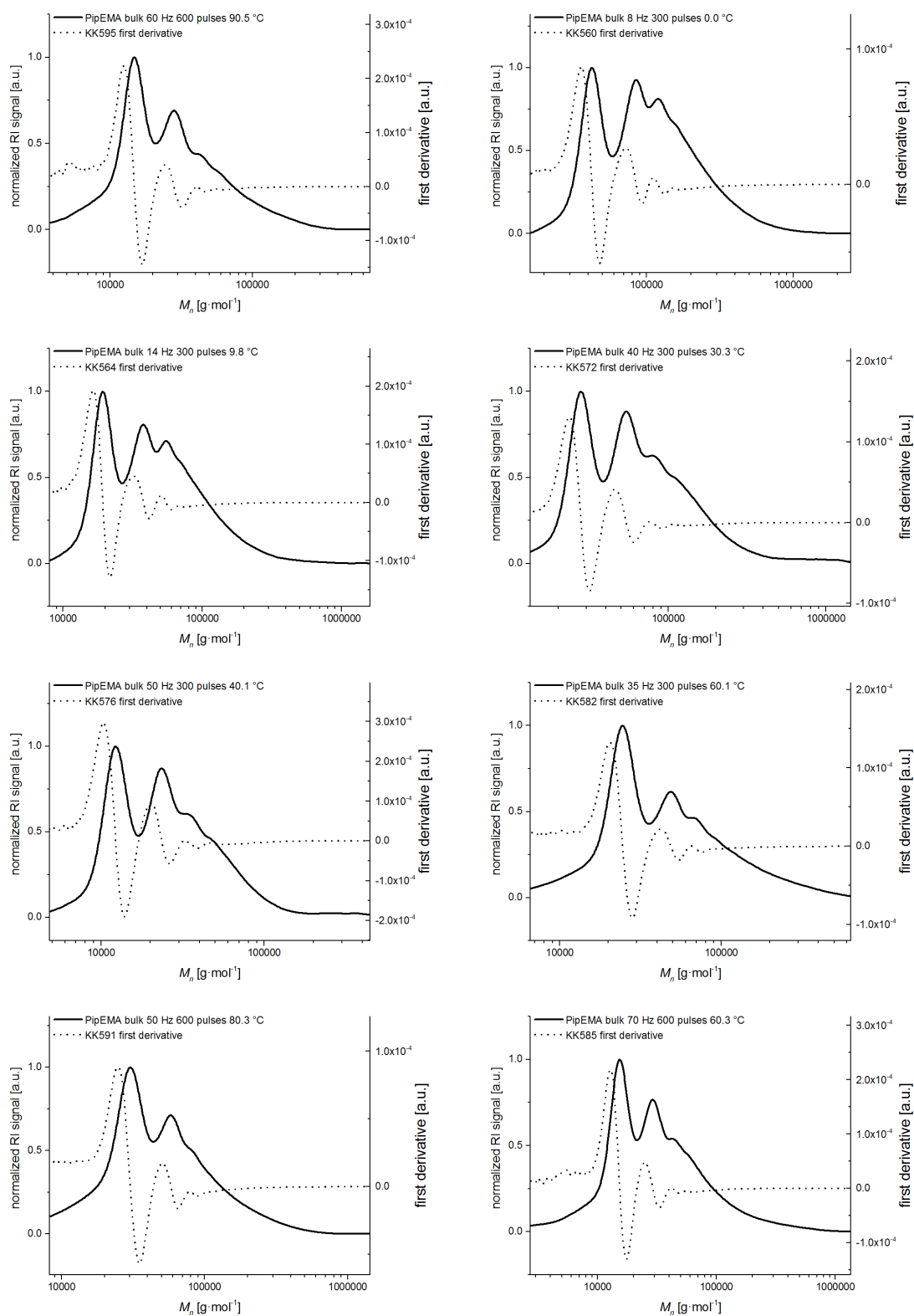


Figure A.9.: Representative molecular weight distributions (solid lines) and their first derivatives (dotted lines) of 2-(1-piperidyl)ethyl methacrylate (PipEMA) in bulk. The sample specific conditions are given in the corresponding diagram and collated in Table A.8. For all samples incorporated into the final Arrhenius plot, the typical PLP structure with at least two inflection points is observed.

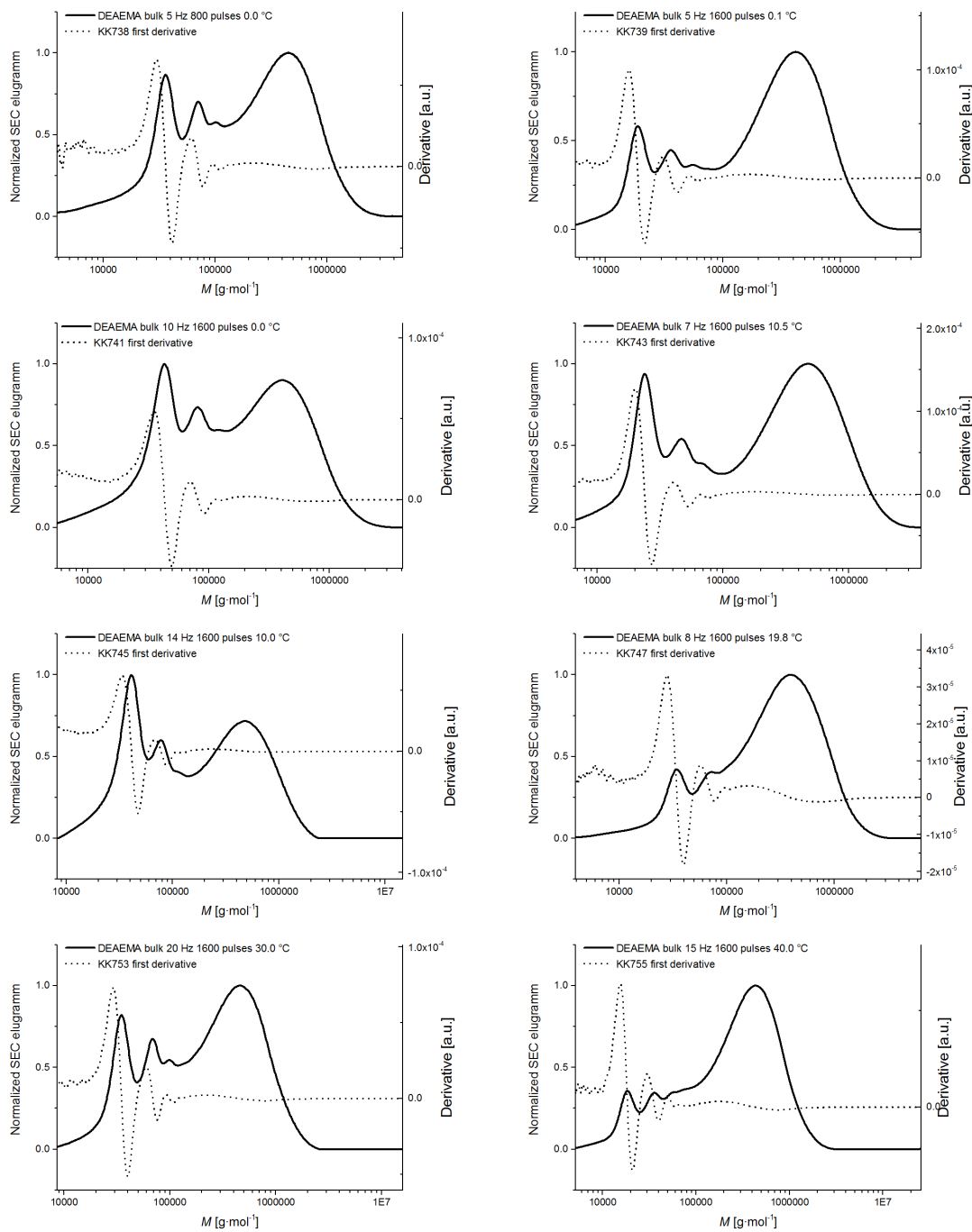


Figure A.10.: Representative molecular weight distributions (solid lines) and their first derivatives (dotted lines) of 2-(*N,N*-diethylamino)ethyl methacrylate (DEAEMA) in bulk. The sample specific conditions are given in the corresponding diagram and collated in Table A.9. For all samples incorporated into the final Arrhenius plot, the typical PLP structure with at least two inflection points is observed.

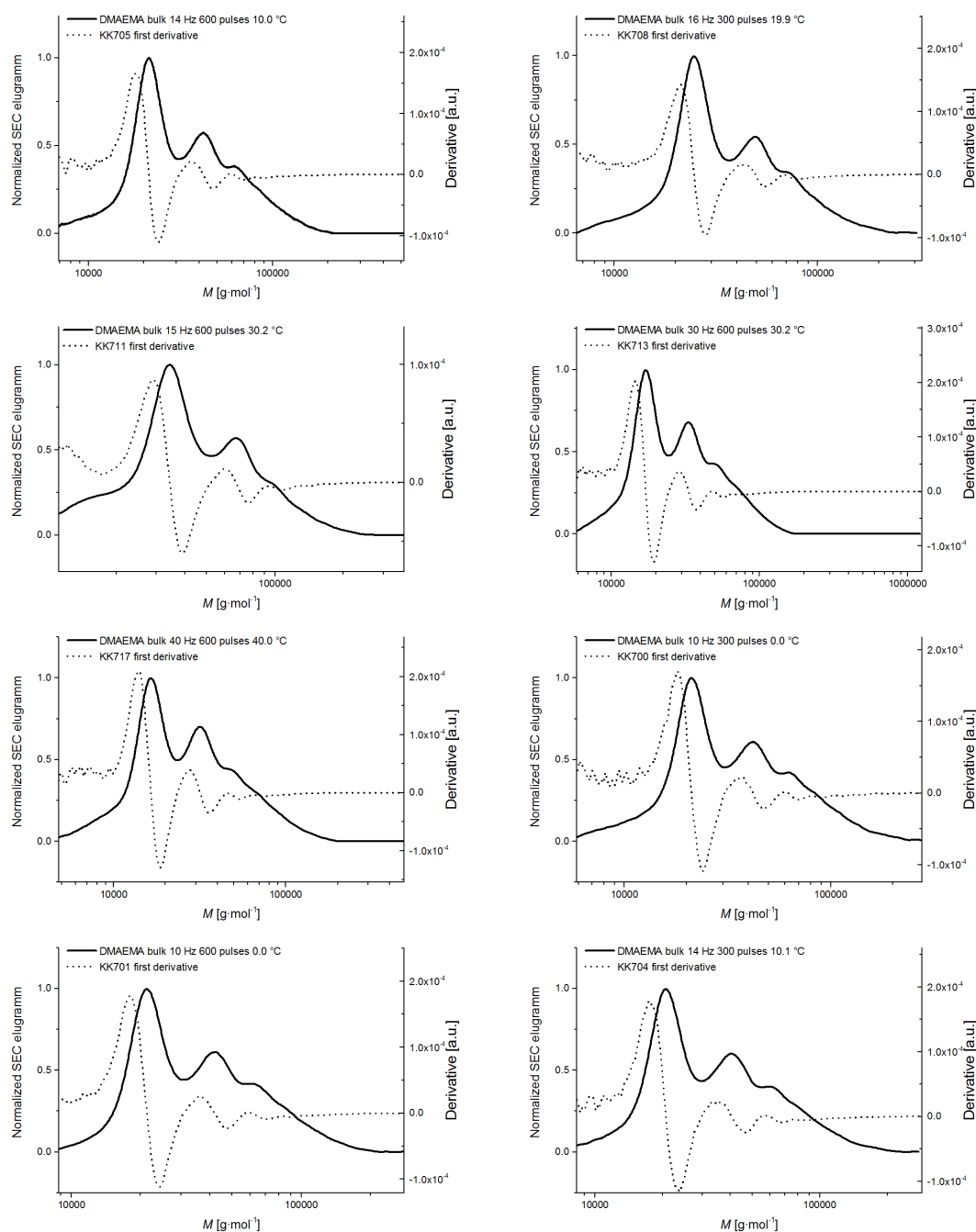


Figure A.11. Representative molecular weight distributions (solid lines) and their first derivatives (dotted lines) of 2-(*N,N*-dimethylamino)ethyl methacrylate (DMAEMA) in bulk. The sample specific conditions are given in the corresponding diagram and collated in Table A.10. For all samples incorporated into the final Arrhenius plot, the typical PLP structure with at least two inflection points is observed.

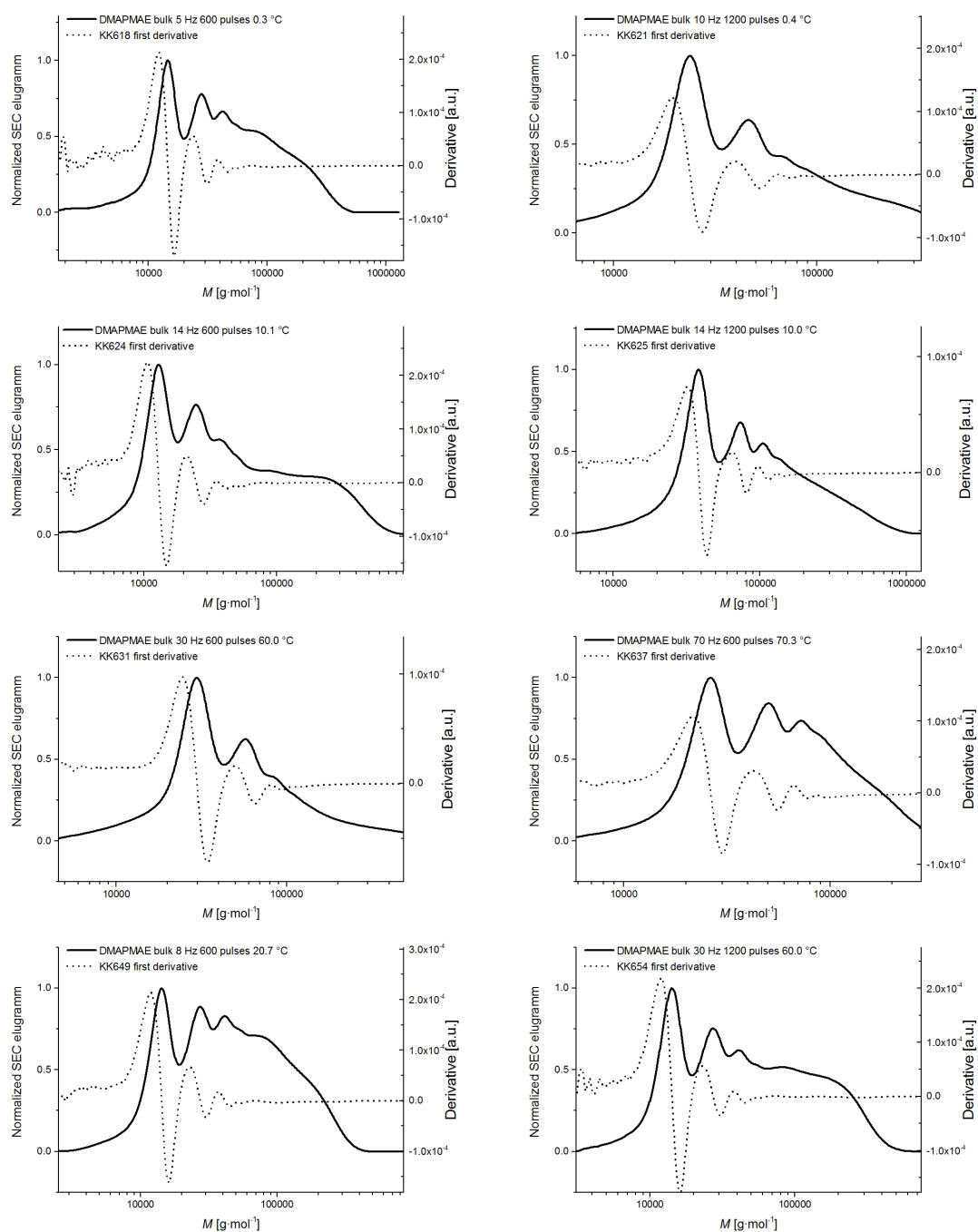


Figure A.12.: Representative molecular weight distributions (solid lines) and their first derivatives (dotted lines) of 3-(*N,N*-dimethylamino)propyl methacrylate (DMAPMAE) in bulk. The sample specific conditions are given in the corresponding diagram and collated in Table A.11. For all samples incorporated into the final Arrhenius plot, the typical PLP structure with at least two inflection points is observed.

Table A.6.: Detailed PLP sample conditions of all samples incorporated in the final Arrhenius plot, absolute molecular weights of the first and second inflection point, as well as the resulting propagation rate coefficients for 2-(*N*-ethylanylino)ethyl methacrylate (NEAEMA) in bulk.

sample	f Hz	n -	θ °C	T^{-1} 10^{-3} K^{-1}	$\ln(k_p)$ -	k_{p1}/k_{p2} -	M1 $\text{g}\cdot\text{mol}^{-1}$	M2 $\text{g}\cdot\text{mol}^{-1}$	c_M $\text{mol}\cdot\text{L}^{-1}$	k_{p1} $\text{mol}\cdot\text{L}^{-1}\cdot\text{s}^{-1}$	k_{p2} $\text{mol}\cdot\text{L}^{-1}\cdot\text{s}^{-1}$
KK1038	7	1000	9.8	3.534	5.7619	1.02	47441	93430	4.477	318	313
KK1039	14	1000	10	3.532	5.8219	1.01	25182	50101	4.476	338	336
KK1040	12	1000	21	3.400	6.0809	0.98	37726	76605	4.436	437	444
KK1041	24	1000	20.3	3.408	6.1522	1.06	20269	38313	4.439	470	444
KK1042	20	1000	29.8	3.301	6.3641	0.98	29832	60782	4.405	581	591
KK1043	40	1000	29.8	3.301	6.4585	1.05	16392	31144	4.405	638	606
KK1044	25	1000	39.9	3.194	6.6479	0.98	31436	64057	4.368	771	786
KK1045	50	1000	40	3.193	6.7243	1.04	16965	32603	4.368	832	800
KK1046	35	1000	49.7	3.097	6.9104	0.99	28958	58255	4.333	1003	1009
KK1047	70	1000	49.7	3.097	6.8742	1.05	13965	26633	4.333	967	922
KK1048	40	1000	59.8	3.003	7.0524	0.98	28958	59146	4.296	1156	1180
KK1049	80	1000	59.8	3.003	7.1589	1.05	16106	30706	4.296	1285	1225
KK1050	45	1000	70	2.914	7.3412	0.98	34065	69576	4.26	1543	1575
KK1051	90	1000	70	2.914	7.3947	1.06	17969	33919	4.26	1627	1536
KK1052	50	1000	80.4	2.828	7.3657	0.97	31144	64057	4.222	1581	1626
KK1053	100	1000	80.5	2.828	7.5558	1.06	18830	35528	4.222	1912	1804
KK1054	60	1000	89.5	2.757	7.7280	0.99	36993	75108	4.189	2271	2305
KK1055	120	1000	89.5	2.757	7.7070	1.06	18112	34211	4.189	2224	2100

Table A.7.: Detailed PLP sample conditions of all samples incorporated in the final Arrhenius plot, absolute molecular weights of the first and second inflection point, as well as the resulting propagation rate coefficients for 2-morpholinoethyl methacrylate (MOMA) in bulk.

sample	f Hz	n -	θ °C	T^{-1} 10^{-3} K^{-1}	$\ln(k_p)$ -	k_{p1}/k_{p2} -	M1 $\text{g}\cdot\text{mol}^{-1}$	M2 $\text{g}\cdot\text{mol}^{-1}$	c_M $\text{mol}\cdot\text{L}^{-1}$	k_{p1} $\text{mol}\cdot\text{L}^{-1}\cdot\text{s}^{-1}$	k_{p2} $\text{mol}\cdot\text{L}^{-1}\cdot\text{s}^{-1}$
KK511	24	300	20	3.411	6.1414	1.07	20256	37729	5.252	465	433
KK512	24	600	20	3.411	6.1344	1.09	20113	36869	5.252	461	423
KK513	20	300	30.8	3.29	6.3561	1.01	29848	59244	5.203	576	572
KK514	20	600	30.8	3.29	6.3845	1.03	30708	59388	5.203	593	573
KK515	40	300	30.9	3.289	6.4502	1.08	16395	30421	5.202	633	587
KK516	40	600	31	3.288	6.4590	1.07	16538	30994	5.202	638	598
KK517	25	300	40.1	3.192	6.5582	1.00	28989	58240	5.161	705	708
KK518	25	600	40.1	3.192	6.6064	1.04	30421	58383	5.161	740	710
KK519	50	300	40.1	3.192	6.6900	1.07	16538	30994	5.161	804	754
KK520	50	600	40.1	3.192	6.6814	1.07	16395	30564	5.161	797	743
KK521	30	300	49.8	3.096	6.9744	1.00	36296	72883	5.114	1069	1073
KK522	30	600	50.1	3.094	6.9506	0.99	35436	71878	5.113	1044	1059
KK523	60	300	50.1	3.094	6.9567	1.04	17825	34433	5.113	1050	1014
KK524	60	600	49.8	3.096	6.9957	1.03	18540	35866	5.114	1092	1056
KK525	35	300	60.2	2.999	7.2776	1.00	41743	83369	5.067	1447	1445
KK526	35	600	60.2	2.999	7.1417	0.99	36439	73889	5.067	1264	1281
KK527	70	300	60.2	2.999	7.1436	1.03	18254	35436	5.067	1266	1229
KK528	70	600	60.1	3.001	7.1819	1.04	18969	36439	5.067	1315	1263
KK529	45	300	70.2	2.912	7.3285	0.98	33859	69437	5.022	1523	1562
KK530	45	600	70.3	2.912	7.3244	0.96	33716	70586	5.021	1517	1588
KK531	90	300	70.3	2.912	7.3721	1.04	17682	33859	5.021	1591	1523
KK532	90	600	70.3	2.912	7.3640	1.04	17539	33859	5.021	1578	1523
KK533	50	300	80.7	2.826	7.4392	0.97	33716	69293	4.974	1701	1748
KK534	50	600	80.8	2.825	7.5090	0.98	36152	73745	4.974	1824	1861
KK535	100	300	80.7	2.826	7.4787	1.03	17539	34003	4.974	1770	1716
KK536	100	600	80.9	2.824	7.4625	1.03	17253	33430	4.973	1741	1687
KK537	60	300	90.8	2.748	7.8057	1.03	40166	77767	4.929	2455	2376
KK538	60	600	90.8	2.748	7.7162	0.96	36726	76187	4.929	2244	2328
KK539	120	300	90.7	2.748	7.7023	1.03	18111	35149	4.929	2213	2148
KK540	120	600	90.8	2.748	7.8693	1.04	21401	41313	4.929	2616	2525
KK541	8	300	-0.1	3.662	5.5429	0.97	33859	69724	5.324	255	263
KK542	8	600	-0.2	3.664	5.6004	0.98	35866	73027	5.324	271	275
KK543	16	300	-0.2	3.664	5.6259	1.03	18397	35579	5.324	278	268
KK544	16	600	-0.2	3.664	5.6715	1.07	19255	36152	5.324	290	273
KK545	10	300	10.3	3.528	5.8982	1.00	38302	76761	5.277	364	365
KK546	10	600	10.4	3.527	5.9278	1.00	39449	79059	5.277	375	376
KK547	20	300	10.5	3.525	5.9754	1.06	20686	39019	5.276	394	371
KK548	20	600	10.4	3.527	5.9959	1.02	21115	41599	5.277	402	396
KK549	12	300	20.5	3.405	6.2157	1.00	43463	86674	5.231	501	499
KK550	12	600	20.2	3.409	6.2350	1.02	44324	87105	5.232	510	501

Table A.8.: Detailed PLP sample conditions of all samples incorporated in the final Arrhenius plot, absolute molecular weights of the first and second inflection point, as well as the resulting propagation rate coefficients for 2-(1-piperidyl)ethyl methacrylate (PipEMA) in bulk.

sample	f Hz	n -	θ °C	T^{-1} 10^{-3} K^{-1}	$\ln(k_p)$ -	k_{p1}/k_{p2} -	M1 $\text{g}\cdot\text{mol}^{-1}$	M2 $\text{g}\cdot\text{mol}^{-1}$	c_M $\text{mol}\cdot\text{L}^{-1}$	k_{p1} $\text{mol}\cdot\text{L}^{-1}\cdot\text{s}^{-1}$	k_{p2} $\text{mol}\cdot\text{L}^{-1}\cdot\text{s}^{-1}$
KK558	4	300	0.0	3.661	5.4354	1.1	67327	122367	5.032	229	208
KK559	4	600	0.0	3.661	5.4651	1.09	69358	126947	5.032	236	216
KK560	8	300	0.0	3.661	5.4539	0.96	34293	71393	5.032	234	243
KK561	8	600	0.0	3.661	5.4745	0.96	35004	73060	5.032	239	249
KK562	7	300	9.7	3.535	5.7717	1.02	53389	104332	4.989	321	314
KK563	7	600	9.9	3.533	5.8021	1.04	55030	105845	4.988	331	318
KK564	14	300	9.9	3.533	5.7914	0.98	27223	55395	4.988	327	333
KK565	14	600	9.9	3.533	5.8357	0.98	28453	58137	4.988	342	350
KK566	12	300	19.7	3.415	6.0963	0.98	42703	87029	4.945	444	453
KK567	12	600	20.2	3.409	6.1176	0.97	43603	89651	4.942	454	467
KK568	24	300	20.7	3.403	6.1264	1.00	21984	43964	4.94	458	458
KK569	24	600	20.7	3.403	6.1575	0.99	22679	45588	4.94	472	475
KK570	20	300	30.2	3.297	6.3550	0.96	32872	68619	4.898	575	601
KK571	20	600	30.3	3.295	6.4281	0.95	35361	74172	4.897	619	649
KK572	40	300	30.3	3.295	6.3980	1.00	17156	34293	4.897	601	600
KK573	40	600	30.3	3.295	6.4177	0.99	17499	35361	4.897	613	619
KK574	25	300	40	3.193	6.5762	0.96	32517	68065	4.854	718	751
KK575	25	600	40.1	3.192	6.7331	0.95	38038	80307	4.854	840	886
KK576	50	300	40.1	3.192	6.5997	0.98	16643	33937	4.854	735	749
KK577	50	600	40.1	3.192	6.6788	0.99	18014	36252	4.854	795	800
KK578	30	300	50.1	3.094	6.9733	0.94	39829	84411	4.797	1068	1131
KK579	30	600	50.2	3.093	6.9823	0.94	40187	85159	4.796	1077	1142
KK580	60	300	50.1	3.094	6.9901	0.99	20253	40726	4.797	1086	1092
KK581	60	600	50.2	3.093	6.9902	0.99	20253	40726	4.796	1086	1092
KK583	35	600	60.3	2.999	7.1723	0.95	41264	87029	4.752	1303	1374
KK584	70	300	60.4	2.998	7.2437	0.99	22158	44685	4.751	1399	1411
KK585	70	600	60.3	2.999	7.1873	0.99	20944	42343	4.752	1323	1337
KK586	45	300	70.3	2.912	7.4673	0.95	42703	90026	4.707	1750	1844
KK587	45	600	70.2	2.912	7.3885	0.94	39470	84038	4.708	1617	1722
KK588	90	300	70.2	2.912	7.3619	0.98	19217	39291	4.708	1575	1610
KK589	90	600	70.2	2.912	7.4885	0.97	21811	44865	4.708	1787	1838
KK591	50	600	80.3	2.829	7.5651	0.92	41983	90776	4.663	1930	2086
KK592	50	600	80.2	2.83	7.5434	0.93	41085	88527	4.663	1888	2034
KK593	100	600	80.3	2.829	7.6501	0.98	22853	46491	4.663	2101	2137
KK595	60	600	90.5	2.75	7.7268	0.94	40726	86281	4.617	2268	2403
KK596	120	300	90.4	2.751	7.7382	0.99	20598	41803	4.618	2294	2328
KK597	120	600	90.5	2.75	7.8268	0.99	22505	45588	4.617	2507	2539

Table A.9.: Detailed PLP sample conditions of all samples incorporated in the final Arrhenius plot, absolute molecular weights of the first and second inflection point, as well as the resulting propagation rate coefficients for 2-(*N,N*-diethylamino)ethyl methacrylate (DEAEMA) in bulk.

sample	f Hz	n -	θ °C	T^{-1} 10^{-3} K^{-1}	$\ln(k_p)$ -	k_{p1}/k_{p2} -	M1 $\text{g}\cdot\text{mol}^{-1}$	M2 $\text{g}\cdot\text{mol}^{-1}$	c_M $\text{mol}\cdot\text{L}^{-1}$	k_{p1} $\text{mol}\cdot\text{L}^{-1}\cdot\text{s}^{-1}$	k_{p2} $\text{mol}\cdot\text{L}^{-1}\cdot\text{s}^{-1}$
KK740	10	800	0.0	3.661	5.4437	0.97	21746	44675	5.074	231	238
KK741	10	1600	0.0	3.661	5.4645	0.98	22203	45152	5.074	236	240
KK744	14	800	10	3.532	5.8105	0.97	22203	45948	5.026	334	345
KK745	14	1600	10	3.532	5.8376	0.98	22813	46426	5.026	343	349
KK747	8	1600	19.8	3.414	6.1391	0.96	53469	111634	4.979	464	484
KK748	16	800	19.9	3.412	6.1475	0.97	26957	55722	4.979	468	483
KK749	16	1600	19.7	3.415	6.1643	0.96	27420	56851	4.98	475	493
KK750	10	800	30	3.299	6.3988	0.95	54917	115671	4.93	601	633
KK751	10	1600	30	3.299	6.4806	0.98	59597	121067	4.93	652	663
KK755	15	1600	40	3.193	6.7443	0.95	51222	107605	4.883	849	892
KK756	30	800	40	3.193	6.6551	0.97	23425	48501	4.883	777	804
KK757	30	1600	40	3.193	6.6998	0.97	24497	50580	4.883	812	839
KK760	40	800	49.9	3.095	6.9080	0.97	22356	45948	4.825	1000	1028
KK761	40	1600	49.9	3.095	6.9282	0.95	22813	48021	4.825	1021	1074
KK764	50	800	60.2	3.001	7.1749	0.99	23119	46904	4.776	1306	1325
KK765	50	1600	59.9	3.003	7.2007	0.94	23731	50420	4.777	1340	1424
KK768	60	800	70.2	2.912	7.3934	0.96	23731	49300	4.728	1625	1688
KK769	60	1600	70.2	2.912	7.3606	0.93	22966	49300	4.728	1573	1688
KK772	70	800	79.9	2.832	7.5828	0.97	24343	49940	4.682	1964	2015
KK773	70	1600	80	2.832	7.4909	0.97	22203	45630	4.681	1792	1841
KK774	40	800	90.2	2.752	7.8734	0.97	56367	116008	4.633	2626	2703
KK776	80	800	90.1	2.753	7.6818	0.95	23272	48980	4.633	2168	2282
KK777	80	1600	90.1	2.753	7.7639	0.93	25264	54273	4.633	2354	2529

Table A.10.: Detailed PLP sample conditions of all samples incorporated in the final Arrhenius plot, absolute molecular weights of the first and second inflection point, as well as the resulting propagation rate coefficients for 2-(*N,N*-dimethylamino)ethyl methacrylate (DMAEMA) in bulk.

sample	f Hz	n -	θ °C	T^{-1} 10^{-3} K^{-1}	$\ln(k_p)$ -	k_{p1}/k_{p2} -	M1 $\text{g}\cdot\text{mol}^{-1}$	M2 $\text{g}\cdot\text{mol}^{-1}$	c_M $\text{mol}\cdot\text{L}^{-1}$	k_{p1} $\text{mol}\cdot\text{L}^{-1}\cdot\text{s}^{-1}$	k_{p2} $\text{mol}\cdot\text{L}^{-1}\cdot\text{s}^{-1}$
KK698	5	300	0.0	3.661	5.6233	0.98	52619	107549	6.046	277	283
KK699	5	600	0.0	3.661	5.6403	0.99	53519	107697	6.046	282	283
KK700	10	300	0.0	3.661	5.6986	1.02	28368	55616	6.046	298	293
KK701	10	600	0.0	3.661	5.6716	0.99	27610	55616	6.046	290	293
KK702	7	300	9.8	3.534	6.0060	0.96	54568	113763	5.987	406	423
KK703	7	600	10.9	3.521	6.0315	0.99	55915	112580	5.98	416	419
KK704	14	300	10.1	3.53	5.9960	1.01	27004	53369	5.985	402	397
KK705	14	600	10	3.532	6.0236	0.99	27762	55915	5.986	413	416
KK706	8	300	20.1	3.41	6.3324	0.99	65486	132963	5.925	562	571
KK707	8	600	19.9	3.412	6.3276	1.00	65187	130603	5.926	560	561
KK708	16	300	19.9	3.412	6.3233	0.99	32454	65784	5.926	557	565
KK709	16	600	19.9	3.412	6.3326	0.99	32757	66083	5.926	563	568
KK710	15	300	30.2	3.297	6.5080	0.97	41203	84853	5.864	671	690
KK711	15	600	30.2	3.297	6.5920	0.99	44814	90944	5.864	729	740
KK712	30	300	30.2	3.297	6.6006	1.04	22599	43461	5.864	736	707
KK713	30	600	30.2	3.297	6.5870	1.01	22295	44363	5.864	726	722
KK714	20	300	40	3.193	6.7180	0.99	37738	76223	5.804	827	835
KK715	20	600	40	3.193	6.8557	1.01	43310	85893	5.804	949	941
KK716	40	300	40	3.193	6.8359	1.01	21229	41956	5.804	931	920
KK717	40	600	40	3.193	6.8430	1.02	21381	41956	5.804	937	920
KK720	50	800	50	3.095	7.0751	0.97	21381	43912	5.753	1182	1214
KK721	50	1600	50	3.095	7.1169	0.98	22295	45565	5.753	1233	1260
KK722	30	800	60.2	2.999	7.2878	0.95	43611	91538	5.691	1462	1535
KK724	60	800	60.1	3.001	7.2892	0.98	21838	44663	5.692	1464	1498
KK725	60	1600	59.9	3.003	7.3300	0.99	22751	46016	5.693	1525	1543
KK727	35	1600	70	2.914	7.5127	0.95	46317	97028	5.632	1831	1918
KK728	70	800	70	2.914	7.5082	0.99	23055	46617	5.632	1823	1843
KK729	70	1600	70	2.914	7.4746	0.97	22295	46166	5.632	1763	1825
KK730	40	800	79.9	2.832	7.6982	0.96	48269	100587	5.572	2204	2297
KK732	80	800	80	2.832	7.8328	0.98	27610	56065	5.571	2522	2561
KK733	80	1600	80	2.832	7.7225	0.97	24727	50970	5.571	2259	2328
KK734	50	800	89.9	2.754	7.9134	0.96	47368	98808	5.511	2734	2851
KK736	100	800	89.9	2.754	7.8996	1.00	23359	46767	5.511	2696	2699
KK737	100	1600	89.9	2.754	7.9253	1.00	23967	47819	5.511	2766	2760

Table A.11.: Detailed PLP sample conditions of all samples incorporated in the final Arrhenius plot, absolute molecular weights of the first and second inflection point, as well as the resulting propagation rate coefficients for 3-(*N,N*-dimethylamino)propyl methacrylate (DMAPMAE) in bulk.

sample	f Hz	n -	θ °C	T^{-1} 10^{-3} K^{-1}	$\ln(k_p)$ -	k_{p1}/k_{p2} -	M1 $\text{g}\cdot\text{mol}^{-1}$	M2 $\text{g}\cdot\text{mol}^{-1}$	c_M $\text{mol}\cdot\text{L}^{-1}$	k_{p1} $\text{mol}\cdot\text{L}^{-1}\cdot\text{s}^{-1}$	k_{p2} $\text{mol}\cdot\text{L}^{-1}\cdot\text{s}^{-1}$
KK612	30	300	30.2	3.297	6.1725	1.05	14571	27769	5.325	479	457
KK613	30	600	30.2	3.297	6.2618	1.06	15932	30123	5.325	524	496
KK614	20	300	40.1	3.192	6.4633	1.04	28946	55509	5.273	641	615
KK615	20	600	40.2	3.191	6.5198	1.04	30627	59162	5.272	678	655
KK616	40	300	40.1	3.192	6.4098	1.03	13719	26759	5.273	608	593
KK617	40	600	40.2	3.191	6.4222	1.00	13889	27769	5.272	615	615
KK618	5	600	0.0	3.661	5.2863	1.04	37167	71753	5.492	198	191
KK619	5	1200	0.0	3.661	5.3086	1.03	38004	73572	5.492	202	196
KK620	10	600	0.0	3.661	5.3343	1.05	19496	37167	5.492	207	198
KK621	10	1200	0.0	3.661	5.3851	1.05	20512	39175	5.492	218	208
KK622	7	600	10	3.532	5.6678	1.01	38506	76381	5.439	289	287
KK623	7	1200	10	3.532	5.7431	1.02	41515	81169	5.439	312	305
KK624	14	600	10	3.532	5.7312	1.04	20512	39510	5.439	308	297
KK625	14	1200	10	3.532	5.7637	1.05	21189	40345	5.439	319	303
KK626	25	300	50	3.095	6.6100	0.99	26590	53847	5.228	742	752
KK627	25	600	50	3.095	6.7784	1.00	31467	62646	5.228	879	875
KK628	50	300	50	3.095	6.8429	1.04	16782	32306	5.228	937	902
KK629	50	600	50	3.095	6.8429	1.02	16782	32978	5.228	937	921
KK630	30	300	60	3.002	6.7637	0.97	25579	52683	5.176	866	892
KK631	30	600	60	3.002	7.0278	1.00	33313	66954	5.176	1128	1133
KK632	60	300	60	3.002	6.9285	1.02	15082	29451	5.176	1021	997
KK633	60	600	60	3.002	7.0149	1.03	16442	31971	5.176	1113	1082
KK635	35	600	70	2.914	7.2365	0.98	34822	71422	5.123	1389	1425
KK636	70	300	70	2.914	7.1584	0.99	16102	32642	5.123	1285	1302
KK637	70	600	70	2.914	7.2961	1.03	18479	35995	5.123	1474	1436
KK638	40	300	80	2.832	7.2683	0.96	31131	65132	5.071	1434	1500
KK639	40	600	80	2.832	7.5109	1.00	39677	79353	5.071	1828	1828
KK640	80	300	80	2.832	7.3334	1.00	16612	33145	5.071	1531	1527
KK641	80	600	80	2.832	7.3334	0.98	16612	33816	5.071	1531	1558
KK642	50	300	90	2.754	7.4407	0.98	29283	59992	5.018	1704	1745
KK643	50	600	90	2.754	7.6187	0.98	34990	71257	5.018	2036	2073
KK644	100	300	90	2.754	7.4815	1.00	15252	30627	5.018	1775	1782
KK645	100	600	90	2.754	7.3376	0.97	13207	27264	5.018	1537	1586

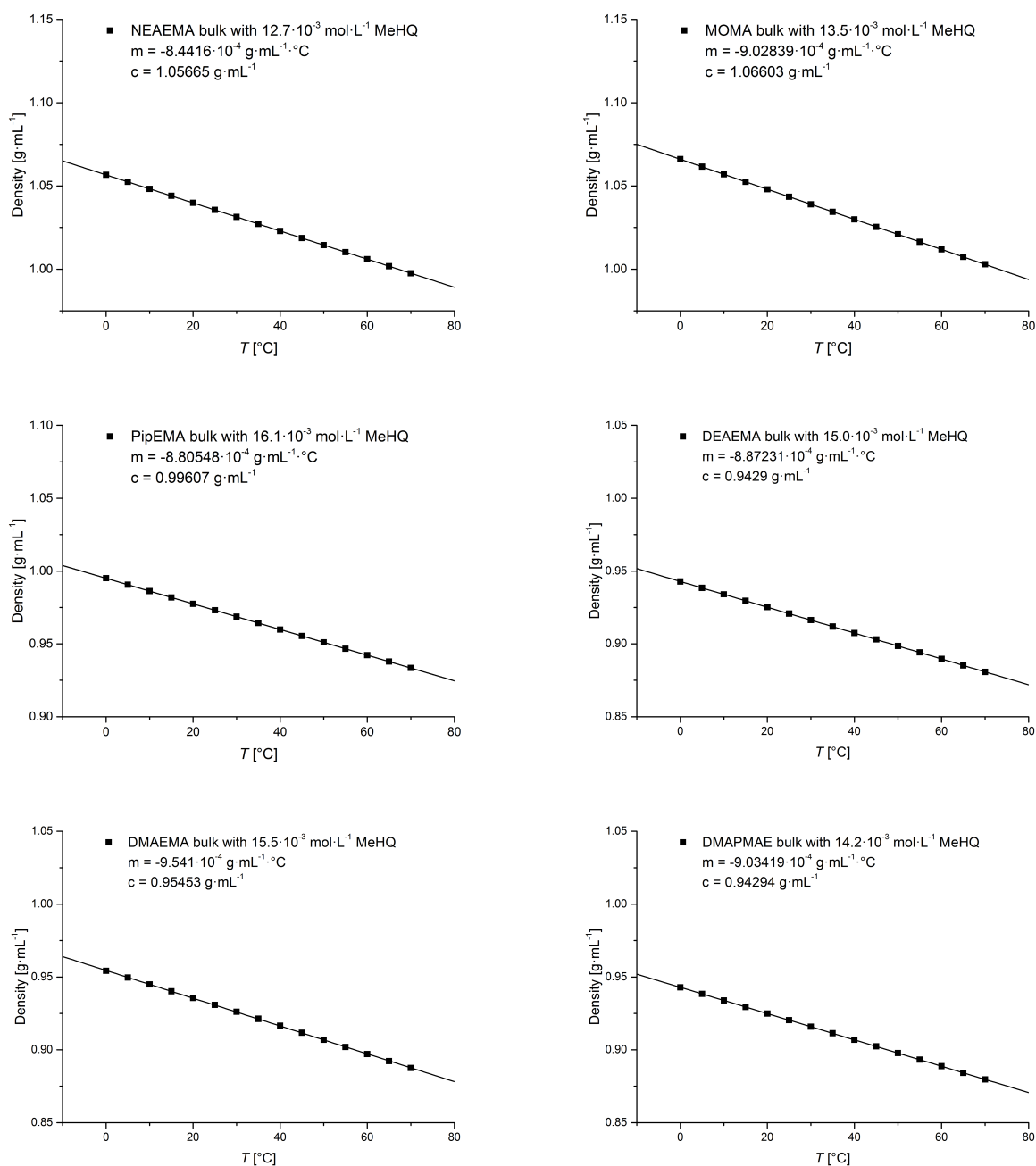


Figure A.13.: Temperature dependent densities for the herein studied monomers NEAEMA, MOMA, PipEMA, DEAEMA, DMAEMA, and DMAPMAE in bulk. To prevent the solutions from polymerizing inside the measurement device, methyl hydroquinone (MeHQ) was added. The temperature dependent densities are furthermore collated in Table 3.1 in Chapter 3.

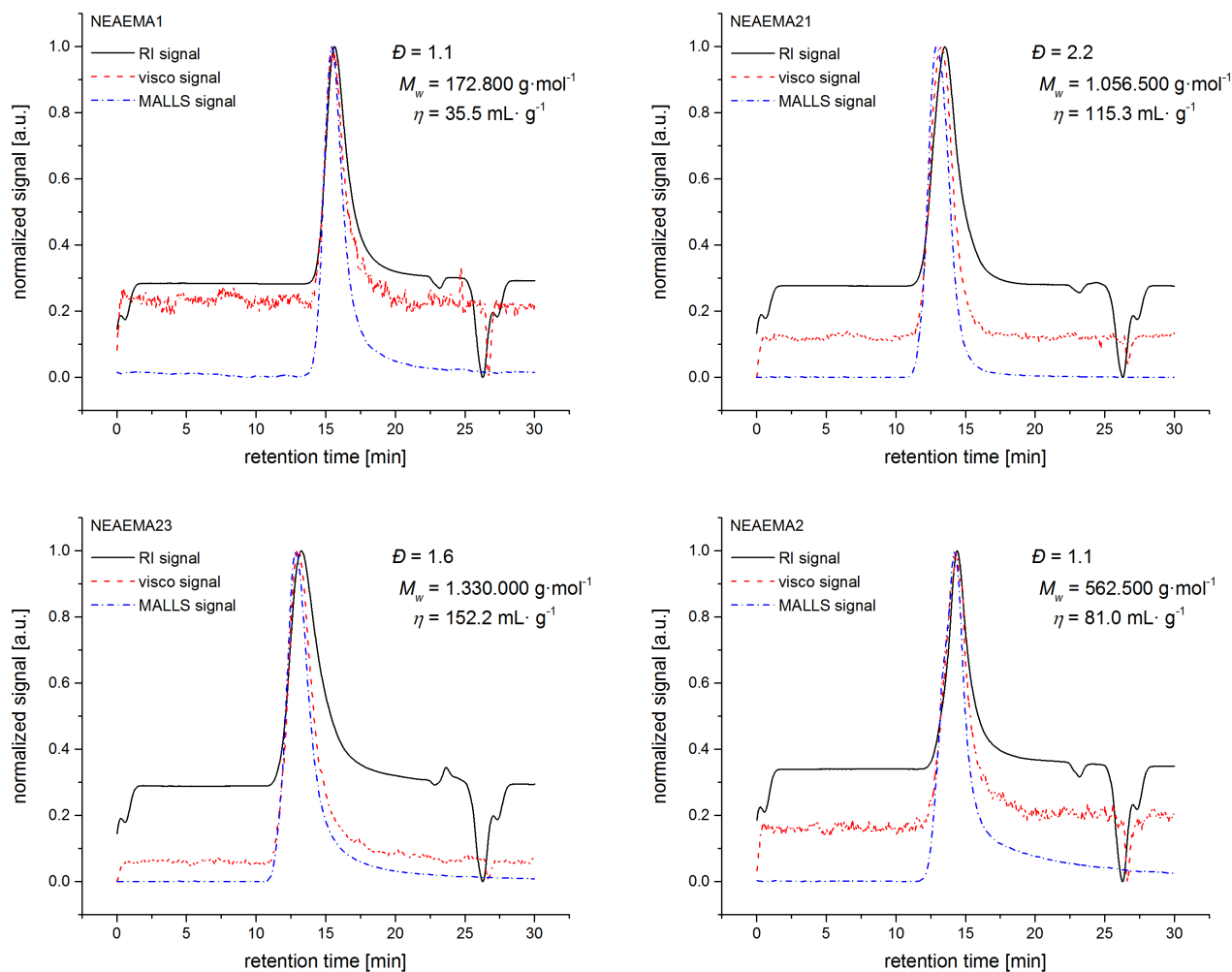


Figure A.14.: Representative triple detection SEC traces with refractive index (RI, black solid line), MALLS (blue dot-dashed line), and viscosimeter (visco, red dashed line) detector signals for NEAEMA. All data incorporated into the final MHKS plot are collated in Table A.12

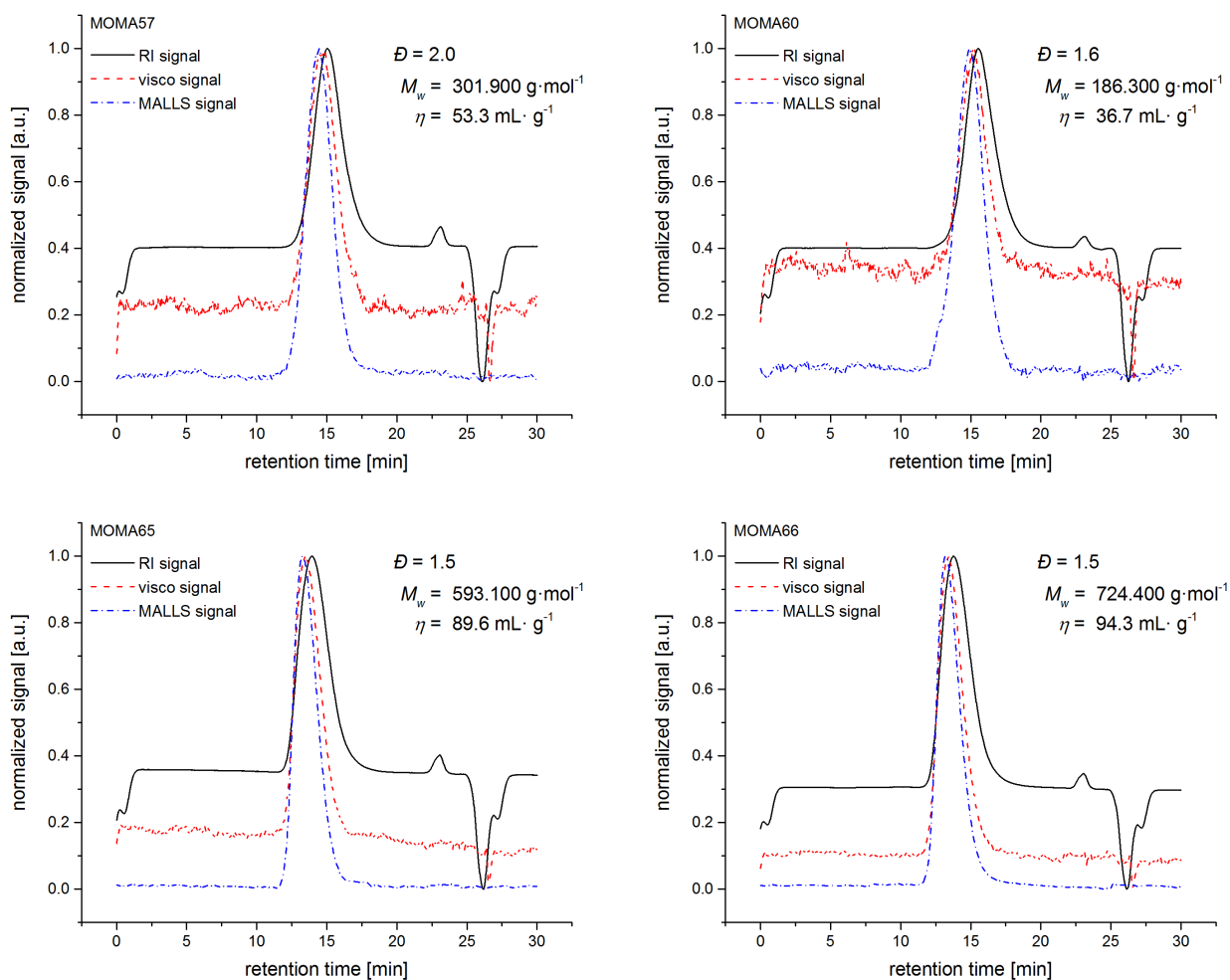


Figure A.15.: Representative triple detection SEC traces with refractive index (RI, black solid line), MALLS (blue dot-dashed line), and viscosimeter (visco, red dashed line) detector signals for MOMA. All data incorporated into the final MHKS plot are collated in Table A.12

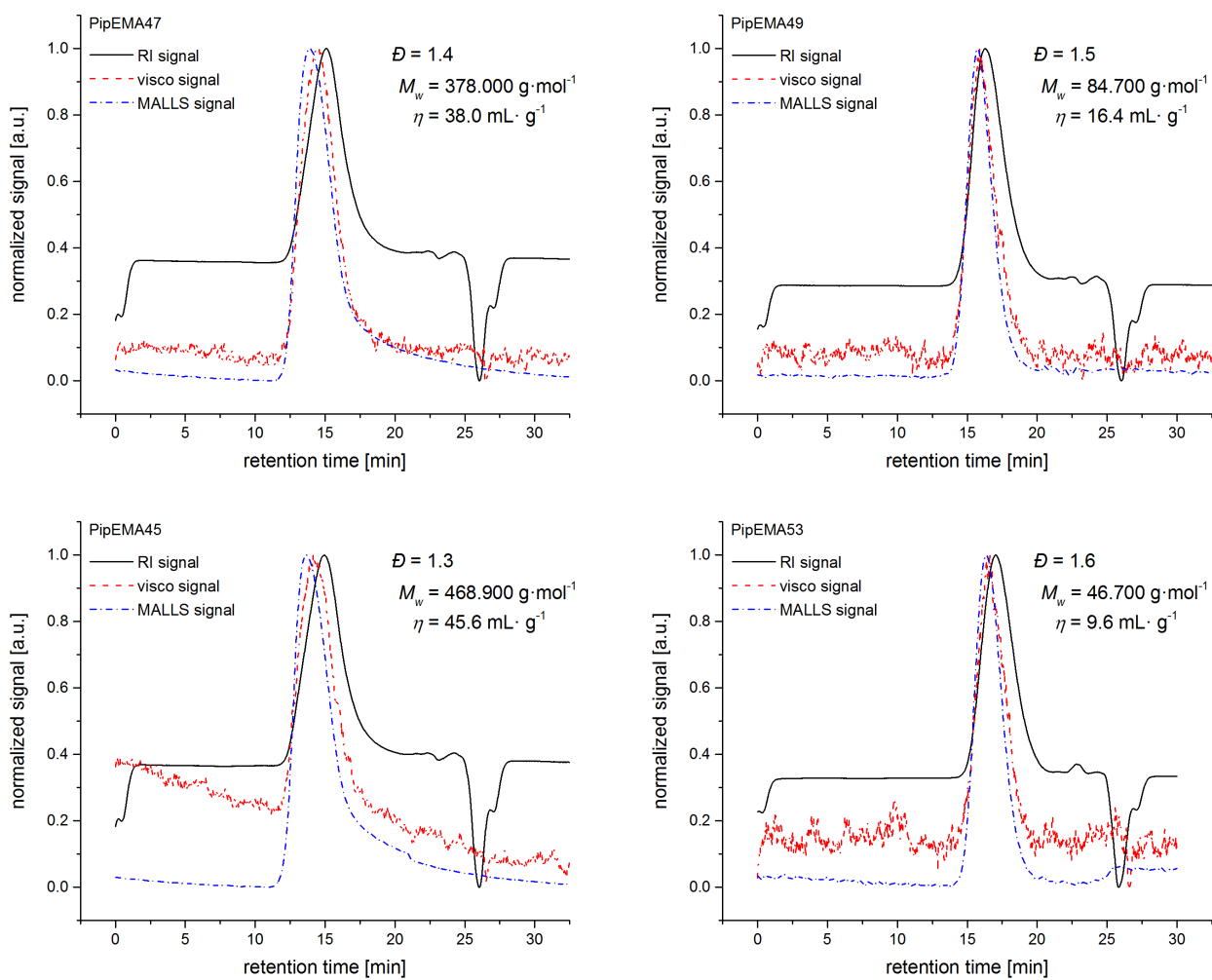


Figure A.16.: Representative triple detection SEC traces with refractive index (RI, black solid line), MALLS (blue dot-dashed line), and viscosimeter (visco, red dashed line) detector signals for PipEMA. All data incorporated into the final MHKS plot are collated in Table A.12

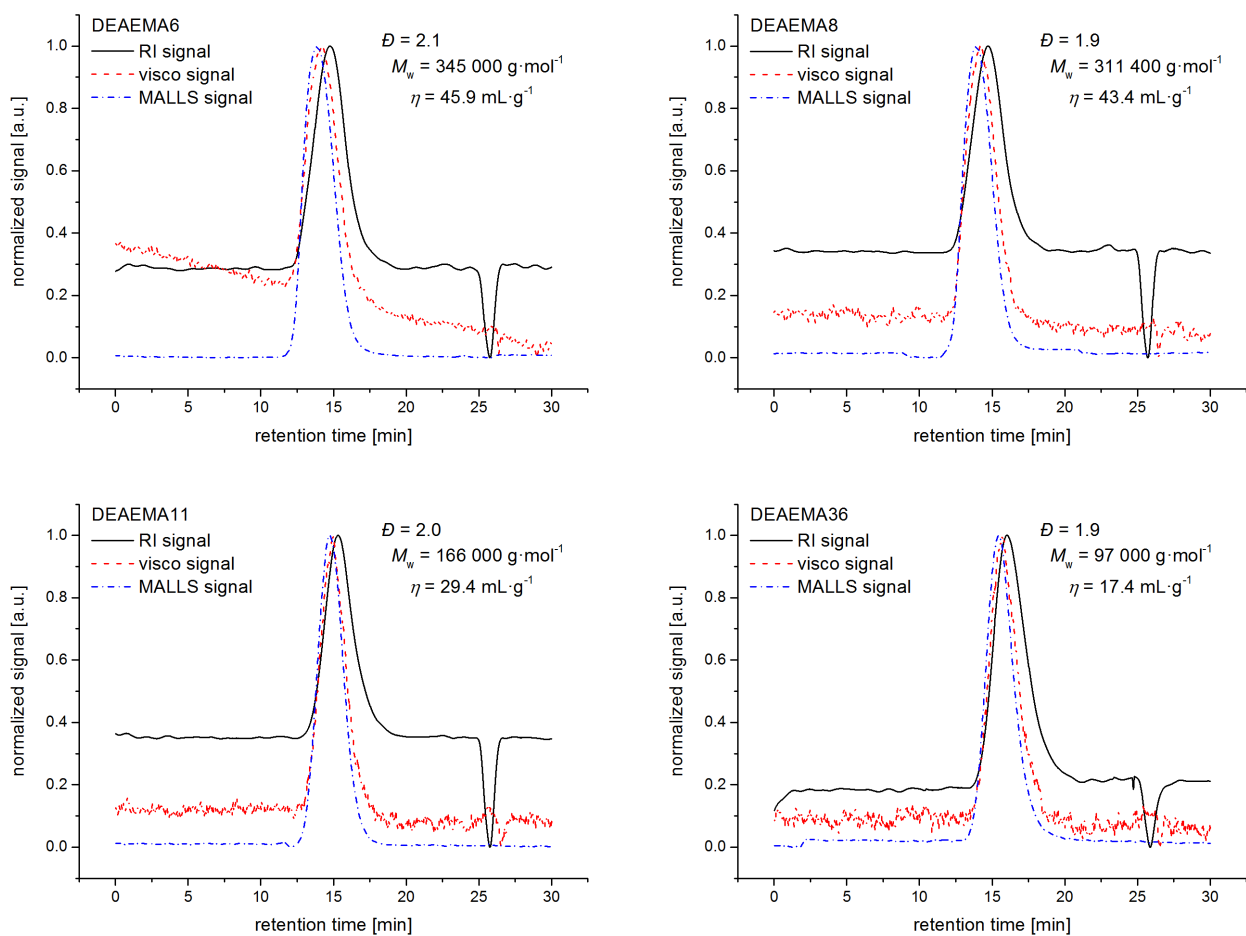


Figure A.17.: Representative triple detection SEC traces with refractive index (RI, black solid line), MALLS (blue dot-dashed line), and viscosimeter (visco, red dashed line) detector signals for DEAEMA. All data incorporated into the final MHKS plot are collated in Table A.13

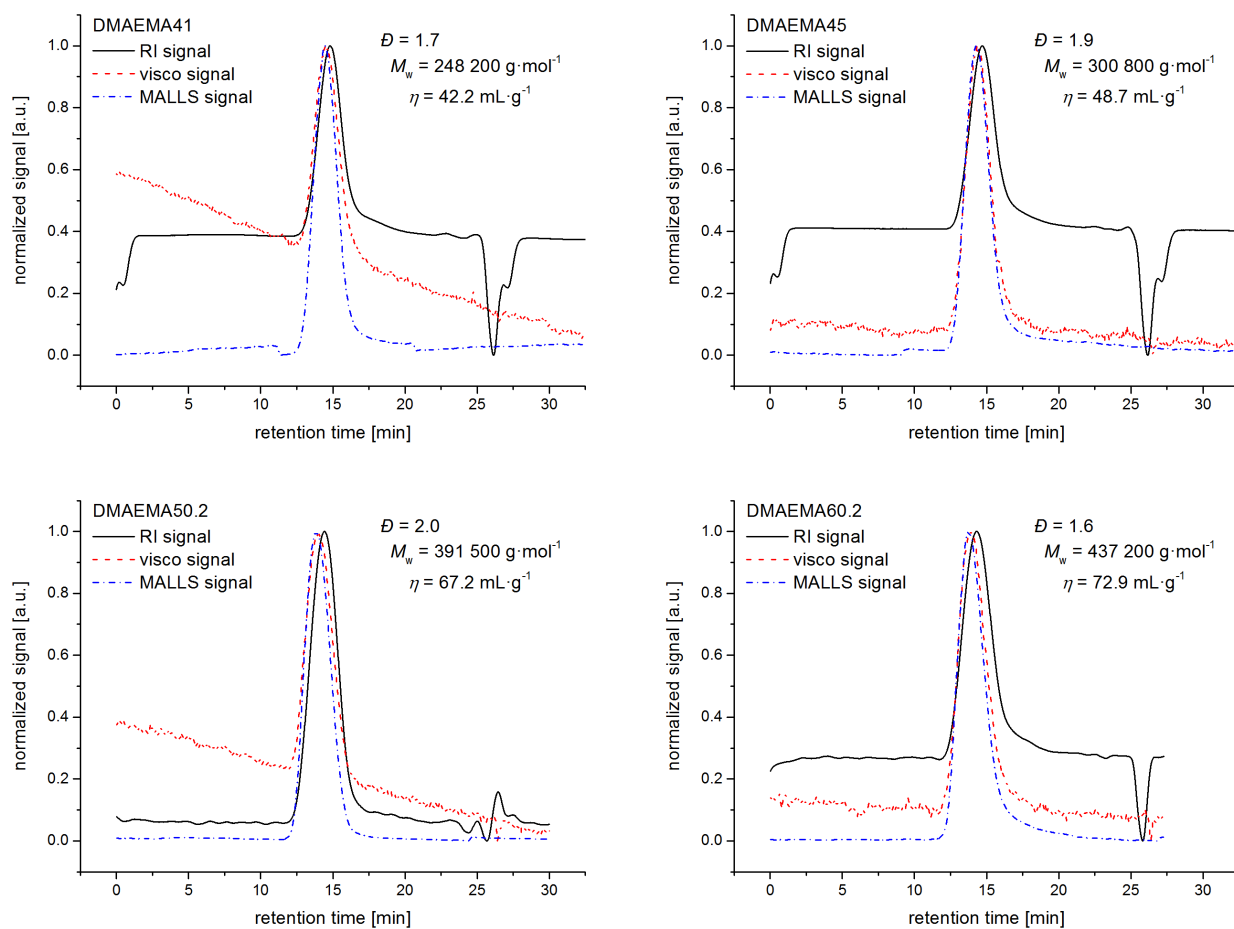


Figure A.18.: Representative triple detection SEC traces with refractive index (RI, black solid line), MALLS (blue dot-dashed line), and viscosimeter (visco, red dashed line) detector signals for DMAEMA. All data incorporated into the final MHKS plot are collated in Table A.13

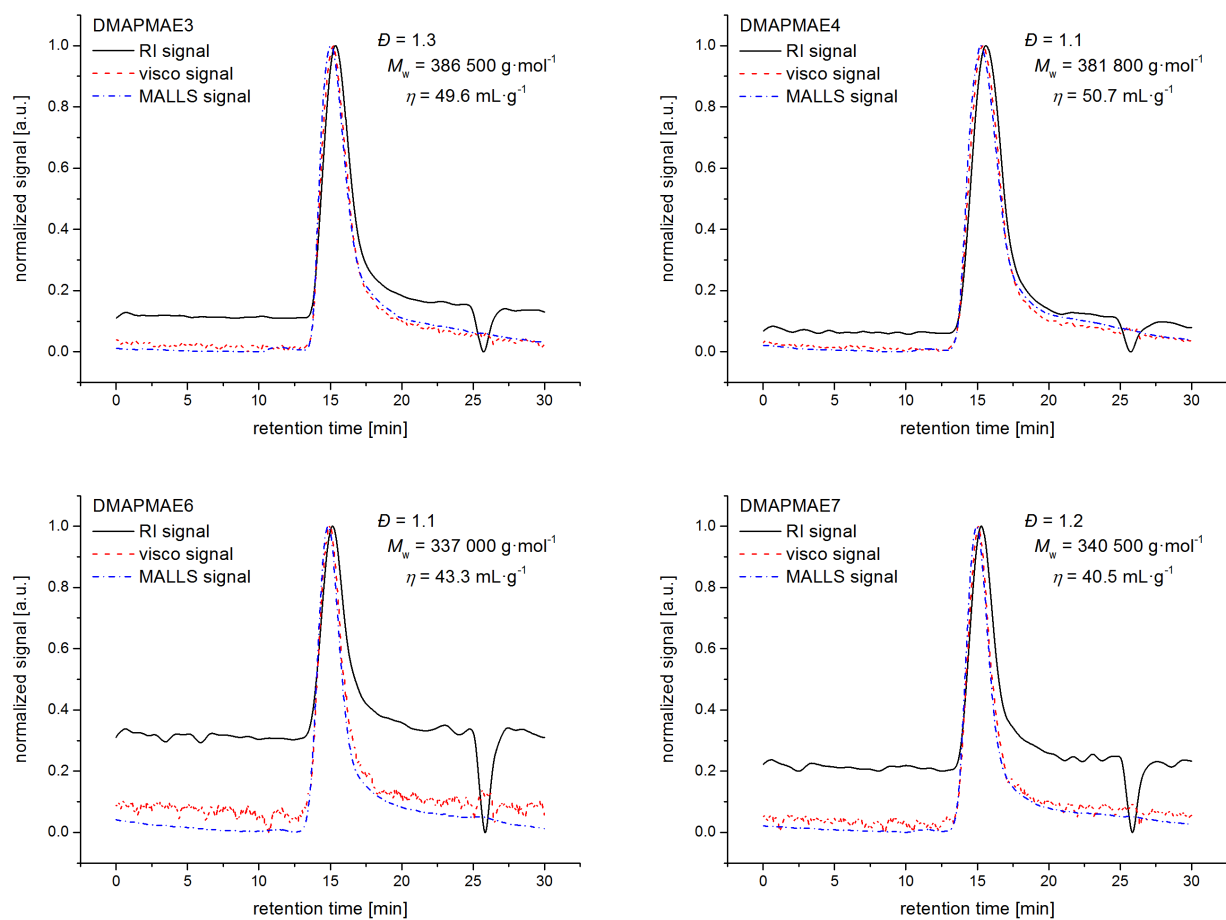


Figure A.19.: Representative triple detection SEC traces with refractive index (RI, black solid line), MALLS (blue dot-dashed line), and viscosimeter (visco, red dashed line) detector signals for DMAPMAE. All data incorporated into the final MHKS plot are collated in Table A.13

Table A.12.: Weight average molecular weights, M_w , and corresponding intrinsic viscosities, $[\eta]$, for the determination of MHKS parameters of NEAEMA, MOMA, and PipEMA. All data were obtained using the MALLS and viscosimeter detector signal of the triple detection SEC.

NEAEMA				MOMA				PipEMA			
sample no.	Mw g·mol ⁻¹	$[\eta]$ mL·g ⁻¹	\bar{D}	sample no.	Mw g·mol ⁻¹	$[\eta]$ mL·g ⁻¹	\bar{D}	sample no.	Mw g·mol ⁻¹	$[\eta]$ mL·g ⁻¹	\bar{D}
1	172800	35.3	1.1	30	1193200	131.3	2.5	20	112600	18.2	1.8
2	562500	81.0	1.1	31	528600	76.7	1.8	21	126500	19.2	1.7
3	968800	89.5	2.5	35	372600	71.0	1.8	33	125800	18.0	1.6
4	1646000	130.2	2.2	36	874800	110.3	2.5	35	618400	49.6	1.7
5	1158800	112.6	2.2	49	113300	29.2	1.9	40	47000	10.5	1.5
17	993600	103.2	1.9	50	130300	32.0	1.5	44	357200	34.0	1.5
19	62600	20.5	2.1	51	128900	26.1	2.4	45	468900	45.6	1.3
21	1056500	115.3	2.2	52	86100	22.7	1.5	46	226300	25.7	1.7
23	1330000	152.2	1.6	53	96000	22.7	1.5	47	378000	38.0	1.4
38	590900	77.4	2.4	55	69100	17.4	1.7	48	107900	18.3	1.6
39	145400	24.9	1.7	57	301900	53.3	2.0	49	84700	16.4	1.5
40	49400	12.7	1.6	60	186300	36.7	1.6	51	75800	14.4	1.8
41	26600	10.5	1.4	61	219900	38.2	1.4	52	64000	13.2	1.5
42	23100	9.1	1.4	65	593100	89.6	1.5	53	46700	9.6	1.6
				66	724400	94.3	1.5				
				67	619100	76.9	1.7				

Table A.13.: Weight average molecular weights, M_w , and corresponding intrinsic viscosities, $[\eta]$, for the determination of MHKS parameters of DEAEMA, DMAEMA, and DMAPMAE. All data were obtained using the MALLS and viscosimeter detector signal of the triple detection SEC. – continued on next page.

DEAEMA				DMAEMA				DMAPMAE			
sample no.	M_w $\text{g}\cdot\text{mol}^{-1}$	$[\eta]$ $\text{mL}\cdot\text{g}^{-1}$	D	sample no.	M_w $\text{g}\cdot\text{mol}^{-1}$	$[\eta]$ $\text{mL}\cdot\text{g}^{-1}$	D	sample no.	M_w $\text{g}\cdot\text{mol}^{-1}$	$[\eta]$ $\text{mL}\cdot\text{g}^{-1}$	D
6	345000	45.9	2.1	41	248200	42.2	1.7	1	483000	61.6	1.1
7	245800	36.6	2.1	42	148800	31.1	1.8	2	459400	54.9	1.1
8	311400	43.4	1.9	43	132300	25.3	2.0	3	386500	49.6	1.3
9	254100	38.4	2.2	44	89100	21.2	1.6	4	381800	50.7	1.1
10	206500	35.1	1.8	45	300800	48.7	1.9	5	360000	50.8	1.1
11	166000	29.4	2.0	46	58500	16.2	2.0	6	337000	43.3	1.1
12	151200	27.7	1.7	47	48600	13.3	1.8	7	340500	40.5	1.2
13	118300	23.1	1.7	48	52600	15.2	1.9	8	293100	42.9	1.1
14	85500	19.0	1.8	49	54100	13.9	1.8	9	262200	41.0	1.2
15	41100	11.7	1.9	50	390500	60.4	2.0	10	182400	29.6	1.8
16	361600	51.4	1.5	51	249200	43.8	2.2	2.2	436600	54.1	1.3
17	297900	47.8	1.4	52	230000	41.1	1.9	3.2	407600	52.1	1.3
18	337100	51.2	1.8	53	209100	38.4	1.6	4.2	356700	49.2	1.5
19	280100	46.6	1.3	54	192200	36.8	2.0	5.2	329300	46	1.5
20	357500	50.1	1.7	55	150700	30.2	1.8	6.2	293600	41.6	1.3
21	338600	46.4	1.6	56	140600	30.1	2.0	7.2	267900	39.5	1.6
22	332300	47.1	1.7	57	91100	22.6	2.0	8.2	253300	32.6	1.8
23	284800	43.5	1.9	58	58200	14.2	1.8	9.2	211100	31.8	1.5
24	367500	47.6	1.6	59	23000	7.6	1.6	10.2	191700	30.9	1.7
25	289900	41.1	1.6	50.2	391500	67.2	2.0	1.3	339300	44.1	2.0
27	394400	46.0	1.6	51.2	251500	42.6	2.0	2.3	425200	55.2	1.4
28	452000	44.0	1.5	52.2	219800	41.7	1.8	3.3	398300	50.3	1.2
29	395800	40.4	1.6	53.2	192000	37.4	1.6	4.3	338900	44.9	1.5
30	442500	46.3	1.5	54.2	184400	32.5	2.2	5.3	309200	39.8	1.4
31	404300	43.0	1.5	55.2	148700	29.7	1.8	6.3	281600	41.0	1.5
32	379500	39.8	1.5	56.2	136400	27	2.1	7.3	240800	35	1.4
33	285800	33.0	1.8	57.2	92000	20	2.2	8.3	267600	34.9	1.3
34	223400	28.9	1.9	58.2	57000	12.9	1.8	9.3	210600	31.5	1.8
35	247700	27.8	2.0	59.2	28900	9.4	1.7	10.3	181300	29.2	2.0
36	97000	17.4	1.9	50.3	395600	60.2	1.9				
37	566900	48.8	1.2	51.3	248600	44.3	2.2				
				52.3	233400	41.4	1.8				
				53.3	212400	38.2	1.8				
				54.3	195200	37.5	1.9				
				55.3	151800	30.1	1.9				
				56.3	142900	27.5	2.2				
				57.3	89300	21.1	2.0				
				58.3	56500	14.6	1.7				
				60	484500	73.5	1.5				

DEAEMA			DMAEMA				DMAPMAE				
sample no.	Mw g·mol ⁻¹	[η] mL·g ⁻¹	Đ	sample no.	Mw g·mol ⁻¹	[η] mL·g ⁻¹	Đ	sample no.	Mw g·mol ⁻¹	[η] mL·g ⁻¹	Đ
				61	362200	61.4	1.6				
				62	348200	52.7	1.8				
				63	405400	58.9	1.7				
				64	307500	47.7	1.7				
				65	171800	29.8	2.0				
				66	226200	41.1	1.9				
				67	303100	47.3	1.6				
				68	167900	30.4	1.9				
				69	186200	33.6	1.9				
				60.2	437200	72.9	1.6				
				61.2	360500	57.4	1.6				
				62.2	350100	54.4	1.8				
				63.2	406300	61.7	1.9				
				64.2	306300	50.1	2.0				
				65.2	173400	31	2.0				
				66.2	225800	38.8	1.8				
				67.2	306400	46	1.5				
				68.2	166400	32.7	1.6				
				69.2	186500	33.6	2				

Table A.14.: Detailed sample conditions and resulting isolated yield for the RAFT polymerization of NEAEMA in bulk at 66 °C.

sample	reaction time h	m(AIBN) mg	c(AIBN) 10 ⁻⁴ mol·L ⁻¹	m(RAFT agent) mg	m(NEAEMA) g	isolated yield %
1	3.5	0.1	2.08	1.2	3.0434	19
2	19	0.1	2.29	1.2	2.767	58
3	18.5	0.2	6.36	3.50 (TRITT)	1.992	65
4	25	0.2	6.35	3.50 (TRITT)	1.9944	84
5	25	0.2	6.04	3.50 (TRITT)	2.096	87
17	19	0.04	1.29	0.62	1.9711	54
19	48	0.04	2.51	0.38	1.0104	4
21	40.5	0.02	1.30	0.19	0.973	18
23	26	0.02	1.24	0.2	1.0198	31

Table A.15.: Detailed sample conditions and resulting isolated yield for the polymerization with thiol as transfer agent for NEAEMA in bulk at 66°C.

sample	reaction time h	m(AIBN) mg	c(AIBN) $10^{-3} \text{ mol}\cdot\text{L}^{-1}$	m(Thiol) mg	Thiol mol%	m(NEAEMA) g	isolated yield %
38	1	0.5	2.66	1.8	0.18	1.189	50
39	1	0.2	1.16	5.3	0.53	1.0946	47
40	1	0.5	3.12	13.7	1.48	1.014	54
41	1	0.4	2.32	21.8	2.19	1.0925	45
42	1	1.0	6.03	41.1	4.3	1.0509	50

Table A.16.: Detailed sample conditions and resulting isolated yield for the RAFT polymerization of MOMA in bulk at 66 °C.

sample	reaction time h	m(AIBN) mg	c(AIBN) $10^{-4} \text{ mol}\cdot\text{L}^{-1}$	m(RAFT agent) mg	m(MOMA) g	isolated yield %
30	9	0.08	9.98	0.39	0.5005	65
31	15	0.08	9.68	0.39	0.5154	72
35	25	0.08	9.57	0.39	0.5211	85
36	30	0.08	9.78	0.39	0.5100	76

Table A.17.: Detailed sample conditions and resulting isolated yield for the polymerization with thiol as transfer agent for MOMA in bulk at 66°C.

sample	reaction time h	m(AIBN) mg	c(AIBN) $10^{-3} \text{ mol}\cdot\text{L}^{-1}$	m(Thiol) mg	Thiol mol%	m(MOMA) g	isolated yield %
49	1	0.4	2.49	3.2	0.29	1.0279	38
50	1	0.5	2.62	4.8	0.37	1.2198	28
51	1	0.4	2.59	4.8	0.46	0.9893	35
52	1	0.7	4.14	6.7	0.58	1.08	39
53	1	0.8	5.06	7.1	0.66	1.0102	36
55	1	0.6	3.48	8.9	0.76	1.1016	30
57	0.75	0.8	4.92	1.5	0.14	1.0391	18
60	0.75	0.8	5.07	3.4	0.32	1.009	32
61	0.75	0.8	5.07	2.9	0.27	1.0088	36
65	0.75	1.6	5.11	1.1	0.05	2.0026	42
66	0.75	1.6	5.11	1.3	0.06	2.0038	42
67	0.75	1.6	5.20	1.6	0.08	1.9667	35

Table A.18.: Detailed sample conditions and resulting isolated yield for the polymerization with thiol as transfer agent for PipEMA in 50% solution in THF at 66°C. ^aPolymerization carried out in butyl acetate.

sample	reaction time h	m(AIBN) mg	c(AIBN) 10 ⁻³ mol·L ⁻¹	m(Thiol) mg	Thiol mol%	m(PipEMA) g	m(solvent) g	isolated yield %
20 ^a	1	0.4	0.99	9.1	0.84	1.0093	1.0118	20
21 ^a	1	0.5	1.41	7.3	0.67	1.0069	1.0096	24
33 ^a	1	0.6	1.69	9.3	0.86	1.0003	1.0088	21
35 ^a	1	0.7	1.92	0.6	0.05	1.0597	1.0121	18
40 ^a	1	0.8	2.00	11	0.92	1.1158	1.1514	18
44	0.75	0.4	2.16	0.4	0.07	0.5045	0.4335	10
45	0.75	0.4	2.17	0.6	0.11	0.5073	0.4384	20
46	0.75	0.3	2.12	0.9	0.16	0.5126	0.4215	19
47	0.75	0.4	2.18	1.2	0.22	0.501	0.4366	21
48	0.75	0.4	2.07	2.1	0.34	0.5764	0.4545	20
49	0.75	0.4	2.28	2.5	0.45	0.5106	0.4848	19
51	0.75	0.3	2.09	2.7	0.49	0.5134	0.4108	18
52	0.75	0.4	2.16	3.5	0.63	0.512	0.4379	19
53	0.75	0.4	2.19	5.1	0.93	0.5111	0.4514	18

Table A.19.: Detailed sample conditions and resulting isolated yield for the polymerization with thiol as transfer agent for DEAEMA in bulk at 66°C.

sample	reaction time h	m(AIBN) mg	c(AIBN) $10^{-3} \text{ mol}\cdot\text{L}^{-1}$	m(Thiol) mg	Thiol mol%	m(DEAEMA) g	isolated yield %
6	1	1.2	7.1	0.13	0.011	1.0801	35
7	1	1.2	6.85	0.91	0.071	1.1206	26
8	1	1.2	7.44	0.28	0.024	1.0319	29
9	1	1.2	6.91	0.36	0.028	1.1106	30
10	1	1.1	6.84	0.62	0.053	1.0277	31
11	1	1.2	7.39	1.09	0.092	1.0386	34
12	1	1.1	6.88	1.26	0.108	1.0216	35
13	1	1.2	7.23	2.05	0.169	1.0607	33
14	1	1.2	7.49	3.58	0.305	1.0243	36
15	1	1.2	7.04	7.48	0.599	1.0898	32
16	1	0.8	9.91	0.01	0.002	0.5162	36
17	1	0.8	10.12	0.02	0.003	0.5053	36
18	1	0.8	10.22	0.03	0.005	0.5003	32
19	1	0.9	10.91	0.05	0.008	0.5277	31
20	1	0.8	10.09	0.06	0.01	0.507	34
21	1	0.8	10.15	0.08	0.014	0.5039	31
22	1	0.7	8.91	0.09	0.016	0.5025	30
23	1	0.8	9.68	0.12	0.02	0.5287	27
24	1	0.7	8.93	0.13	0.023	0.501	29
25	1	0.6	7.56	0.16	0.028	0.5075	25
27	2	1.2	16.66	0.05	0.009	0.4606	47
28	2	1.3	17.31	0.08	0.015	0.4801	57
29	2	1.5	16.61	0.15	0.023	0.5776	59
30	2	1.2	17.06	0.24	0.047	0.4497	67
31	2	1.2	16.62	0.35	0.066	0.4616	67
32	2	1.1	16.34	0.39	0.079	0.4304	69
33	2	1.1	17.51	0.45	0.098	0.4018	66
34	2	1.1	15.89	0.58	0.114	0.4427	70
35	2	1.4	16.61	0.85	0.138	0.5388	61
36	2	1.5	16.68	1.8	0.273	0.5749	64
37	4	1.1	16.17	0.05	0.01	0.435	81

Table A.20.: Detailed sample conditions and resulting isolated yield for the polymerization with thiol as transfer agent for DMAEMA in bulk at 66°C. – continues on next page.

sample	reaction time h	m(AIBN) mg	c(AIBN) $10^{-3} \text{ mol}\cdot\text{L}^{-1}$	m(Thiol) mg	Thiol mol%	m(DMAEMA) g	isolated yield %
41	0.75	0.8	5.11	0.80	0.059	1.0013	21
42	0.75	0.8	5.04	2.00	0.146	1.015	18
43	0.75	0.8	5.1	2.80	0.207	1.0022	20
44	0.75	0.8	5.09	3.80	0.28	1.0047	20
45	0.75	0.8	5.11	0.40	0.03	1.0004	21
46	0.75	0.8	4.84	6.10	0.427	1.0572	15
47	0.75	0.8	5.02	7.80	0.567	1.0187	12
48	0.75	0.8	4.81	7.40	0.515	1.0644	19
49	0.75	0.9	5.2	9.40	0.629	1.1059	19
50	0.75	1.1	6.96	0.27	0.02	1.0099	25
51	0.75	1.1	7.02	0.37	0.027	1.0026	23
52	0.75	0.9	6.76	0.37	0.032	0.8509	19
53	0.75	0.8	7.31	0.36	0.038	0.7002	23
54	0.75	0.7	6.91	0.44	0.05	0.6475	22
55	0.75	1.0	7.38	1.00	0.085	0.867	23
56	0.75	0.7	7.19	1.00	0.119	0.6222	24
57	0.75	0.7	7.19	1.80	0.214	0.6229	23
58	0.75	0.9	7.97	4.20	0.431	0.7218	22
59	0.75	0.7	7.39	8.20	1.002	0.6056	19
50.2	0.75	1.1	6.96	0.27	0.02	1.0099	25
51.2	0.75	1.1	7.02	0.37	0.027	1.0026	23
52.2	0.75	0.9	6.76	0.37	0.032	0.8509	19
53.2	0.75	0.8	7.31	0.36	0.038	0.7002	23
54.2	0.75	0.7	6.91	0.44	0.05	0.6475	22
55.2	0.75	1.0	7.38	1.00	0.085	0.867	23
56.2	0.75	0.7	7.19	1.00	0.119	0.6222	24
57.2	0.75	0.7	7.19	1.80	0.214	0.6229	23
58.2	0.75	0.9	7.97	4.20	0.431	0.7218	22
59.2	0.75	0.7	7.39	8.20	1.002	0.6056	19
50.3	0.75	1.1	6.96	0.27	0.02	1.0099	25
51.3	0.75	1.1	7.02	0.37	0.027	1.0026	23
52.3	0.75	0.9	6.76	0.37	0.032	0.8509	19
53.3	0.75	0.8	7.31	0.36	0.038	0.7002	23
54.3	0.75	0.7	6.91	0.44	0.05	0.6475	22
55.3	0.75	1.0	7.38	1.00	0.085	0.867	23
56.3	0.75	0.7	7.19	1.00	0.119	0.6222	24
57.3	0.75	0.7	7.19	1.80	0.214	0.6229	23
58.3	0.75	0.9	7.97	4.20	0.431	0.7218	22
60	1	0.8	4.99	0.09	0.006	1.0258	28

sample	reaction time h	m(AIBN) mg	c(AIBN) $10^{-3} \text{ mol}\cdot\text{L}^{-1}$	m(Thiol) mg	Thiol mol%	m(DMAEMA) g	isolated yield %
61	1	0.8	5.05	0.13	0.01	1.0123	27
62	1	0.8	5.09	0.20	0.015	1.0047	25
63	1	0.8	5.06	0.26	0.019	1.0118	22
64	1	0.8	5.08	0.32	0.024	1.0063	26
65	1	0.8	5.07	0.54	0.04	1.0087	22
66	1	0.8	5.11	0.71	0.05	1.0008	13
67	1	0.8	5.06	1.00	0.07	1.0115	25
68	1	0.8	5.08	1.53	0.11	1.0067	24
69	1	0.8	5.1	2.54	0.19	1.0026	25
60.2	1	0.8	4.99	0.09	0.006	1.0258	28
61.2	1	0.8	5.05	0.13	0.01	1.0123	27
62.2	1	0.8	5.09	0.20	0.015	1.0047	25
63.2	1	0.8	5.06	0.26	0.019	1.0118	22
64.2	1	0.8	5.08	0.32	0.024	1.0063	26
65.2	1	0.8	5.07	0.54	0.04	1.0087	22
66.2	1	0.8	5.11	0.71	0.05	1.0008	13
67.2	1	0.8	5.06	1.00	0.07	1.0115	25
68.2	1	0.8	5.08	1.53	0.11	1.0067	24
69.2	1	0.8	5.1	2.54	0.19	1.0026	25

Table A.21.: Detailed sample conditions and resulting isolated yield for the polymerization with thiol as transfer agent for DMAPMAE in bulk at 66°C.

sample	reaction time h	m(AIBN) mg	c(AIBN) $10^{-3} \text{ mol}\cdot\text{L}^{-1}$	m(Thiol) mg	Thiol mol%	m(DMAPMAE) g	isolated yield %
1	1	0.8	10.11	0.16	0.025	0.5062	15
2	1	0.8	10.18	0.2	0.032	0.5026	30
3	1	0.8	9.93	0.25	0.039	0.5151	32
4	1	0.7	8.99	0.27	0.044	0.498	27
5	1	0.7	8.93	0.32	0.051	0.5015	32
6	1	0.7	8.88	0.38	0.061	0.5042	29
7	1	0.7	9.14	0.44	0.072	0.4897	30
8	1	0.7	9.16	0.52	0.086	0.4887	33
9	1	0.6	7.67	0.63	0.102	0.4999	31
10	1	0.7	8.32	0.92	0.138	0.5383	28
2.2	1	0.8	10.18	0.2	0.032	0.5026	30
3.2	1	0.8	9.93	0.25	0.039	0.5151	32
4.2	1	0.7	8.99	0.27	0.044	0.498	27
5.2	1	0.7	8.93	0.32	0.051	0.5015	32
6.2	1	0.7	8.88	0.38	0.061	0.5042	29
7.2	1	0.7	9.14	0.44	0.072	0.4897	30
8.2	1	0.7	9.16	0.52	0.086	0.4887	33
9.2	1	0.6	7.67	0.63	0.102	0.4999	31
10.2	1	0.7	8.32	0.92	0.138	0.5383	28
1.3	1	0.8	10.11	0.16	0.025	0.5062	15
2.3	1	0.8	10.18	0.2	0.032	0.5026	30
3.3	1	0.8	9.93	0.25	0.039	0.5151	32
4.3	1	0.7	8.99	0.27	0.044	0.498	27
5.3	1	0.7	8.93	0.32	0.051	0.5015	32
6.3	1	0.7	8.88	0.38	0.061	0.5042	29
7.3	1	0.7	9.14	0.44	0.072	0.4897	30
8.3	1	0.7	9.16	0.52	0.086	0.4887	33
9.3	1	0.6	7.67	0.63	0.102	0.4999	31
10.3	1	0.7	8.32	0.92	0.138	0.5383	28

A.3. Chapter 4: PLP with Lewis Acids

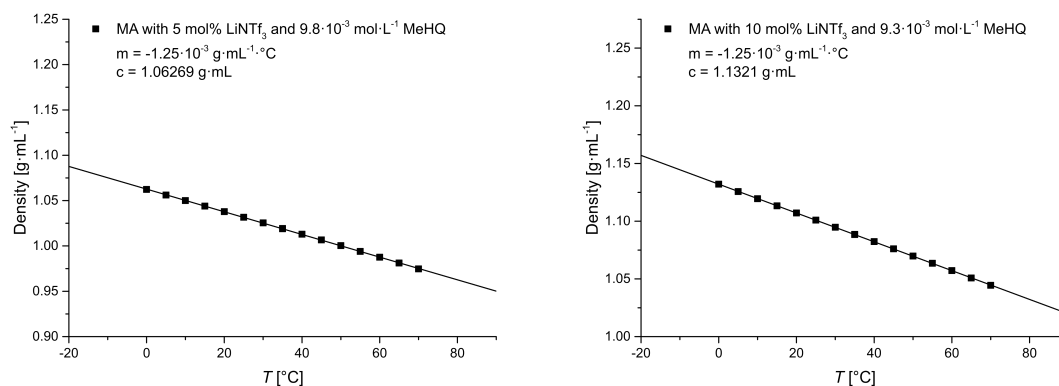


Figure A.20.: Temperature dependent densities for MA in bulk with 5 and 10 mol% of the Lewis acid LiNTf_3 . To prevent the solutions from polymerizing inside the measurement device, methyl hydroquinone (MeHQ) was added.

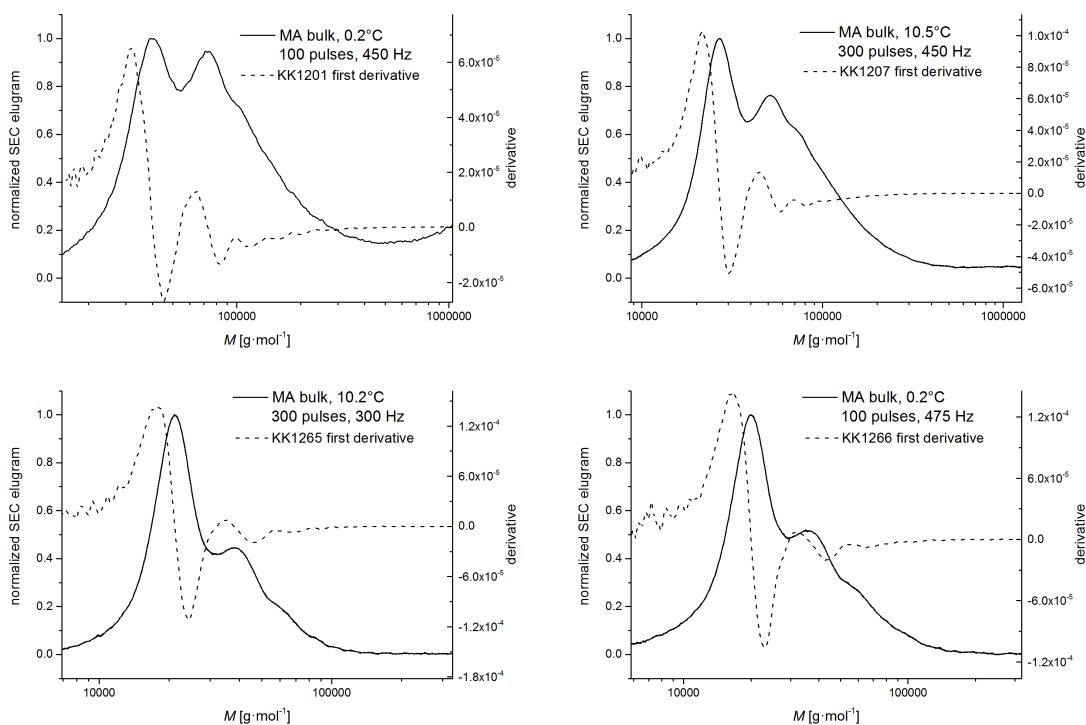


Figure A.21.: Representative molecular weight distributions (solid lines) and their first derivatives (dotted lines) of methyl acrylate (MA) in bulk.

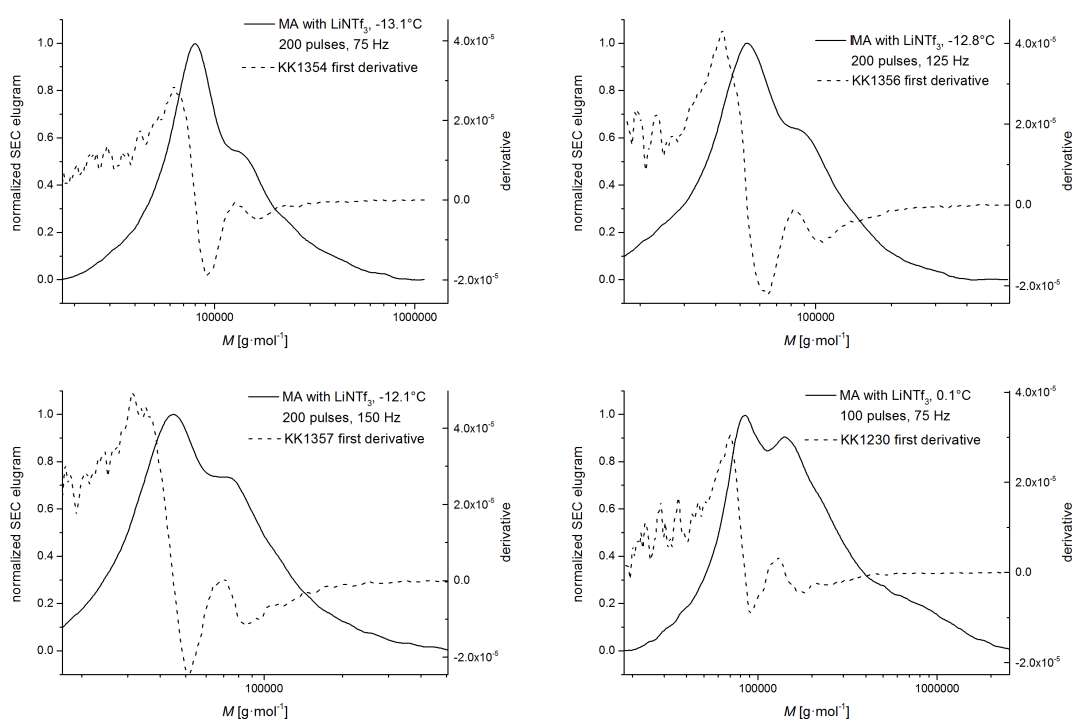


Figure A.22.: Representative molecular weight distributions (solid lines) and their first derivatives (dotted lines) of methyl acrylate (MA) with LiNTf₃.

Table A.22.: Detailed PLP sample conditions, absolute molecular weights of the first and second inflection point, as well as the resulting propagation rate coefficients for methyl acrylate (MA) samples incorporated into the frequency series at 10 °C.

sample	f Hz	n -	θ °C	T^{-1} 10^{-3} K^{-1}	$\ln(k_p)$ -	k_{p1}/k_{p2} -	M1 $\text{g}\cdot\text{mol}^{-1}$	M2 $\text{g}\cdot\text{mol}^{-1}$	c_M $\text{mol}\cdot\text{L}^{-1}$	k_{p1} $\text{mol}\cdot\text{L}^{-1}\cdot\text{s}^{-1}$	k_{p2} $\text{mol}\cdot\text{L}^{-1}\cdot\text{s}^{-1}$
KK1192	75	300	10.5	3.525	9.0962	1.00	114800	230200	11.210	8921	8945
KK1193	100	300	10.5	3.525	9.1293	1.03	89000	173400	11.210	9222	8984
KK1194	125	300	10.5	3.525	9.1706	0.98	74200	150800	11.210	9610	9766
KK1195	150	300	10.5	3.525	9.1925	1.01	63200	125600	11.210	9823	9761
KK1196	175	300	10.4	3.527	9.2111	1.04	55200	106100	11.212	10008	9618
KK1197	200	300	10.5	3.525	9.2009	1.07	47800	89200	11.210	9906	9243
KK1198	225	300	10.4	3.527	9.2057	1.03	42700	83100	11.212	9954	9686
KK1199	250	300	10.4	3.527	9.2023	1.04	38300	73700	11.212	9920	9544
KK1200	275	300	10.2	3.529	9.2044	1.04	34900	67400	11.215	9941	9599
KK1201	300	300	10.2	3.529	9.2202	1.01	32500	64400	11.215	10099	10005
KK1202	325	300	10.5	3.525	9.2071	1.00	29600	59200	11.210	9968	9968
KK1203	350	300	10.5	3.525	9.1930	0.98	27100	55200	11.210	9828	10009
KK1204	375	300	10.3	3.528	9.2087	0.99	25700	52100	11.213	9983	10119
KK1205	400	300	10.4	3.527	9.2132	0.96	24200	50500	11.212	10029	10464
KK1206	425	300	10.5	3.525	9.2100	0.96	22700	47200	11.210	9996	10393
KK1207	450	300	10.5	3.525	9.2035	0.96	21300	44500	11.210	9932	10375
KK1208	475	300	10.3	3.528	9.2190	0.96	20500	42600	11.213	10087	10481
KK1209	500	300	10.5	3.525	9.2154	0.95	19400	40700	11.210	10051	10543

Table A.23.: Detailed PLP sample conditions, absolute molecular weights of the first and second inflection point, as well as the resulting propagation rate coefficients for methyl acrylate (MA) samples with 10 mol% LiNTf₃ incorporated into the frequency series at 10 °C. For certain samples, no second inflection point was observed, however, the data have been incorporated into the frequency series since the determined propagation rate was in agreement with the remaining data.

sample	f Hz	n -	θ °C	T^{-1} 10^{-3} K^{-1}	$\ln(k_p)$ -	k_{p1}/k_{p2} -	M1 $\text{g}\cdot\text{mol}^{-1}$	M2 $\text{g}\cdot\text{mol}^{-1}$	c_M $\text{mol}\cdot\text{L}^{-1}$	k_{p1} $\text{mol}\cdot\text{L}^{-1}\cdot\text{s}^{-1}$	k_{p2} $\text{mol}\cdot\text{L}^{-1}\cdot\text{s}^{-1}$
KK1171	50	300	10.4	3.527	9.1454	0.97	157500	-	9.762	9371	-
KK1172	75	300	10.6	3.524	9.1465	-	117600	-	9.759	10498	-
KK1174	125	300	10.3	3.528	9.4530	1.00	85700	175800	9.763	12746	13073
KK1175	150	300	10.5	3.525	9.4724	-	72800	-	9.760	12996	-
KK1176	175	300	10.6	3.524	9.4773	-	62700	125600	9.759	13060	13080
KK1177	200	300	10.6	3.524	9.4446	0.99	53100	-	9.759	12640	-
KK1178	225	300	10.5	3.525	9.5200	-	50900	-	9.760	13629	-
KK1179	250	300	10.4	3.527	9.4998	-	44900	91100	9.762	13357	13551
KK1180	275	300	10.7	3.523	9.4749	1.03	39800	-	9.758	13028	-
KK1181	300	300	10.4	3.527	9.4640	0.93	36100	-	9.762	12887	-
KK1183	350	300	10.5	3.525	9.4756	0.90	31300	60900	9.760	13037	12683
KK1187	450	300	10.3	3.528	9.4569	0.94	23900	51300	9.763	12796	13733
KK1188	475	300	10.5	3.525	9.4728	1.02	23000	50900	9.760	13002	14387
KK1189	500	300	10.6	3.524	9.4843	0.95	22100	46900	9.759	13152	13955

Table A.24.: Detailed PLP sample conditions, absolute molecular weights of the first and second inflection point, as well as the resulting propagation rate coefficients for methyl acrylate (MA) samples incorporated into the frequency series at -12 °C.

sample	f Hz	n -	θ °C	T^{-1} 10^{-3} K^{-1}	$\ln(k_p)$ -	k_{p1}/k_{p2} -	M1 $\text{g}\cdot\text{mol}^{-1}$	M2 $\text{g}\cdot\text{mol}^{-1}$	c_M $\text{mol}\cdot\text{L}^{-1}$	k_{p1} $\text{mol}\cdot\text{L}^{-1}\cdot\text{s}^{-1}$	k_{p2} $\text{mol}\cdot\text{L}^{-1}\cdot\text{s}^{-1}$
KK1372	25	200	-12.5	3.837	8.4362	1.07	177900	333300	11.204	4611	4319
KK1374	75	200	-11.8	3.826	8.5162	1.02	64200	125800	11.197	4995	4894
KK1376	125	200	-11.3	3.819	8.4898	0.96	37500	78500	11.192	4865	5092
KK1377	150	200	-11.6	3.823	8.5288	0.95	32500	68100	11.195	5058	5299
KK1378	175	200	-12.1	3.831	8.5263	1.01	27800	55100	11.200	5046	5000
KK1379	200	200	-12.5	3.837	8.5125	0.95	24000	50300	11.204	4976	5215
KK1380	225	200	-12.8	3.841	8.5012	0.98	21100	43100	11.207	4921	5026
KK1381	250	200	-13	3.844	8.5068	0.87	19100	43700	11.209	4948	5661
KK1382	275	200	-13.2	3.847	8.5144	1.00	17500	34900	11.211	4986	4972
KK1383	275	200	-13.4	3.850	8.5200	1.05	17600	33400	11.213	5014	4757
KK1384	300	200	-13.5	3.851	8.5363	1.01	16400	32400	11.214	5096	5034
KK1386	350	200	-13.4	3.850	8.5251	0.95	13900	29200	11.213	5040	5294
KK1388	400	200	-13.1	3.845	8.5447	1.02	12400	24200	11.210	5140	5015
KK1389	425	200	-13.1	3.845	8.5300	0.95	11500	24300	11.210	5064	5351
KK1390	450	200	-13	3.844	8.5872	0.96	11500	24000	11.209	5363	5596

Table A.25.: Detailed PLP sample conditions, absolute molecular weights of the first and second inflection point, as well as the resulting propagation rate coefficients for methyl acrylate (MA) samples with 5 mol% LiNTf₃ incorporated into the frequency series at -12 °C. For certain samples, no second inflection point was observed, however, the data have been incorporated into the frequency series since the determined propagation rate was in agreement with the remaining data.

sample	f Hz	n -	θ °C	T^{-1} 10^{-3} K^{-1}	$\ln(k_p)$ -	k_{p1}/k_{p2} -	M1 g·mol ⁻¹	M2 g·mol ⁻¹	c_M mol·L ⁻¹	k_{p1} mol·L ⁻¹ ·s ⁻¹	k_{p2} mol·L ⁻¹ ·s ⁻¹
KK1352	25	200	-13.4	3.850	0.9925	0.99	171100	344800	10.582	4695	4731
KK1353	50	200	-13.2	3.847	1.0337	1.03	105700	204500	10.580	5802	5613
KK1354	75	200	-13.1	3.845	1.0275	1.03	71100	138400	10.579	5855	5699
KK1355	100	200	-13	3.844	0.9762	0.98	53400	109400	10.578	5864	6007
KK1356	125	200	-12.8	3.841	1.0193	1.02	42300	83000	10.575	5808	5698
KK1357	150	200	-12.1	3.831	1.0317	1.03	35800	69400	10.567	5903	5722
KK1358	175	200	-13.5	3.851	1.0347	1.03	29800	57600	10.584	5724	5531
KK1359	200	200	-13.8	3.856	1.0386	1.04	26900	51800	10.587	5903	5683
KK1360	225	200	-13.8	3.856	0.9651	0.97	23500	48700	10.587	5801	6011
KK1361	250	200	-13.8	3.856	0.9953	1.00	21300	42800	10.587	5842	5870
KK1362	275	200	-13.7	3.854	0.9684	0.97	19900	41100	10.586	6005	6201
KK1364	325	200	-13.3	3.848	0.9851	0.99	16500	33500	10.581	5887	5976
KK1369	450	200	-13.2	3.847	-	-	12300	-	10.580	6077	-

Table A.26.: Detailed PLP sample conditions, absolute molecular weights of the first and second inflection point, as well as the resulting propagation rate coefficients for methyl acrylate (MA) samples determined with the Nd:YAG Laser system in the absence (upper part) and presence (lower part) of LiNTf₃ at 10, 25, and 50 Hz.

sample pure MA	f Hz	t s	θ °C	T^{-1} 10^{-3} K^{-1}	$\ln(k_p)$ -	k_{p1}/k_{p2} -	M1 g·mol ⁻¹	M2 g·mol ⁻¹	c_M mol·L ⁻¹	k_{p1} mol·L ⁻¹ ·s ⁻¹	k_{p2} mol·L ⁻¹ ·s ⁻¹
KK1325	10	30	-13.8	3.856	8.1709	0.90	341500	762400	11.216	3537	3948
KK1326	10	30	-13.5	3.851	8.1591	-	337400	-	11.213	3495	-
KK1327	25	15	-14.2	3.862	8.2641	0.94	150000	319800	11.220	3882	4138
KK1328	25	15	-13.6	3.853	8.2812	0.94	152500	325600	11.214	3949	4216
KK1329	25	15	-13.7	3.854	8.3012	0.94	155600	329800	11.215	4029	4270
KK1331	50	10	-12.5	3.837	8.4491	1.03	90100	175500	11.204	4671	4549
KK1332	50	10	-12.9	3.842	8.4520	1.09	90400	166100	11.208	4685	4304

sample LiNTf ₃	f Hz	t s	θ °C	T^{-1} 10^{-3} K^{-1}	$\ln(k_p)$ -	k_{p1}/k_{p2} -	M1 g·mol ⁻¹	M2 g·mol ⁻¹	c_M mol·L ⁻¹	k_{p1} mol·L ⁻¹ ·s ⁻¹	k_{p2} mol·L ⁻¹ ·s ⁻¹
KK1336	10	30	-13.8	3.856	8.3205	1.01	383100	755400	10.835	4107	4049
KK1337	10	30	-13.4	3.850	8.3238	1.07	384200	720100	10.830	4121	3862
KK1338	10	30	-12.5	3.837	8.2958	1.00	373200	745300	10.818	4007	4001
KK1340	25	15	-14.1	3.860	8.5262	1.00	188300	377500	10.838	5045	5057
KK1341	25	15	-13.6	3.853	8.4894	0.98	181400	369500	10.832	4863	4953
KK1342	50	10	-13.8	3.856	8.6993	1.10	111900	204300	10.835	5998	5476
KK1343	50	10	-12.9	3.842	8.6713	1.00	108700	217500	10.823	5833	5836

Table A.27.: Detailed PLP sample conditions, absolute molecular weights of the first and second inflection point, as well as the resulting propagation rate coefficients for methyl acrylate (MA) samples in the absence and presence of LiNTf₃ incorporated into the Arrhenius plot.

sample pure MA	f Hz	n -	θ °C	T^{-1} 10^{-3} K^{-1}	$\ln(k_p)$ -	k_{p1}/k_{p2} -	M1 g·mol ⁻¹	M2 g·mol ⁻¹	c_M mol·L ⁻¹	k_{p1} mol·L ⁻¹ ·s ⁻¹	k_{p2} mol·L ⁻¹ ·s ⁻¹
KK1381	250	200	-13	3.844	8.5068	0.87	19100	43700	11.209	4948	5661
KK1382	275	200	-13.2	3.847	8.5144	1.00	17500	34900	11.211	4986	4972
KK1383	275	200	-13.4	3.850	8.5200	1.05	17600	33400	11.213	5014	4757
KK1263	400	100	0.2	3.658	8.9473	1.00	18800	37600	11.364	7687	7687
KK1264	425	100	0.1	3.660	8.9531	1.01	17800	35400	11.365	7732	7688
KK1265	450	100	0.1	3.660	8.9584	1.03	16900	32800	11.365	7773	7543
KK1205	400	300	10.4	3.527	9.2132	0.96	24200	50500	11.212	10029	10464
KK1206	425	300	10.5	3.525	9.2100	0.96	22700	47200	11.210	9996	10393
KK1207	450	300	10.5	3.525	9.2035	0.96	21300	44500	11.210	9932	10375
KK1208	475	300	10.3	3.528	9.2190	0.96	20500	42600	11.213	10087	10481
KK1402	300	100	20.5	3.405	9.5047	0.94	41900	89200	10.878	13423	14288
KK1403	350	100	20.2	3.409	9.5179	0.98	36400	74000	10.881	13600	13825
KK1404	400	100	19.8	3.414	9.5222	0.95	32000	67300	10.885	13659	14364
KK1121	400	300	30.3	3.295	9.6742	0.97	37400	76800	10.927	15903	16328
KK1122	425	300	30.3	3.295	9.6512	0.96	34400	71500	10.927	15541	16151
KK1123	450	300	30.3	3.295	9.6759	0.96	33300	69300	10.927	15929	16575
KK1426	500	100	40	3.193	9.9465	0.99	38400	77300	10.681	20879	21015
KK1427	500	100	40	3.193	9.9923	0.98	40200	82200	10.681	21858	22347

sample LiNTf ₃	f Hz	n -	θ °C	T^{-1} 10^{-3} K^{-1}	$\ln(k_p)$ -	k_{p1}/k_{p2} -	M1 g·mol ⁻¹	M2 g·mol ⁻¹	c_M mol·L ⁻¹	k_{p1} mol·L ⁻¹ ·s ⁻¹	k_{p2} mol·L ⁻¹ ·s ⁻¹
KK1357	150	200	-12.1	3.831	1.0317	1.01	35800	69400	10.567	5903	5722
KK1359	200	200	-13.8	3.856	1.0386	1.07	26900	51800	10.587	5903	5683
KK1361	250	200	-13.8	3.856	0.9953	1.00	21300	42800	10.587	5842	5870
KK1235	200	100	0.2	3.658	9.3166	1.04	47400	91100	9.901	11122	10688
KK1238	275	100	0.2	3.658	9.3203	1.06	34600	65000	9.901	11163	10485
KK1241	350	100	0.2	3.658	9.3135	1.05	27000	51400	9.901	11086	10553
KK1174	125	300	10.3	3.528	9.4530	0.97	85700	175800	9.763	12746	13073
KK1176	175	300	10.6	3.524	9.4773	1.00	62700	125600	9.759	13060	13080
KK1179	250	300	10.4	3.527	9.4998	0.99	44900	91100	9.762	13357	13551
KK1414	225	100	20.5	3.405	9.7155	1.00	64700	129800	10.203	16573	16625
KK1418	350	100	20.3	3.408	9.8073	1.06	45600	86300	10.205	18166	17190
KK1433	500	100	40	3.193	10.1607	0.96	44900	93100	10.081	25867	26818

Hiermit erkläre ich wahrheitsgemäß, dass ich die vorliegende Doktorarbeit im Rahmen der Betreuung durch Professor Christopher Barner-Kowollik im Zeitraum von März 2014 bis März 2017 selbstständig verfasst und keine anderen als die angegebenen Hilfsmittel und Quellen verwendet habe. Des Weiteren erkläre ich, dass ich mich zur Zeit in keinem laufenden Promotionsverfahren befinde und keine vorausgegangenen Promotionsversuche unternommen habe.

Karlsruhe, 10.03.2017

.....

(Katrin Kockler)

Curriculum Vitae

Date of Birth: April 27th, 1989
Place of Birth: Birkenfeld, Germany
Nationality: German

Education

03/2014 - 04/2017 **Doctoral Studies in Chemistry**
Under the Supervision of Prof. Dr. Barner-Kowollik
Karlsruhe Institut of Technology (KIT), Germany
“Taking the Pulse of Polymerization Kinetics: A Systematic PLP-
SEC Study of Industrially Relevant (Meth)acrylates“

09/2016 - 11/2016 **Research Period**
Under the Supervision of Prof. Dr. Coote
Australian National University (ANU), Canberra, Australia

01/2014 **Diploma in Chemistry**
Under the Supervision of Prof. Dr. Meier
Karlsruhe Institut of Technology (KIT), Germany
“Recyclable polymeric reagents for a sustainable approach in
organic synthesis“

10/2008 - 02/2014 **Studies of Pure Chemistry**
Universität Karlsruhe (TH) (later: Karlsruhe Institut of Technology
(KIT)), Germany

07/2008 **High School Certificate**
St. Wendel, Germany

Professional Experience

09/2011 - 11/2011 Institute of Organic Chemistry, Group of Prof. Dr. Meier
Karlsruhe Institute of Technology (KIT), Germany
Complementary Scientist

08/2010 - 11/2010 Engler Bunte Institute, Bereich Gas, Erdöl, Kohle
Karlsruhe Institute of Technology (KIT), Germany
Complementary Scientist

Publications and Conference Contributions

Peer Reviewed Publications

- 1. Solvent Effects on Acrylate k_p in Organic Media? – A Systematic PLP-SEC Study**
Haehnel, A. P.; Wenn, B.; Kockler, K.; Bantle, T.; Misske, A. M.; Fleischhaker, F.; Junkers, T.; Barner-Kowollik, C. *Macromol. Rapid Commun.* **2014**, *5*, 2029–2037.
- 2. No Apparent Correlation of k_p with Steric Hindrance for Branched Acrylates**
Kockler, K. B.; Haehnel, A. P.; Fleischhaker, F.; Schneider-Baumann, M.; Misske, A. M.; Barner-Kowollik, C. *Macromol. Chem. Phys.* **2015**, *216*, 1573–1582.
- 3. Solvent Effects on Acrylate k_p in Organic Media? – A Systematic PLP-SEC Study – Statement to the Response**
Haehnel, A. P.; Wenn, B.; Kockler, K.; Bantle, T.; Misske, A. M.; Fleischhaker, F.; Junkers, T.; Barner-Kowollik, C. *Macromol. Rapid Commun.* **2015**, *36*, 1984–1986.
- 4. Determining Free-Radical Propagation Rate Coefficients with High Frequency Lasers: Current Status and Future Perspectives**
Kockler, K. B.; Haehnel, A. P.; Junkers, T.; Barner-Kowollik, C. *Macromol. Rapid Commun.* **2016**, *37*, 123–134.
- 5. Investigating the Propagation Kinetics of a Novel Class of Nitrogen-Containing Methacrylates via PLP-SEC**
Kockler, K. B.; Fleischhaker, F.; Barner-Kowollik, C. *Polym. Chem.* **2016**, *7*, 4342–4351.
- 6. A Complete Kinetic Study of a Versatile Functional Monomer: Acetoacetoxyethyl Methacrylate (AAEMA)**
Zoller, A.; Kockler, K. B.; Rollet, M.; Lefay, C.; Gigmes, D.; Barner-Kowollik, C.; Guillaneuf, Y. *Polym. Chem.* **2016**, *7*, 5518–5525.
- 7. An alternative method to estimate the bulk backbiting rate coefficient in acrylate radical polymerization**

Marien, Y. W.; Van Steenberge, P. H. M.; Kockler, K. B.; Barner-Kowollik, C.; Reyniers, M.-F.; D'hooge, D. R.; Marin, G. B. *Polym. Chem.* **2016**, *7*, 6521–6528.

8. Free Radical Propagation Rate Coefficients of N-Containing Methacrylates: Are We Family?

Kockler, K. B.; Fleischhaker, F.; Barner-Kowollik, C. *Macromolecules* **2016**, *49*, 8572–8580.

9. Estimating Photodissociation Quantum Yields from PLP-SEC Peak Heights

Marien, Y. W.; Van Steenberge, P. H. M.; Kockler, K. B.; Barner-Kowollik, C.; Reyniers, M.-F.; Marin, G. B.; D'hooge, D. R. **2017**, *in press*.

Conference Contributions

1. Understanding the Fundamentals – Investigating the Kinetics of a Novel Class of N-containing Monomers via PLP-SEC

K. B. Kockler, F. Fleischhaker, C. Barner-Kowollik

Warwick Polymer Conference 2016, Coventry, United Kingdom.

2. Free Radical Propagation Rate Coefficients of N-Containing Methacrylates: Are We Family?

K. B. Kockler, F. Fleischhaker, C. Barner-Kowollik

36th Australasian Polymer Conference 2016, Lorne, Australia.

Danksagung – Acknowledgements

Mein Dank geht in erster Linie an Prof. Dr. Christopher Barner-Kowollik für die Möglichkeit dieses interessante Thema in seiner Arbeitsgruppe zu bearbeiten. Seine rege fachliche Unterstützung, Motivation und das Vertrauen in mich und meine Fähigkeiten haben den Weg für diese Doktorarbeit geebnet. Wie auch immer mein weiterer Karriereweg aussehen mag, ich kann mir keine bessere Basis vorstellen als zu den Macroarcians zu gehören.

Des Weiteren danke ich Dr. Andrea Misske und Dr. Friederike Fleischhaker von der BASF Ludwigshafen für eine ausgezeichnete Kooperation, einsichtsreiche Projekttreffen, eine tolle Arbeitsatmosphäre und rege Diskussionen sowie die Versorgung mit den Monomeren, auf denen diese Arbeit aufgebaut ist. Dank der Zusammenarbeit mit der BASF durfte ich einen interessanten Einblick in den Alltag in der chemischen Industrie gewinnen. Vielen Dank an Frau Dr. Maria Schneider-Baumann für die Einführungen an den zahlreichen GPC-Systemen und die großartige und schnelle Hilfe sowohl mit praktischen als auch theoretischen Problemen. Ihr unermüdlicher Einsatz für das Wohlbefinden der Analysegeräte hat meine Arbeit sehr erleichtert und ohne Sie wäre ich an dem einen oder anderen Geräteproblem gescheitert. Dr. Alexander Hähnel gebührt mein Dank für die kompetente Einführung in das Thema PLP-SEC, das Vertrauen sein Thema in meine Hände abzugeben und offene Ohren bei allerlei (intelligenten und weniger intelligenten) Anfängerfragen auch über das Ende seiner Zeit in der Arbeitsgruppe hinaus.

I'm furthermore grateful to Prof. Dr. Michelle Coote and Dr. Leesa Smith for the opportunity to gain deeper insight into the field of Lewis acids, Dr. Ben Noble for fruitful discussions, Dr. Naomi Hayworth for the help with the paper war and swiping me out of the building in the evenings, and all other members of the Coote group for the nice and welcoming atmosphere during my research stay at ANU. Gaining insight into the working routine in Australia and at RSC in particular has broadened my experiences in many respects and gave me the opportunity to get to know and fall in love with a particularly beautiful country full of amazingly friendly people.

Ich danke dem Karlsruhe House of Young Scientists (KHYS) für die finanzielle Förderung meines Auslandsaufenthaltes an der Australian National University (ANU) in Canberra, Australien.

Dr. Michael Kaupp und Dr. Bryan Tuten danke ich für die geopfert Zeit für das Korrekturlesen dieser Arbeit und das Behalten zahlreicher Tippfehler. Alle, die noch übrig sind, lass ich Euch bei Gelegenheit zukommen. Dem ganzen Macroarc-Team bin ich

meinen Dank schuldig für viele interessante Diskussionen, gute Stimmung im Labor, offene Ohren und offene Arme und eine unglaublich sympathische Arbeitsatmosphäre, die das PhD-Leben deutlich einfacher gemacht hat. Wenn ich noch einmal von vorne anfangen könnte, würde ich es wieder mit den Macroarcians tun.

Meinen Eltern danke ich ganz besonders für die großartige Unterstützung während meines gesamten Studiums, angefangen mit Ermutigungen, sich an das Studentenleben zu wagen, über Geldspritzen, um Miete und Essen zu zahlen, vielen Fahrten nach Karlsruhe, langen Tagen an Krankenhausbetten, bis hin zum Stolz sein auf das "Töchterchen" mit dem Diplom in der Hand. Ohne Euch wäre es mir nicht möglich, heute die zwei magischen Buchstaben vor meinen Namen schreiben zu dürfen.

Mein ganz spezieller Dank geht auch an das "kleine Office"-Team, allen voran Dr. Michael Kaupp und Matthias Eing, für die tolle Zeit mit Euch, viel Spaß und Unfug und vor allem für Eure Freundschaft, die mehr wert ist als "Eine Millionen Yen!". Bryan, Dir danke ich für zahlreiche Gespräche in Deutsch-Englisch-Wechsel, kreatives Brainstorming, schwarze Schafe und den unermüdlichen Hinweis darauf, wie man 'idea' richtig ausspricht. Deine Begeisterung für Chemie und dein unerschöpflicher Vorrat an Ideen wird dich noch weit bringen und ich hoffe, mich in Zukunft noch öfter davon anstecken lassen zu können. Iroh forever!

Es war mir ein Fest.

Everything is theoretically impossible, until it's done.

Robert A. Heinlein

Hurray for science! Woo!

Bart Simpson